Aspects of Feasibility of a Shipboard Algal Photobioreactor to Capture Carbon Dioxide Emissions

PhD Thesis

Submitted for the degree of Doctor of Philosophy

PhD Candidate:	**Konstantina Koutita**
Supervisory Team:	Professor Julia Stegemann
	Dr Tristan Smith
	Dr Nithin Rai
Studentship Funding:	UCL Impact Award
	Octoply Ltd.

Centre for Resource Efficiency & the Environment

Department of Civil, Environmental and Geomatic Engineering

University College London

November, 2016

Dedicated to

My parents, Christopher and Maria,

My brother, George,

and my sister, Maria-Christina.

Acknowledgements

I would like to sincerely thank my supervisors for patiently helping me start and complete this project, by always being there to provide advice, offering to help with any kind of problem, and carefully reading through and commenting on my thesis. Specifically, I am grateful to Professor Julia Stegemann for her valuable guidance, for teaching me to be more efficient in my research and for motivating to work. I also greatly appreciate the focused, constructive and wise advice and the support given by Dr Tristan Smith. Last but not least, Dr Nithin Rai, the industrial sponsor of this project, provided the idea of this topic and numerous inspiring and creative suggestions throughout the project.

I would also like to express my thanks to the financial support for my project from: (i) UCL Impact Award, (ii) Octoply Ltd, (iii) the Spark Award by Knowledge Transfer Network, and (iv) Community by Design social enterprise, for funding the photobioreactor materials purchase. I need to mention that the CEGE department of UCL offered me a friendly environment to work in, which is most vital for PhD studies.

Special thanks would go to my fellow colleague, Alessandro Marco Lizzul, for his help in the lab and the great co-operation I had with him and his supervisor, Dr Luiza Campos. I would also like to thank the students Rena Seyidova, Michael Gonzalez, Shao Zong Wu, Xin Min Lee and Liusixing He, for their help with lab measurements and some schematics drawing.

Regarding the lab work, my honest thanks go to Ian Sturtevant, Dr Judith Zhou, Catherine Unsworth, Dr Melisa Canales and the workshop's staff for their assistance in using lab equipment and for helping with occasional construction work. I am also thankful to Dr Jong Kyu Kim, Dr Anna Bogush and Sajida Rasheed, for lending lab equipment; to Rokiah Yaman and Hamid Aghili for their help with the photobioreactor construction; to Professor Brian Whitton for the wild algae identification; and to Dr Sofie Vonlanthen for helping with some lab measurements.

I also greatly appreciate the advice provided by Dr Alexandros Kiparissides, as well as Dr Mazaher Molaei Chalchooghi and the gPROMS technical support team, regarding gPROMS modelling issues I faced, being the only person in the department to use this software. Many thanks go to Dr Andy Chow for his help with statistical analysis, to Dr Frank Baganz for his advice during my upgrade viva, to Dr Christos Markides for motivating me, and to Rukayya I. Muazu for her companionship in UCL. Most special thanks go to my family for the continuous support and encouragement and for always believing in me, it has been most important during this period. Finally, I would like to thank in advance the examiners for reading through my thesis.

Declaration of Authenticity

I, Konstantina Koutita, hereby declare that this thesis and the work presented in it is entirely my own. Where I have consulted the work of others, this is always clearly stated. To the best of my knowledge and belief, this thesis contains no material previously published or written by another person, except where due reference has been made.

Konstantina Koutita

University College London

16 October 2015

Abstract

The CO_2 contribution of shipping to global emissions is about 3.1% and emission reductions are becoming urgent as part of global measures to combat air pollution. This study was the first to investigate the implementation of an algal photobioreactor (PBR) on a ship to treat its gas emissions and produce biomass for commercial purposes. The research examined various aspects of the challenges faced, focusing on the biomass cultivation process of the application. The target was to use the waste streams of the ship (i.e., flue gas, waste heat and wastewater) to fulfil the PBR's material and energy needs.

A PBR configuration is proposed and constructed, considering the additional complications of a shipboard system. Algae from natural surrounding water were cultivated in lab conditions to explore the potential of this approach in a shipboard PBR. A theoretical hydrodynamic model was developed to compute gas hold-up and liquid velocity in airlift PBRs. The different bubble sizes and drag coefficients used were shown to greatly impact the results, but the effect of bubbles is not easily distinguished in the experiments. A model of the effects of light intensity, nutrient concentration and temperature on microalgal growth kinetics was also developed, for use in optimising the operating conditions.

Finally, practical aspects of integrating the PBR into the shipboard system were examined. Availability of space in the ballast tanks of tankers and ferries in the existing fleet to accommodate a PBR to treat their total emissions was estimated. The need for a large water mass limits this application, but the comparatively higher potential of tankers for this implementation was demonstrated. Maintaining the PBR's temperature by sparging with hot flue gas was proven to be unfeasible and a novel heat exchanger design was suggested and modelled, using an input produced by the hydrodynamic model.

Glossary

Absorptance	Absorptance of the surface of a material is its effectiveness in absorbing radiant energy.
Algae – Microalgae	Algae are aquatic photosynthetic organisms, and they may be microscopic and mostly unicellular (microalgae), or large and poses plant-like characteristics (macroalgae). Macroalgae are not relevant to the present work; the term “algae” is therefore generally used in the following to refer to microalgae.
ANOVA	Analysis of variance (ANOVA) is a procedure for comparing more than two groups and the effect of independent variables on dependent ones, as well as the interaction among the independent variables. It can be 1-way, where is one independent variable (one factor) with more than two conditions; or 2-way, where are two independent variables (factors) and can have multiple conditions.
Broth	Microalgal culture in water, including potential nutrient media, traces and impurities in liquid form.
CH_4	Methane
Class – genus – species – strains	In biological taxonomic classification, ranks in descending order of size are life, domain, kingdom, phylum, order, class, family, genus, and species. Class is a distinct rank of biological classification having its own distinctive name. A genus contains one or more species. Each named species of algae is referred to by its genus and species name. In a binomial algae name, the first part is the genera name, the second represents the species. A strain is an isolate that has been studied in the laboratory so that the details of the appearance and behaviour of the cells become known. For example, for the microalga Botryococcus braunii KMITL 2, Botryococcus is the genera, Botryococcus braunii is the species and KMITL 2 is the specific strain.
CO_2	Carbon dioxide
Downcomer	Airlift bioreactors are pneumatic gas-liquid contacting devices, in which gas injected into the bioreactor “riser” causes circulation of liquid via a linked “downcomer” where there is no sparging but smaller bubbles move downwards carried by the stream of the liquid which recirculates due to the density difference
EEDI	Energy Efficiency Design Index
Exhaust gas – Flue gas	The report mainly uses the term flue gas to describe the exhaust gas from combustion process. Exhaust gas is mentioned in the description of the “exhaust gas cleaning systems” of the ship, to keep consistency with the term used in the literature.
Fixation	Microalgal contribution to the reduction of CO_2 contained in the flue gas, by using it as carbon source. This process is known as biofixation of CO_2, but referred to simply as fixation in this study.
Gas hold-up	The ratio of gas phase volume to total volume
HE	Heat exchanger

IMO	International Maritime Organisation
Mixture	When not determined by the context, it implies the mixture of algal broth with bubbles flowing within the liquid.
MV Sound	Motor Vessel Sound. A ship owned by Octoply Ltd
N	Nitrogen (element)
N_2	Nitrogen (molecular)
Net energy ratio	Energy production divided by consumption, which is the combustion energy of the produced algae divided by the total energy demand of the reactor. Hence when being higher than 1 the PBR is able to produce more energy than it consumes.
NO_x	Nitrogen oxides (NO_x and NO_2)
P	Phosphorus (element)
PAR	Photosynthetic Active Radiation (measured in μmol/s/m^2). Illumination on algae is measured in these units in this report.
PBR	Photobioreactor
Petri dish	A Petri dish is a cylindrical glass or plastic lidded dish used to culture cells in the lab.
Productivity	Refers to aerial, volumetric or daily biomass productivity and reported as grams of dry algae per square meter per littre, or per square meter per littre per day, respectively. When it refers to production of lipids, it is determined as lipid productivity.
Pseudoreplication	Pseudoreplication involves treatments that are not replicated but are treated as the same in statistical testing, e.g., t-test or ANOVA. There are several types of pseudoreplication: simple, sacrificial, temporal and implicit. Sacrificial pseudoreplication (referred to simply as sacrificial in this study) uses a number of wells/bottles/Petri dishes per experimental unit equal to the number of samples that need to be taken over time. Temporal pseudoreplication (resampling in this study) uses only one well/bottle/Petri dish, which is repeatedly sampled over time (South & Somers, n.d.).
P-value	In relation to statistical testing, P-value refers to the probability of finding the observed, or more extreme, results when the null hypothesis of a study question is true. It either validates or refutes the null hypothesis. Null hypothesis refers to a general statement or default position that there is no relationship between two measured phenomena, or no association among groups.
Response	This term illustrates the changes of the characteristics or metabolites of an algal species to conditions or environmental changes.
Riser	See “Downcomer”
Roll-on-roll-off	Vessels designed to carry wheeled cargo without requirement for turning.
R1, R2, R3	Reactor configuration 1, 2 and 3 (in Chapter 5)
Salinity	Salinity is defined as the dissolved salt content of various salts

	such as sodium chloride (NaCl), magnesium and calcium sulphates and bicarbonates. In the Practical Salinity Scale, salinity is redefined as the conductivity ratio of a seawater sample to a standard KCl solution. Seawater contains predominantly NaCl, but other salts as well. The studies reviewed in this report have examined salinity of natural seawater or with artificial seawater made with introduction of NaCl and probably other additional salts. Salinity in the present report will refer to total salt concentration since most of the reports do not define the composition of the saltwater used, but it will state which studies have worked with salinity specifically caused by the introduction of NaCl. Salinity is reported in a variety of units, including 1 ppt (parts per thousand) = 1 ‰ = 0.1 % = 1 psu (practical salinity unit) = 1 gL^{-1} ≈ 1/58 M. All of these have been converted to gL^{-1} for consistency.
Scrubbing	Scrubber systems are used to remove particulates or gas components from industrial flue gas. They use liquid or dry reagent, or slurry to absorb unwanted pollutants. The term scrubbing in the text is used to describe the removal of SO_x, NO_x, particulate matter, or CO_2 by means other than algae (see fixation above).
Sky temperature	For practical calculations in radiative heat transfer, it is often convenient to treat the sky as a black radiator having some appropriate temperature. This effective sky temperature usually lies between 5 and 30 K below the ground level air temperature. The sky temperature decreases as the amount of water vapour in the air goes down (Lienhard Iv & Lienhard, 2008).
SO_x	Sulphur oxides
S1, S2, S3	Spargers 1, 2 and 3 (refer to the spargers used in Chapter 5)
Tolerance	In the present report, this term refers to the limits below which a species can survive, though perhaps not optimally.
t-test	t-test is a statistical hypothesis test that allows for the comparison of two data populations and their means. It can be used to determine if two sets of data are significantly different from each other. A null hypothesis (defined in the P-value definition) can be created where the means of the returns of the two samples do not differ. t-test is well-suited for a small set of data.
UV	Ultraviolet light (UVA, UVB, UVC wavelengths)
WHR	Waste Heat Recovery
Wild algae	Algal strains harvested from natural waters.
1st, 2nd, 3rd generation biofuels	This classification is variously based on type of feedstock, conversion technology used, or properties of the fuel molecules produced. To overcome confusion, a more scientific definition can be described based on the carbon source from which the biofuel is derived. 1st generation are the conventional biofuels made from starch, sugar, or vegetable oil, directly extracted from a plant. 2nd generation are biofuels made from lignocellulosic biomass or woody crops (e.g., agricultural, forestry wastes or residues, or purpose-grown non-food feedstocks). 3rd generation biofuels are derived from aquatic autotrophic organism (e.g., algal biomass).

Nomenclature

Symbols

A	Surface area of the tube [m^2]
A_1, A_2	Preexponential factors [h^{-1}]
a	Cross section area [m^2]
a_i	Interphase area [m^2]
a_s	Initial slope of light response curve [day^{-1}]
a_d	Cross-sectional area of the downcomer [m^2]
a_i	Cross-sectional area of a fitting with different diameter from the main tube [m^2]
a_r	Cross-sectional area of the riser [m^2]
a_{solar}	Absorptance from the sun [dimensionless]
B	Regression coefficient for the Arrhenius-Eyring-Polanyi equation [K^{-1}]
b	Factor in Tamiya light intensity model [dimensionless]
C_b	Biomass concentration [g/L]
C_{CO_2}	Gas CO_2 concentration [L/L]
$C_{CO_2 l}$	Dissolved CO_2 concentration in the liquid phase [L/L]
$C^*_{CO_2 l}$	Concentration of CO_2 in the liquid phase that could equilibrate its measured partial pressure [L/L]
C_f	Carbon emission factor [g/g]
C_N	Extracellular nitrogen substrate concentration [g/L]
$C_{N,0}$	Extracellular nitrogen substrate concentration in the feed stream [g/L]
C_P	Extracellular phosphorus substrate concentration [g/L]
$C_{P,0}$	Extracellular phosphorus substrate concentration in the feed stream [g/L]
C_S	Substrate concentration [g/L]
$C_{S,0}$	Substrate concentration in the feed stream [g/L]
C_f	Carbon emission factor [tonnes CO_2 / tonnes fuel]
c_D	Drag coefficient [dimensionless]
c_{p_g}	Specific heat capacity of the gas [$JK^{-1}kg^{-1}$]
$c_{p_{hf}}$	Specific heat capacity of the heating fluid [$JK^{-1}kg^{-1}$]
c_{p_l}	Specific heat capacity of the liquid [$JK^{-1}kg^{-1}$]
c_{p_m}	Specific heat capacity of the mixture [$JK^{-1}kg^{-1}$]
D	Dilution rate [h^{-1}]
d	Diameter or depth of the PBR [m]
d_b	Mean diameter of the bubbles [mm]
d_d	Diameter of the downcomer tube [m]
d_i	Inner diameter of the tube (equal to d_r) [m]
d_o	External diameter of the tube [m]

d_r	Diameter of the riser tube [m]
E_a	Activation energy [kJ/mol]
E_{a1}, E_{a2}	Activation energy [kJ/mol]
F_B	Buoyancy force [N, or $kgms^{-2}$]
F_{CO_2}	CO_2 flow rate [tonnes/h]
F_D	Drag force [N, or $kgms^{-2}$]
F_F	Wall friction force [N, or $kgms^{-2}$]
F_f	Fuel flow rate [tonnes/h]
F_{fuel}	Fuel consumption [tonnes/day]
F_g	Flue gas flow rate into the heat exchanger [kg/s]
$F_{w,1}$	Water flow rate through valve 1 [kg/s]
$F_{w,1,o}$	Threshold flow rate through valve 1 that leads to overflow of the storage tank [kg/s]
$F_{w,1,p}$	Threshold flow rate through valve 1 that leads to inadequate heating rate provision [kg/s]
$F_{w,2}$	Water flow rate through valve 2 [kg/s]
$F_{w,2,b}$	Threshold flow rate through valve 2 that leads to inadequate water in the storage tank [kg/s]
f	Darcy-Weisbach friction factor [dimensionless]
f_{fix}	CO_2 fixation factor [g/g of dry algae]
f_{scr}	Percentage ratio of CO_2 fixed [gCO_2/gCO_2]
g	Gravitational acceleration [ms^{-2}]. The value of 9.810 was used for this fixed parameter as a modelling input
g_r	Regression coefficient [$h^{-1/2}\,K^{-1}$]. The value of 9.810 was used for this fixed parameter as a modelling input
Gz	Graetz number [dimensionless]
h	Heat transfer coefficient [$Wm^{-2}K^{-1}$ or $kgs^{-3}K^{-1}$]
h_D	Height of the liquid in the riser after gas entrance, hence height of the dispersion [m]
h_e	Heat transfer coefficient of the ambient air [$Wm^{-2}K^{-1}$ or $kgs^{-3}K^{-1}$]
h_f	Head due to sum of friction on the wall [m]
h_{fr}	Head due to friction [m]
h_L	Height of the liquid in the riser before gas entrance [m]
h_{mf}	Head due to friction in the fittings [m]
h_m	Heat transfer coefficient of the mixture in the PBR [$Wm^{-2}K^{-1}$ or $kgs^{-3}K^{-1}$]
I	Light intensity [$\mu E/m^2/sec$]
I_{av}	Space averaged light intensity within the PBR [$\mu E/m^2/sec$]
I_{opt} , I_{max}	Optimal light intensity [$\mu E/m^2/sec$]
I_0	Incident light intensity on the surface of the PBR [$\mu E/m^2/sec$]
K_A	Acid dissociation constant [mol/L]
K_a	Biomass light absorption (extinction) coefficient [m^2/g]

K_{CO2}	Half saturation constant for CO_2 [L/L]
K_{cont}	Equivalent frictional velocity head loss coefficient due to contractions [dimensionless]
K_{exp}	Equivalent frictional velocity head loss coefficient due to expansions [dimensionless]
K_{fit}	Equivalent frictional velocity head loss coefficient from the fittings in the loop [dimensionless]
$K_{H_{CO_2}}$	Henry's constant [mol/L/atm]
K_I	Bioenergetics efficiency of light utilisation (or irradiance necessary for half maximum photosynthesis rate) [μE/m^2/sec]
K_i	Light inhibition constant [μE/m^2/sec or g.s/L/μmol^2/m^4]
K_l	Additional frictional loss coefficient, equivalent number of velocity heads [dimensionless]
K_N	Half saturation constant for nitrates [g/L]
K_P	Half saturation constant for phosphates [g/L]
K_S	Half saturation constant for substrate [g/L]
k	Thermal conductivity [$Wm^{-1}K^{-1}$ or $kgms^{-3}K^{-1}$]
k_B	Frictional loss coefficient for the bottom connecting section of the PBR tubes [dimensionless]. The value of 5.0 was used for this fixed parameter as a modelling input
k_l	Liquid phase mass transfer coefficient [mol/(s·m^2)/(mol/m^3)]
k_m	Thermal conductivity of the mixture in the tube [$Wm^{-1}K^{-1}$ or $kgms^{-3}K^{-1}$]
k_t	Thermal conductivity of the walls of the tube [$Wm^{-1}K^{-1}$ or $kgms^{-3}K^{-1}$]
k_0	Frequency factor or the total number of collisions between reacting species per unit time [s^{-1}]
l	Total length of the PBR [m]
l_d	Length of the downcomer [m]
l_{HE}	Length of the heat exchanger [m]
l_r	Length of the riser [m]
LF_{ME}	Load factor of the main engines [-]
$LMTD$	Logarithmic Mean Temperature Difference [K]
LPD	Lag phase [days]
m	Exponent of the hyperbolic Monod model [dimensionless]
m_a	Specific maintenance rate [h^{-1}]
m_S	Maintenance supply rate of minimum substrate consumption to maintain cells [h^{-1}]
$m_{S/N}$	Maintenance supply rate of minimum nitrates consumption to maintain cells [h^{-1}]
$m_{S/P}$	Maintenance supply rate of minimum phosphates consumption to maintain cells [h^{-1}]
$\dot{m}$	Mass flow rate [kgs^{-1}]
N	Number of the bubbles in the tube [dimensionless]
n	Factor in the Arrhenius equation of enzyme-mediated reactions response [dimensionless]

Nu_d	Nusselt number based on the inner diameter of the tube [dimensionless]
N_{CO2}	Mass transfer rate of CO_2 to the liquid [mol/m^3]
OD	Optical density [-]
P	Perimeter of the tube [m]
P_B	Power generated from the buoyancy force [W]
P_{CO_2}	Partial pressure of CO_2 [L/L]
P_F	Power consumed by the friction on the wall and the fittings [W]
P_{ME}	Power of the main engines [hp]
P_V	Volumetric productivity [g/L/h]
Pr	Prandtl number [dimensionless]
Pr_{PBR}	Productivity of the PBR [g/L/day]
p	Pressure [Pa or $kgm^{-1}s^{-2}$]
q	Heat transferred [W]
q_g	Gas sparging rate [m^3s^{-1}]
q_{hf}	Flow rate of the heating fluid [m^3s^{-1}]
q_l	Mean flow rate of the liquid [m^3s^{-1}]
q_{loss}	Heat lost through a section of the wall to the environment [W]
q_m	Heat transferred in the mixture from its entrance to its exit of a selected system [W]
q_{max}	Maximum heating rate output from the heat exchanger at the exhaust [W]
q_{radial}	Heat transferred through a section of the wall to the environment [W]
q_{solar}	Average global sunlight intensity over year [W/m^2]
R	Gas constant [J/K/mol]
$R_{t_{cond}}$	Absolute thermal resistance by conduction [KW^{-1}]
$R_{t_{conv}}$	Absolute thermal resistance by convection [KW^{-1}]
$\mathrm{R_{t_m}}$	Absolute thermal resistance by convection in the mixture [KW^{-1}]
$\mathrm{R_{t_e}}$	Absolute thermal resistance by convection in the ambient air [KW^{-1}]
$\mathrm{R_{t_t}}$	Absolute thermal resistance by conduction in the tube and [KW^{-1}]
r	Relative roughness of the pipe [m]. The value of 0.0000025 was used for this fixed parameter as a modelling input
r_t	Radial dimension of the tube [m]
r_e	External radius of the PBR tube [m]
r_i	Internal radius of the PBR tube [m]
r_{oper}	Day operation ratio [dimensionless]
r_s	Slope of the linear regression [$h^{-1}K^{-1}$]
Re	Reynolds number [dimensionless]
Re_b	Reynolds number of the bubbles [dimensionless]
Re_l	Reynolds number of the liquid [dimensionless]
$S_{fp,ME}$	Specific fuel consumption per main engine power unit [tonnes/hp]

s	Thickness of the wall [m]
T	Temperature [K]
T_e	Ambient temperature [K]
$T_{g_{in}}$	Temperature of the gas fed in the PBR [K]
$T_{hf_{in}}$	Temperature of the heating fluid in the entrance [K]
$T_{hf_{out}}$	Temperature of the heating fluid in the exit [K]
T_m	Temperature of the mixture [K]
$T_{m_{in}}$	Temperature of the mixture at thermal quasi-equilibrium between the liquid in the entrance and the sparged gas [K]
$T_{m_{out}}$	Temperature of the mixture at the end of the PBR and reintroduced in the entrance [K]
T_{max}	Maximum temperature allowed for growth [K]
T_{min}	Minimum temperature allowed for growth [K]
T_{opt}	Optimal temperature where the maximum growth rate is obtained [K]
T_{ref}	Reference temperature [K]
T_{sky}	Sky temperature [K]
T_w	Temperature at the wall of the tube [K]
$T_{w_{ex}}$	Temperature at the external diameter of the tube wall [K]
$T_{w_{in}}$	Temperature at the internal diameter of the tube wall [K]
T_0	Conceptual temperature with no metabolic significance [K]
t	Time [h]
t_g	Residence time of the bubbles in the riser [s]
t_l	Residence time of the liquid in the riser [s]
tpd	Daily fuel consumption of ship engines [tonnes/day]
U	Overall heat transfer coefficient [$Wm^{-2}K^{-1}$ or $kgs^{-3}K^{-1}$]
u_b	Mean velocity of bubbles in the riser relative to the liquid [ms^{-1}]
u_g	Superficial gas velocity in the riser [ms^{-1}]
u_l	Superficial liquid velocity of the liquid mobilised by the bubbles in the riser [ms^{-1}]
u_m	Velocity of the mixture [ms^{-1}]
$\bar{u}_g$	Gas rise velocity in the riser estimated according to the sum of u_b and $\bar{u}_l$ [ms^{-1}]
$\bar{u}_l$	Liquid circulation velocity in the riser [ms^{-1}]
V_g	Volume of gas in the riser tube [m^3]
V_l	Volume of liquid in the riser tube [m^3]
V_{PBR}	Volume of the PBR [m^3]
V_{riser}	Volume of the riser [m^3]
$Y_{b/N}$	Yield over nitrates [g of biomass/g of N]
$Y_{b/P}$	Yield over phosphates [g of biomass/g of P]
$Y_{C/S}$	Yield over substrate [g of biomass/g of substrate]

z	Depth of light penetration in the PBR [m]

Greek characters

ε	relative roughness of the pipe [m]
ε_d	Gas hold-up in the downcomer [dimensionless]
ε_{IR}	Emittance [dimensionless]
ε_{mean}	Mean gas hold-up in the PBR [dimensionless]
ε_r	Gas hold-up in the riser [dimensionless]
θ_j	j^{th} parameter to be estimated [dimensionless]
θ_j^*	Final value of that parameter to be estimated [dimensionless]
θ_j^L	Lower bound imposed on the parameter to be estimated [dimensionless]
θ_j^U	Upper bound imposed on the parameter to be estimated [dimensionless]
μ	Dynamic viscosity [$kgm^{-1}s^{-1}$]. The value of 0.798 x 10^{-3} was used for the fixed parameter of the liquid in the PBR as a modelling input
μ_r	Growth rate [1/h]
μ_j	Lagrange multiplier that corresponds to the bound constraints imposed on the parameter [dimensionless]
μ_m	Dynamic viscosity of the mixture in the PBR [$kgm^{-1}s^{-1}$]
μ_{max}	Maximum growth rate [1/h]
μ_{opt}	optimal growth rate which can be reached at the optimal temperature [1/h]
μ_0	Specific growth rate at 0 °C [1/h]
ν	Kinematic viscosity of water [m^2s^{-1}]. The value of 0.801 x 10^{-6} was used for the fixed parameter of the liquid in the PBR as a modelling input
π	Ratio of circumference to diameter of a circle [dimensionless]. The value of 3.142 was used for this fixed parameter as a modelling input
ρ	Density [kgm^{-3}]
ρ_g	Density of the sparged gas [kgm^{-3}]. The value of 1.225 was used for this fixed parameter as a modelling input
ρ_{hf}	Density of the heating fluid [kgm^{-3}]. The value of 1000 was used for this fixed parameter as a modelling input
ρ_l	Density of the liquid in the PBR [kgm^{-3}]. The value of 1000 was used for this fixed parameter as a modelling input
ρ_m	Density of the mixture (gas and liquid) in the PBR [kgm^{-3}]
σ	Stefan-Boltzmann constant [5.6704×10^{-8} $W/m^2/K^4$]
φ	Utilisation factor [dimensionless]
Φ^*	Final value of the maximum likelihood objective function [dimensionless]

Subscripts

b	Bubbles

g	Gas
hf	Heating fluid
I	Illumination
l	Liquid
m	Mixture
N	Nitrates
P	Phosphates
S	Substrate
T	Temperature
w	Water

Table of Contents

List of Figures

List of Tables

1 Introduction

1.1 Motivation and aim

The Third International Maritime Organisation (IMO) Greenhouse Gas Study estimates that annual carbon dioxide (CO_2) emissions from the shipping industry exceed 1 billion tonnes with projected growth by a factor of up to 2.5 by 2050. The CO_2 contribution of shipping to global emissions is about 3.1%. Currently there are no regulatory limits for CO_2 emissions from shipping, but they are likely to soon become taxable and some existing schemes and mechanisms promote energy efficiency in shipping. The Energy Efficiency Design Index (EEDI), the Ship Energy Efficiency Management Plan, the Maritime Emissions Trading Scheme and market-based measures (IMO - Marine Environmental Protection Committee, 2014; IMO, 2011; Psaraftis, 2012) incentivise reduction of both input fuel use and exhaust emissions. Route optimisation and modifications to the engine or the fuel (Harrould-Kolieb & Savitz, 2010; The International Council on Clean Transportation, 2011) can also decrease CO_2 emissions, and there is a further potential to treat emissions by scrubbing. Other emissions in shipping flue gas, such as sulphur and nitrogen oxides (SO_x and NO_x), are controlled by the IMO Scheme B and are reduced by modifications to the fuel, the engine, or scrubbing (Entec, 2010; IMO, 2009).

CO_2 capture with algal photobioreactors (PBR) of various configurations (Carvalho et al., 2006) is a biologically-based fixation method that has been implemented for the treatment of CO_2 emissions from on-shore smokestacks (Borkenstein et al., 2011; Myer, 2006). PBRs grow algal biomass in water, using heat, light, CO_2 and other macronutrients. Algal biomass production not only ties up CO_2, but can be used to produce chemicals, biofuels and supplements for human and animal foods (Ugwu et al., 2008). The use of algal cultivation systems to generate third generation biofuels avoids problems faced by first and second generation biofuels, such as high water consumption and the use of land needed for food cultivation (Brennan & Owende, 2010).

The idea of using a shipboard PBR to capture CO_2 emissions from ship engines was conceived by Dr Nithin Rai, the industrial supervisor of the present project who sponsored it through his company, Octoply. The company's concept is to use waterways to develop novel products and services whereby transport could be utilised for the provision of social, health and educational activities (its vessels are presented in

3.2 and Appendix II). The literature does not show any evidence of previous implementation of a shipboard PBR for cultivation of algae. The aim of this study was to investigate important aspects of the technical challenges and basic sustainability of using a PBR to treat the ship engine's CO_2 emissions and produce biomass in a commercially viable way. The goal is to use waste streams of the ship (i.e., flue gas, waste heat and wastewater, as shown in Figure 1.1) to provide system independence and reduce operating costs in future implementation of the system.

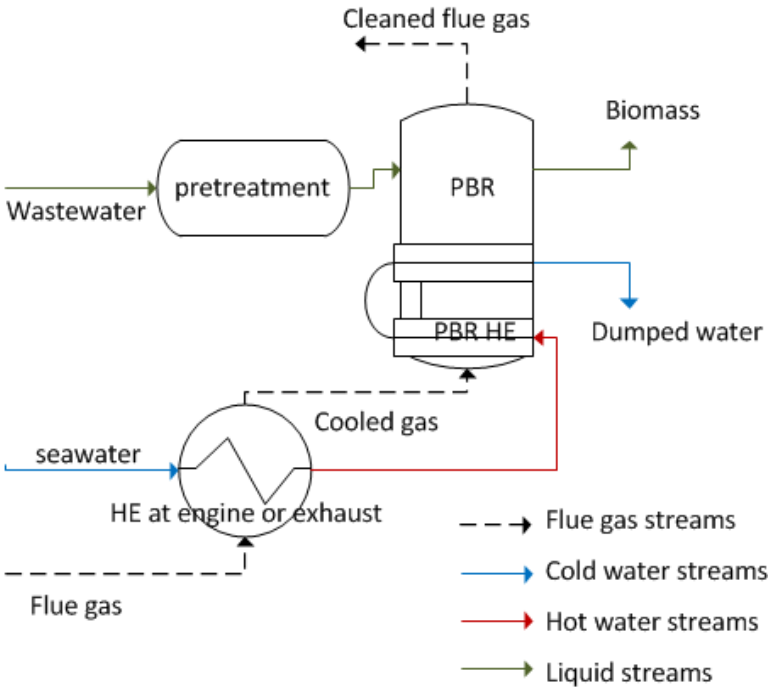

Figure 1.1. Overall system for the use of the flue gas, the wastewater and the waste heat produced in the ship to feed the photobioreactor.

1.2 Structure of the thesis

This thesis is organised into nine chapters. Chapter 2 reports on review of the literature related to: 1) ship emissions, ship emission reduction and ship heat exchange systems and 2) algal cultivation systems. This leads to an examination of the challenges and opportunities of a shipboard PBR.

Chapter 3 articulates the research questions arising from this examination, which will be addressed by this thesis, and the overall approach adopted. Each of Chapters 4 to 7 describes a separate aspect of the feasibility of a shipboard algal PBR, with a separate introduction, method, results, discussion and conclusions section for each.

Chapter 4 examines some other practical aspects of the shipboard PBR implementation. Specifically, it suggests a PBR design and reports on experiments to

study the performance of gas bubble flow. It then considers the effects of the NO_x and SO_x present in flue gas, as well as the fluctuations in salinity due to shipping route transitions from riverine, through estuarine and marine environments, on algal growth. Also, lab cultivation of various wild algae samples around London was investigated, to assess the potential for using local water for algae production. Part of this work was presented at a conference (Koutita et al., 2013a).

Chapter 5 focuses on the hydrodynamics of PBR designs of the same group as the airlift design suggested in Chapter 4. A model developed from physical first principles estimates the liquid velocity induced in the selected reactor design. The model was successfully validated by a number of laboratory scale experiments. This work has been published as a journal paper (Koutita et al., 2015).

A model of algal growth kinetics is developed in Chapter 6, which takes into account the simultaneous effects of several factors that influence growth, to predict the productivity under different conditions. Part of this work was presented at a conference (Koutita et al., 2014). An attempt to calibrate the model used data produced from lab experiments to estimate model parameters. The model is used to examine the conditions for semi-continuous operation of the PBR that would be beneficial for the growth of wild algae, which grow more slowly than most commercial varieties (Chapter 4). Different objective functions were dynamically simulated as case studies for potential optimisation and the variety of the control variables needed in each case were discussed.

Chapter 7 examines the availability of suitable space in different ship types and sizes, to accommodate the treatment of the total flue gas emissions with an algal PBR system. It includes a fundamental model developed using Clarkson's World Fleet Register database (Clarkson Research Services Limited, 2011). The reactor could be supported by either partitioning the reactor between the deck and the ballast tanks, or just by artificial illumination in the tanks. This work was presented at conference (Koutita et al., 2013b). This chapter also describes a waste heat recovery system, which stores the heat recovered from the flue gas in the ballast tanks when the engines are off, to provide an uninterrupted source of heat for the PBR. A way to integrate a heat exchanger (HE) with the PBR without adding significant mass or affecting its photosynthetic efficiency is suggested. The heat transfer model uses the liquid velocity computed by the model developed in Chapter 5 as an input.

The overall conclusions of the research are summarized in Chapter 8, whereby these represent the contributions to knowledge of this project, and lead to recommendations for further work.

2 Literature review

2.1 Introduction

The research presented in this thesis has been undertaken at the intersection of two very different subject areas: 1) control of emissions and waste streams from shipping, and 2) cultivation of algae. This literature review, therefore, summarises the main background understanding in these areas, which is relevant to the development of the research.

The main flue gas components from ship engines are examined to evaluate the composition of the gas feed stream to the PBR (Figure 1.1). The regulations being developed for the emissions control are then summarised, which provides evidence that installations to capture CO_2 are likely to be unavoidable in the future. Other waste streams relevant to the shipboard algal PBR are the ballast water and the sewage. Existing methods used to reduce the different emissions and waste streams are then briefly reviewed, including an overview of the Waste Heat Recovery (WHR) methods and the HE systems on ships that need to provide the heating and cooling for algal cultivation.

CO_2 sequestration by cultivation of algae in a PBR requires knowledge of algal cell biology. Thus algal physiology is briefly introduced and the most important factors that determine algal composition and growth for CO_2 sequestration and biofuels are discussed. The most significant factors that would affect the sequestration process in shipboard algal PBRs are temperature, pH, SO_x and NO_x concentration, light distribution and mixing, culture species, culture density, critical CO_2 concentration and CO_2 mass transfer (Juneja et al., 2013). The applicability and characteristics of different types of PBRs for algae-based CO_2 sequestration are then compared. A suitable PBR vessel was identified to be designed, to better understand the operational aspects of carbon capture onboard a vessel. The choice of a PBR design depends on several factors, including energy requirements and the location onboard a ship.

Typical existing land-based algal systems and their CO_2 capturing efficiency are then discussed, along with other potential uses of a PBR onboard a ship, including biogas conditioning and wastewater treatment. Modelling approaches that describe the influence of PBR parameters on productivity on board are reviewed for application to dimensioning of the shipboard PBR and optimization of productivity. The findings of the

literature review are synthesized into a consideration of the challenges and opportunities associated with the proposed shipboard algal PBR.

2.2 Shipping waste streams

2.2.1 Gas emissions from shipping

2.2.1.1 Flue gas

Ship engines burn either heavy fuel oil, marine gas oil, or their blend, marine diesel oil (Moreno-Gutierrez et al., 2007). Marine diesel oil is less carbon intensive than heavy fuel oil (Harrould-Kolieb & Savitz, 2010), as marine gas oil contains pure distillates of crude oil (MAN Diesel, 2008), whereas heavy fuel oil is normally a mixture of residual fuel oil (RO) and distillates and its viscosity varies a lot depending on the crude oil used and the process (MAN Diesel, 2008).

The carbon-containing emissions from combustion of marine fuels in a ship engine include the main gases associated with climate change, CO_2, carbon monoxide, volatile organic compounds and particulate matter. The amount of CO_2 emitted per vessel tonne in a year depends mainly on the dead weight tonnage and type of ship, as well as its operation time and mode (David Cooper, 2002; Defra, 2010; IMO, 2009), rather than the type of fuel or engine (Psaraftis & Kontovas, 2008). Carbon monoxide and volatile organic compounds are toxic products of imperfect combustion. Carbon-based particulate matter generation is related to the consumption of the engine lubricant oil (IMO, 2009). Land-based particulate matter emissions are associated with respiratory and toxic effects (Schlesinger et al., 2006) and marine emissions of particulate matter raise the same concerns when weather patterns result in their landfall; their impact on the marine environment and algae is not well understood and needs further exploration (Van Den Hende et al., 2012). Volatile organic compounds and carbon monoxide are also associated with serious health issues (Jones, 1999; Schlink et al., 2010).

Other main flue gas emissions include SO_x (95 – 97% SO_2 and 3 – 5% SO_3, depending on the combustion temperature, pressure, excess air and fuel sulphur content), NO_x (NO and NO_2), and heavy metals. Sulphur is present in most fuels and the amount oxidized to SO_x depends on the fuel type. A typical sulphur level in residual marine fuel oil in 2009 was a little over 3% w/w (Psaraftis & Kontovas, 2008). A small part of nitrogen (N_2) in the charge air and the majority in the fuel is also oxidised in the fuel combustion to form nitric oxide (NO) and ground level ozone. The total amount of

NO_x emissions is therefore mainly related to the design and operation of an engine, the combustion temperature and the amount of excess air, rather than the nitrate content of the fuel (DNV, 2008). The main problem with both SO_x and NO_x emissions is that, dissolved in water, they are converted to sulphuric and nitric acids and ground level ozone, causing acid precipitation, respiratory problems, eutrophication and oxygen (O_2) depletion of natural waters (West, 2009). Finally, toxic heavy metals, such as lead, cadmium and arsenic, are vaporized at the high temperature of the combustion system (Hutto, 2001).

Table 2.1 shows the main inputs and outputs of a two-stroke diesel engine – which is a popular main propulsion ship engine (Anish, 2011) – and the quantities of the different pollutants. A more comprehensive table that summarises gas emissions quantities from different engine types and operations is shown in Appendix I. The main difference between ship emissions and other automotive emissions is the high SO_x concentration of the former, as sulphur in residual marine fuel oil has been measured to be 2.7%, whereas it is only 10 mg/kg in automotive diesel fuels (IMO, 2009).

Table 2.1. Summary of typical emissions from a slow speed 2-stroke diesel engine burning heavy fuel oil (West, 2009).

	Source	Components (w/w)	Amount consumed or emitted
Input streams	Air	21 % O_2 79 % N_2	8,500 g/kWh
	Fuel	97 % HC* 3 % S	175 g/kWh
	Lube	97 % HC 2.5 % Ca 0.5 % S	1 g/kWh
Output stream	Flue gas	13 % O_2 76 % N_2 5.2 % CO_2 5.4 % H_2O 1500 mg/kg NO_x 600 mg/kg SO_x 60 mg/kg CO** 180 mg/kg VOCs*** 120 mg/Nm^3 PM****	8,676 g/kWh (mass balance)

*HC is hydrocarbons, **CO is carbon monoxide, ***VOC the volatile organic compounds and ****PM is particulate matter.

2.2.1.2 Regulation of ship flue gas emissions

Since shipping is an international activity, international regulators, such as the IMO, have the authority to regulate emissions, as global measures are more effective for emissions control. Apart from the regulations, other schemes and mechanisms may control shipping emissions. Although shipping transport is often touted for its low CO_2 emissions per unit of mass and distance travelled relative to aviation, it is an important emissions contributor (Chapter 1) and some regulations for their reduction have been implemented in some areas. The measures are applied on the carbon intensity of the ships and they use metrics such as gCO_2/t.km. Therefore, they incentivise reduction of both the input fuel and the flue gas emissions (IMO, 2013).

Currently there are no fixed thresholds for CO_2 emissions, but some schemes and mechanisms exist that promote energy efficiency in shipping:

- EEDI international agreement requirements demand that new ships over 400 tonnes have a low fuel consumption divided by speed and deadweight tonnage per tonne-mile (IMO, 2011). Specifically, ships built after 2015 have to improve their efficiency by 10%, ships built between 2020 and 2024 by 15% and those built after 2024 by 30%. EEDI are currently not applied to ships in developing countries (European Federation for Transport and Environment, 2011). According to the IMO, the EEDI deal could reduce emissions by 45 to 50 million tonnes a year by 2020 (Pearce, 2011).
- Ship Energy Efficiency Management Plan is a mechanism to monitor performance against a benchmark (e.g., the Energy Efficiency Operational Indicator) and improve energy efficiency of ship operations. The ship owner and operator are also recommended to review and consider operational practices and technology upgrades to optimise the performance at each stage of the operation of the ship.

Apart from the mandatory measures mentioned, there are a couple of candidate future regulations that do not apply at the moment. These are the market-based measures and the Maritime Emissions Trading Scheme. They allow the shipping sector to buy allowances from other sectors and they take technical and operational measures regarding fuel consumption and emissions, aiming to improve the 400 gross registered tonnage to submit CO_2 allowances or credits matching its fuel consumption in order to be allowed to load and unload at ports. The Maritime Emissions Trading Scheme is becoming a net buyer of emission allowances and emission credits by setting a threshold for permissible emissions (Goulielmos et al., 2011; Kageson, 2009). The

most recent EU-wide regulation proposed by the European Commission requires Monitoring, Reporting and Verification (MRV) of CO_2 emissions for ships of 5,000 gross registered tonnage. This will not only provide insight into the changing status of CO_2 emissions from shipping, but will also stimulate investments to improve performance of ships, and reduce the capital cost of the implementation of carbon capture systems, as the measuring sensors will already be installed. MRV is therefore expected to cut 2% of the emissions (MarineLog, 2013).

Regulations for NO_x and SO_x started being applied many years ago and are stricter than those for CO_2 in shipping. Scheme B from the IMO exhaust gas cleaning system Guidelines require the SO_2/CO_2 ratio to be continuously recorded. Regulation 14 MARPOL (Marine Pollution) Annex VI sets limits for maximum sulphur content in fuels burnt within the Emission Control Areas (ECA) (Defra, 2010; Pedersen, 2011; Resolution MEPC.184(59) Annex 9, 2009). Continuous monitoring of NO_x emissions is not required, but there are Tiers (emission standards) since 2000 that set limits to their emissions (Defra, 2010; Pedersen, 2011; Resolution MEPC.184(59) Annex 9, 2009; West, 2009). There is no particular effort to reduce heavy metals (Lloyd & Veritas, 2006), carbon monoxide and volatile organic compounds, but particulate matter is required to be greatly reduced within the ECA and globally (IMO, 2009).

2.2.1.3 Existing methods to reduce ship flue gas emissions

This section focuses on mitigation of the emissions, which are associated with or would affect an algal PBR system. Table 2.2 summarises the treatment methods for the main polluting flue gases, CO_2 and NO_x and SO_x. CO_2 reduction methods have not been developed as much as those for other pollutants due to the current lack of strict regulation. Most studies to reduce CO_2 emissions are through route or speed optimization, aiming mainly to increase cost efficiency (Chang et al., 2013; Smith, 2014), and other technological measures to produce energy such as kites and solar power generated on deck (De Rosa & Holtshausen, 2011; The International Council on Clean Transportation, 2011). Studies have recently started proposing solutions for CO_2 capture on ships (Zhou & Wang, 2014), however, complex modification of the engines would be required and the whole design of ships would need to be adapted, to ensure the technical feasibility of the implementation.

Land-based CO_2 capture and storage techniques are categorised according to the process and to the technology used. The first criterion divides them into three main

capture processes, depending on the processed stream (Florin & Fennell, 2010; Hillebrand et al., 2016; Kunze & Spliethoff, 2012; Mondal et al., 2012):

- Post-combustion, where CO_2 is separated from the flue gas after the combustion chamber.
- Pre-combustion, where the fuel is converted into hydrogen and CO_2 prior to the combustion and the hydrogen is used as the new fuel.
- Oxy-fuel combustion, where the fuel is combusted with pure oxygen making the flue gas to contain high CO_2 concentration and allowing its direct storage.

Depending on the process, various methods for CO_2 capture can be used, including absorption, adsorption, membranes, and hybrid applications of these (Liang et al., 2015). For instance, post combustion processes use monoethanolamine or amine solvent scrubbing, solid sorbent, ionic liquids, membrane separation for CO_2 and algal-biological capture. The main pre-combustion processes include integrated gasification combined cycle systems, sorbent enhanced reforming using carbonate looping and membrane separation for hydrogen. Oxy-fuel processes include an oxy-fuel boiler by cryogenic air separation, chemical looping combustion using solid metal O_2 carriers, and membrane separation of O_2 (Florin & Fennell, 2010).

Reviews in the literature use various criteria (e.g., impact on climate change, health impact, cost, impact on other technologies, leakage of captured CO_2, public perception, technology readiness) to compare the above capture methods, making it difficult to distinguish which criteria are best to use for method selection (Choptiany et al., 2014). Also, the optimal method for each case and the economic performance of each method depends on the location, the size of the plant, and the diverse operating conditions (Choptiany et al., 2014; Kuramochi et al., 2012).

Based on patents and articles, post-combustion is the only industrial CO_2 capture process being demonstrated at full commercial scale (Liang et al., 2015). The most frequently applied process in post-combustion is amine sorbents (Kunze, Splliethof). A post-combustion capture facility is a conceptually simple upgrade for the existing technology (Hillebrand 2016, Quintella 2011) and can be retrofitted (Figueroa 2008) with minor impact on the power conversion process (Kunze & Spliethoff, 2012). Some concerns with this method are the low CO_2 concentration in the flue gas which limits the process efficiency, the intense solvent regeneration energy (Figueroa et al., 2008; Kunze & Spliethoff, 2012), corrosion of equipment in the presence of O_2 and other

impurities, high solvent degradation rates, potential emissions of solvent to the environment, cost of materials, low capture capacity and very large equipment requirements (Figueroa et al., 2008, Florin & Fennell, 2010, Kunze & Spliethoff, 2012).

Pre-combustion CO_2 capture is used in integrated gasification combined cycle plant. Although it has a higher driving force for separation due to the high CO_2 partial concentration (Figueroa et al., 2008), it is not feasible in conventional steam power plants (Kunze & Spliethoff, 2012). Its main drawback is that it requires a chemical plant in front of the turbine and it is therefore applicable mainly to new power plants (Figueroa et al., 2008; Mondal et al., 2012). Its complicated chemical processes also cause extra shut-downs of the plant, which can result in a lower power output (Mondal et al., 2012). Other disadvantages are cost of equipment and difficulty in commercialisation (Figueroa et al., 2008; Florin & Fennell, 2010).

The oxy-fuel approach has the advantage of avoiding NO_x formation and of a high CO_2 concentration in the flue gas which makes it more efficient in absorbing. However, recycle of cooled CO_2 is required which would decrease efficiency (Figueroa et al., 2008). It is also costly, energy intensive, associated with degradation of oxygen carriers (Florin & Fennell, 2010). and it has a higher impact on the power plant process, which complicates retrofitting (Kunze & Spliethoff, 2012; Mondal et al., 2012).

Most non-algal land-based CO_2 capture and storage techniques are based on absorption and adsorption (Florin & Fennell, 2010; Mondal et al., 2012; Quintella et al., 2011), with monoethanolamine being the most promising absorption method (Aaron & Tsouris, 2005). Absorption is a mature and retrofitable method with easy application and a low energy penalty, suggesting investment in further research and improvement (Aaron & Tsouris, 2005; Mondal et al., 2012). While this method is currently most promising, the development of ceramic and metallic membranes for membrane diffusion should produce membranes significantly more efficient at separation than liquid absorption (Aaron & Tsouris, 2005). Literature supports that the energy requirements of the four technologies are highest for the cryogenic, followed by absorption, adsorption and membrane methods, whereas the CO_2 recovery is highest for the cryogenic, decreasing for the absorption, membrane and adsorption methods (Mondal et al., 2012).

The lack of information and the small number capture units, implemented at large scale, most of which are pilot projects, imply that it is early to extrapolate outcomes from the obtained data for each technology and to identify the future dominating technology, as admitted by the available reviews (Choptiany et al., 2014; Kuramochi et

al., 2012). For instance, although oxy-fuel was mentioned earlier to be energy intensive and difficult to retrofit, other review studies and modelling research support opposite statements (Figueroa et al., 2008; Vatopoulos & Tzimas, 2012).

Summarising, the issues with non-algal land-based CO_2 capture and storage techniques that would make them problematic for a shipboard implementation are their significant energy penalties, high costs, immaturity as technologies, and low capacities. Also, they consist of inflexible operations that cannot be easily retrofitted, and they are linked to corrosion and require waste absorbent disposal (Van Den Hende et al., 2012). There are additional limitations in shipboard CO_2 capture, though preliminary studies using chemical absorption examine how to overcome them (Zhou & Wang, 2014). Chemical and physical CO_2 treatment technologies are relatively costly (Van Den Hende et al., 2012). Biological processes, including algal-based capture, are further from commercialisation (Figueroa et al., 2008), but it can be achieved through continued research, development, and demonstration.

NO_x reduction methods tend to increase the volatile organic compounds and carbon monoxide emissions and fuel consumption, but SO_x scrubbers are able to reduce particulate matter as well. SO_x scrubbers are the systems that are most similar to a PBR in terms of the process and are analysed further. Exhaust gas cleaning systems allow the use of conventional high sulphur fuels and are cheaper over their lifetime than the use of low sulphur fuels. SO_2 can be removed from the flue gas by wet scrubbers or dry scrubbers using lime. Such technologies have been in use for several decades in oil tankers (Leigh-Jones, 1998). According to chief Shipping Analyst at BIMCO, Peter Sand, “for a ship with 10 years of commercial life left, the vessel should sail in an Emission Control Area 33% of the time for a scrubber to break even” (Fathom Shipping, 2013b). The process is energy consuming, as wet scrubbers require 10 – 30 kW per MW of the engine (Fathom, 2011). Many flue gas cleaning systems companies offer pilot systems but only a few are in commercial operation (e.g., Hamworthy Krystallon) (West, 2009).

The wet scrubber system may be an “open” type, where seawater is taken from the sea, used for scrubbing, treated and discharged back to sea. Otherwise, it is a “closed” type, where freshwater is treated with an alkaline chemical for buffering and scrubbing. The two systems are shown in Figure 2.1. The pH of the wash water from an exhaust gas cleaning system can be as low as 3. Typically, open seawater systems use 45 m^3/MWh water, whereas closed freshwater systems have a water discharge rate 0.1 – 0.3 m^3/MWh (West, 2009). As a result, closed systems do not need an

Environmental Impact Assessment by a local Environmental Protection Agency (Knudsen, 2010), but the IMO requires a specific assessment and applies additional wash water discharge criteria for systems that use chemicals (West, 2009).

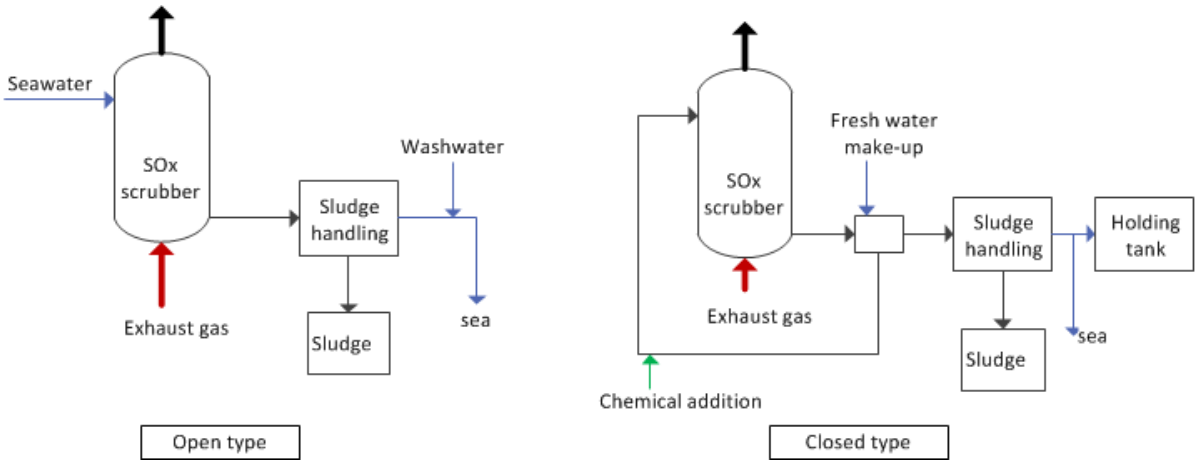

Figure 2.1. Marine wet scrubber systems operating with seawater and recirculating freshwater respectively. Figure reproduced from West (2009).

SO_2 solubility increases with decreasing temperature. Therefore, hot flue gas, typically in excess of 300 °C, benefits from passing through a cooling system within the exhaust gas cleaning system unit. In general, a demister removes condensed droplets (West, 2009).

2.2.2 Waste emissions from shipping

Ship operation generates four main types of liquid and solid waste streams that are relevant to the concept of the shipboard algal PBR:

1. Sewage from washing and use of toilets by the crew, which contains phosphorus, nitrogen, potassium, sulphur and organic contamination (measured in biochemical oxygen demand – BOD) and traces of various metals such as zinc, copper and nickel.
2. Food waste, which also contains the macronutrients present in the sewage.
3. Bilge water collected at the lower parts of the ship containing a mixture of fuel, detergents and lubricants.
4. Wash water, which is the used water from gas scrubbing emissions and contains sulphuric acid.
5. Ballast water used to maintain ship stability, containing biological organisms present in natural waters which may be considered as pollutants if discharged in different natural waters.

The quantity of each stream is dependent on the type and size of the ship. The main environmental impact faced regarding sewage and food waste is eutrophication (Han et al., 2006). Bilge water and wash water affect the pH, polycyclic aromatic hydrocarbon concentrations and turbidity of the water; they need to be monitored and their dumping is allowed only when their pH is over 6.5 (Resolution MEPC.184(59) Annex 9, 2009).

Monitoring of transfer of harmful aquatic organisms and pathogens with ballast water is rarely undertaken. There is a lack of international standards for ballast management, but the IMO prepared the Ballast Water Management Convention in 2004 for national ballast water management. The comprehensive test program evaluates the performance and suitability of ballast water management systems, which includes large scale land-based and shipboard tests. Apart from this, risk assessments are also suggested to be crucial (David & Gollasch, 2015). Table 2.2 includes some common ballast water treatment methods used.

Table 2.2. Key abatement techniques for main pollutant sources, CO_2, NO_x, SO_x and ballast water (and their corresponding evaluated reduction efficiencies). Data taken from Balland & Ntnu (n.d.); IMO (2009); Chang et al. (2013); David & Gollasch (2015); Jalkanen et al. (2009); Smith et al. (2013).

Pollutant	Abatement technique	Reduction efficiency
CO_2	Logistics (e.g., route optimisation)	N/A
	Engine modification	N/A
	Wind assistance	N/A
SO_x	Fuel switch seawater scrubbing	44 – 81%
	Cylinder lubrication	75 – 98%
NO_x	Slide valves	20%
	Water injection	50%
	Humid air	70%
	Selective catalytic reduction	90%
	Exhaust gas recirculation	35%
	Emulsion combustion	10%
	High scavenge pressure and compression Ratio	N/A
Ballast water organisms	Chemical (e.g., chlorination, ozonation)	N/A
	Physical (e.g., ultraviolet, radiation, deoxygenation, filtration, heat)	N/A
	Biological (bioaugmentation)	N/A

2.2.3 Waste heat and waste heat recovery in ships

Marine diesel engines are classified according to their speed (slow, medium and high speed), their operating cycle (the strokes completed by the piston in each engine cycle; two-stroke and four-stroke) and their construction (crosshead and trunk) (Ayub, 2009). Their emissions concentrations differ as shown for some examples in Table I.1 of Appendix I. Two-stroke engines are the most powerful, reaching the highest attainable efficiency of piston engines of 55% (Bosch Gmbh, 2003). Apart from the main engines, ships also use auxiliary engines for the operations and boilers for heat generation. Auxiliary engines typically represent a 5% of the installed power, but run at lower load than the main engines (around 50%), with great variety across the different ship types.

The non-adiabatic compression and expansion, and mechanical losses due to friction, along with other lost heat, reduce the thermal efficiency of the engine (i.e. heat energy obtained by the combustion) to around 40% of a diesel cycle. The various main losses during the operation of a diesel engine are shown in Figure 2.2. However, some losses depend on the engine type and the whole system. Heat lost in the flue gas, conducted through the piston, cylinder and cylinder head, leads to very high temperatures generated in the propulsion engines with diesel temperatures ranging from 120 – 720 °C (Zheng, 2004) and an average flue gas temperature of approximately 380 °C with a pressure of 220 kPa (Maersk, n.d.).

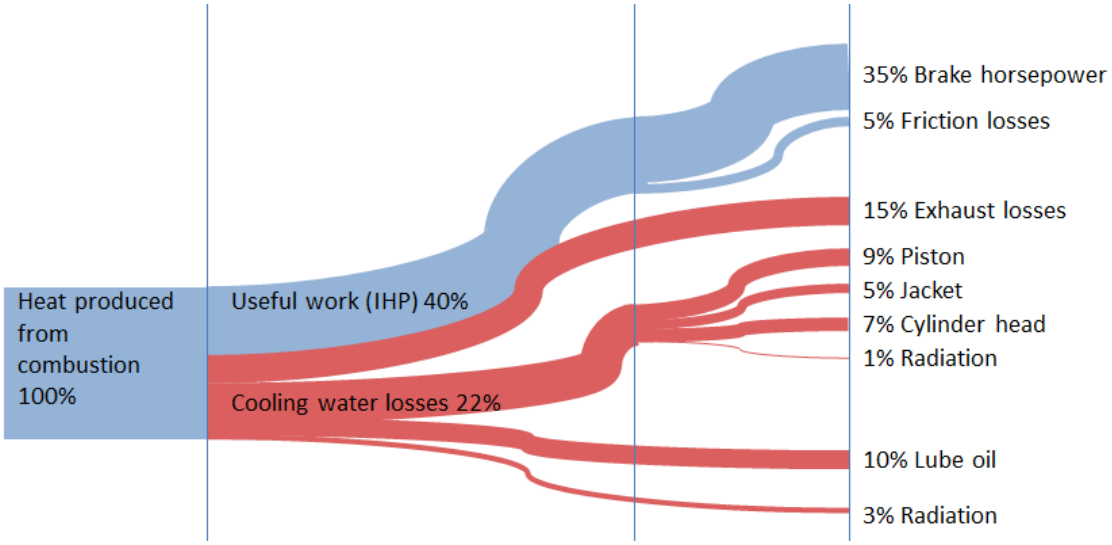

Figure 2.2. Heat balance for a ship propulsion engine. Data provided in Ayub (2009).

The engine cooling system absorbs heat in cool water or oil, to avoid unsafe heat accumulation and thermal stresses in the engine. Modern engines increasingly use oil for cooling the piston as it requires simpler piston design due to the lower thermal stresses developed, and it does not require a separate cooling system and chemical treatment to prevent corrosion and scaling. On the other hand, use of oil removes less heat per volume than water, requires a large oil purification plant, and may cause oil carbonisation at high temperatures. Medium speed engines use freshwater circulated through cylinder heads for cooling, usually connected to the main engine jacket cooling water system (Ayub, 2009). The jacket cooling water temperature at the inlet of the main engine is maintained at 55 °C and at the outlet 80 – 85 °C, in order to maintain the liner temperature between 150 °C and 220 °C. An independent cooling system circulates coolant in the inner spaces of the piston crown, as its temperature is higher than in the cylinder line (Ayub, 2009).

In seawater circulation systems, seawater is used as a medium to cool the various components, the lube oil, the charge air to air compressors and to generate freshwater (Ayub, 2009). An alternative system is the central cooling that supplies seawater only to cool freshwater, which is the coolant medium in the various HEs. This system has the benefit of minimising maintenance work. In both cases, the heated seawater is discharged overboard. The heat lost through cooling represents an energy loss in the system (Ayub, 2009). The latter system is commonly found on smaller vessels as it minimises maintenance work, i.e., limiting the effect of sea water corrosion to the various ship components that require cooling.

WHR systems manage and utilize the two major energy losses that together account for approximately half of the energy produced by the combustion: 1) the heat conducted to the engine components, and 2) the heat lost from the flue gas stream. The high temperature and pressure of the flue gas is utilised with turbochargers and sometimes with steam turbines or combined heat and power hybrid systems. Turbochargers can utilise approximately 65% of this energy, supplying charge air to the engine with higher density causing more efficient combustion of the fuel (Fathom Shipping, 2013). The steam turbine hybrid system produces useful steam from the exhaust heat for on board heating, and to drive a steam turbine for extra electricity generation (Maersk, n.d.). Apart from the heating uses, tri-generation, or a power-heat-refrigeration-coupling system, could produce cooled water and air with thermal-driven chillers. This would be useful for cargo that needs refrigeration, or for air-conditioning generally (Fischer, 2011).

The engines also require heating during start-up and there are also fuel handling systems which heat the fuel to temperatures as high as 160 °C to reduce viscosity (Bosch Gmbh, 2003). Also, heating is required for passenger ships types, for the operation of radiators.

All of the above options reduce fuel utilisation and consequently carbon footprint. The best option will depend on the electricity needs and operational profile of the ship, as well as how much complexity is accepted by the owner and the shipyard. Several engine manufacturers (Wartsila, Mitsubishi Heavy Industries, ManDiesel&Turbo) state that their high-efficiency WHR systems can obtain fuel savings of 4 – 12% with a return on investment of less than 5 years (Fathom Shipping, 2013).

2.3 Algal systems

2.3.1 Physiology of algae

Microalgae are unicellular or multicellular microorganisms; most of those identified are eukaryotic. They are grouped according to their pigment composition, ultrastructure, life cycle and biochemical constituents. According to the Aquatic Species Program, the main physiologically similar algae classes are (Borowitzka & Borowitzka, 1988; Borowitzka, n.d.; Sheehan et al., 1998):

- diatoms (*Bacillariophyceae* class)
- green algae (*Chlorophyceae* class)
- golden-brown algae (*Chrysophyceae* class)
- prymnesiophytes (*Prymnesiophyceae* class)
- eustigmatophytes (*Eustigmatophyceae* class) and
- the prokaryotic blue-green algae, or cyanobacteria (*Cyanophyceae* class) (Sheehan et al., 1998).

Microalgae can be photoautotrophic (photosynthesizing inorganic compounds), heterotrophic (consuming organic compounds), mixotrophic (photosynthesizing but also using organic compounds), auxotrophic (form of heterotrophy where only small amounts of organic compounds are required), photoheterotrophic (light is required to use organic carbon sources for growth) or phagotrophic (consuming solid food particles) (Borowitzka, n.d.; Schaechter, 2009). Photoautotrophic algae are relevant in the present context, as they are capable of absorbing CO_2 when light is provided and producing organic compounds and O_2. Figure 2.3 shows the photosynthetic reactions. Algae not only sequester CO_2 from flue gas, but other compounds, such as NO_x (Chiu et al., 2011; Gardner, 2011; Kumar et al., 2010), which is produced in diesel combustion. The gross content of carbohydrates, proteins and lipids among algal species of one group may vary as much as among different algae genera, according to the compositions listed for some algae types in Sialve et al. (2009). Other metabolic characteristics of the cells include growth rate, chlorophyll, proline, glycine and carotene contents, as well as metal accumulation. Growth rate is the combination of photosynthesis and respiration, and is usually estimated from cell counts, cell density, or on a chlorophyll basis (Kirst, 1989)

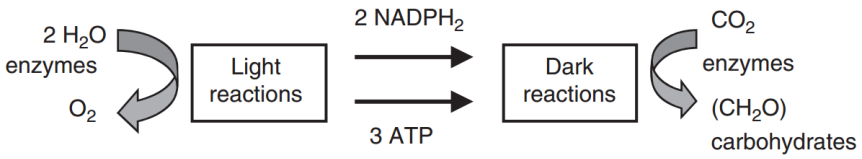

Figure 2.3. Major products of the light and dark reactions of photosynthesis with the use of adenosine triphosphate (ATP) energy and consumption of the enzyme $NADPH_2$ for the sugars production. Figure adapted from Richmond (2004).

2.3.2 Factors affecting growth and carbon sequestration

2.3.2.1 Species selection

According to The Algal Industry Survey (Edwards, 2009), species selection is the most critical variable for successful mitigation of CO_2, followed by light penetration, temperature and pH (weight factors are shown in Table I.2 of Appendix I). The most usual criteria for deciding a species' suitability for CO_2 fixation include growth rate, temperature range, resistance to shear stress (hydrodynamic stress parallel to the cell wall), product value, robustness to potential contamination, and/or content of important biological molecules (González López et al., 2009). Apart from this, the harvesting energy requirements, which are affected by the lipid content, need to be considered (Becker, 1994). Optimisation of one characteristic might negatively affect another desirable characteristic and any individual strain cannot exhibit all the desired traits. Therefore, different algal species may be the most suitable solution depending on the specific requirements for each case and each PBR design. For example, if algae are grown for CO_2 capture, then high overall algal productivity would be desired, whereas for production of biodiesel, high lipid productivity would be the most desired, rather than carbohydrates or proteins. However, algae with high oil content may show slower growth and hence have low lipid productivity. This would mean that it is less difficult to extract the given amount of lipids from the amount of biomass produced, but a larger facility is required to produce the same amount of lipid products per time. Therefore, the selection of an algal species must optimise lipid content together with growth rates, for optimisation of CO_2 fixation. According to Becker (1994), *Chlamydomonas*, *Chlorella*, *Dunaliella* and *Nannochloropsis* are genera with species that can produce a high proportion of lipids and are also widely cultivated for various applications. However, the literature is inconsistent about the benefits of some species, e.g., according to other studies *Chlamydomonas* genus does not accumulate lipids (Sheehan et al., 1998). *Chlorella* seems to be a most common genus that been widely

used (Sheehan et al., 1998), and is very tolerant to higher CO_2 concentrations (Ono & Cuello, 2001; Westerhoff et al., 2010). Therefore, this genus will be examined as a potential candidate for the application of this study. Figure 2.4 shows lipid content and productivity for a variety of species.

There is evidence that thermophilic strains (see also 2.3.2.3) can tolerate higher CO_2 concentration. For instance, when cyanobacterium *Synechococcus elongates* was bubbled with various concentrations of CO_2 at different temperatures, the drop in pH at 52 °C with 60% CO_2 was comparable to the drop in pH at 25 °C with 20% CO_2 (Miyairi, 1995).

Algae can grow in fresh potable water, saline or brackish water, or municipal and industrial wastewaters (Mallick, 2002; Muñoz & Guieysse, 2006). Different microalgal species prefer different salinities and some halotolerant species can grow well in both environments (Araújo et al., 2009). Salinity level is reported to influence not only the growth, but also the harvesting efficiency of microalgae and the CO_2 quantity stripped from the water (Borgvang, 2011; Sukenik et al., 1988). The most important cell characteristics that have been reported to be influenced by salt levels are growth rate, lipid, chlorophyll, carbohydrates, proteins, proline, glycine and carotene contents, as well as metal accumulation.

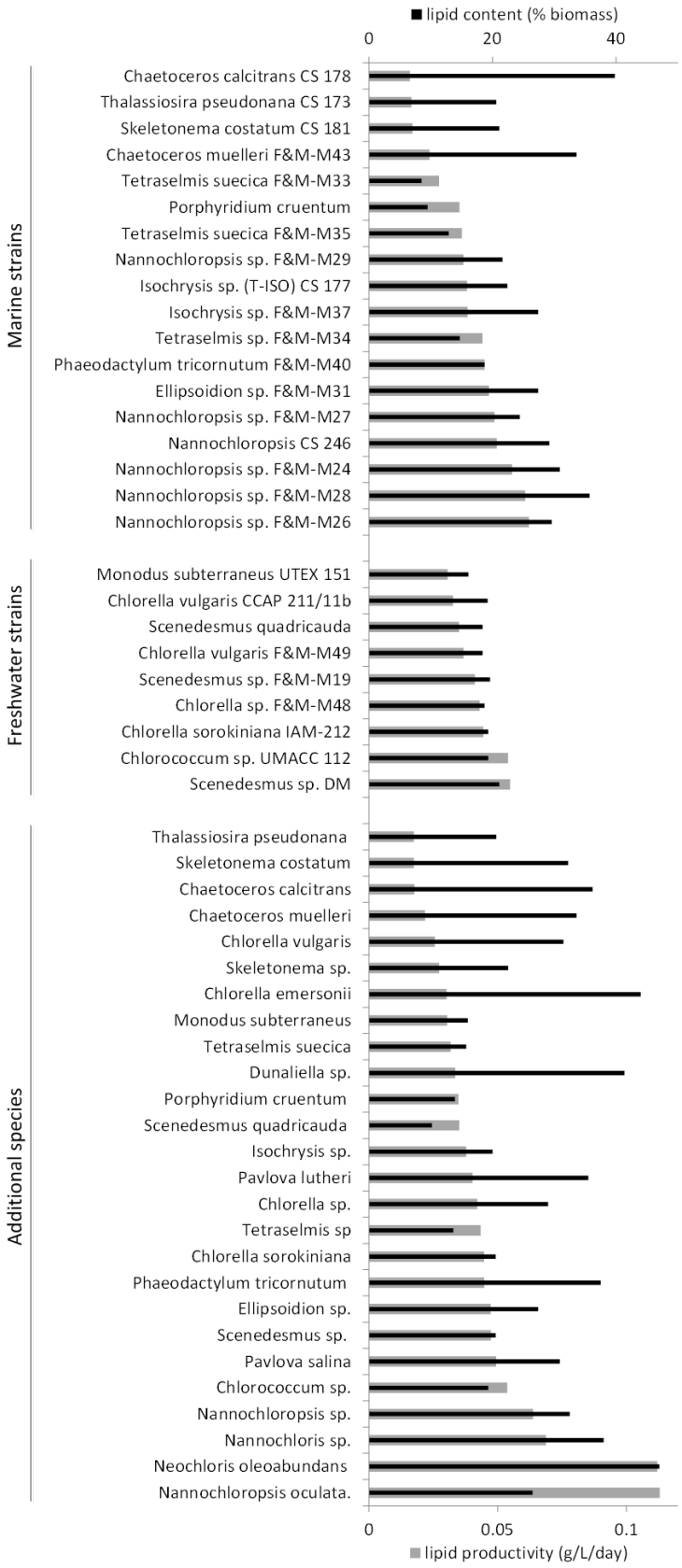

Figure 2.4. Total lipid contents and lipid productivities for some marine and freshwater species and for various microalgal species. Data taken from Rodolfi et al. (2009) and Mata et al. (2010).

2.3.2.2 Light – cell density – mixing

Light is one of the most important factors for the growth of the photoautotrophic algae strains, and below the optimal light intensity, it becomes a limiting factor. Light affects cell growth through its wavelength and its intensity, which are determined by the light source, the broth mixing and the cell concentration. In addition, there is also intensive research on the beneficial effect of light and dark cycles of specific ratios on the growth, caused by static mixers or the operation cycles of lamps (Barbosa et al., 2003; Gonçalves et al., 2014; Huang et al., 2014; Liu et al., 2007), which could be crucial for a shipboard PBR divided within the deck and the ballast (4.1).

Algae grow best in the visible light spectrum (390 – 750 nm). Near-ultraviolet light has a detrimental effect on algal growth, and infrared light, on the other side of the spectrum, primarily causes overheating of the culture (Asenjo, 1995). Blue and red light wavelengths are best utilised by the microalgae. Fluorescent lamps are used to enhance productivity (Araújo et al., 2009a; Solovchenko et al., 2007).

Saturation light intensity (I_S) is a crucial parameter, which, together with incident light intensity (I_0), determines light utilisation efficiency. Overload of the system with the incoming light results in the production of reactive O_2 species, causing photoinhibition and/or photooxidative death. I_0 has to be lower than I_S, but not much, as it would be insufficient for optimal productivity. Therefore, selection of algal species having high I_S, or approaches to decrease I_0 below I_S, are advisable (Kumar et al., 2011). Proper mixing minimises time of each cell being exposed to I_0. It also creates a flashing light effect, which can increase the productivity in tubular PBRs by up to 40% (Ugwu et al., 2002). However, the mixing rate and technique should be chosen to prevent the detrimental effect of high shear stress on algae viability.

Proper geometry of PBRs can reduce the weakening of light with depth in the algal suspension (Kumar et al., 2011). Many special light systems have been tried on PBRs to evenly distribute I_0, through splitting of light sources among many parts of the PBR, and consequently increase CO_2 sequestration (Lee et al., 1995; Morita et al., 2000). Some other special sunlight-harnessing devices have been reported to providing high algal productivity, by focusing visible light into a fiber optic cable, or by filling columns with tubular fiber optic light radiators (Asenjo, 1995). Cell concentration affects productivity and light utilization efficiency. Below the optimal concentration, the light is only partially captured by the cells while above the optimum concentration many cells

are left in the dark zone (Zhang et al., 2001). On the other hand, a high cell concentration makes algae more tolerant to higher CO_2 concentrations (Chiu et al., 2008).

2.3.2.3 Temperature – Heating requirements

The temperature range tolerated by most algal cultures is 15 – 40 °C (Konopkat & Brock, 1978; Maeda et al., 1995; Shang et al., 2010). Levin et al. (1962) support that the optimal temperature for *Chlorella sp*. is 39 °C. Photosynthesis is an endothermic reaction, but a substantial part of the light energy absorbed in the photic zone is transformed to heat because the capacity of algae to fix light energy is limited (Janssen et al., 1999). Hence, outdoor tubular PBRs are expected to require cooling during hot periods (Chisti, 2007; Stephenson et al., 2010) to prevent the culture temperature from rising above the maximum temperature tolerated. Also, indoor cultivation with the use of fluorescent lighting (other than cool white) produces additional heat for removal (Chiu et al., 2008).

A shipboard facility has two additional variables that affect heat requirements: the potentially low ambient temperatures that cause great heat loss, and the high temperature of the flue gas. All heat gains and losses must be taken into account to determine whether a specific PBR needs heating or cooling at any given time of operation. Therefore, it seems likely that algal CO_2 fixation onboard a ship can only be feasible with installation of a heat exchange system.

Temperature control methods used in algal PBRs, either for cooling or for heating, are water baths, immersed coils or tubes, water spraying and shading tubes. Temperature regulation of the feeding or recirculating stream has also been examined (Kumar et al., 2011). The case of controlling the temperature by adjusting the temperature of the sparged gas has not been investigated. Evaporative cooling has shown to be favoured economically over the use of HE (Kumar et al., 2011). All heating and cooling systems add operating costs. Specifically, water baths add significant weight to the system and decrease light absorption, important parameters for the case of a shipboard application.

Significant energy and heat would also be required during shipboard harvesting too. For instance, one way to vaporise the water from the microalgal slurry is by contacting it with superheated steam, which is energy intensively produced. Also, filters with biomass need to be dried at 105 °C and allowed to cool (Janssen et al., 1999).

Froth flotation is a more efficient harvesting technique, but the addition of chemicals leads to downstream problems (Christenson & Sims, 2011).

2.3.2.4 Macronutrients

The most important inorganic macronutrients for photosynthesizing microalgae are:

a. nitrogen (N), which is absorbed mainly in the form of ammonium and nitrates (NH_4^+, NO_3^-, NO_2^-) to synthesize aminoacids (Martinez et al., 1999);
b. phosphorus (P), which is absorbed mainly as inorganic salts, sodium or potassium phosphates, and is used in the cellular processes related to energy transfer and nucleic-acid synthesis (Martinez et al., 1999);
c. carbon (C), which is absorbed through CO_2, and sometimes through HCO_3^- to produce the cell mass (Borowitzka & Borowitzka, 1988).

Other required macronutrients are sulphur, calcium, magnesium, sodium, potassium, chlorine, silicon, iron (Borowitzka & Borowitzka, 1988; Borowitzka, n.d.). In addition to macronutrients, microalgae are able to not only scrub, but increase their lipid accumulation as well when fed with heavy metals from the media solution (Kalesh & Nair, 2005; Yang, Cao, Xing, & Yuan, 2014), and thereby with the flue gas that is being fed to it. The effects of nitrate and phosphate concentrations on growth, and their optimal values for various conditions and species have been extensively examined both experimentally and numerically (Ruiz et al., 2011; Xin et al., 2010). Again, finding an optimal value is not a straightforward process and depends on whether the objectives are to maximise lipid content, growth rate, or lipid productivity. For instance, nitrate deficiency has been reported to benefit lipid accumulation in certain green algal species (Sheehan et al., 1998). Its concentration affects the lipid content of different species differently, as shown in Table 2.3, so general conclusions are difficult.

Table 2.3. Lipid content (% dry weight) of a variety of freshwater (f) and marine (m) microalgal species, chosen from references related to CO_2 fixation or biofuel production under different nitrogen (N) conditions.

Species	N starvation	N deficiency	N sufficiency
Chlorella vulgaris (f)	18 [1]	40 [1]	27 [2]
Chlorella protothecoides (f)	11 [1]	23 [1]	14 [4]
Chlorella emersonii (f)	29 [1]	63 [1]	-
Neochloropsis oleoabundans(f)	56 [6]	38 [7]	-
Nannochloropsis sp. (m)	60 [8]	-	29 [9]

Data taken from: [1] (Illman et al., 2000), [2] (Francisco et al., 2010), [3] (Liang et al., 2009), [4] (Sieg, 2008), [5] (Xiong et al., 2008), [6] (Olguín, 2012), [7] (Li et al., 2008a), [8] (Rodolfi et al., 2009), [9] (Gouveia & Oliveira, 2009). Empty cells indicate data not available.

The dissolved CO_2 is computed from using its partial pressure as given by Henry's Law (Buhr & Miller, 1983) in Eq.1 and Eq.2. In an aqueous environment, dissolved CO_2 exists in different carbonate forms in equilibrium; as carbonate (CO_3^{2-}), bicarbonate (HCO_3^-), CO_2 and carbonic acid (H_2CO_3), and the partitioning between these species depends on pH and temperature (Baird & Cann, 2012). The equilibrium is shown in Eq.4.

$$CO_{2(g)} + H_2O \leftrightarrow CO_{2(aq)} \tag{1}$$

$$c_{CO_2 l} = K_{H_{CO_2}} P_{CO_2} \tag{2}$$

where $K_{H_{CO_2}}$ is a function of temperature:

$$K_{H_{CO_2}} = exp\left[-8.1403 + \frac{842.9}{(T + 151.5)}\right] \tag{3}$$

$$CO_{2(aq)} + H_2O \leftrightarrow H_2CO_3 \leftrightarrow H^+ + HCO_3^- \leftrightarrow H^+ + CO_3^{2-} \tag{4}$$

The equilibrium is not affected by algal fixation, due to the fast reaction kinetics. Microalgal cells preferentially take up HCO_3^- over CO_2 (Carvalho et al., 2006). The mass transfer of CO_2 from the gas into the algal cell includes the following steps; (i) transport from the main body of gas to the thin gaseous film immediately adjacent to the gas/liquid interface; (ii) diffusion through the thin gas film; (iii) transition of the gas/liquid interface; (iv) diffusion into the adjacent thin liquid film; (v) transport to the main body of the liquid phase; (vi) diffusion into the thin liquid film in the vicinity of the

cell wall; (vii) free diffusion through the outer cell liquid film (Carvalho et al., 2006). The slow step that controls the process is reported to be the gas-liquid transport resistance (Markl, 1977). A smaller bubble size increases the interface area and mixing maintains maximum driving force for diffusion (Carvalho et al., 2006). The rate of mass transfer of CO_2 to the liquid, N_{CO_2}, is given by the following formula (Carvalho et al., 2006).

$$N_{CO_2} = k_L a_i (C^*_{CO_2 L} - C_{CO_2 L}) \quad (5)$$

where k_L is the liquid phase mass transfer coefficient, a_i the interphase area, $C^*_{CO_2 L}$ the concentration of CO_2 in the culture broth that would equilibrate with its measured partial pressure on the gas side, and $C_{CO_2 L}$ is the concentration of CO_2 in the bulk of culture broth. The opposite process is CO_2 desorption from the liquid to the air, either spontaneously (outgassing), or deliberately (degassing) (Weissman et al., 1988).

Many algal cultivation experiments have been executed with control gas (ambient air), or simulated flue gas, fewer with flue gas from on-shore plants (Borkenstein et al., 2011; Chiu et al., 2011; Douskova et al., 2009; Koberg et al., 2011; Kumar et al., 2010; Rosenberg et al., 2011; Zeng et al., 2011). Most of the existing integrated algal cultivation systems are fed with flue gas, either cleaned or not, with a CO_2 concentration of more than 10% (Chiu et al., 2011; Douskova et al., 2009; Koberg et al., 2011). Flue gas of land-based engines and industrial smokestacks usually contains a concentration of CO_2 of the range 20 – 25% and the growth potential of the algae types has been also evaluated when aerated directly with flue gas of this concentration (Chiu et al., 2011). The growth rates of *Chlorella sp.* and its mutant strain, *Chlorella sp. MTF-7*, were 48% higher when they were aerated with flue gas from the coke oven of a steel plant (containing 25% CO_2, 4% O_2, 80 mg/kg NO and 90 mg/kg SO_2), than with air enriched with CO_2 (2%, 10%, or 25%). Although the lipid content was slightly lower for the flue gas case, the overall lipid productivity was higher due to the higher growth rate. It was not clear whether the improved growth observed with the flue gas aeration was because of the nutrients included in it, such as NO and SO_x (which may also have a detrimental effect on algae, see 2.3.2.4 and 4.3), or because of the low O_2 concentration.

High CO_2 concentrations become toxic for algae (Nagaich et al., 2014) as it reduces pH (according to the equilibrium shown in 2.3.2.4 and as discussed in 2.3.2.5). However, several species have been tested under high CO_2 concentrations and many of them have adaptation techniques which enable them to tolerate very high concentrations. For instance, Kodama et al. (1993) showed that *Chlorococcum littorale*

could grow with a feed of 60% CO_2 by feeding in a series of distinct stages (stepwise adaptation technique). However, the maximum growth rate for this tolerant species is under lower CO_2 concentrations (Ono & Cuello, 2001). Since growth conditions vary among different experiments, a direct comparison of the tolerance of various species to CO_2 is difficult. Kumar et al. (2011) have summarised some CO_2 fixation rates of various species from different studies, using influent CO_2 concentration from 2 to 60% and showing a 16 to 63% sequestration approximately and up to 2 g/L/day fixation rate.

Although studies have been optimising the growth conditions in order to enhance CO_2 retention time in the PBR and thereby increase its removal efficiency (Chiang et al., 2011), only a small portion of around 38% v/v of the CO_2 contained in the flue gas is sequestered by algae and there are many losses, as shown in Figure 2.5.

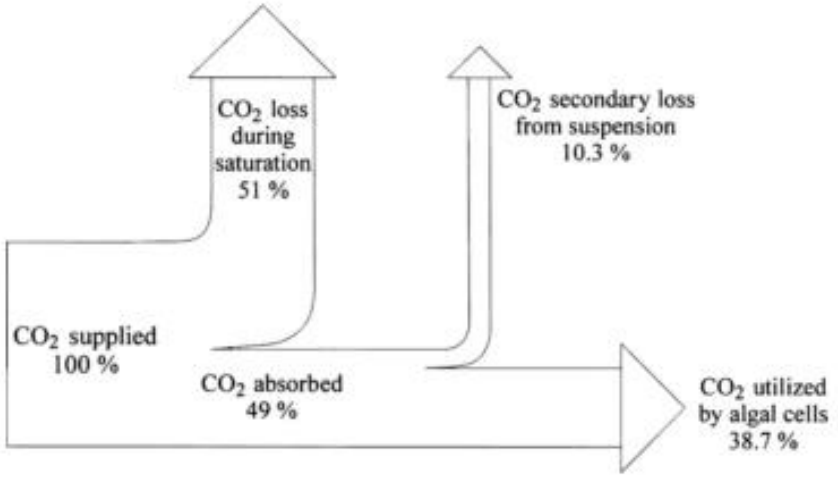

Figure 2.5. Scheme for CO_2 mass balance for an algal PBR fed with flue gas of 8% v/v CO_2. Figure adapted from Doucha et al. (2005).

2.3.2.5 pH

Algae optimally grow under a pH range of 5 to 9 (Weisse & Stadler, 2003).The dissolved CO_2 and SO_x from the flue gas influence the pH of the culture broth. Specifically, pH can drop down to 5 with elevated CO_2 concentrations (due to formation of carbonic acid, see equation Eq.4), and high SO_x concentrations can even drop it to pH 2.6 (due to formation of sulphuric acid) (Maeda et al., 1995; Westerhoff et al., 2010). Compared to the pH change caused by CO_2 concentration, the pH drop due to the SO_x has been reported to have a great influence on the algal growth and even completely inhibit growth. If a detrimental pH drop is prevented by suitable buffers,

growth rates can exceed those at lower SO_x concentrations (Kumar et al., 2011; Maeda et al., 1995). This indicates that the growth is not directly influenced by SO_x concentration, but mainly by the resulting pH change.

2.3.2.6 Oxygen accumulation

Photosynthetic efficiency is decreased by trapped O_2 in the culture, as it causes toxic effects such as photo-bleaching. Hence, efficient degassing systems are required in order to remove O_2 from the system (Kumar et al., 2011).

2.3.3 Microalgal cultivation systems

2.3.3.1 Open pond raceways versus photobioreactors

Various systems are used for algal cultivation, including open ponds (inclined, circular and raceway) and the main different types of PBRs: vertical tubular (bubble columns, airlifts and annular), helical, flat panels, horizontal tubular, stirred tanks, plastic bags, hollow fibre membranes and hybrid designs of these types (Wolkers et al., 2011). The main cultivation systems are shown in Figure 2.6. Commercial cultivation of algae is mostly carried out in open systems and natural ponds due to their low cost. However, open ponds usually occupy a larger footprint and it is difficult to monitor and control their conditions, e.g., temperature, compared to closed systems, and they are susceptible to contamination (by fungi, bacteria, protozoa or other algae) and water evaporation (Carvalho et al., 2006).

PBRs are easier to control and have higher yields than open systems. Sparging of gas bubbles at the bottom of the PBRs provides mixing, mass transfer of CO_2 and removal of O_2 produced by photosynthesis. PBRs regularly produce biomass of the order of 5 g L^{-1}, compared to the 0.5 – 1.5 g L^{-1} produced by raceway ponds (Chiu et al., 2009; Rosenberg et al., 2011). However, they have higher energy costs because of the gas sparging to circulate liquid suspension and of the materials construction. PBRs may be constructed of glass, transparent polyvinyl chloride, acrylic (e.g., Plexiglas) or polycarbonate (e.g., Lexan), or polymethyl methacrylate, to allow light penetration (Tredici & Zittelli, 1998). The information presented in the next section on the PBRs characteristics has been systematically collected in Table I.3 of Appendix I.

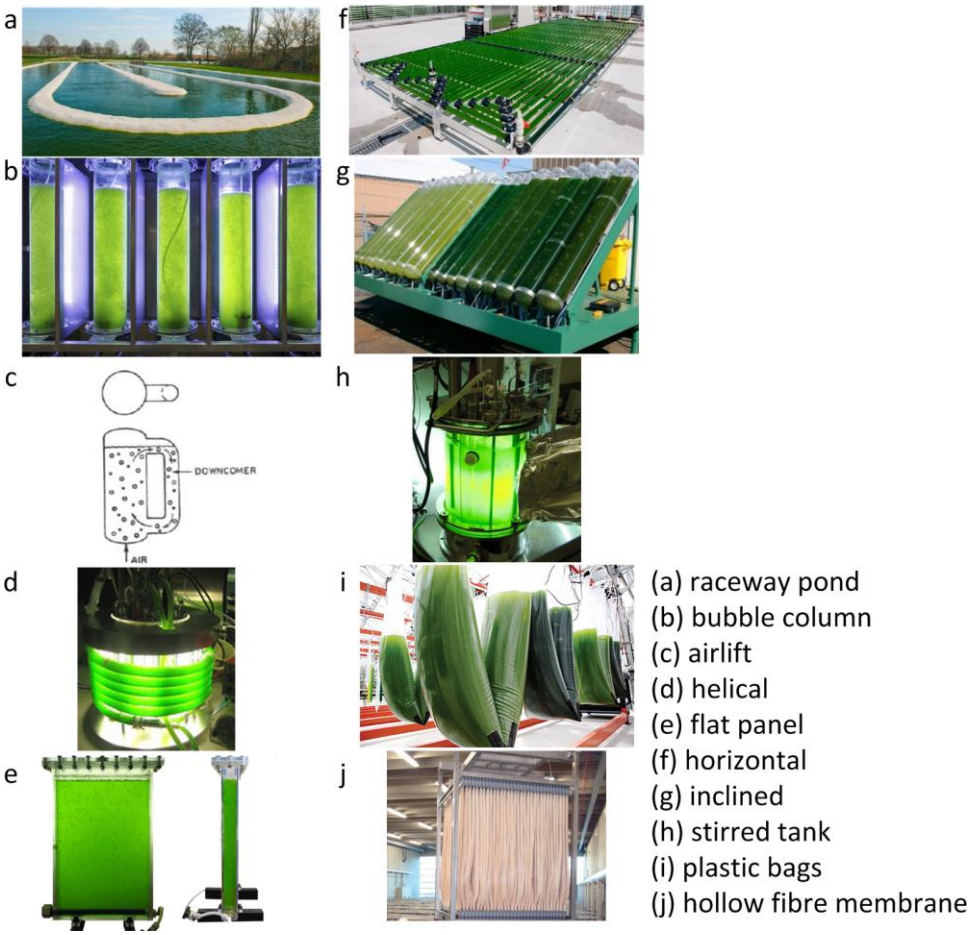

Figure 2.6. Photobioreactor types. Figures adapted from: (a)(Wolkers et al., 2011), (b) (Oneal, 2015), (c) (Chisti, 1989), (d) (Wiscombe, 2010), (e) (Bochum, n.d.), (f) (Wolkers et al., 2011), (g) (Sieg, 2008), (h) ("Indiamart," 2015), (i) (Dubyne, 2015), (j) (Electric, 2013).

2.3.3.2 Photobioreactors

2.3.3.2.1 Vertical tubular photobioreactors

Vertical tubular PBRs might be either bubble columns, or airlift PBRs based on their mode of liquid flow. The main parts of the bubble columns are a tube containing the algal broth and a sparger immersed inside the algal broth, providing a supply and mixing of gas for the photosynthesis reaction. Bubble columns' advantages compared to the other PBR types are low capital costs, high surface-to-volume ratio, lack of moving parts, satisfactory heat and mass transfer and efficient O_2 release and residual gas mixture produced by the reactions (Kumar et al., 2011). The liquid flow in this PBR type is stated as independent of the gas flow, while large liquid transport is impossible without significant recycle rates inside the tube (Chisti, 1989). Photosynthetic efficiency depends mainly on gas flow rate; increased flow rate increases light and dark cycles'

frequency (Kumar et al., 2011), which have been reported to influence the photosynthesis rate (Barbosa et al., 2003).

Airlift bioreactors encompass a broad family of pneumatic gas-liquid contacting devices, in which gas injected into the bioreactor “riser” causes circulation of liquid via a linked “downcomer” where there is no sparging but smaller bubbles move downwards carried by the stream of the liquid which recirculates due to the density difference. The circulatory patterns are a function of the geometry and velocity within the system and differ from the flow in a bubble column (Shah et al., 1982). Airlift bioreactors have a wide range of applications in bioprocessing, chemical processing and wastewater treatment (Merchuk & Siegel 1988; Moo-Young & Chisti 1994). In particular, they have a variety of operational benefits for cultivation of algae in relation to other PBR types, including high gas and mass transfer, increased exposure to light due to uniform turbulent mixing, low hydrodynamic stress and ease of control, particularly of liquid velocity (Kumar et al., 2011). They also display flatter dissolved O_2 profiles compared to bubble columns (Chisti, 1989), with the circulation velocity and O_2 removal characteristics reported to be closely linked (Molina et al., 2001). Figure 2.7 illustrates common airlift bioreactor configurations, with either an internal or external loop. Internal loop airlifts separate their riser and downcomer either with a draft tube or a split-cylinder. In external loop airlifts the two areas are separated physically, as two separate interconnected tubes (Kumar et al., 2011). External loop airlifts are found to give lower mass transfer coefficient for given gas velocities, compared to bubble columns and internal loop airlifts (Chisti, 1989). Another type of vertical column is the draught tube type which includes an inner tube that either serves as an airlift (Kumar et al., 2011), or as a chamber for the illumination from the inside in an annular PBR type (Loubiere et al., 2011).

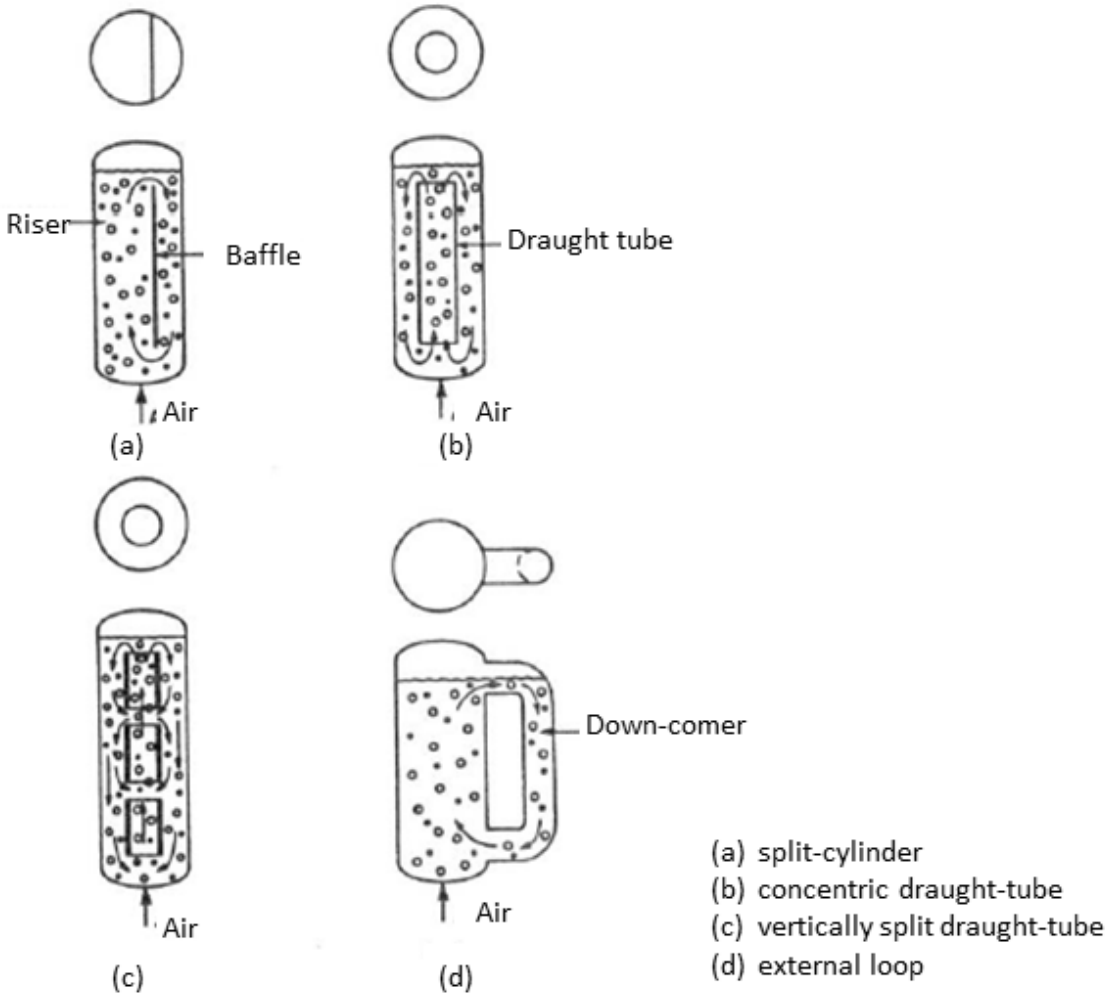

Figure 2.7. Types of airlift bioreactors with internal (a, b, c) and external loop (d). Figure adapted from Chisti (1989).

2.3.3.2.2 Helical photobioreactors

Helical PBRs consist of coiled transparent and usually flexible tubes with a degassing unit, which may be attached to the top of the tube or separate as a part of a manifold, to remove the accumulated O_2 and the residual gas (significant quantities in this type of PBR due to their low inclination). The culture is driven to the degassing unit by a centrifugal pump (Kumar et al., 2011). The gas mixture can be circulated from either direction, but it has been proven that injection from the bottom gives better photosynthetic efficiency (Morita et al., 2000). Rigid vertical structures are used to support the coiled flexible tube at the minimum inclination that will avoid bubble coalescence.

Advantages of helical PBRs are the small footprint occupied by long tubes to enable a longer residence time for better CO_2 transfer from gas to liquid phase

(Watanabe et al., 1995). One disadvantage of this type of PBRs is the bubble coalescence appearing at low inclinations, which strictly define the angle and height of the tube of the conical helical system and impede scaling-up. Therefore, scale-out can be realised by using a larger number of helical units. However, the energy required by the centrifugal pump to recirculate the culture, which also causes high shear stress, as well as the high O_2 accumulation over the high gas residence time, limit their commercial use. Also, fouling in the inside of the PBR is a common disadvantage, as they are more difficult to clean (Kumar et al., 2011).

The configuration of the conical helical PBR results in a lower centre of gravity, adding stability for the case of its implementation on ships (Watanabe et al., 1995). This type of PBR gives relatively high photosynthetic efficiency for given energy input, which is reported to be able to increase by a factor of 2 relative to the non-conical helical PBR, due to higher exposure to the light (Morita et al., 2000).

2.3.3.2.3 Flat panel, horizontal, stirred tank, bags, membrane and hybrid photobioreactors

Flat panels (or flat plate) PBRs are either vertical or inclined panels. They are described to be the most productive, avoiding the problem of O_2 accumulation due to their high surface-to-volume ratio and open gas disengagement systems, but they have many disadvantages such as high energy requirements for mixing, and complexities in adding concentrated CO_2 and scaling up (Wolkers et al., 2011). Mixing is provided either by sparged gas though a perforated tube, or by mechanical rotation through motor. There have also been applied modifications such as addition of baffles to improve mixing (Zhang et al., 2001), or V shape PBRs to improve agitation and minimize shear stress and cell adhesion to the walls. Scale-out is carried out by placing several plates over an area. The highest productivity of green algae achieved so far is 12.2 $gL^{-1}d^{-1}$, in a continuous culture of *Chlorella sorokiniana* in a flat panel with short path length under over-saturating light conditions (2,100 $\mu mol/m^2/s$) (Cuaresma et al., 2009).

Horizontal PBRs are advantageous for outdoor cultures due to their orientation and may achieve volumetric productivity and photosynthetic efficiency higher than a flat panel PBR Tredici and Zittelli (1998). Their design can be parallel set of tubes, loop shape, ‘a’ shape, that have either near horizontal or horizontal orientation. Gas mixture is introduced into the tube connection via a gas exchange system, where bubbles exist

for a particular time to transfer gas mass into the liquid. Horizontal PBRs drawbacks are large ground footprint, high O_2 accumulation efficiency (Kumar et al., 2011) and the high energy consumption to reach high linear liquid velocities (Posten, 2009). However, on a ship installation, footprint of the horizontal shapes might not be a problem as it can provide more efficient packing, by being run along the hull occupying spaces that would otherwise not be utilised by other ship systems, provided there is sufficient exposure to artificial light.

Stirred tanks are the most conventional and cheap PBR type. Agitation is delivered by impellers. Illumination is mostly provided externally via fluorescent lamps or optical fibres. They include large disengagement zones to separate O_2 produced and residual gas from the liquid. The main disadvantage of these PBRs is the low surface-to-volume ratio, which decreases the light harvesting efficiency, and the high shear stress due to energy intensive mechanical agitation (Kumar et al., 2011).

Plastic bag PBRs are inexpensively built, compact, with low energy consumption and low shear stress. However, they have a short life and relatively low surface-to-volume ratio for light harvesting (Christenson & Sims, 2011). They are also prone to growth of algae on the inside walls (Li et al., 2013) due to the less uniform mixing obtained compared to vertical columns.

The greater mass transfer area of the hollow fibre membranes cultures have shown improved CO_2 and NO_x sequestration, overcoming one of the most important challenges of the PBR systems, the gas transfer and residence time. However, they show higher pressure drop (Gardner, 2011; Kumar et al., 2010).

When it comes to applications with specific characteristics and requirements, hybrid PBRs may be advantageous because they exploit the advantages of more than one PBR type to overcome the individual disadvantages.

2.3.3.3 Comparison of the photobioreactor types

Photos of the main cultivation systems are shown in Figure 2.6. A comparison of all the PBR types in the literature is difficult, because there are many variables involved and there is a lack of information about the operating conditions in some references. Table I.4 in Appendix I summarises the literature productivity values for different PBR designs. It has been claimed (Asenjo, 1995) that surface-to-volume ratio controls production potential; given otherwise comparable conditions, both volumetric productivity and areal productivity increase as surface-to-volume ratio increases.

However, the collection of literature data of the past decade and older shows significant variation in the productivities of each design (summarised in Figure 2.8), due to the variety of species and operating conditions used among the different studies. Overall, it is not clear that any reactor types are definitively associated with better performance.

Another important parameter to be taken into consideration for the shipboard application is the net energy ratio (energy production divided by consumption, whereby a value higher than 1 indicates that the PBR is able to produce more energy than it consumes). Girdhari (2011) estimated a net energy ratio of 0.36 for the flat plate PBR, 1.3 for the tubular PBR and 6.27 for the open pond PBR.

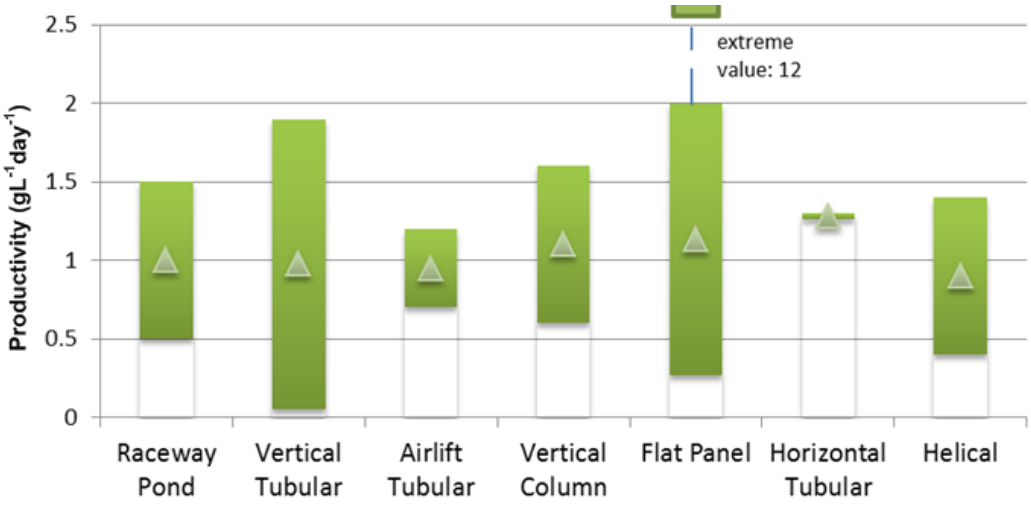

Figure 2.8. Ranges of productivities found in the literature for the main PBR designs. Data taken from Table I.4.

2.3.4 Photobioreactor design characteristics required for shipboard application

2.3.3 covers some of the design variables to consider when selecting an appropriate PBR design for a particular application. The importance of these variables within land-based algal carbon capture systems is shown in Table I.2 of Appendix I. For the case of a shipboard PBR to treat the emissions from fuel combustion, the main requirements are related either to the algal productivity or to the net energy ratio, as algal productivity is linked to the quantity of CO_2 captured, and the energy requirements imply additional emissions generated. The following specific design requirements were

taken into account and were considered to be the most important for a shipboard PBR that captures CO_2 from combustion as the primary feedstock:

- high surface-to-volume ratio to increase light harvesting
- high gas retention time to increase mass transfer of CO_2 from the flue gas to the liquid
- good mixing of the broth to increase nutrient delivery and prevent fouling
- minimal maintenance and easy control of design parameters (e.g., temperature, pH) to reduce handling requirements for the crew
- high physical stability of the PBR to reduce the effect of movements (e.g., ship movements from waves)
- low pumping or mixing energy requirements
- low ground footprint for a given volume to avoid space issues inside the ship
- low O_2 accumulation to prevent oxidation.

An attempt to compare the characteristics of the different designs by using data from Table I.3 of Appendix I is shown in the bar chart of Figure 2.9. The figures used for the production of this diagram are the integers 1, 2 and 3 representing, low/poor/difficult, medium and high/good/easy, respectively, for the characteristics light utilisation, gas retention, mixing, maintenance, control stability and oxygen release; while integers 1 and 3 represent high/big and low/small, respectively, for the characteristics of energy requirement and ground footprint. Therefore, integers 1, 2 and 3 are used to represent an inconvenient, a neutral (medium) and a convenient characteristic.

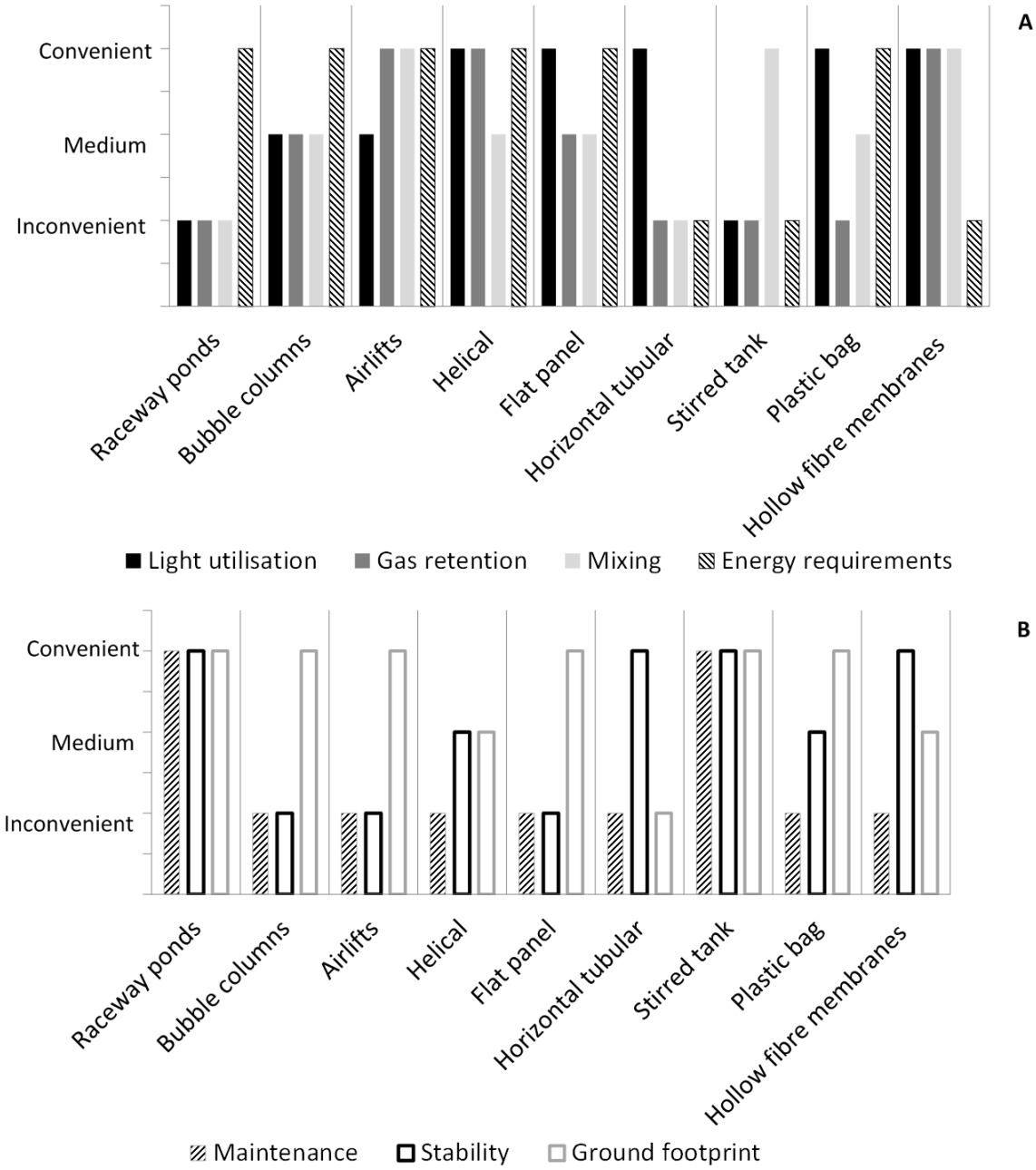

Figure 2.9. Illustrative comparison of the characteristics (plot A: light utilisation, gas retention, mixing, energy requirements; plot B: maintenance, stability, ground footprint) of different algal cultivation systems. Data taken from: Scott et al., (2010), Kumar et al. (2011), Chisti (1989), Molina et al. (2001), Morita et al. (2000), Watanabe et al. (1995), Wolkers et al. (2011), Tredici and Zittelli (1998), Posten 2009), Lee et al. (1995), Christenson and Sims (2011), Gardner (2011), as well as Brennan and Owende, 2010; Carvalho et al., 2006; Girdhari, 2011), as summarised in Table I.3 of Appendix I.

None of the PBRs presented addresses all of the required design characteristics. The largest sum, indicative of more advantageous characteristics, was obtained by airlift, the hollow fibre membrane and helical PBR types. However, other characteristics, such as cost and ease of scale-out were not taken into account due to

difficulties in comparing the available information in the literature. It should be emphasized that the comparison in the graph was made with respect to the specific shipboard application. Although its method might be different when considering other applications, it gives similar outcomes to the statements in the literature. For example, airlift systems are reported in (Kumar et al., 2011) as the most suitable PBRs for CO_2 sequestration since they combine high gas transfer, uniform mixing, low stress on algae cell walls and ease of control. Also, vertical tubular, helical tubular and flat panel PBRs are stated to be more advantageous to most of these characteristics than the other types discussed (Carvalho et al., 2006), which is roughly verified by the interpretation of different literature studies produced in Figure 2.9.

2.3.5 Application of algal cultivation systems

2.3.5.1 Description of generic algal carbon capture systems

The overall facilities of systems that cultivate algae for carbon sequestration consist of four processes; preparation, culturing, harvesting, dewatering and processing/biorefining. They require the integration of other processes in the system, such as connected detectors of the environmental conditions, in order to produce a valuable product. In the preparation stage of seawater systems such as the system in this study, seawater is recommended to be collected, filtered and buffered with anti-chlorine solution to be tolerable by algae. At the end of the cultivation cycle, the water is then treated and recycled (Alwi, Algaetech Group of Companies, Rahman, & Norsham Bin Che Yahya, 2010). The CO_2 provision to the system includes the steps shown in Figure 2.10. The flue gas collected has to pass through a HE (cooling system) (Alwi et al., 2010; Brennan & Owende, 2010), is pressurized by a blower, collected and compressed in a flue gas chamber before being fed to the algae.

Figure 2.10. Process diagram for the supply of CO_2 in an algae-based sequestration unit. Figure reproduced from Oilgae (2011b).

The harvesting techniques that are used for the separation of the algal suspension from the media are centrifugation, flotation with flocculation, and the comparatively less expensive techniques of sedimentation with flocculation and filtration extraction of the biomass (Borowitzka & Borowitzka, 1988).

2.3.5.2 Land-based algal carbon capture systems

The main purpose for the implementation of a PBR onboard a ship is considered in this study to be the flue gas carbon capture. Several land-based applications demonstrate the use of algae for CO_2 fixation, either integrated industrially, or at pilot scale, where the flue gas treated originates directly from an industrial smokestack. They are able to remove up to 85% CO_2, 73% NO_x and 55% SO_x (Chiu et al., 2011; Kumar et al., 2010) and exhibit fixation rates of up to 4.4 g CO_2 L^{-1} 24 h^{-1} (Douskova et al., 2009). Different algal species have been used in these facilities, including *Chlorella vulgaris*, *Chlorella emersonii*, *Chlorella sp*., *Scenedesmus obliquus*, *Dunaliella salina*, *Spirulina platensis* and *Anabaena sp*, in various systems including flat panels, raceways, airlifts, hollow fibre membranes and vertical thin films (Borkenstein et al., 2011; Chiang et al., 2011; Chiu et al., 2011; Douskova et al., 2009; Gardner, 2011; Kastánek et al., 2010; Koberg et al., 2011; Kumar et al., 2010; Rosenberg et al., 2011; Tesař & Bandalusena, 2010; Zeng et al., 2011). These facilities fix the flue gas produced by biorefineries, coal power stations, cement plants, coke ovens of steel plants but none has been applied to a ship engine. Open-loop "raceway" ponds are used for treating gases from bigger plants or greater emission quantities and ultimately achieve greater than 90% utilization of sequestered CO_2 (Atkins, 2010; Koberg et al., 2011; Rosenberg et al., 2011).

Research to decrease the biomass production costs in microalgal facilities that fix the CO_2 in coal-fired plant emissions began in 1978, when the U.S. Department of Energy's Office of Fuels Development funded the Aquatic Species Program to grow algae-based fuel (Sheehan et al., 1998). Over 3,000 species of algae were tested and contributed to the current biofuels state of the art. Many PBR applications have been tested too for integration to emission treatment from smokestacks (Borkenstein et al., 2011, Chiu et al., 2011; Douskova et al., 2009; Tesař & Bandalusena, 2010; Zeng et al., 2011).

The costs of the systems for emissions treatment and biomass production from algae differ in the various studies depending on the assumptions taken. Capital costs of PBRs range between \$60 – 100/m^2 (Oilgae, 2011b). Algal carbon capture is much more costly than chemical scrubbing of CO_2, with estimated costs of up to \$1,500/tonne CO_2, but under optimal conditions the costs are offset by the revenues generated from biodiesel or other products (Oilgae, n.d.-a; Chisti, 2007).

2.3.5.3 Considerations for shipboard algal carbon capture systems

2.3.5.3.1 Overall concept

In the case of the shipboard application, the utilisation of water around the ship for the PBR arises as an opportunity. However, water pre-treatment, such as sterilisation with antibiotics or ultraviolet (UV) light, if used, would increase the operation costs. The continuous or semi-continuous operation of the PBR might then be required in order to maintain a high concentration of the selected algal species and decrease acclimation times. However, the continuous operation of the PBR would give rise to the complication of increasing salinity due to evaporation. By starting with a wild algae mixture and maintaining a continuous process, each ship could acclimate the species that benefit most from the given specific conditions under which they operate. Salt accumulation would also be a problem with the use of local water. These aspects are further analysed in 2.4.1.

Regarding the flue gas of the ship, its high concentration in sulphur oxides (SO_x) of around 600 mg/kg (as shown in Table 2.1) (Ayub, 2009) would make it intolerable to the culture. Therefore, a SO_x scrubber is potentially required before the flue gas enters the PBR.

Flue gas temperature is around 300 °C and exiting the SO_x scrubbers it is 60 – 100 °C (Oilgae, 2011a). Cooling of the flue gas before its entry to the PBR is essential, as its temperature is not tolerable to algae and would also cause plastic materials commonly used in PBRs to fail, while also reducing the efficiency of the SO_x scrubber. PBRs that are integrated with smokestacks of plants require prior cooling of the flue gas to approximately 30 °C (Kastánek et al., 2010). Even if an SO_x scrubber is used before the PBR, the gas exit temperature from SO_x scrubbers is 60 – 100 °C, which is too high for the PBR materials.

Provision of sunlight to a PBR in the ballast tanks could be facilitated by a system to concentrate sunlight with lenses (Mori et al., 1987). Alternatively, the algal broth could be circulated from the deck to the ballast, obtaining light and dark cycles ideally in specific ratios that would have a beneficial effect on the growth (2.3.2.2), although the influence of medium-duration light/dark cycles (of the order of a few minutes) is not clear (Janssen, 2002). Finally, it may be possible to use the motion of the ship to mix the algal broth for more even exposure of the algae to light, though such a system may be difficult to control. For a combined light and dark set-up, the external installation

could be on the deck and/or along the topsides. The advantage of deck mounting is ease of installation and accessibility. The PBR would be less likely to get damaged by waves or when mooring alongside another structure. One of the advantages of mounting along the topsides is that it could offer a shorter piping run to the ballast tank and more area for light penetration and less crowding on the deck.

Regarding the shipboard PBR design, the three largest sums of performance with regard to the characteristics examined in 2.3.4 were obtained by the airlifts, the hollow fibre membranes and the helical types. A hybrid conical helical airlift PBR could combine the advantages of several different reactor types for shipboard implementation. For instance, apart from the characteristics summarised in Table I.3, a helical PBR has also lower pumping requirements, compared to vertical tubes of the same volume due to its inclination. Also, it is as robust as a tubular PBR and not prone to breaking, as in the case of flat panels and plastic bags. Moreover, the conical shape could harvest sunlight for more hours during the day and, by lowering the centre of gravity, it is more stable, requiring less securing to the vessel. The main disadvantage of the helical PBR, which is O_2 accumulation (2.3.3.2.2), could be overcome by integrating a degassing zone at the top of the structure. Different configurations of various dimensions could be examined by adjusting the flexible tubing.

2.3.5.3.2 Waste streams

On ships, the ready availability of the surrounding water and the nutrients (as mentioned in 2.2) contained within and sourced from ship waste, such as that found in grey and black water could make maintaining the algal growth medium more cost effective. Since algae metabolise inorganic nitrate and phosphate, they can be used for tertiary treatment (i.e., removal of ammonium, nitrate and phosphate) of wastewater and quinary treatment (i.e., removal of inorganic salts and heavy metals). The PBR could potentially treat the wastewater stream of the ship (indicated in the schematic of Figure 1.1), as algae have been successfully used for wastewater treatment (Christenson & Sims, 2011). They also require relatively lower energy input compared to other wastewater treatment processes, but one drawback is that they fail to meet suspended solids limits (Noüe et al., 1992; Oilgae, 2010).

In addition, ships, especially passenger ships, produce food waste which cannot be offloaded in the sea. Food waste can be processed in anaerobic digesters to produce biogas, digestate and solid sludge. Biogas is a valuable fuel, which could be used in fuel cells or simply onboard combustion with lower CO_2 emissions. Its main components are methane (CH_4), CO_2, and hydrogen sulphide, (Abatzoglou & Boivin,

2009). It has to undergo a process of purification to increase the CH_4 concentration and remove hydrogen sulphide.

Currently, the methods for CO_2 removal from biogas include several physicochemical techniques and biological methods, or their combinations (Abatzoglou & Sherbrooke, 2009; Chung et al., 2003; Kapdi et al., 2005). Most of the physicochemical methods are now developed commercially by companies, but the conditioning effect is suboptimal (Mann et al., 2009). The application of algae could avoid the use and disposal of expensive chemicals. However, it may be uneconomical due to high energy needs and low productivity of PBRs (Mann et al., 2009). The studies that examined algal fixation of CO_2 from biogas used synthetic biogas made of CO_2 and N_2 (Mandeno et al., 2005), synthetic biogas from CH_4 and CO_2 (Mandeno et al., 2005), or raw biogas (Conde et al., 1993; Mann et al.. 2009). With biogas, the resulting biomass was almost 5 times higher than that for the same media without biogas (Conde et al., 1993) and the CO_2 concentration was reduced from 40% to <5% Mandeno et al. (2005). However, productivity under biogas feeding greatly depends on experimental conditions and the algal species used. Mann et al. (2009) reduced the hydrogen sulphide concentration by more than 50%, due to its high solubility in water and partial uptake by algae as a source of sulphur. On the other hand, photosynthesis in blue-green algae is stated to be inhibited by sulphide (Castenholz & Utkilen, 1984). Excessive O_2 levels are considered a problem, but explosive CH_4/O_2 mixture concentrations could be avoided, as CH_4 ignition limits (concentrations between which a gas or a vapour in air is capable of producing a flash of fire in presence of an ignition source) are 5 – 60% and biogas that is being cleaned contains 60% or more CH_4 (Mandeno et al., 2005; Mann et al., 2009).

Moreover, an improvement in growth rates (up to 4.8-fold) and biomass production (up to 8.7-fold) has also been shown for various cultures after their adaption to the nutrient rich effluent digestate from anaerobic digestion (Wahal, 2010). A lot of studies examine the use of grown algae as a biomass feedstock for biogas production and the process was reported to be economically feasible and sustainable (Sialve et al., 2009).

2.3.5.3.3 Use of ballast tanks

As discussed in 2.4 and 7.2, ballast is one promising place to locate the algal PBR. Although algae grown in PBRs can reuse the water involved (Aitken, 2012), they still generate liquid waste volume that would need to be processed (2.2.2). Besides, the

water volume to be disposed does not only depend on the operation of the PBR, but the stability requirements of the ship at any given time. In addition to the general ballast water management processes, harvesting techniques would have to be incorporated to separate the algal broth, or else the total broth volume would have to be transported to a plant on-shore.

Ballast tanks exist in many ship types to provide balance, depending on dynamic factors such as the ship load and sea conditions. They can be loaded with the local natural water (e.g., seawater) to provide additional weight and to eliminate increased buoyancy that can result in lack of propeller immersion, inadequate inclination, stresses on the hull and instability (David & Gollasch, 2015). Ballast tanks are important for the implementation of a PBR and the system integrated with it, as their space can contribute significantly to the accommodation of the large water mass required for algal growth.

The ballast tanks occupy approximately 37% of the deadweight tonnage of the ship, depending on the ship type (Table I.5 in Appendix I). They have various positions in different ship types, such as in the vessel's double bottom (double bottom tanks), port and starboard along the sides, in the bow (forepeak tank), in the stern (after peak tank), port and starboard underneath the main deck (topside tanks or upper wing tanks) (David & Gollasch, 2015). After peak and forepeak tanks exist in almost all ships, often in combination with other tanks (Figure 2.11). The fact that one tank can be divided into different compartments could facilitate the accommodation of water mass dedicated to different aspects of the PBR system. Nevertheless, direct implementation of the PBR with storzge of the broth in the ballast place would not be a simple consideration of even more complex modification of the whole design of the ships would be required to ensure the technical feasibility, instead of taking a simple decision to directly storage the PBR or the broth in ballast space.

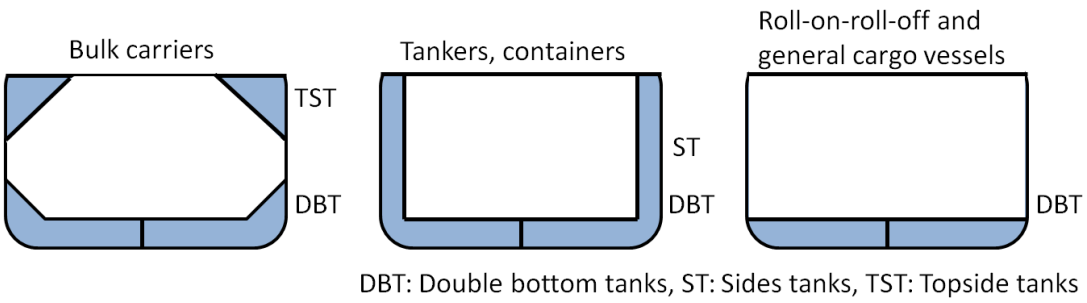

Figure 2.11. Cross sections of common ballast tank positions in some ship types. Figure reproduced from David and Gollasch (2015).

2.3.6 Photobioreactor performance modelling needs and approaches

2.3.6.1 Introduction

Carbon capture needs the study of numerical hydrodynamic models, which are useful in optimising PBR design and operation for carbon capture without expensive experimentation. Additionally, models of algal growth kinetics are important for study of the influence of operating conditions on the productivity and consequently the carbon capture rate. In both cases, there are many experimentally validated models for individual algal PBRs, but there is no standardised approach to modelling and models cannot be generalised for wide use and reproduction (Costache et al., 2013; Derakhshan et al., 2014; Gonçalves et al., 2014; Vunjak-Novakovic et al., 2005).

Building validated models to the requirements of each application is important, as operating conditions could be highly variable due to weather, sea state, latitude, engine load, etc. A new approach for validation of a generic algal growth kinetics model and the gradual addition of layers of complexity would ensure more valid predictions for such a complex system.

2.3.6.2 Hydrodynamic models

Bitog et al. (2011), Merchuk (2003) and Petersen and Margaritis (2001) have reviewed fluid dynamic models for airlift PBRs. Discrepancies in literature relationships between gas hold-up, superficial gas velocity, effect of any solid phase, and column diameter were attributed to different measuring techniques. Review of two- and three-phase system models by Merchuk (2003) showed discrepancies in model predictions to be due to the use of different drag coefficients and frictional loss estimates, as well as the fact that many models are configuration specific. They emphasised the lack of a generalised equation with wide range validity and requirements for massive data to validate the empirical correlations proposed by some studies. Bitog et al. (2011) showed the progress in computational fluid dynamics studies, mostly of bubble columns employing the Eulerian-Eulerian mixture model. They confirmed the lack of a systematic method for scale-out and highlighted the importance of drag coefficient estimation for algal systems.

Only a few studies have examined the effect of bubble size, gas flow rate and reactor dimensions on flow characteristics: Law & Battaglia (2013) and Zhang et al.

(2005) examined gas hold-up and liquid velocity dependence for bubbles with the same average size but different distributions; Camarasa et al. (2001) studied the effect of bubble size on the gas hold-up and the pressure but the range of bubble diameters was small (2 – 2.5 mm); Saez et al. (1998) introduced the buoyancy force in the model by Young et al. (1991) for computationally intensive modelling of the effect of bubble size on the gas hold-up and the liquid velocity, but validated it for only one size; Marquez et al. (1999) further introduced a differential equation to estimate the phase change due to reaction in this model but their experimental results are restricted to one gas flow rate.

The existing studies for external loop reactors are based on two parallel approaches, either using continuity and momentum balance equations (Camarasa et al. 2001; Young et al. 1991), or power balance equations (Chisti, 1989; García-Calvo et al. 1999).

The well-known model by Chisti (1989) incorporates an empirical correlation to estimate gas hold-up and has been widely validated for a great range of sizes and configurations of algal airlift reactors. Chisti's model assumes dependence of the liquid velocity mainly on the geometric configuration of the circulation loop, and the difference in gas hold-up in the riser and the downcomer zones (Chisti, 1989; Molina et al., 2001). This method is based on the principle of energy conservation, taking into account the energy input due to isothermal gas expansion and energy lost due to wakes, friction and stagnant gas in the downcomer (Chisti, 1989). For an external-loop airlift, where the top and bottom connections are very similar in geometry, the superficial liquid velocity is estimated according to the model as:

$$u_l = \sqrt{\frac{2gh_D(\varepsilon_r - \varepsilon_d)}{k_B\left(\frac{1}{(1-\varepsilon_r)^2} + \left(\frac{a_r}{a_d}\right)^2 \frac{1}{(1-\varepsilon_d)^2}\right)}} \quad (6)$$

where u_l is the superficial liquid velocity, h_D is the dispersion height, ε_d is the gas hold-up in the downcomer, k_B is the friction loss coefficient for the bottom connecting section of the PBR tubes, a_r and a_d are the cross-sectional areas of the riser and downcomer, respectively. The values for ε_r and ε_d are estimated from the following empirical formulae:

$$\varepsilon_r = \frac{u_g}{0.24 + 1.35(u_g + u_l)^{0.93}} \quad (7)$$

$$\varepsilon_{\mathrm{d}} = 0.79\varepsilon_{\mathrm{r}} - 0.057 \quad (8)$$

Also, $\mathrm{h_D}$ is described as the height of the liquid with no gas displacement and is found from the following equations:

$$\varepsilon_{mean} = \frac{a_r\varepsilon_r + a_d\varepsilon_d}{a_r + a_d} \quad (9)$$

$$h_D = \frac{h_L}{(1 - \varepsilon_{mean})} \quad (10)$$

where $\varepsilon_{\mathrm{mean}}$ is the mean gas hold-up in the PBR and $\mathrm{h_L}$ is the height of the liquid. The superficial gas velocity and the liquid circulation velocity are given respectively as:

$$u_g = \frac{q_g}{\pi\frac{d_r^2}{4}} \quad (11)$$

$$\bar{u}_l = \frac{u_l}{(1 - \varepsilon_r)} \quad (12)$$

Finally, the frictional loss coefficient for the connecting section in the present study is assumed to have a mean value of $\mathrm{k_B}$=5 (Chisti, 1989). Eq. 6 – 12 are solved by iteration with assumed superficial liquid velocity values, allowing determination of the liquid circulation velocity and gas hold-up.

2.3.6.3 Models of algal growth kinetics

2.3.6.3.1 Specific growth rate and productivity

Several models for algal growth simulation are based on the first order reaction equation developed by Prokop and Erickson in Asenjo (1995) and used in different studies (Huesemann et al., 2013; Cheenkachorn et al., 2011; Molina Grima et al., 1994). This generic equation represents the dynamic behaviour of the biomass concentration ($\mathrm{C_b}$) over time, t, where μ is the specific growth rate (referred to simply as growth rate in this study) and takes the form of Eq.13 when the specific maintenance rate ($\mathrm{m_a}$) and dilution rate (D) are considered as part of the process. The specific maintenance rate is defined as a negative relative growth rate, which, multiplied by the microbial biomass, equals the loss of cell material through maintenance (van Bodegom, 2007).

$$\frac{dC_b}{dt} = C_b(\mu - m_a - D) \tag{13}$$

Under optimal growth conditions, where none of the independent variables (temperature, light, nutrients) are limited, the growth rate takes a constant maximum value and growth increases exponentially. However, in reality, at least one of the affecting variables will be limited at some point and thus growth rate is multiplied by a utilisation factor, which changes for different growth phases. A typical growth curve involves the six phases indicated in Figure 2.12.

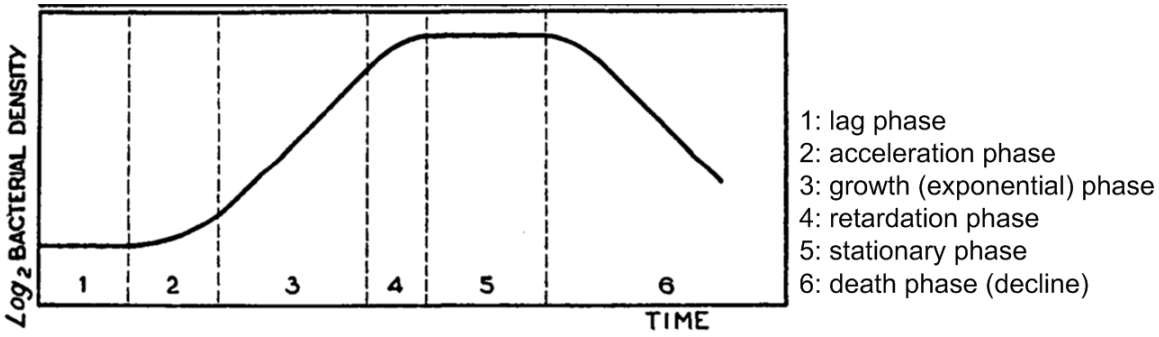

Figure 2.12. Stages of a typical microbial growth curve. Figure adapted from Monod (1949).

2.3.6.3.2 Light utilisation and growth under light limited conditions

Most of the reaction schemes that have been suggested to estimate the growth rate when light is a limiting factor are empirical, although loosely based on enzymatic kinetics. Kinetic models include rectangular hyperbolic (similar to the Monod model and Michaelis-Menten enzyme kinetics) (He, Subramanian, & Tang, 2012), generalised hyperbolic (Bannister model), inverted exponential (Van Oorschot) and other modifications like the Aiba model. All of the models consist of the maximum growth rate, $\mu_{max,I}$, at the saturated light intensity multiplied by a light utilisation factor $\varphi(I)$. The formulae for light utilisation factor are summarised in Table 2.4 and some of the curves are shown in relation to experimental data in Figure 2.13. The first-order linear model and the rectangular hyperbolic and generalised hyperbolic models give similar results and are widely used. There is no indication of which is the most appropriate, although Monod's model is the one most frequently used (Asenjo, 1995). On the other hand, an inverted exponential has been reported to give better fit than the three models mentioned to experimental data for photosynthesis-irradiance curves, but is criticised for being insufficiently based on a mechanistic understanding (Zonneveld, 1998). Aiba's model is an extension of Monod's model (Table 2.4), where K_I is the

bioenergetics efficiency of light utilization, for the case when light inhibition is present and, therefore, deviates from the other models above threshold light intensity.

The hyperbolic model was modified by Molina Grima who added an exponent describing the abruptness of the transition from weakly to strongly illuminated regions (Acien Fernandez et al., 1998; Fernandez et al., 2001; Fernandez et al., 1998; Molina Grima et al., 1994). It has been widely used (Brindley et al., 2011), but there are also other less common representations of the effect of light on algae when the considered irradiance range is not orders of magnitude lower than the optimal one, such as the Jessby and Platt model, the Peeters and Eilers model and the Haldane expression based on polynomial rational fraction (Bernard & Rémond, 2010; Pereira et al., 2014; Molina Grima et al., 1999). In dilute cultures with minimum self-shading effect, the growth rate increases to its maximum when the light intensity reaches the saturation value and sometimes it decreases after that point due to photoinhibition.

Table 2.4. Models used for the estimation of the light utilisation factor, $\varphi(\mathrm{I_{av}})$.

Model	Equation for $\boldsymbol{\varphi(I_{av})}$	Eq. number	Reference
Monod	$\frac{I_{av}}{K_I + I_{av}}$	(14)	(Asenjo, 1995)
Monod with overall integration	$\int_{z=0}^{z=d} \frac{I(z)}{K_I + I_{av}}$	(15)	(Huesemann et al., 2013)
Banister	$\frac{I_{av}}{(K_I^m + I_{av}^m)^{1/m}}$	(16)	(Asenjo, 1995)
Van Oorschot	$1 - e^{-\frac{I_{av}}{K_I}}$	(17)	(Acién Fernández et al., 2013; Geider et al., 1997)
Aiba	$\frac{I_{av}}{K_I + I_{av} + \frac{I_{av}^2}{K_i}}$	(18)	(Asenjo, 1995; Molina Grima et al., 1999)
Molina Grima	$\frac{I_{av}^m}{K_I^m + I_{av}^m}$	(19)	(Molina Grima et al., 1994)
Jassby and Platt	$tanh\left(\frac{aI_{av}}{\mu_{max}}\right)$	(20)	(Van Wagenen et al., 2014)
Bernard	$\frac{I_{av}}{I_{av} + \frac{\mu_{max}}{a_s}\left(\frac{I_{av}}{I_{opt}} - 1\right)^2}$	(21)	(Bernard & Rémond, 2010)
Steele	$\frac{I_{av}}{I_{max}} e^{\left(1 - \frac{I_{av}}{I_{max}}\right)}$	(22)	(Molina Grima et al., 1999)
Tamiya	$\frac{bI_{av}}{1 + \frac{bI_{av}}{\mu_{max}}}$	(23)	(Molina Grima et al., 1999)

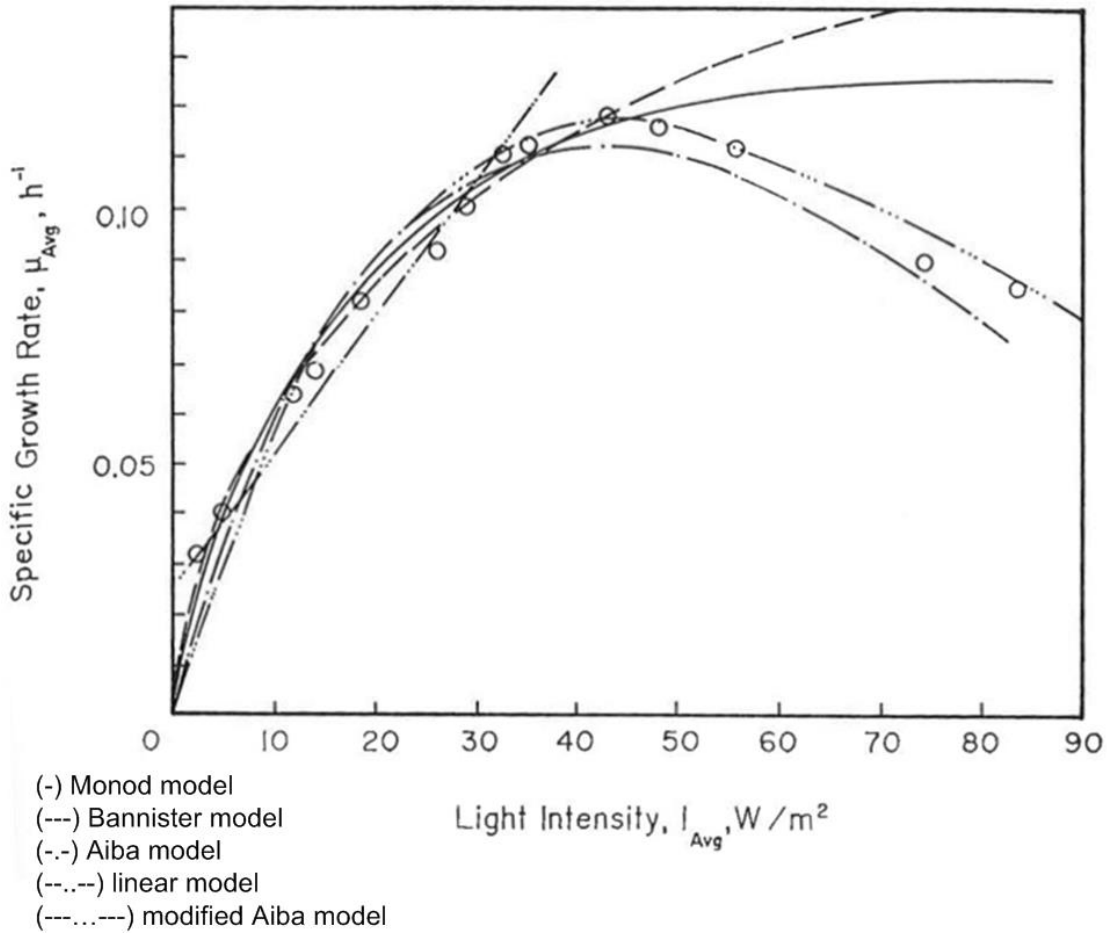

Figure 2.13. Comparison of experimental data relating average specific growth rate to average light intensity for biomass concentration 0.04 g/L. Figure adapted from Asenjo (1995).

In optically dense cultures, the light intensity cannot be described as a uniform light condition because it changes with depth in the PBR, so the photosynthesis rate is different in different regions within the PBR. Scattering is an important consideration when determining local light intensities. Light attenuation at a specific point of the PBR has generally been described by Beer-Lambert's law (Eq.24), which has been used in numerous studies from the literature (Acién Fernández et al., 2013; Acien Fernandez et al., 1998; Asenjo, 1995; Huesemann et al., 2013; Jean, 2013; Kim, Nag-Jong, Suh, Hur, & Lee, 2002; Molina Grima, Garcia Camacho, Sgnchez Perez, Acien Fernandez, & Fernandez Sevilla, 1997; Molina Grima, Sanchez Perez, Garcia Camacho, Fernandez Sevilla, & Acien Fernandez, 1996; Molina Grima et al., 1994; Quinn, de Winter, & Bradley, 2011):

$$I(z) = I_0 exp(-K_a C_b z) \quad (24)$$

where I_0 is the incident light on the surface of the PBR and z is PBR depth or radius. K_a is the biomass light absorption (extinction) coefficient which varies with pigment concentration, under the assumption that the light is monochromatic. For polychromatic light, the wavelength dependence on K_a must be considered or an average value is used (Asenjo, 1995). Molina Grima et al. (1994) have proposed determination of K_a by means of two parameters, the total pigment absorption and pigment free biomass (Molina Grima et al., 1994). Other existing representations, such as the photon flux divided by the biomass concentration and the PBR depth, are more empirical and not widely used (Zijffers et al., 2010). Substituting Eq.24 into Monod's equation from Table 2.4 gives Eq.25.

$$\mu_r = \frac{\mu_{max,I} I_0 exp(-K_a C_b z)}{K_I + I_0 exp(-K_a C_b z)} \tag{25}$$

Mixing has an important effect on growth in dense cultures by increasing the frequency of light to dark periods of the cells (Quinn et al., 2011). A space-averaged irradiance is, therefore, needed to describe the system at any time. The simplicity of the rectangular hyperbolic type model is preferably used for the integration within the PBR's geometry (Asenjo, 1995). The estimation of the growth rate for a specific time interval consequently takes the form of Eq.26.

$$\mu_r = \frac{\mu_{max,I} \int_{z=0}^{z=d} I(z)dz}{K_I + \int_{z=0}^{z=d} I(z)dz} \tag{26}$$

Eq.26 assumes a constant supply of the incident light on the surface of the PBR, which happens only with artificial illumination. Some studies, though, have estimated the fluctuation of natural light supplied outdoors and have transformed it to the space-averaged intensity for cylindrical PBRs (Brindley et al., 2011; Ribeiro et al., 2008).

2.3.6.3.3 Growth under nutrient depletion

Most models focus on light-inhibited growth, but some others have examined growth under nutrient limitation (Zonneveld, 1998). The synthesis of chlorophyll may be restricted in nutrient-limited growth, so nutrients are implicitly accounted for models which use the chlorophyll to carbon ratio as an input, and can be applied to both light- and nutrient-limited growth. On the other hand, if the chlorophyll to carbon ratio is considered as a state variable, then the maximum carbon specific rate of photosynthesis has to be described as a function of the nutrient availability. The second type of model is more common, as the chlorophyll to carbon ratio is usually

difficult to measure. An example of this type of model based on the Monod equation has been described by Geider et al. (1997). Monod's model has often been used to describe growth under nutrient-limited conditions (Cheenkachorn et al., 2011; Quinn et al., 2011; Xin et al., 2010). When there is more than one nutrient component present, often only the most limiting nutrient is modelled (Arrigo & Sullivan, 1994). Aiba's model, with an inhibition factor, has been used for cases where the nutrient becomes toxic above certain concentrations (He et al., 2012). The efficiency factor $\varphi(S)$ this time refers to the uptake of nutrients, which could represent nitrate (Quinn et al., 2011), phosphate (Xin et al., 2010), or the CO_2 concentration (Cheenkachorn et al., 2011), depending on which component is the growth-limiting factor. The maximum growth rate $\mu_{max,S}$ is also the value that the growth rate takes at the saturation nutrient concentration. Monod's generic model for substrate utilisation takes the form of Eq.27.

$$\mu_r = \mu_{max,S}\varphi(S) = \frac{\mu_{max,S}S}{K_s + S} \tag{27}$$

here S is the substrate extracellular concentration at a given time and K_S is the half velocity or saturation constant for the growth. In cases where the concentration of the growth-limiting nutrient exceeds the saturation concentration, another formula is used and an inhibition constant is introduced as is the case for CO_2 above certain concentrations (Cheenkachorn et al., 2011; Lian He et al., 2012). In reality, the concentration in the model should be the internal concentration in the cell, as nutrients are not directly absorbed and utilised by the cells, and rather pass through a metabolic pathway (Aníbal et al., 2014)

The dynamic behaviour of the substrate is given by Eq.28, where $Y_{C/S}$ is the yield over substrate, m_s the maintenance supply rate of minimum substrate consumption to maintain cells and S_0 is the substrate concentration fed in by the dilution mixture (Nyholm and Biochemistry, 1977; Ruiz et al., 2011; van Bodegom, 2007).

$$\frac{-dS}{dt} = \frac{1}{Y_{C/S}}\frac{dC_b}{dt} + m_s C_b - \frac{1}{Y_{C/S}}D(S_0 - S) \tag{28}$$

In contrast to Martinez et al. (1999) study, this study assumes Y to be stable and independent of the nutrient concentrations. The equation for dynamic substrate behaviour equation is useful as the nutrient concentration can be measured in real time to validate Eq.28 and predict the maximum growth rate.

2.3.6.3.4 Temperature effect on growth

The effect of temperature on microorganisms has been summarised comprehensively by Swinnen et al. (2004), but there are a minor number of studies that actually model its effect on algal kinetics. It is a very important parameter, as it is the environmental factor responsible for the largest part of the variance in growth (Geider et al., 1997; Quinn et al., 2011). In particular, excessively high temperatures reached in PBRs are reported to strongly reduce the growth rate (Bernard & Rémond, 2010).

Contrary to light (the average absorbed intensity through the algae that grow with time) and nutrients, which are time variant resources, temperature is a modulating factor and is not exhaustible (Zonneveld, 1998). It is described to affect cell growth in two ways. The first is to affect the metabolism by changing the rates of the processes occurring (thus all rate parameters can be assumed to be temperature dependent) and some other parameters such as the half-saturation constant (Zonneveld, 1998). The second way it to affect the maximum growth rate (Geider et al., 1997) and contribute to a lag phase in a culture's growth, which is defined as the reciprocal of the adaptation rate of the microorganisms (Giannuzzi et al., 1998). Lag phase is also affected by culture history and pH (Swinnen et al., 2004). There are two levels of models developed to describe the lag phase, regarding their structure; primary and secondary (Swinnen et al., 2004). Primary models describe evolution of the microbial numbers with time at a constant rate, and can be either stochastic or deterministic (e.g., Koutsoumanis et al., 2000). Secondary models link the primary model parameters to environmental factors, such as temperature, through the lag phase (Swinnen et al., 2004).

The effect of temperature on the maximum growth rate in biological systems has been described in several ways; by different modifications of the Arrhenius equation, by square root equation, by linear models, as listed in (Giannuzzi et al., 1998), and by cardinal temperature values with inflection (Bernard & Rémond, 2010; Pereira et al., 2014). The effect of temperature is represented by an efficiency factor, $\varphi(\mathrm{T})$, which in most algae models is described by modifications of the generalised Arrhenius equation (Eq.29) (Giannuzzi et al., 1998):

$$\mu_{max} = \mu_{opt}\varphi(T) = k_0 e^{(-\frac{E_a}{RT})} \quad (29)$$

In this equation, k_0, the frequency factor or the total number of collisions between reacting species per unit time, could be replaced by another exponential term that includes a reference temperature to normalise the equation, as shown in Geider et al.

(1997). Also, Costache et al. (2013) have added another identical term with pre-exponential factor and activation energy in order to normalise the photosynthesis rate. Alexandrov and Yamagata (2007) have suggested another alteration of the Arrhenius equation to make it applicable to enzyme-mediated reactions response to temperature as shown in Table 2.5, where n is 2 for photosynthesis reactions. Finally, Huang et al. (2011) have used a modified Arrhenius-Eyring-Polanyi equation derived from the transition state theory, to give a better fit to the non-linear data of microbial growth measurements. The Arrhenius equation has been gradually built up with modifications and addition of parameters in order to better simulate the unique nature of the temperature dependence of microorganisms, but is has not found a wider application in predictive microbiology (Huang et al., 2011).

Table 2.5. Models used for the estimation of the maximum growth rate with temperature as the limiting factor.

Model	Equation for $\mu_{max}(T)$	Eq. number	Reference
Arrhenius type	$1/LPD = k_0 exp(-E_a/RT)$	(30)	(Giannuzzi et al., 1998)
Linear model	$\mu_0 r_s T$	(31)	(Giannuzzi et al., 1998)
Square root	$[g_r(T - T_0)]^2$	(32)	(Giannuzzi et al., 1998)
Cardinal temperature	$\begin{cases} 0 \; for \; T < T_{min} \\ \mu_{opt}\varphi(T) \; for \; T_{min} < T < T_{max} \\ 0 \; for \; T > T_{max} \end{cases}$	(33)	(Bernard & Rémond, 2010)
	where, $\mu_{opt}\varphi(T) = \mu_{opt} \frac{(T-T_{max})(T-T_{min})^2}{(T_{opt}-T_{min})[(T_{opt}-T_{min})(T-T_{opt})-(T_{opt}-T_{max})(T_{opt}+T_{min}-2T)]}$		
	(Bernard & Rémond, 2010)		
Normalised Arrhenius	$\mu_{opt} exp\left[-\frac{E_a}{R}\left(\frac{1}{T} - \frac{1}{T_{ref}}\right)\right]$	(34)	(Geider et al., 1997)
Normalised Arrhenius with additional factor	$A_1 exp(-E_{a1}/RT) - A_2 exp(-E_{a2}/RT)$	(35)	(Costache et al., 2013)
Arrhenius applicable to enzyme-mediated reactions	$\varphi(T) = \frac{n \cdot exp\left[\frac{E_a}{RT}\frac{(T - T_{opt})}{T_{opt}}\right]}{(n-1) + exp^n\left[\frac{E_a}{RT}\frac{(T - T_{opt})}{T_{opt}}\right]}$	(36)	(Alexandrov and Yamagata, 2007)
modified Arrhenius-Eyring-Polanyi	$k_0 exp(-E_a/RT)\left[1 - \exp\left(B(T - T_{max})\right)\right]$	(37)	(Huang et al., 2011)

2.4 Key challenges and opportunities associated with the shipboard photobioreactor implementation and upstream process

2.4.1 Challenges

As presented in 2.3.2, the PBR system requirements that need to be considered to allow its operation are water and algal culture (2.3.2.1), light (2.3.2.2), heat (2.3.2.3) and CO_2 and other nutrients (2.3.2.4). To these should be added the question of space and location in the PBR. These challenges can be addressed by taking advantage of the system of the ship and the marine environment, as discussed below, always acknowledging the fact that a more complex modification of the engines and the whole ship design would need to be considered, to ensure the technical feasibility of the implementation.

1. **Water**: Since the use of freshwater supplies is a major concern, especially for ships, the ability to cultivate algae using the seawater or river water around the ship reduces this constraint on algae production. Not all areas, however, can provide a water quality which promotes the fast growth of contained algae. Some might need dilution of their salinity and some might require the injection of a concentrated algal culture. It should be added that a water treatment unit for the discharge from the PBR might also be required, together with a residue collection tank, due to biodiversity and biosecurity concerns (2.3.5.3.1).
2. **Algal species**: Selection of culture strain is one of the most important steps for successful mitigation of CO_2 (2.3.2.1). While the use of a commercial algae strain would guarantee the system's quality (i.e., the product characteristics would not vary under given grow conditions), expenses would be added (Sieg, 2008). On the other hand, using algae sourced from the shipping route might make it easier to maintain and resistant to invasion by other organisms; but strain identification might be difficult and the strains present locally might not have high lipid productivity. Also, wild algal species existing in the seawater are exposed to more microorganisms that might compete with the growth of the chosen algal species. Another issue is that the variety and quantity of the microorganisms fluctuate during the course of the year and across different areas (analysed in 2.3.5.3.1 and 4.4.7), hence, the dominating species in the PBR might be different on each journey of a specific ship and frequent tests for the water quality are needed. The comparative costs nevertheless could favour the use of wild algae.

3. **Light**: Sunlight provision on deck would save illumination energy requirements, but as mentioned above, ship stability requires the PBR to be positioned close to the waterline where light is limited. Some solutions were proposed in 2.3.5.3.1.
4. **Heat**: A PBR placed on a ship, either on the deck or in the ballast and operating in a cold climate, would face significant heat loss and require heating in order to maintain its temperature within the range tolerated by algal cultures (20 – 40 °C) (Konopkat & Brock, 1978; Maeda et al., 1995). The opportunity thus arises to taking advantage of the waste heat from combustion (Figure 2.2), carried by the flue gas or the cooling fluid of the engine. The use of the hot flue gas (2.3.5.3.1) would require minimal modifications to be retrofitted.

   However, the operating hours of the engines depend on the ship type and most of them do not operate full time; they either work for some hours during the day or operate for a number of days and then stay anchored. Therefore, it is of vital priority to determine a solution for the operation of the PBR when flue gas and heat are not supplied from the engines, since the biological nature of the PBR requires a more or less continuous supply of heat as well as light and air.

5. **CO_2**: The engine provides an unlimited supply of CO_2 during its working hours but it is not always operating. Therefore, an algal species or consortium capable of growth under a wide range of CO_2 concentrations is required (2.3.2.4). Moreover, the growth potential of some species is reported to be higher when aerated with flue gas compared to being aerated with control gas enriched with CO_2. However, the concentration and the temperature of the compounds in the flue gas of the ship may not be optimal for biomass growth. In particular, the high concentration of flue gas of the ship in sulphur oxides (SO_x) of around 600 mg/kg (as shown in Table 2.1) (Ayub, 2009) would make it intolerable to the culture.

   PBR performance needs to be optimised to maximise the CO_2 quantity captured with one pass through the PBR and reduce pumping requirements from potential recirculation of the gas back to the PBR. Considering the low residence time in the PBR and the high volumes of flue gas emitted from the engines, the optimisation of the gas rate is crucial for the minimisation of the energy required for its cooling, transfer and sparging, and for the maximisation of the CO_2 absorption and fixation. The higher the gas flow rate, the higher the energy required for the compressions and the higher the CO_2 quantity passed

through the PBR without being absorbed. On the other hand, a very low gas flow rate may result in an underperformance of the PBR and hence the fixation of a smaller quantity of flue gas than the maximum potential anticipated.

6. **Location:** Given the considerable water mass required for the emissions treatment, the PBR units need to be placed in appropriate positions taking into consideration the ship's stability requirements, which are dynamic, depending on weather conditions and cargo transported. On this basis, It would be tempting to place a high volume PBR low down within the hull either adjacent to or within the ballast tank (2.3.5.3.3). However, the purpose of the ballast load is to stabilise the ship depending on the cargo mass (2.2.2) and there would be a requirement for either artificial lighting or light tunnels. Therefore, at each loading and unloading, volumes of the biomass might have to be diluted, or harvested and replenished. Also, the PBR needs to be either robust enough to cope with the flushing and refilling, or placed in a separate compartment in the ballast area.

Affecting all the above issues and their solutions are questions of cost as well as the need to ensure that the solution does not have a greater carbon footprint than the CO_2 it manages to reduce. Thus the key risks of this project are the commercial viability and the energy penalty of implementation. Some additional challenges are the following:

- Freight costs also have to be considered, given the large volume of water needed to be transported. This could be optimised by maximising the concentration of the algal broth in the PBR.
- While new vessels can be designed to incorporate the spatial requirements of the PBR system and SO_x scrubber, the retrofitting of existing ships may be very costly and represents a limiting factor.
- Dealing with engine exhaust emissions, hot gas and water streams requires many crew safety considerations, and the operation of the whole facility will need to be constantly monitored. Training, maintenance and managerial issues will be time consuming for the crew. System controls, however, could eliminate the need for manual PBR operation.
- Finally, the overall sustainability of the proposal is an issue. The R&D challenges suggested by the National Algal Biofuels Technology Roadmap (Fishman et al., 2010) include the environmental risks and impacts of algal

cultivation. An integrated estimation of the sustainability of algal PBR implementation will contribute to a critical evaluation of the overall CO_2 reduction and sustainable biomass production, this being the main purpose of this implementation.

2.4.2 Opportunities

Although there are many challenges in implementation of a shipboard algal PBR, there are arguments on the other side that support this project:

1. **Regulations**. Business opportunities in carbon capture and biofuel production exist for CO_2 emitters, such as regulations and carbon prices to be imposed (2.2.1.2). The high costs of PBR systems may well be surpassed in the near future by the imposition of high carbon taxes. For instance, if CO_2 limits are implemented for ships (2.2.1.2), then ships which exceed those limits will have to either buy costly permits for their excess emissions or install on board carbon capture and storage. The carbon capture system may be sized to capture only the excessive emissions (beyond the limit) rather than the whole amount. A PBR system would have the added advantage of being able to reduce the NO_x emissions (2.3.2.4).
2. **Know-how on scrubbers**. Existing know-how of HEs required for SO_x scrubbers (2.2.1.3) is an opportunity for the successful development of a PBR.
3. **Waste streams utilisation**. Treatment of wastewater or food waste products of the ships, including biogas and digestate (2.2.2) could provide considerable potential for the operation of the PBR during the hours that the main engines are not working and not providing CO_2.
4. **Biomass utilisation**. The production of a valuable product, either for use on board (e.g., emulsified biomass in the fuel) or for treatment on-shore for more valuable products (2.3.2.4), would counter-balance the extra costs of operating the PBR.
5. **Integration of HE with water provision system**. It is vital, not only for the bioremediation system, but also for the sustainability of the ship, to design an integrated heat exchange system. It could take advantage of a novel fresh-water-from-brackish provision system and would provide low cost freshwater for the PBR and the needs of the ship, as well as cooling to the

flue gas to enter the PBR and heating the water of the PBR (2.3.2.3) when the ambient temperature is not adequate.

3 Research questions and approach

3.1 Research questions

The aim of the project was to analyse and investigate technical challenges associated with developing a commercially viable shipboard algal PBR system, for the treatment of flue gas emissions from the engine. The literature review in Chapter 2 has identified the key challenges associated with the implementation of a shipboard algal bioreactor. The questions addressed by the research are:

Research question 1 (addressed in Chapter 4): How can a PBR be customised for shipboard carbon capture (see 2.4, challenges 1, 2, 3 and 5)? Three subquestions were addressed as part of this question:

- Which PBR designs are suitable for shipboard carbon capture (2.4, challenges 3 and 5)?
- What is the effect of high concentrations of NO_x and SO_x in the flue gas and water salinity variations, which are typical marine conditions, on the PBR (2.4, challenges 1 and 5)?
- Is it feasible to cultivate wild algae samples for use in a PBR (2.4, challenge 2)?

Research question 2 (addressed in Chapter 5): How does the PBR design affect the hydrodynamics of the PBR and its efficiency (2.4, challenge 5)? Subquestions were:

- How does bubble size affect the gas hold-up and liquid velocity in the selected airlift-type PBR?
- How can the effect of the bubble size help in dimensioning of the PBR to attain desired gas hold-up and liquid velocity levels?

Research question 3 (addressed in Chapter 6): How could algal growth be predicted in a system with multiple growth-limiting factors and the model be used to improve productivity and water volume requirements (2.4, challenges 3 and 5)? There were two subquestions:

- How can an algal growth kinetics model, taking into account various factors affecting the algal growth, be developed and validated?

- Can the model be used to control concentration of nutrients and optimise biomass production and water volume requirements?

Research question 4 (addressed in Chapter 7): What are the practical aspects of the shipboard integration of the PBR (2.4, challenge 1, 4 and 6)? Four subquestions were considered:

- Can the water requirements of an algal PBR to fully treat ship CO_2 emissions be accommodated in the ballast tanks of typical ships that are currently part of the global fleet (2.4 challenge 1 and 6)?
- How can the PBR HE be integrated into a flue gas cooling system for the provision of heating during engine non-operating hours at a reduced operating cost (2.4, challenges 4 and 6)?
- How do the flue gas flow rate and the liquid velocity affect the heat loss from the PBR (2.4, challenge 4)?
- How can the temperature of the PBR be controlled (2.4 challenge 4)? Is adjusting the temperature of the sparged flue gas adequate for heating the PBR or is there a better alternative?

3.2 Approach

This study is the first to examine PBR implementation on a ship for carbon capture and the research was approached by discretising it based on the research questions, which cover different aspects of the challenges.

The PBR design was investigated in relation to a future small scale implementation on the deck of Octoply's vessel MV Sound (Figure II.1 to Figure II.3 of Appendix II), thus providing easy access for experiments to examine the effect of exhaust on the PBR and of the PBR on the ship performance. Two test PBRs were constructed, one at the Camley Street Park pilot microanaerobic digestion site (in collaboration with Community by Design; LEAP, n.d.), and the other on the vessel Tamesis in the Thames (in collaboration with Octoply). The Tamesis is a former Dutch cargo barge that is currently used as a bar and is permanently moored on the Thames (in Vauxhall area), with ready access to shore services including water and electricity. It is easily accessible and secured to two piles, making it a practical site to test out some of the design aspects being investigated.

In Chapter 4 the effects of the NO_x and SO_x in the flue gas, as well as the water salinity, on algae were approached through a literature review, concluding with a

number of points for further research. The cultivation of wild algae samples obtained from London's waterways (the example city of this case study) was examined in a short series of experiments. Their productivity was compared with that of commercial algae and results led to a conclusion on the advisability of using algae from local waters in the PBR.

In relation to the PBR design suggested in Chapter 4, the following three chapters then present three models developed to simulate different aspects of this design, though they can be extended to be applied to modified designs too. The hydrodynamic model from first principles was coded in the MATLAB environment and takes into account the effect of bubble size, which is known to be an important variable for optimising gas absorption and energy input. It estimates the gas hold-up and liquid velocity for use in the dimensioning of the PBR. The liquid velocity will also be an input variable for the estimation of the PBR temperature when it is integrated with the proposed heat exchanger design.

The next model, on algal growth kinetics, taking into account various factors affecting algae growth, is built in the gPROMS environment with the purpose of optimising productivity by controlling the operating conditions of the system. It incorporated the effect of three different factors and its calibration proved to be difficult due to its complexity. It was therefore simplified using parameter values from the literature.

A rough estimation of the space requirements was computed. Ballast capacities of ships were considered as potential space to locate the PBRs, using data for tankers and ferries from the Clarkson's World Fleet Register database. This led to overall conclusions about the ship types that are most appropriate for the implementation, based on their emissions, size and style of operation.

The final model simulates a heat exchanger design suggested for the PBR. The flow rate of the broth fluid is computed from the liquid velocity estimated in Chapter 5. The practical aspects of PBR integration to the ship are investigated. A flow sheet model of potential integration of the heat exchanger into a WHR system is designed in gPROMS, to provide an overall idea of the effect of the flow rates selected on the effectiveness of PBR heating during the engine's non-operating hours.

4 Photobioreactor design modifications for shipboard carbon capture

4.1 Introduction

Regarding the first set of research questions (3.1), this chapter identifies a suitable PBR design to implement onboard a ship for future use in practical carbon capture experiments. It also examines the effect of the conditions within the ship and the surrounding marine environment that would affect the PBR. In detail, the chapter explores the following issues:

i) The design considered practical aspects related to the effectiveness of CO_2 capture. As an initial attempt, a prototype PBR system was designed and installed at the site of the Camley Street Park, and a deck mounted copy of it was installed on Tamesis (3.2). This approach aims to first test the design on land and to later try it on a small stable vessel, to understand and map the complexity of the system, in order to allow future work for the test of a vessel that moves. The purpose of building the reactor on board was to allow experiments to be conducted and future examination of the effect of the flue gas on the PBR, and the effect of the PBR on the operation of the ship.

ii) The effect of tube inclination on bubble size was studied to identify the desired angle for the helical bioreactor and flue gas flow rates to facilitate mass transfer between the gas CO_2 and the liquid. Tube inclination is a characteristic of not only different helical PBR design modifications, but also the ship movements due to sea conditions.

iii) Also, the effects of the high SO_x and NO_x in the flue gas on the algal growth are considered and algae's tolerance limits are studied by examining previous literature.

iv) The effect of the water salinity on the algal growth and products is discussed to assess the feasibility of using surrounding water from the ships voyage waters for the algal cultivation.

v) Samples of natural waters from several sites in London were obtained and naturally occurring algae in them were cultivated in the lab to examine the potential for the onboard PBR to use wild algae from the surrounding water of the ship. The responses of the wild algae in the different water samples

towards different combinations of CO_2 concentration and gas flow rates were studied. Some of the species grown in the different experiments were isolated and identified, as knowledge on the species grown in London's waterways is limited.

4.2 Proposed photobioreactor design

4.2.1 Photobioreactor design concept

As concluded in 2.3.5.3.1, the tubular helical airlift design was chosen as a concept that would be suited for a small vessel with deck space, and that could have aesthetic appeal (which is important in relation to Octoply's business). It was used for the pilot PBR onboard Tamesis (design is shown in Figure 4.1), though that one was not conical shape (as suggested in 2.3.5.3.1), as this would have complicated its construction. The PBR was installed on an available part of the deck to increase photosynthetic efficiency and decrease lighting needs. Figure III.1 and Figure III.2 of Appendix III demonstrate the PBRs installed at Camley Street Park and onboard Tamesis. The two reactors constructed were identical, with minor variations of the inclination and turn degrees of the helix close to the fittings.

The PBR helices were made of flexible polyvinyl chloride tubing, their downcomers and degassers were rigid clear polyvinyl chloride-u (resistant to degradation by ultraviolet light), as were the fittings. Ambient air was inserted by an air compressor (Hailea AC0-009E 112W), of maximum output 140 L/min and minimum pressure output 0.035 MPa, via a gas flow meter and a 35 mm x 50 mm ceramic air stone sparger connected by 5 mm diameter piping. The treated gas outlets were at the top of the riser and via a hole drilled at the top of the degasser. The PBR dimensions listed in Table 4.1 were chosen to provide a volume of 10 L with a small enough tube diameter for adequate light penetration. An 1.3 m downcomer was selected, which corresponds to a moderate hydrostatic pressure (approximately 30 kPa lower compared to the same volume placed vertically). The inclination was chosen as 40° from the horizontal, to provide 3 loops of the helix for the given height. The degasser diameter was twice that of the downcomer, to decrease the linear liquid velocity and allow the liquid more time to release its accumulated O_2.

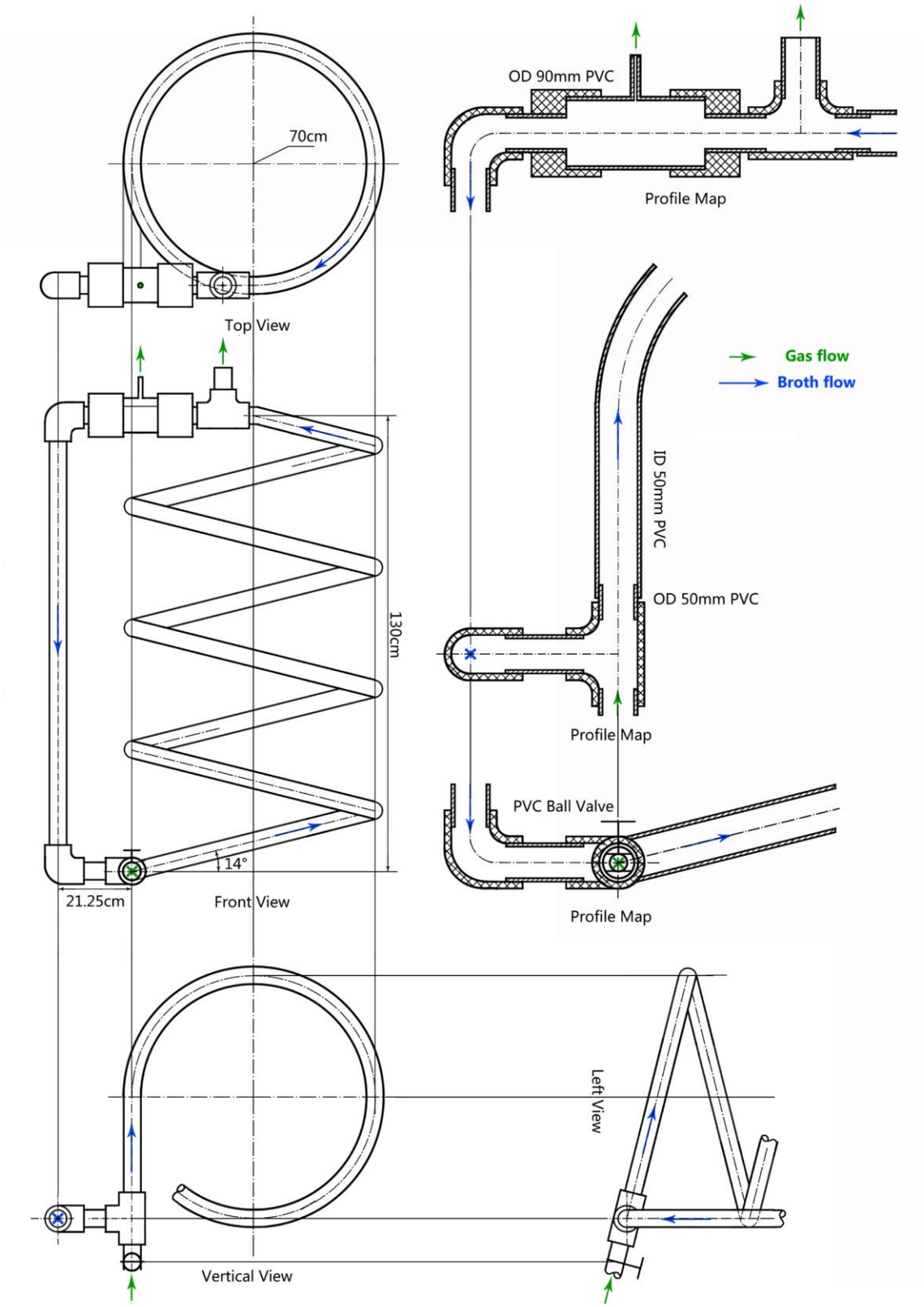

Figure 4.1.Hybrid helical airlift design for the pilot-scale PBR.

Table 4.1. Dimensions of the two pilot hybrid helical airlift photobioreactors.

	Dimensions (m) of the PBRs constructed
Helix length	~3.00
Downcomer length	1.30
Degasser length	0.30
Total length	~4.60
Helix tube inner diameter	0.05
Downcomer inner diameter	0.05
Degasser inner diameter	0.09
Number of helix turns	2.5
Elevation from horizontal	40°

Both pilot PBRs leaked, necessitating water to be added periodically into the system, mainly due to the connection of the flexible inclined tube to the fittings. This would be possible to be fixed with proper construction work. On running the system, gas bubbles were found to coalesce at the end of the first loop of the PBR as shown in Figure III.1 of Appendix III. The coalescence was due to the low inclination of the tubing from the horizontal, as the wall became an obstacle to the vertical rise of the bubbles, causing them to merge. Although bubbles coalesced in the first loop of the helix, they were able to induce recirculation to the liquid. The time taken for the liquid recirculation was measured by observing circulation of food dye added at the top of the riser. One recirculation took approximately 50 seconds which corresponds to a recirculation velocity of 0.092 m/s. Nevertheless, bubble coalescence reduces the surface area for mass transfer between the gas and liquid, and therefore reduces the efficiency of CO_2 fixation.

4.2.2 Examination of the effect of inclination on the bubble coalescence

4.2.2.1 Method

A series of experiments were conducted with the help of an MSc student (He, 2014), to determine the inclination of the PBR above which the bubbles stopped coalescing. To simplify these experiments, a straight rigid bubble column was used. The 0.5 m long transparent polyvinyl chloride-u column tube with inner diameter 0.045 m and approximate thickness of 0.005 m was supported by a metal clamp holder and tested at the inclinations 20°, 30°, 40°, 50° and 60° from the horizontal, as shown in Figure 4.2. The bubble sizes were measured at various flow rates ranging from 0.1

L/min, which was the minimum flow rate regulated by the flow meter, up to 1.5 L/min, above which bubbles had a spherical cap shape (values shown in Table III.1 of Appendix III and Figure 4.3). The bubbles were measured by photographing them with a Canon camera, first placed 1 cm above the sparger (to measure the bubbles at the bottom of the column) and near the surface of the water, in approximately 0.4 m distance from the first camera (to measure the bubbles at the top of the column). The effect of refraction was less than 10% based on comparative measurements using a ruler as a reference. Bubble size was taken as the average diameter of the bubbles taken in each photo.

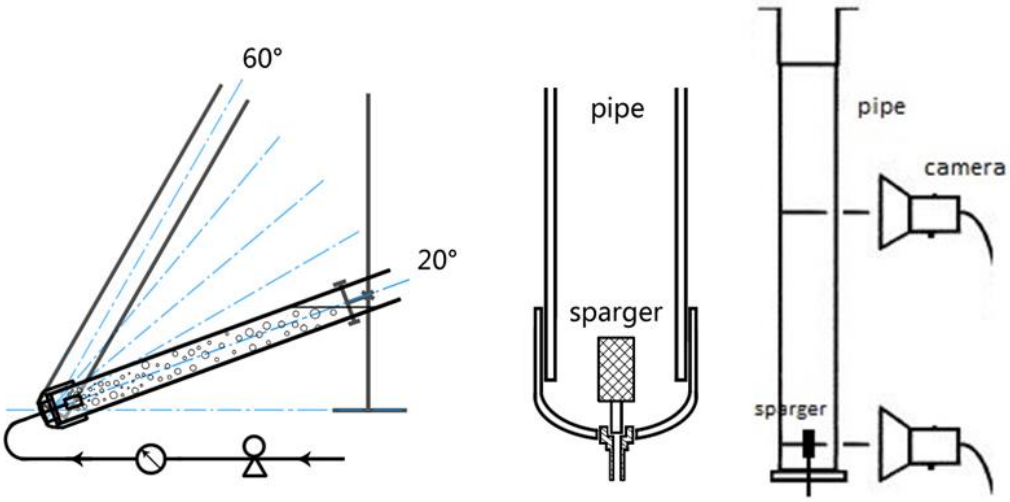

Figure 4.2. Bubble column apparatus tested at different inclinations.

4.2.2.2 Results and Discussion

The average sizes of the bubbles photographed at each inclination and area of the column for various gas flow rates are shown in Figure 4.3 (data taken from Table III.1 of Appendix III). Example photo representing the bubble measuring method is shown in Figure 5.6 of the next chapter.

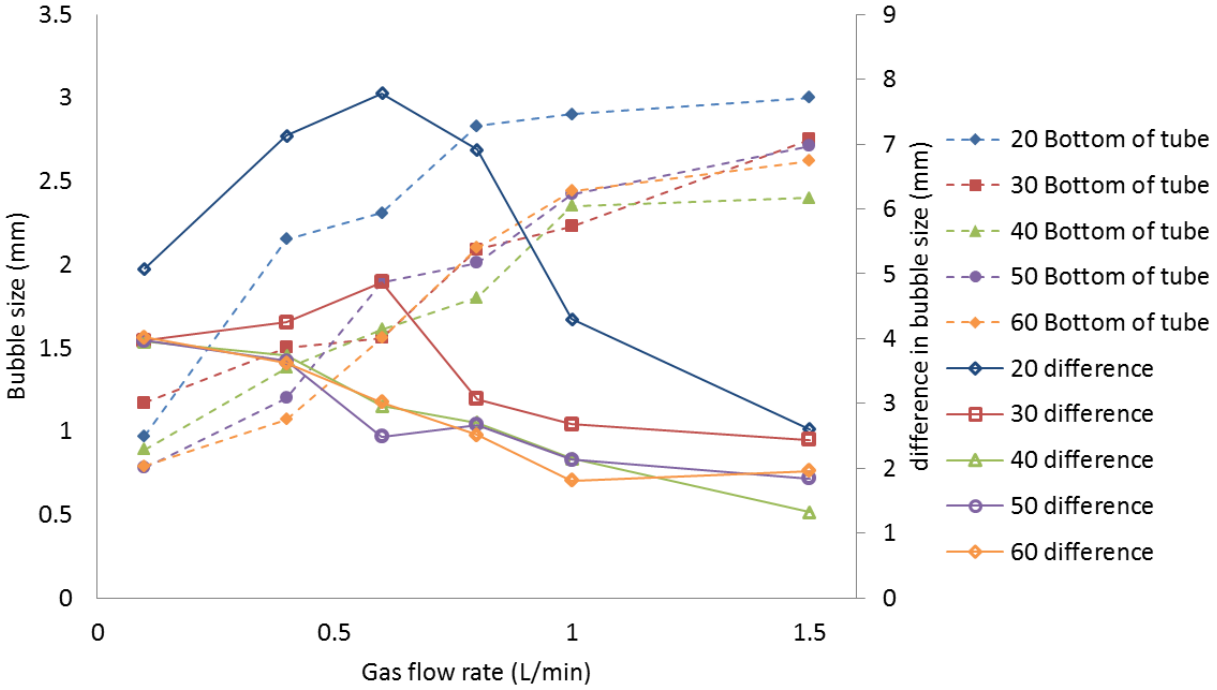

Figure 4.3. Bubble size (primary ordinate) at the bottom of the tube, and difference in bubble size (secondary ordinate) between the top and bottom of the column, as a function of gas flow rates for five different inclinations (°) from the horizontal. Lines joining points are for visual clarity and do not represent a known physical reality.

In general, bubble size increased with the gas flow rate for all inclinations. The bubble size difference between the top and bottom of the column decreases with gas flow rate increase, which could be attributed either to the greater number of bubbles being detached from the sparger at increased turbulence, or to the splitting of the large bubbles produced at high flow rates after obtaining a potential maximum size allowed for each turbulence. 2-way analysis of variance (ANOVA) P-values showed significant effect of both the gas flow rates (P-values 2.2×10^{-11} and 0.00027, respectively) and the inclinations (P-values 8.2×10^{-5} and 9.4×10^{-6}) on both the bottom bubble sizes and their difference from the top bubble sizes. In conclusion, the increase in average bubble size between the bottom and top of the column is similar for inclinations greater than 40°, implying that beyond this limit major coalescence due to inclination stops being significant for the given reactor length. However, significant coalescence was actually observed in the actual helical PBR constructed with 40° inclination (4.2.1) for all flow rates below 1.5 L/min. Verification of the results could be done with the use a helical airlift apparatus, as coalescence might behave differently under the different liquid velocities induced in the two designs. Also, continuous captures of the bubbles with a high-speed camera would allow – in addition to the bubble size measurement –

verification of not only whether there are coalesced bubbles at inclinations above 40°, but also the reason for the decrease in bubble size difference at the high flow rates (hence, if there are bubbles being split along the tube).

Average bubble size increased by up to 100% at the 20° inclination at low flow rates. This increase is translated as a 57% decrease in surface area (320 mm^2 and 60 mm^2 bubble surface for inclination 20° and 50°, respectively, at 0.6 L/min) of a given gas volume. This increase of the bubble size difference and its decrease at higher flow rates, suggests that bubble coalescence starts only above a flow rate that produces enough bubbles that they find each other during their travel; any bubble size difference occurring below this flow rate could just be a gas expansion effect. Coalescence would imply wasted energy in compression of the gas to form small bubbles which end by coalescing. On the other hand, increasing the inclination with a given PBR volume increases the compression energy required to counter the high hydrostatic pressure, plus it moves the centre of gravity of the PBR higher which could create stability issues for a shipboard application. This confirms the statement in 2.3.3.2.2 that bubble coalescence is one of the main problems with the conical helical systems. Therefore, scale-out would require an increase in the number of harvesting units, perhaps by adding more helices on the same frame connected in parallel to a bigger manifold to save space.

Further analysis of the effect of coalescence, bubble size and inclination on the hydrodynamics of a PBR, and of the CO_2 mass transfer from the gas to the liquid, are needed. Also, a better measuring technique for bubble volume is required, as a limitation with using only photographic techniques is known. A more sophisticated approach involves laser illumination of a plane of liquid containing fluorescent dye, to revealing the bubbles within that plane. This, coupled with image processing, offers a more automated and potentially more accurate approach to bubble sizing and counting (Busciglio et al., 2013). The effect of bubble size on the fluid dynamics of an airlift PBR is studied in Chapter 5.

4.3 Tolerance of algae to nitrogen and sulphur oxides

4.3.1 Introduction

The tolerance to CO_2, NO_x and SO_x exhaust is particularly important for the shipboard implementation of a PBR for emissions fixation, considering the higher concentrations emitted from ships (1500 mg/kg and 600 mg/kg NO_x and SO_x) as compared with land-based power plants (2.2.1.1). Algal species tested by Zeiler et al. (1995) and Nagase et al. (1998) were found not to tolerate NO_x and SO_x concentrations exceeding 1,000 mg/kg and 200 mg/kg respectively (Chiu et al., 2011; Lee et al., 2000; Matsumoto et al., 1995; Ono & Cuello, 2001; Zeiler et al., 1995). There is a lack of work on the effect of the different flue gas toxic compounds on different algal species and the operating conditions, such as gas flow rates, media initial concentration, controlled pH in the broth (Lee et al., 2000). CO_2 and NO_x are included in the nutrients of algae (2.3.2.4), however, excessive CO_2, NO_x and SO_x are found to have a toxic effect on the growth (tolerance of various species is summarised in Table III.2 of Appendix III).

4.3.2 Nitrogen oxides

It is reported that gaseous NO dissolves in the algal broth and can diffuse across the cell membrane (Chiu et al., 2011). NO absorbed by the medium can then be transformed to NO_2^- and be further oxidised to NO_3^- and utilised as a nitrate source, as verified by Nagase et al. (2001) using *Dunaliella tertiolecta*. Some algal species are able to grow well under a concentration of 100 mg/kg NO, including *Nannochloris sp.* and *Dunaliella tertiolecta,* which was able to remove 51 – 96% of NO, when fed with 15% CO_2 (Nagase et al., 1998; Oilgae, n.d.-a). *Tetraselmis sp.* is reported to grow under conditions of 125 mg/kg NO_x, 185 mg/kg SO_x and 14.1% CO_2 (Matsumoto et al., 1995). The removal efficiency of NO by *Chlorella sp*. MTF-7 cultures of 2 gL^{-1} biomass cultivation with flue gas can range from 60 – 100% (Chiu et al., 2011).

High density cultures outweigh the toxic effect of NO, and then NO can contribute as a nitrate source (Chiu et al., 2011). For instance, Yoshihara (1996) found that strain *NOA-113* with a cell concentration of 1.5 $g{\cdot}L^{-1}$, grew and retained almost 50% NO when fed by a simulated flue gas containing up to 300 mg/kg NO_x at flow rates lower than 300 mL/min. Change in media pH is suggested as the fundamental cause of the toxicity. Controlling media pH is a reported way to overcome toxic effects. For instance, Lee et al. (2000) found that productivity of a culture fed with NO_x-free gas was

equivalent to that of a culture fed with 300 mg/kg NO_x gas when the pH was adjusted to within tolerable limits (2.3.2.5) with NaOH.

4.3.3 Sulphur oxides

The main form of SO_x found in the flue gas is SO_2. If the flue gas is directly introduced to the culture, SO_x forms sulphurous acid and can decrease the pH to 2 or 1 (Kumar et al., 2011; Packer, 2009). Oxidative traces of bisulphite (HSO_3^-), sulphite (SO_3^{2-}) and sulphate (SO_4^{2-}) formed from SO_2 can lead to peroxidation of membrane lipids and bleaching of chlorophyll (Chiu et al., 2011). Different *Chlorella* species show different tolerance levels to this gas compound. For example, it has been reported that the growth of *Chlorella HA-1* is completely inhibited by SO_2 concentrations higher than 50 mg/kg, whereas isolated mutant strain *Chlorella sp.* MTF-7, with initial biomass concentration 0.5 g L^{-1}, grew well in indoor cultures in presence of gas containing 90 mg/kg SO_2 (Chiu et al., 2011).

Similarly to the case of NO_x, suppressed growth of the *Chlorella KR-1* strain at SO_2 concentration higher than 150 mg/kg was found to be overcome by a five-fold increase in initial biomass concentration (Chiu et al., 2011). Also, controlling pH by adding NaOH solution achieved approximately the same productivity as for feeding with SO_2-free gas (Lee et al., 2000). Also, acidophilic algae are resistant to SO_2, e.g., *Cyanidium caladrium,* which shows growth for the first 20 h under 200 mg/kg SO_2 (Kurano et al., 1995).

Removal efficiency of SO_2 by *Chlorella sp*. MTF-7 cultures of 2 gL^{-1} biomass cultivation under flue gas aeration can range from 40 to 80% (Chiu et al., 2011). Most land-based power stations are equipped with a desulphurisation unit to control SO_x below 100 mg/kg, although some algal species seem to be able to capture the three components from raw flue gas (Chiu et al., 2011). However, concentrations close to 600 mg/kg have not been widely tested (Chiu et al., 2011; Lee et al., 2000; Matsumoto et al., 1995; Ono & Cuello, 2001; Zeiler et al., 1995). The ship exhaust which is characterised by even higher SO_x concentration would have to pass through a SO_x scrubber before its entry to the PBR in order to ensure good continuous algal growth.

4.4 Effect of salinity conditions on algal growth

4.4.1 Introduction

Algae can grow in fresh water, saline or brackish water (2.3.2.1). The growth, CO_2 sequestration rate and harvesting of different species is affected by salinity, which will affect the potential for cultivation of algae in a shipboard PBR (2.3.2.1). Different algal species and strains differ in their responses to salinity and other stress conditions (2.3.2.1). Adaptive mechanisms that make cells survive under the influence of environmental stresses include changes in morphological form as well as in metabolic processes (Borgvang, 2011; Hiremath & Mathad, 2010; Kirst, 1989; Ruangsomboon, 2011).

The effect of salinity is important even in land-based algal PBRs, in which salinity increases due to evaporative water loss, and the use of freshwater supplies is a major concern for biofuel production. However, it is particularly important in relation to operation of an algal PBR on a ship since freshwater becomes an even more valuable resource off-shore. The ability to cultivate algae in ocean water gives a big advantage. The algae industry recently revealed a study by the University of California at San Diego, has shown that marine algae can be as capable as freshwater algae for biofuel production (Algal Biomass Organisation, 2012).

The most important cell characteristics that have been reported to be influenced by salt levels are mentioned in 2.3.2.1. The impact of salt concentration on algae growth could be either detrimental or beneficial (for example some freshwater species maximize some of their growth parameters with slight increase of salinity), depending on the algal preferences, as shown in the following sections. In addition to the direct effects on algal growth, there are other indirect impacts that mostly affect the cost of the process. For instance, if algae are grown in saltwater, the need to wash the salt off the biomass and to pass it through a filter press or centrifuge for a second time is costly and energy consuming (Alabi et al., 2009).

To understand the influence of salinity on algal growth, the following section reviews experimental data from the some species, focusing on both marine and freshwater species of the *Chlorella* genera, many of which show high levels of lipid content (2.3.2.1). This study summarises the effects reported for these response of compounds and also includes effects on CO_2 and O_2 concentrations of the water.

4.4.2 Tolerance of algae to salinity

Microalgal species can generally be divided into two categories based on whether they grow optimally in freshwater or saltwater. Salt levels affect the productivity and the individual production rates of lipids and carbohydrates in each strain of algae (Kunjapur & Eldridge, 2010). However, algae have shown several other responses to salinity changes. Marine microalgae are very tolerant to changes in salt concentration, but most species are cultured in diluted seawater because they grow best at a salt concentration that is slightly lower than that of their native habitat (Lavens & Sorgeloos, 1996).

The reason why algae are affected by salinity in the media is controversial. Some, such as Alyabyev et al. (2007), support that the influence is based on the Na^+ and Cl^- ions and others base it on the osmotic pressure effect (Greenway & Setter, 1979). Irrespective of the osmotic substance used, either NaCl or raffinose osmotica (non-ionic), a similar growth reduction was shown (Setter & Kuo, 1982). Kirst (1989) examined the effect of two forms of osmotic stress, dehydration and salinity, on photosynthesis of various species. Both stresses reduce water potential within the cell, resulting in an increase in the cellular ionic strength. However, during desiccation, the ion proportions remained constant, whereas under salinity stress there were changes in ion ratios owing to selective uptake. Kirst assumed that osmotic stress increases algae permeability to ions and observations with *Dunaliella* showed that ionic stress is a greater inhibitor of growth than osmotic stress (osmotic substances can sometimes be non-ionic as reported in Lloret et al., 1995). Thus, the explanation for growth reductions under high salinity might be species specific, and there is a lack of understanding of the reaction mechanisms.

Generally, the optimal salinity range for most algal species, including marine and freshwater, is *12 – 40 gL^{-1}* and a more specific salinity range of *20 – 24 gL^{-1}* has been proposed to be optimal by Lavens and Sorgeloos (1996). However, the range is species specific (some optimal salinities for maximum productivity and salinities tolerated for various species are shown in Table III.3 of Appendix III), and sometimes strain specific, as there are genera such as *Chlorella* and *Chlamydomonas*, which have both freshwater and marine species (Wetherell, 1961). Consequently, the variance in the ranges might either be attributed to the tolerance of the different strains of each species, or hide the influence of the environmental conditions to the tolerance levels of the strains. Indeed, the limits of tolerance have been reported to change with changes in environmental conditions. For instance, tests of 13 species cultured in dilutions with

freshwater, made by Wetherell et al. (1961), showed that when seawater was enriched with appropriate concentrations of nitrate, phosphate and iron salts and when pH was reduced in order to prevent precipitation of the nutrients, algae culture had grown satisfactorily. However, the addition of a variety of organic substances was reported not to alter the tolerance limits (Wetherell, 1961).

The most successful commercially used genera are *Dunaliella*, *Spirulina* and *Chlorella*, because they can all tolerate and bloom in extreme environments and inhibit competition. These genera are shown to grow in environments with raised salinity, alkalinity and nutrients, respectively, conditions which would be intolerable for other species (Aitken & Antizar-Ladislao, 2012; Kunjapur & Eldridge, 2010).

4.4.3 Response of algae to salinity changes

The response of the algae to changes in salinity is a controlled two-phase osmotic acclimation process, where water fluxes cause pressure and volume changes to the cells and then osmolytes are adjusted to a new steady state (Kirst, 1989). An important characteristic of the salt-tolerant microorganisms is their adaption to NaCl stresses without using all their energy capabilities to maintain their structural-functional integrity. This can be illustrated by the change in heat production of algae in different salinities, which, for instance, increased in the salt-tolerant *Dunaliella* cells in conditions up to 116 g/L salt in the medium (Alyabyev et al., 2007).

The parameters that have been repeatedly reported to respond to salinity changes include: (a) growth rate, (b) photosynthesis-respiration and (c) concentration of various compounds in the cells, such as the lipid content. The first two are related, as growth rate is the combination of photosynthesis and respiration, as mentioned in 2.3.2. Further:

a. Growth rate is affected because the availability of certain ions, such as K^+ and Ca^{2+} may govern or affect growth. The presence of Ca^{2+} has been found to increase the salinity tolerance limits (Kirst, 1989).
b. Photosynthesis in species with strong cell walls has appeared to be less sensitive to extensive hypoosmotic shocks (e.g., *Stichococcus bacillaris*) according to Kirst (1989), while most wall-less species appear to be more sensitive.
c. The effect on the fine structure of the cell due to osmotic stress mainly causes compartmentation by the development of vacuoles (Kirst, 1989). Increase in

salt content increases carotenogenesis and enhances metal assimilation (Kalesh & Nair, 2005), which would also mean higher heavy metal scrubbing from the flue gas. Also the lipid content is influenced by salinity, but the impact varies with the cultures. For example, an increase in salinity may result in a slight increase in lipid content of Botryococcus braunii, but, Botryococcus braunii KMITL 2 cultured in Chlorella broth showed higher lipid content with no salinity, compared to salinities of 5, 10, 15 and 20 gL^{-1} (Ruangsomboon, 2011). Thus, salinity stress does not increase lipid yield in all algal strains and there is no overall correlation between lipid content and growth in a fresh or salt water environment.

4.4.4 Special tolerant algae types

Some algal species are able to adapt to higher salinities and tolerate wider ranges and are called halotolerant (such as *Dunaliella salina* tolerating from 3 gL^{-1} to over 280 gL^{-1} NaCl). According to Alyabyev et al. (2007), this might be due to the ability of those cells to pump out Na^+ ions more effectively, or to the mechanism of regulation of osmotic pressure (Araújo et al., 2009).

Under physiological stresses that retard cell growth, such as high light intensities, high salinities, high temperatures and high nutrient deficiencies (sulphate or nitrate limitation), b-carotene accumulation was shown to be induced, resulting in an increase of up to 14% of the alga dry weight (Araújo et al., 2009). Halotolerant *Dunaliella maritime* adapts to high salinity; with NaCl concentration increase, the O_2 uptake rate and heat production from this species increased as well (Alyabyev et al., 2007).

However, the influence of the salt concentration on halotolerant species depends on other factors as well. For instance, the salinity range of 58 – 174 gL^{-1} affected *Dunaliella salina*‘s specific growth rate for only one of two different light intensities, which could imply that the other intensity used was a more important limiting factor than the salinity. Similar effects were observed for two different temperatures and three different salinities on the photochemical yield of *Dunaliella* species (Araújo et al., 2009). Also, lower thermal inhibition under salinity increase was observed in Henley et al.'s (2002) study on photochemical yield of the halotolerant species *Dunaliella sp. Teodoresco and Nannochloris sp. Naumann*. Although analysis becomes very complex with additional growth affecting factors, Henley’s et al. results could explain the observations of Araújo et al. (2009) for *Dunaliella* which shows a two-fold increase in

the specific growth rate with salinity and irradiance increase, since the increased irradiance may result in higher temperature.

Algae grown in polar regions are also noteworthy, since they tolerate very harsh conditions, including variation in salt levels in the surface, interior and bottom of ice assemblages, and during the seasons (Kirst, 1989). The salinity conditions in the seawater-snow-ice interface and the pools on the ice surface vary from hyperosmotic seawater levels in winter down to about 3 gL^{-1} when ice melts. Conditions in interior assemblages show temperatures as low as -5 °C resulting in more than 100 gL^{-1} NaCl. Bottom assemblages grow between ice crystals and platelets, where salinity is about 29 gL^{-1} to 34 gL^{-1} (close to seawater). Despite the increased salinity, the low temperatures and the reduced volume in brines due to freezing in all those areas, they are densely populated with algae. This might be due to enrichment in nutrients during freezing, and to antifreezing properties of antiosmotic compounds such as proline and glycerol (Kirst, 1989).

4.4.5 Effects of salinity on *Chlorella*

The effect of salt levels on the growth rate, photosynthesis rate, heat production and content of other compounds of the specific algae genera of interest, *Chlorella sp*. (explained in 2.3.2.1), is different for the different species. Cho et al. (2007) found that among the salinities they used in their experiments, the lowest one, *10* gL^{-1}, was the optimal salinity for *Chlorella ellipsoidea*, but also observed its tolerance to higher temperatures and salinities. Other studies on *Chlorella sp*. and *Chlorella virginica* showed optimal biomass growth for salinities of 14 and 15 gL^{-1}, respectively, for a tested range of 0 to 40 gL^{-1} (Alias, 1988; Makarevičienė et al., 2011; Shah et al., 2003). Regarding the CO_2 sequestration efficiency, which roughly corresponds to the growth rate, it can be provisionally concluded that an average optimal salinity is 14 gL^{-1}. This could indicate good growth under the shipboard PBR conditions, with heating provided by high temperature flue gas and use of seawater as the medium.

The total chlorophyll content – hence, the photosynthetic rate – is also reported to benefit from similar salinity levels (Hiremath & Mathad, 2010). Comparison of *Chlorella sp. XQ-200419* and *Chlorella marina NJ-016* at a salinity increase from 0 to 34.8 gL^{-1} has shown that net photosynthetic O_2 evolution decreased for the former, while it increased for the latter (Zheng-Rong et al., 2010). Alyabyev et al. (2007) determined the effect of NaCl level on the respiration of *Chlorella vulgaris*, by measuring the O_2

uptake. At low salt concentrations down to 2.9 gL^{-1}, there was some increase of the O_2 uptake rate by the cells which decreased with salinity increase of up to 58 gL^{-1}.

Decrease in chlorophyll and protein content with cultivation in high saline concentrations was observed, whereas b-carotene, carbohydrates and the compound of defense – glycine betaine (glucogenic amino acid that triggers chloride ion influx) – showed a maximum at *30.7* gL^{-1} (Hiremath & Mathad, 2010). Apparently, the concentrations of such compounds are higher in *Chlorella* strains that are more tolerant to salinity (Kalinkina & Naumova, 1992; Li & Li, 2011). The preference of *Chlorella* species for low salinity was confirmed by an investigation of the heat production by *Chlorella vulgaris*. Alyabyev et al. (2007) found that heat production of the species at a NaCl concentration of 29 gL^{-1}, was lower than that at 2.9 gL^{-1}. Combined Na^+ and Ca^{2+} addition increases photosynthetic rate in this species under salinity stress but reduces respiration and proline content, compared to net NaCl addition (Abdel-Basset, 1993). Therefore, addition of Ca^{2+} could control the growth of the shipboard PBR, to maximize CO_2 absorption at potential salinity increase after evaporation losses.

There is great quantity of experimental results on the response of various *Chlorella's* compounds to salt changes, but there is a lack of information about the lipid content changes with salinity increase, which is important for the evaluation of the potential for biofuel production from the species. Table 4.2 shows the changes in physiology and metabolism that occur as a result of salinity stress on some commonly studied algal species. Different organisms have a different response, which could possibly be due to an inhibition to metabolic reactions that are helpful for the survival (Alyabyev et al., 2007). The missing characteristics from some rows presenting each species just imply a gap in the literature search rather than an absent response to salinity changes. Some of these changes are either common responses or are generated under different conditions that might have affected the outcome; thus, it is difficult to summarise results. The table is to be treated as a source for looking further into this subject as opposed to being a summary of stress response. *Chlorella* has also been singled out because of its wide use and tolerance to CO_2 (2.3.2.1). Its response to salinity changes is summarised in Figure 4.4. Thus, the studies referenced in this table offer a good starting point for the selection of the best salt concentration from the chart below, for a given application.

Table 4.2. Responses of algal strains and *Chlorella* to high salinity stress, obtained from the literature.

Species	Response	Response at high salinity	Reference
Most strains	Carbohydrates	↑	(Kalinkina & Naumova, 1992; Li & Li, 2011)
	Proline	↑	(Hiremath & Mathad, 2010; Kalinkina & Naumova, 1992; Li & Li, 2011)
	Glycine	↑	(Kalinkina & Naumova, 1992; Li & Li, 2011)
	Carotenoids	↑	(Araújo et al., 2009)
	Lipid content	Depends on strain	(Borgvang, 2011)
	Fine structure	Shrinkage	(Kirst, 1989)
	Metal assimilation	Enhanced	(Kalesh & Nair, 2005)
	CO_2 solubility	↑	(Weissman et al., 1988)
	Cell lysis	↓	(Zemke et al., 2010)
	Flocculation performance	↓	(Sukenik et al., 1988)
Most freshwater *Chlorella* species	b-Carotene	↓	(Hiremath & Mathad, 2010)
	O_2 uptake	↓	(Alyabyev et al., 2007)
	Growth rate	↓	(Makarevičienė et al., 2011)
	Chlorophyll content	↓	(Hiremath & Mathad, 2010)
	Heat production	↓	(Alyabyev et al., 2007)
	Protein content	↓	(Hiremath & Mathad, 2010)
Halotolerant species	Heat tolerance	↑	(Henley et al., 2002)
	O_2 uptake	↑	(Alyabyev et al., 2007)

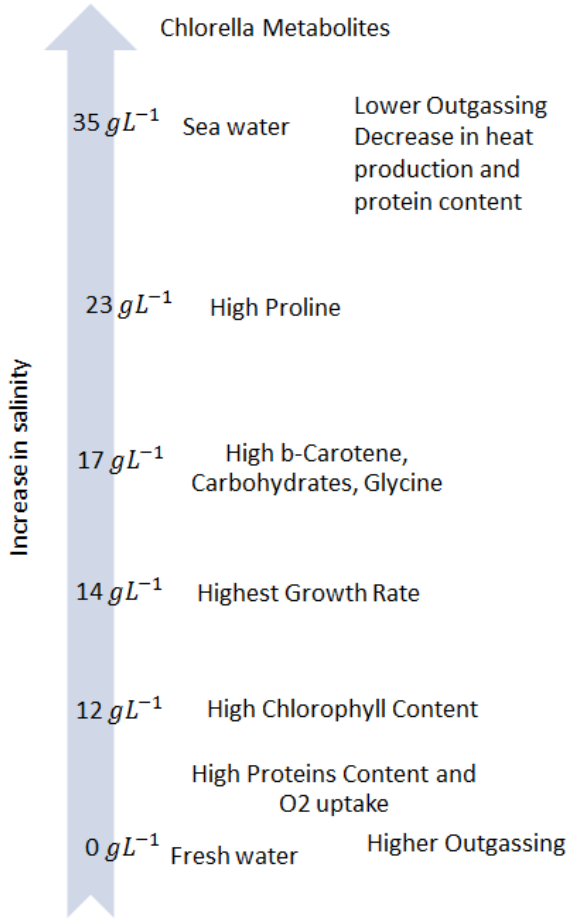

Figure 4.4. Response of *Chlorella sp*. growth characteristics to different salinity levels.

4.4.6 Effects of water salinity on carbon dioxide solubility, fixation and harvesting

In addition to the direct influence of salinity on algal metabolism and consequently on its ability to absorb CO_2, salinity has an impact on the Henry's Law constant for the solubility of CO_2 in water. The decrease of CO_2 in the solution with salinity increase can be calculated as a function of temperature as reported in Valdes et al. study (Valdés et al., 2012). Thus, salinity partially controls dissolution and outgassing rate (2.3.2.4), which determines the CO_2 desorption rate from the media. A study using *Chlorella sp*., reported that outgassing is less in high salinity than in freshwater at a given pH, due to the ionic strength effects on the carbonate equilibrium. However, this was not found to happen at very low CO_2 concentrations, when the outgassing is proportional to alkalinity (Weissman et al., 1988). Therefore, it is difficult to conclude on the exact impact of salinity on the CO_2 fixation by PBRs, since it does not influence solely the algal growth rate, but also dissolution and outgassing rate from the water.

Apart from the CO_2 fixation ability of the PBRs, which is determined by the cells metabolism, gas dissolution and outgassing rate, salinity affects harvesting efficiency too (2.3.2.1). Therefore, there is an indirect factor to consider for an integrated evaluation of the effectiveness of a PBR operation, since harvesting costs and energy consumption might overcome the benefits of high CO_2 fixation. The impact of salt on harvesting might be either beneficial or detrimental. For instance, salt water is sometimes used to wash algae to prevent cell lysis (Zemke et al., 2010), but removing salt from harvested algae might be energy and water intensive, depending on the level of desalting required by the product specifications. Another detrimental impact is that salinity reduces the performance of flocculation with polyesterolytes and requires either high flocculant dosages (5 to 10 times more than in freshwater), or combination of polyesterolytes with inorganic flocculants, or ozone oxidation pretreatment followed by flocculation with inorganic flocculants (Sukenik et al., 1988).

4.4.7 Salinity and wild algae in the Thames

Given that initial implementation of the ship-board PBR is intended for the Thames, the salinity levels along different areas of the river Thames are presented in Table III.4 in Appendix III. As shown, the range along the Thames varies from 0.35 to 32 gL-1, with a salinity of 1.06 gL^{-1} at Woolwich where MV Sound (presented in 3.2 and Appendix II) is based. Daily variations can be attributed to the strong tidal flow of the river which can reach 3 knots. As shown in 4.4.5, the 14 gL-1 optimal salinity level for *Chlorella* species is found in brackish water, therefore the Thames water could be used as the water medium of the shipboard PBR.

However, there is also the potential to use wild algae in a shipboard PBR (introduced in 2.3.5.3.1 and 2.4.1). The main phytoplankton group in rivers is diatoms. Small-celled species also dominate when nutrient concentrations increase. A time series study of phosphorus, nitrate, dissolved reactive silicon and abundance of phytoplankton (measured as chlorophyll-a) of the Thames by Bowes et al. (2012), shows that there is a great fluctuation not only among the years, but during the seasons of a year as well. Another study has used generalized linear modeling (GLM) to predict the response of phytoplankton taxa in the Thames to variation in mean daily discharge rate from the river and during the seasons of the year (Ruse & Love, 1997). The classes that exist in the Thames include Chlorophycae, Cyanobacteria, Centric and Pennate Bacillariophycae and Chryptophycae. Some of the species found growing in the Thames between Inglesham to Windsor have included *Centric*, *Chlorella* oval

small and medium, *Chlorella* round small, *Monoraphidium Contrortum*, *Ankistrodesmus gracilis*, *Chlamydomonas* round and oval small, *Cocconeis placentula*, *Pennate diatom spp*., *Nintzschia acicularis*, *Melosira varians*, *Diatoma vulgare*, *Blue-green sp.2*, *Gomphonema spp*., *Koliella longiseta*, *Monoraphidium minutum*, *Cryptomonas sp.2*, *Spermatozopsis exsultans*, *Rhodomonas minuta* and *Phormidium spp*. (Ruse & Love, 1997). In addition, enteromorpha might play a contributing role in the Thames flora because they are salt tolerant green algae usually found throughout brackish and marine zones (Thames Estuary Partnership Biodiversity Action Group, n.d.).

4.4.8 Discussion

The water supply choice is important for the operation of the PBR and CO_2 uptake rate, if freshwater *Chlorella* species is to be used for cultivation. *Chlorella* species exist in the Thames, alternatively other halotolerant species could better adapt to changes in salinity due to evaporation from the continuous operation of the onboard PBR. Almost all osmolytes and regulating components concentrations in *Chlorella* continue to increase until the increase of salinity to 17 gL^{-1} (4.4.5). If the value of 10 – 15 gL^{-1} is exceeded then dilution with freshwater may be required. This poses an economic issue, as it requires – more often than in the case of freshwater – freshwater pumped and treated for desalination, or supplied from on-shore.

The data for spatial salt concentration along the river Thames have indicated that the area where MV Sound is based in Woolwich is much lower than the highest level tolerated by *Chlorella* species. Salinity levels along the Thames are suitable for cultivation of most algal species. However, salt concentration in the tidal river changes during the day and the seasons, so the suitability of local water for the PBR operation needs to be carefully considered. The PBR could be loaded with water from the Thames up to an area close to Littlebrook where salinity is close to the optimal level. However, other microorganisms and components of the Thames water might affect the growth of the chosen algal species. Water from the river Thames would need to be frequently tested for quality parameters, and possibly pre-treated, for use in the PBR.

4.5 Cultivation of wild algae from natural waters around London

4.5.1 Introduction

The objective of this experiment was to examine the feasibility of cultivating wild algae samples, taken from sites in London's inland waterways to compare growth and adaptation with lab grown cultures. The results are needed to observe the potential for the onboard PBR operating conditions to use algae sourced directly from the local environment.

4.5.2 Methods

These experiments were conducted with the help of 3rd year students (Wu & Lee, 2014) and an MSc student (He, 2014). Water samples were taken from the surface of five natural waters in London (Regent's Canal near Camley Street Natural Park, Camley Street Natural Park pond, Boating Lake at Regent's Park, St James's Park Lake and Serpentine Lake at Hyde Park) and a domestic potted plant. The origin and labelling of the samples is shown in Table 4.3. The water quality of all the samples is shown in Table III.5 of Appendix III. Samples RC20/2 – RC20/5 were taken from the same area as RC22/1, but at a different time. 20 mL/L of Bold Modified Basal Freshwater Nutrient Solution (specification in Table III.6 of Appendix III) were added to each sample in cultivation bottles.

Three different main experiments were conducted using the wild algae samples; their cultivation under air sparging, treatment of some of them with UV light and cultivation of some of them under various CO_2 in air flow rates sparged. The bottles used had different volumes, depending on the experiment. Air and CO_2 were sparged at the bottom of each sample directly by an airline pipe for samples RC22/1, RC5/1A – RC5/1D, RC24, PP, CSP, RP, SJP and HP and ceramic airstone spargers for samples RC20/2 – RC20/5, with the gas flow rates and compositions shown in Table 4.3. The illumination was delivered by a fluorescent lamp providing 14 μmol/m^2/s on the surface of the bottles. The temperature during the cultivation was 25 (± 2) °C (set-up shown in Figure III.3 of Appendix III).

Since there was a concern about the effect of bacteria in the natural water samples on the algae, an experiment was conducted using UV light. UV radiation is reported to induce damage to bacterial cells and has been used to remove bacteria from algae cultures (Mehta & Hawxby, 1977). Its effectiveness depends on its intensity, wavelength and exposure time (Solomon et al., 1998). 6 W lamps of different

wavelengths, UV-A (λ = 315 – 400 nm), UV-B (λ = 280 – 315 nm), and UV-C (λ = 200 – 280 nm), were immersed into bottles of samples RC5/1A – RC5/1D for exposure times of 0, 15, 30 and 60 min. At each exposure time, two 15 mL samples were taken from each bottle and placed on bacteria and algae agar plates (18.1 g/L CM0906 R2A agar powder and 15 g/L Fluka 05039 agar powder with 20 mL/L Bold medium were the agar compositions, respectively) for inoculation. Cultivation of the bottles was continued after the final exposure time, and 500 mL were taken from the bottle treated with the most enhancing UV light condition (UVA) for the experiments of the different flow rates of air and CO_2-enhanced air (Table 4.3).

Table 4.3. Cultivation bottles using wild algae from the different locations and their allocated name.

Sample	Source	Initial Volume	Cultivation period	Gas type	Gas flow rate
RC22/1	Regent's Canal near Camley Street Natural Park	1000 mL	22/01/14–03/02/14	air	0.1 L/min
RC5/1A	" "	200 mL from sample RC22/1 diluted to 1000 mL	05/02/14–19/02/14	" "	" "
RC5/1B	" "	" "	" "	" "	" "
RC5/1C	" "	" "	" "	" "	" "
RC5/1D	" "	" "	" "	" "	" "
RC24/1D1	" "	100 mL from sample RC5/1D diluted to 500 mL	24/02/14–03/03/14	air	0.2 L/min
RC24/1D2	" "	" "	" "	10% CO_2	0.2 L/min
RC24/1D3	" "	" "	" "	10% CO_2	0.6 L/min
RC20/2	Regent's Canal near Camley Street Natural Park, close to Granary Sq.	200 mL diluted to 1000 mL	20/06/14–22/08/14	air	0.6 L/min
RC20/3	" "	" "	" "	" "	" "
RC20/4	" "	" "	" "	" "	" "
RC20/5	" "	" "	" "	" "	" "
PP	Indoor potted plant	200 mL diluted to 1000 mL	22/01/14–19/02/14	air	0.1 L/min
CSP	Camley Street Natural Park pond	500 mL	" "	" "	" "
RP	Boating Lake, Regent's Park	" "	" "	" "	" "
SJP	St James's Park Lake	" "	" "	" "	" "
HP	Serpentine Lake, Hyde Park	" "	" "	" "	" "

Biomass concentration was measured with the UV/Vis Spectrophotometer Camspec M550 Double Beam at 750 nm, with a sampling time/growth time ratio lower than 1/48. The calibration curve for these sample measurements was determined for five 200 mL samples from sample RC22/1 diluted with deionised water. In parallel with the spectrophotometer readings, the samples were vacuum filtered using a 0.45 μm pore-sized filter, and then oven dried at 105 °C to constant mass. The data and the calibration curve are shown in Table III.7 and Figure III.4 of Appendix III. The calibration curve should show a linear trend, as predicted by the Lambert-Beer Law for the absorbance measurements (Myers et al., 2013) (discussed further in 6.3). However, a 2nd order polynomial curve had a better fit, possibly due to inaccuracy of the optical density measurements caused by the omission in diluting the higher concentration samples (discussed in 6.5.1 and Appendix V). It should be noted that the present study used directly the produced concentration data for samples RC20/2 – RC20/5, as computed from the calibration curve produced by He (2014); thus, using 10 mL samples for the filtration instead of 200 mL. One limitation of this calibration method is that the dry biomass could have minor quantities of other microorganisms such as bacteria, due to contamination during cultivation.

The algal species were identified by microscopy, as described in Delwiche et al., (1995). Isolation of the colonies after the UV treatment required use of the antibiotic ampicillin, due to competition between the growth of algae and remaining bacteria.

P-values of the three experiments were computed with:

a. A 2-way ANOVA on the effect of time and different sampling sites among the samples taken in the winter (samples RC22/1, PP, CSP, RP, SJP and HP).

b. Similarly a 2-way ANOVA for the samples taken in the summer (RC20/2 – RC20/5).

c. A 1-way ANOVA for the effect of the period (summer and winter) on the productivity of the samples. Since the samples for the two different periods were taken at different times of the cultivation progress, this was accomplished by first analysing the overall productivities of the samples at the peak growth of each. Then the productivities of the samples were analysed at 29 h, which was the longest mutual cultivation duration for all samples (except samples RC22/1). For the purpose of comparing samples of equal size, the ANOVA tests used samples that had the same measurement frequencies; hence, the

first 1-way ANOVA excluded samples PP and CSP which were from pond sites and the second 1-way ANOVA excluded samples RC22/1 and CSP.

d. A 2-way ANOVA for the effect of time and UV wavelength on the growth of samples RC5/1A – RC5/1D.

e. A 2-way ANOVA for the effect of time and gas sparging conditions on the growth of samples RC5/1D1 – RC5/1D3.

4.5.3 Results and discussion

The growth curves for the wild algae samples from the different sites are shown in Figure 4.5 (data taken from Table III.8 in Appendix III). pH ranged from 7 to 9 at all times. All four typical growth phases (2.3.6.3.1) can be identified in the growth curves of the samples RC20/2 – RC20/5 taken from different points of the Regent's Canal. On the other hand, growth of algae in samples RC22/1, PP, CSP, RP, SJP and HP lagged and did not reach a peak, which is possibly attributable to fact that these samples were taken in the winter, whereas RC20/2 – RC20/5 were collected in the summer. The average productivity of all the summer-cultivated samples during their growth period (before the peak for RC20/2 to RC20/5) was 0.021 g/L/day. This is much lower than the average productivities reported for PBRs using commercial algae (Table I.2 of Appendix I).

Statistical analysis showed that the effect of time was significant only for the samples RC20/2 – RC20/5 (P-values 4.1×10^{-6} and 0.18 for the samples RC22/1, PP, CSP, RP, SJP and HP), confirming that the samples collected in the winter remained in a lag phase throughout the experiment. Nevertheless, the effect of the sampling site on the samples at each testing period (winter and summer) was always significant, while comparatively more significant for the winter samples (P-value was 1.5×10^{-11} for samples RC22/1, PP, CSP, RP, SJP and HP and 0.00374 for samples RC20/2 – RC20/5). However, conclusions for this cannot be made, as samples RC20/2 – RC20/5 were obtained from close points of the same area. The effect of the testing period on the maximum productivities of the samples was significant only when productivities were measured for just the first 29 hours (P-value 0.008). In general, the summer samples obtain significantly higher concentrations than the winter samples.

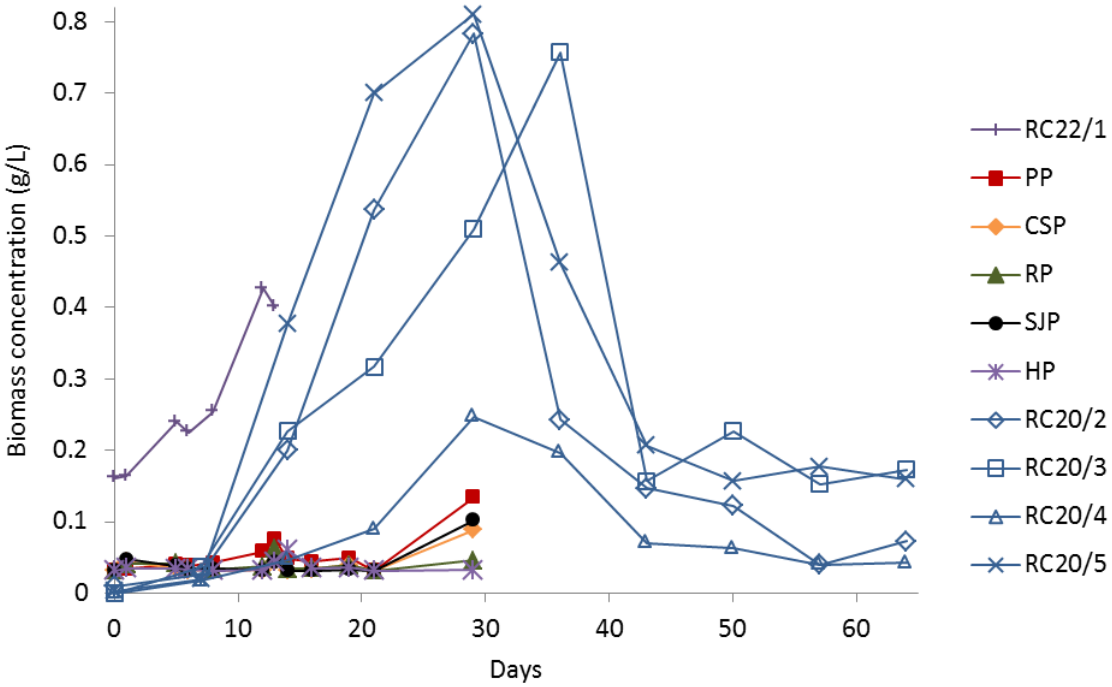

Figure 4.5. Growth of the samples obtained from the different sites. Lines joining points are for visual clarity and do not represent a known physical reality.

The effect of UV light on the growth of algae in the bottles and bacteria in the petri dishes is shown in Figure 4.6 and Figure III.5 of Appendix III, respectively. The effects of UVB, UVC and exposure time on extermination of the bacteria and retardation of algal growth were much stronger than that of UVA and the control sample. Specifically, this effect was more significant with increased exposure duration and with shorter wavelengths (UV-C) than with longer ones (UV-A) (pictures of the bottles at the end of their post-treatment growth shown in Figure III. 6 Appendix III). P-values of the influence of UV light and time were 0.039 and 0.010, respectively, indicating their significant effect on the growth.

Algal growth as a function of the various CO_2 concentrations and flow rates fed to the cultures is shown in Figure 4.7. Sparging 10% v/v CO_2 in the air apparently had the best effect on algal growth, amongst the various concentrations tested. However, two-way ANOVA showed that effects were statistically insignificant (P-values were 0.05 and 0.21 for time and the different gas sparging sets of measurements, respectively). The data used for the production of both figures are shown in Table III.9 of Appendix III.

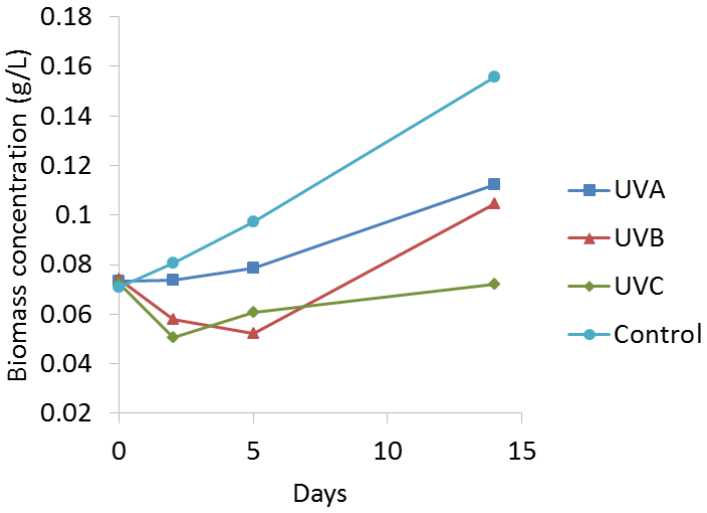

Figure 4.6. Algal growth after UV treatment of samples RC5/1A – RC5/1D using UVA, UVB, UVC and the control, respectively. Lines joining points are for visual clarity and do not represent a known physical reality.

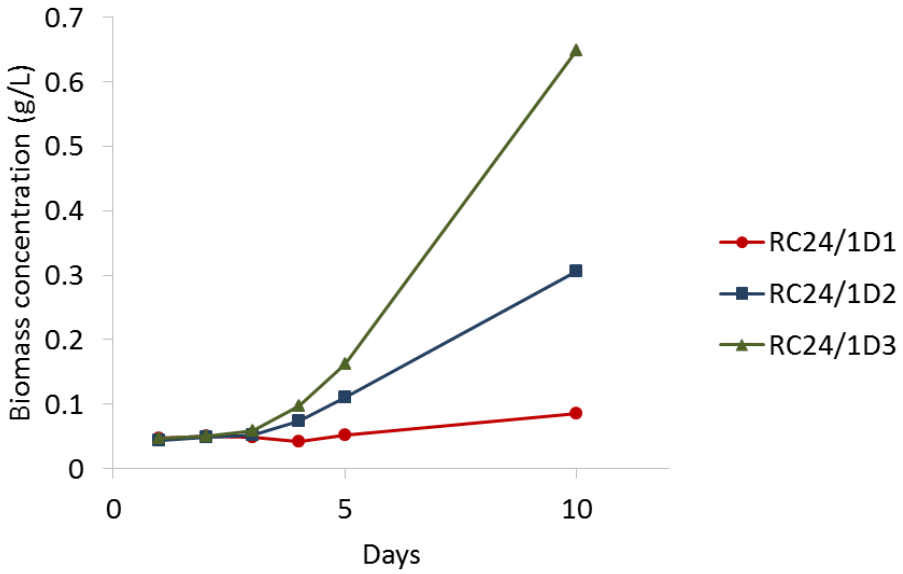

Figure 4.7. Biomass growth in samples RC24/1D1 – RC24/1D3 under different gas sparging conditions. Lines joining points are for visual clarity and do not represent a known physical reality.

Some of the colonies isolated from samples RC22/1, PP, CSP, RP, SJP and HP were observed using a microscope and 12 species in total were identified. Their possible identities are shown in Table III.10 of Appendix III. The species of *Chlorella vulgaris*, *Scenedesmus* genera and *Chlamydomonas* genera were identified and several genera of green algae, cyanophyta and bacillariophyta were visually recognised. Many of the species identified are included are those present in the Thames according to the literature (4.4.7).

4.6 Conclusions

The four different topics that were examined in this chapter, regarding the PBR requirements for modifications on board, showed some difficulties. The experiments on the photobioreactor design showed that bubble size significantly increased with gas flow rate, while the difference in bubble size between the top and bottom of the column decreased. Although coalescence was observed for all flow rates in the pilot helical PBR constructed with 40° inclination, the design experiments suggested that no major coalescence would be observed at inclinations higher than 40°. Coalescence at lower inclinations increased the average bubble size by up to 100%, which would reduce the area for mass transfer of CO_2 into the medium and waste energy used for the bubble production. On the other hand, increased inclination is coupled with higher hydrostatic pressure, hence, an optimal angle and height are anticipated to exist for every helical system. Scale-out would therefore require an increase in the number of harvesting units. In larger ships applications, where large volumes of gas need to be treated, a different PBR design with less material requirements and able to be placed below the ships waterline, could be more beneficial for commercialisation.

Regarding the effect of NO_x and SO_x, experimental work on how actual marine emissions using live algal cultures would benefit from scrubbing or similar form of pre-processing technology is crucial. Although experimental conditions vary among different studies, some quantitative information is presented in this section and it is shown that the flue gas may likely require pre-treatment for better algal growth.

Water supply is important for the efficient operation of the PBR and effective CO_2 uptake. *Chlorella* species can exist in the Thames water, the salinity of which is suitable for most algal species, but if its value exceeds 10 – 15 gL^{-1} then dilution with freshwater may be required. While using local algae might make the system cost effective and resistant to local parasites, strain identification may be difficult and the existing strains might not have high lipid productivity. On the other hand, using a commercial algae strain for a more predictable product quality (see 2.4.1) is likely to add expenses. The need for a water source is also affected by the top up requirements due to accumulating salinity from evaporation. Therefore, supply of freshwater from on-shore might be needed.

Wild algae samples from various waterways around London were successfully grown in lab conditions and growth appeared to be better under enhanced CO_2 air with

10% concentration, compared to ambient air, though this effect could not be statistically proven. However, a relatively longer lag phase, which could be attributed to the season in which the sample was taken and the time needed to adapt to the lab conditions, resulted in a slower growth rate than that for commercial algae, although further experimental work would be required to prove whether this was the case. Treatments of the wild algae samples with UV light to reduce bacteria inhibited algal growth as well as bacteria. A continuous operation of the PBR under exponential growth could limit population growth from competing bacteria.

5 Hydrodynamics in the airlift photobioreactor

5.1 Introduction

2.3.2.4 discussed the importance of understanding the hydrodynamics of the proposed design for the improvement of mass transfer and gas absorption. The effect of the bubble size on the PBR hydrodynamics is examined in this chapter for a straight vertical airlift PBR. Bubble size is known as an important variable for optimising gas absorption and energy input. This chapter demonstrates a new simplified mathematical model developed for an external loop vertical airlift PBR, derived from established chemical engineering formulae, with the minimum possible reliance on empirical correlations with adjustable parameters (Koutita et al., 2015). Bubble slip velocity, liquid circulation velocity and gas hold-up are simply estimated based on bubble diameter, gas flow rate, riser diameter and riser height. The model reveals the contribution of bubble diameter to gas hold-up and liquid circulation velocity, filling a gap in the literature. The model was validated using experimental data measured in the lab (with the help of the fellow doctoral student Alessandro Marco Lizzul) and taken from the literature. The current model was found to provide a better estimate of gas hold-up than the literature model it was compared with, but liquid velocity was overestimated. The impact of using various drag coefficient correlations was also revealed.

In contrast with the models discussed in 2.3.6.1, the proposed model is macroscopic and uses a mean bubble size within the reactor, which allows the momentum balance to be omitted and only an overall mechanical power balance to be used instead. This work resolves some of the literature deficiencies by using a simple generalised equation, validating the model for several reactor sizes and bubble sizes, and by examining whether existing drag coefficient correlations can sufficiently describe the behaviour of the examined bubble size range. Results for the estimation of liquid circulation velocity support the design of airlift reactors, i.e., liquid circulation velocity determines allowable riser tube length, depending on the gas flow rate and riser diameter.

5.2 Model development

5.2.1 Power balance approach

The developed approach uses equilibrium of forces applied on the bubbles to estimate their relative velocity. The model then uses the power conservation principle on the gas/liquid mixture in the PBR to estimate the liquid circulation velocity and the gas hold-up in the riser. As shown in Figure 5.1, the buoyancy force acting upon individual bubbles is opposed by the counteracting drag force from the water. As the bubbles enter the PBR, they reach their equilibrium slip velocity in very short time, implying that the buoyancy force is balanced by the drag. When considering a small fraction of the mixture (bubbles with liquid); the power provided by the buoyancy force is balanced by the power consumed by the frictional forces of the walls and the connections.

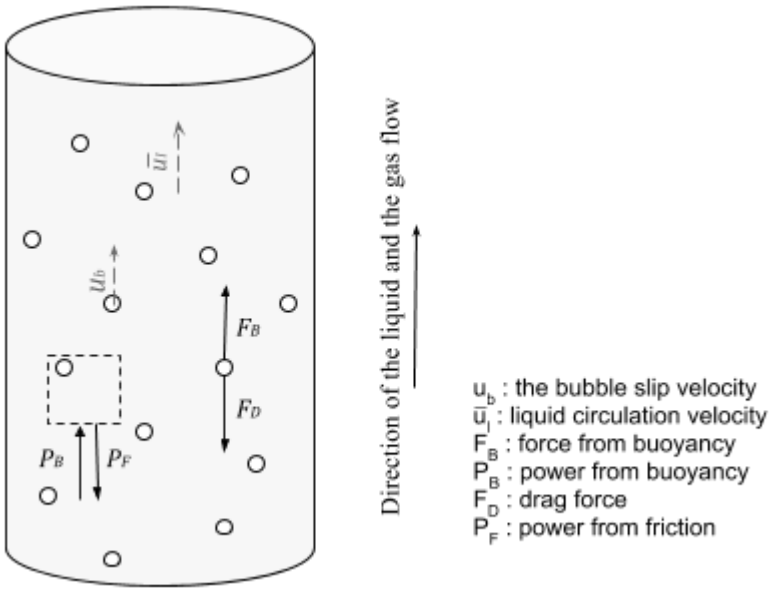

Figure 5.1. Section of the riser tube. The relative velocities of the bubbles and the liquid are shown, alongside the forces acting on each according to the power balance approach.

The buoyancy force acting on a bubble and the interfacial drag force imposed by the surrounding liquid upon each bubble are described respectively by the following equations (Kuiper, 2010):

$$F_B = (\rho_l - \rho_g) g \frac{\pi d_b^3}{6} \tag{38}$$

$$F_D = \frac{1}{2} c_D \rho_l u_b^2 \pi \frac{{d_b}^2}{4} \tag{39}$$

where F_B is the buoyancy force, ρ_l and ρ_g are the liquid and gas densities, respectively, d_b is the bubble diameter, F_D is the drag force, u_b is the bubble slip velocity, and c_D is the drag coefficient calculated from Ishii and Zuber (1979) formula for the particles in the viscous flow regime:

$$c_D = \frac{24}{Re_b}\left(1 + 0.1 Re_b^{0.75}\right) \quad for\ Re_b < 2 \cdot 10^5 \tag{40}$$

$$\text{where } Re_b = \frac{u_b d_b}{\nu_l} \tag{41}$$

where ν_l is the kinematic viscosity of the liquid. This drag coefficient correlation is a classical one used extensively in the literature, including similar experiments (Sáez et al., 1998); the impact on the model of using other common formulae (Karamanev & Nikolov 1992; McCabe et al. 1956; Morisson 2013; Sáez et al. 1998) for the drag coefficient is discussed in 5.4.4. Buoyancy and drag forces are applied to the total riser height. The number of bubbles is calculated using the following expression:

$$N = \frac{V_g}{\frac{1}{6}\pi d_b^3} = \frac{q_g}{\frac{1}{6}\pi d_b^3} t_g = \frac{q_g}{\frac{1}{6}\pi d_b^3} \frac{l_r}{u_b + \bar{u}_l} \tag{42}$$

where N is the number of bubbles, V_g is the volume of the gas, q_g is the gas flow rate, t_g is the gas residence time in the riser, l_r is the riser height (i.e. vertical length) and $\bar{u}_l$ is the liquid circulation velocity.

Considering the force components along the longitudinal axis of the riser, the buoyancy forces should be equal to the sum of the drag forces for the total riser height (Chisti, 1989).

$$\sum F_{B_x} = \sum F_{D_x} \Rightarrow N\left(\rho_l - \rho_g\right) g \frac{\pi d_b^3}{6} = N \frac{1}{2} c_D \rho_l u_b^2 \pi \frac{{d_b}^2}{4} \tag{43}$$

Using the formulae in Eq.40, 41 and 43, the expression for the bubble slip velocity is:

$$u_b = \sqrt{\frac{4gd_b\left(\rho_l - \rho_g\right)}{3\rho_l c_D}} \tag{44}$$

The residence times of the gas and the liquid, the gas hold-up in the riser, and the density of the mixture, are calculated from the following formulae, respectively:

$$t_g = \frac{l_r}{u_b + \bar{u}_l} = \frac{V_g}{q_g} \tag{45}$$

$$t_l = \frac{l_r}{\bar{u}_l} = \frac{V_l}{q_l} \tag{46}$$

$$\varepsilon_r = \frac{V_g}{V_{riser}} = \frac{\frac{l_r q_g}{u_b + \bar{u}_l}}{\frac{\pi d_r^2}{4} l_r} = \frac{4q_g}{\pi d_r^2 (u_b + \bar{u}_l)} \tag{47}$$

$$\rho_m = \frac{\rho_l q_l + \rho_g q_g}{q_l + q_g} \xrightarrow{steady\ \ state} \frac{\rho_l V_l + \rho_g V_g}{V_l + V_g} = \frac{\rho_l \left(\frac{\pi d_r^2}{4} - \frac{q_g}{\bar{u}_l + u_b}\right) + \rho_g \frac{q_g}{\bar{u}_l + u_b}}{\frac{\pi d_r^2}{4}} \tag{48}$$

where t_l is the residence time of the liquid during recirculation in the riser, V_l is the volume of the liquid in the PBR, q_l is the liquid flow rate, ε_r is the gas hold-up in the riser, V_{riser} is the riser volume, d_r is the riser diameter and ρ_m is the mixture density.

Additionally, the gas rise velocity and the superficial gas velocity are respectively estimated from the following formulae:

$$\bar{u}_g = \bar{u}_l + u_b \tag{49}$$

$$u_g = \bar{u}_g \varepsilon_r \tag{50}$$

where $\bar{u}_g$ is the gas rise velocity and u_g the superficial gas velocity.

Considering the force components along the longitudinal axis in Figure 5.1 under steady conditions, the supplied buoyancy power must overcome the wall friction of the mobilised fluid (with upward circulation velocity) and the local resistive forces. Therefore, the power provided by the buoyancy force in the riser tube must be equal to

the power consumed by the friction loss along the PBR. This balance of powers defines the steady flow velocity of the liquid-gas mixture. The two balancing powers are given as:

$$P_B=(\rho_l-\rho_g)g\frac{\pi d_b^3}{6}Nu_b \tag{51}$$

$$P_F=\Delta p\cdot q_l=\rho_l g q_l h_{fr} \tag{52}$$

where P_B is the power provided by buoyancy, P_F is the power lost to friction, Δp is the pressure difference and h_{fr} is the head due to friction, given as:

$$h_{fr}=h_f+h_{mf}=f\frac{l}{d_r}\frac{\bar{u}_l^2}{2g}+K_l\frac{\bar{u}_l^2}{2g} \tag{53}$$

where h_f and h_{mf} are the head losses due to wall friction and fitting friction, respectively. K_l is the additional local frictional loss coefficient, and $\mathrm{f}=\frac{64}{\mathrm{Re}}$ for Reynolds number of the liquid $Re_l<2100$. For $Re_l\geq 2100$, f is calculated from the Churchill formula (Perry et al., 1999):

$$f=\left\{-4log\left[0.27\frac{r}{d_r}+\left(\frac{7}{Re_l}\right)^{0.9}\right]\right\}^2 \tag{54}$$

With the Reynolds number found by the Blasius equation (for $\mathrm{Re}<80{,}000$) (Perry et al., 1999):

$$Re_l=\frac{\bar{u}_l d_r}{\nu_l} \tag{55}$$

The term coupled with $\mathrm{K_l}$ in Eq.53 is the sum of the frictional losses expressed as the frictional velocity head losses due to expansions, K_{exp}, contractions, K_{contr}, and fittings, K_{fit}, in the loop.

By equating the power input with the power consumed, the model is simplified to give the liquid velocity and can be solved by iteration, for given parameters of the fluid characteristics, including PBR diameter, riser and PBR length (which is the sum of the riser and downcomer heights plus the connection lengths), bubble diameter and gas flow rate, after solving first Eq.44:

$$\bar{u}_l^3(\bar{u}_l + u_b) = \frac{8g(\rho_l - \rho_g)u_b q_g l_r}{\pi d_r \rho_l \left[K_l d_r + l\left\{-4log\left[0.27\frac{r}{d_r} + \left(\frac{7\bar{u}_l}{v_l d_r}\right)^{0.9}\right]\right\}^{-2}\right]} \quad (56)$$

The following assumptions were made in developing the model:

For the estimation of the bubble slip velocity from Eq.44, an average bubble size along the tube was used. This does not mean that the isothermal gas expansion of the bubble along its propagation is not considered, as the use of the buoyancy force in the equations implies that density is different at different PBR heights.

1. Bubbles are considered spherical; bubbles have been reported to be spherical for a d_b< 1 mm and ellipsoid for 1 mm < d_b< 1 cm (Clift et al., 1978).
2. The Reynolds number of the bubbles' slip in the liquid is always below the threshold required in Eq.40, based on estimates of Re_b=170 – 2,200 in the experiments.
3. Bubbles have negligible weight compared to the drag and buoyancy forces.
4. The gas flow rate is constant.
5. Flow is at steady state.
6. Flow is turbulent.
7. The drag force is uniform over the cross-section of the tube as bubbles are assumed to be spread evenly after a short distance from their entrance into the PBR.
8. There is negligible bubble recirculation (Chisti, 1989).
9. Bubbles wake friction is negligible.
10. The gas is assumed to instantly obtain the temperature of the liquid by the time it is sparged into it, so compression due to temperature difference of the two phases is not accounted.

The following assumptions were applied in comparing the predictions from Chisti's model (2.3.6.1) with the model developed:

a. The riser of the airlift device is simply a continuous smooth pipe and Re is always between 2.5×10^3 and 10^5.
b. Pipes have smooth walls with negligible friction.
c. The gas hold-up in the downcomer is negligible, leading to a value of zero for Eq.8.

5.2.2 Computational algorithms and parameters

Figure 5.2 illustrates the interrelation of the parameters in the two approaches and Figure 5.3 shows the computational algorithm referring to the equations used to estimate the liquid circulation velocity in each of the two approaches. The models were solved using MathWorks MATLAB Version 7.11.0.584 (R2010b). The whole simulation ran in less than a minute with MATLAB 7.11.0(R2010b) on a 32-bit Intel(R) Core(TM) i5 CPU (code attached in Appendix IV).

Although the two approaches follow the same path, there is a difference in the energy inputs and outputs used. The energy input from the bubble inflow is expressed in the model developed as the power from the buoyancy force, whereas in Chisti's model it as the isothermal gas expansion. The energy outputs considered in the developed power balance approach are due to the wall and fitting friction loss, whereas Chisti's model considers the energy dissipation due to wakes behind the bubbles, energy loss due to stagnant gas and to fluid turn-around friction. Secondly, in its present form, the model developed applies to riser and downcomer tubes of identical diameters and would need modification to describe other systems. Finally, Chisti's model uses empirical formulae for riser and downcomer gas hold-up, which may be configuration dependent (e.g., ε_r in Eq.8 has to be higher than 0.07 in order to give a rational positive ε_d figure. Thus, ε_d was assumed to be zero for the calculations in Eq.8 and Eq.9).

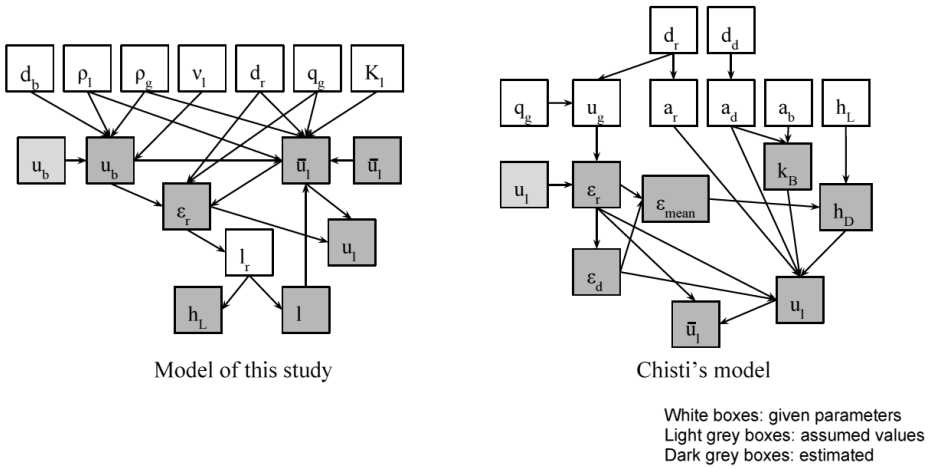

Figure 5.2. The interrelations between parameters within the two models. White boxes: given parameters, light grey boxes: assumed values, dark grey boxes: estimated.

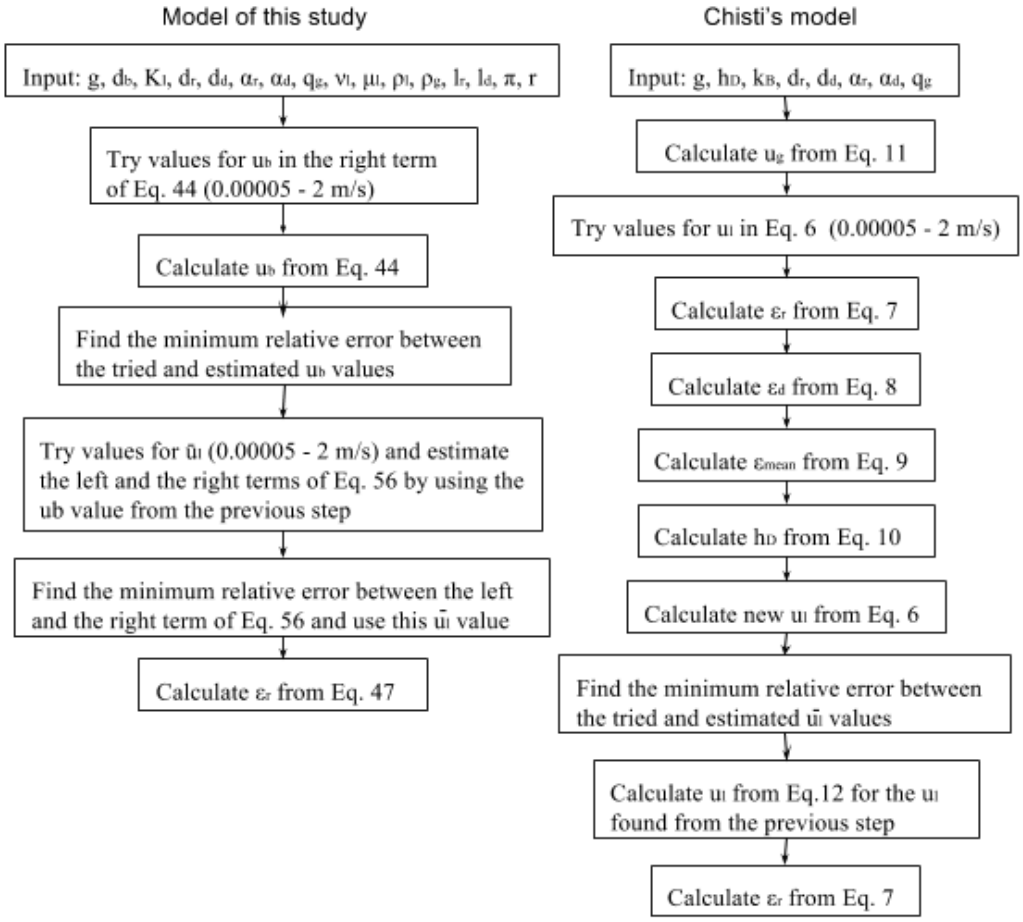

Figure 5.3. Computational algorithms for the estimation of the liquid circulation velocity and gas hold-up in the riser from the two different models.

5.3 Experimental and statistical analysis method

5.3.1 Experimental photobioreactor

The experimental PBRs were constructed from standard polyvinyl chloride piping connectors and polymethylmethacrylate tubing for riser and downcomer sections (Plastock). Five different PBR configurations were used which differed in diameter and height in order to examine their influence on the results. The dimensions of PBRs R1, R2, R3, R4 and R5 are shown in Table 5.1 and are based on designs from the unpublished work of Lizzul. Information for estimation of the frictional losses is shown in Table 5.2. The expansions and contractions are located at the points where flow passes from the main pipes to the fittings and from the fittings to the main pipes, respectively. The 180° close return bends are located at the top of the PBRs where liquid passes from the riser to the downcomer, whereas the 90° standard and square L

fittings are at the bottom of the downcomer and riser, respectively. Each PBR was filled with tap water to the middle of the horizontal degasser zone as shown in Figure 5.4.

The gas was fed by the air-compressor (Hailea AC0-009E 112W) used in the previous experiments. The ambient temperature during the experiments was 23°C and the temperature of the water was 16°C. Three spargers of different porosities (shown in Figure 5.5) were used to conduct experiments with three different average bubble sizes. The first two spargers were 3D-printed from nylon beads. Sparger D1 was slightly perforated and D3 was more perforated. The third sparger (sparger D2) was a porous ceramic sparger. Bubble size within airlift bioreactors is usually 0.5 – 5 mm (Shah et al. 1982; Zimmerman et al. 2011), but can expand in the upper portion of longer tubes.

Table 5.1. Dimensions of the photobioreactors used for the experiments.

PBRs	$\mathbf{d_r}$ (m)	$\mathbf{d_d}$ (m)	$\mathbf{l_r}$ (m)	$\mathbf{l_d}$ (m)	$\boldsymbol{l}$ (m)	$\mathbf{h_d}$ (m)
R1	0.054	0.054	1.04	1.04	2.40	1.04
R2	0.054	0.054	2.04	2.04	4.40	2.04
R3	0.058	0.058	0.54	0.54	1.40	0.54
R4	0.10	0.10	1.04	1.04	2.40	1.04
R5	0.034	0.034	1.04	1.04	2.40	1.04

Table 5.2. Estimation of the frictional losses (velocity head loss).

Loss types	$\boldsymbol{K_l}$ Estimation	Values (Perry et al., 1999)	Frequency in PBRs				
			R1	R2	R3	R4	R5
$\mathbf{K_{fit}}$	180° close returns bends	1.5	2	2	2	2	2
	90° standard L	1.3	1	1	1	1	1
	90° square L	0.75	1	1	1	1	1
$\mathbf{K_{contr}}$	$\sum_{i=1}^{n} 0.5\left(1-\frac{a_{i+1}}{a_i}\right)$	0.4177	2	4	2	2	2
$\mathbf{K_{exp}}$	$\sum_{i=1}^{n}\left(1-\frac{a_i}{a_{i+1}}\right)^2$	0.2464	2	4	2	2	2

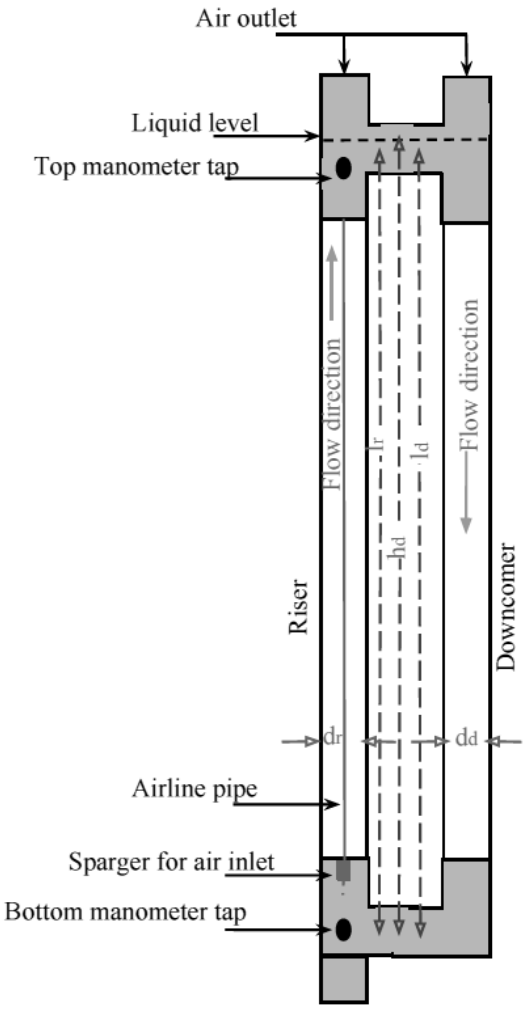

Figure 5.4. Schematic of the external loop photobioreactors used for the experiments (dimensions are shown in Table 5.1).

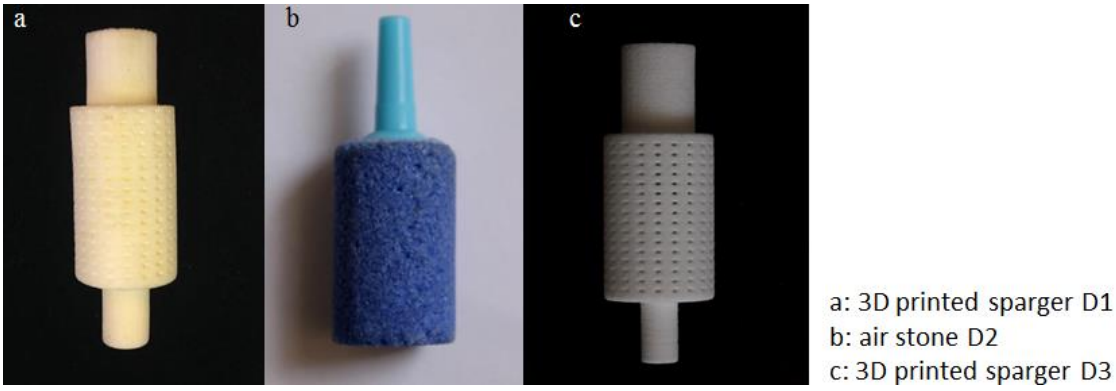

Figure 5.5. Photos of the spargers used.

5.3.2 Bubble size measurement

The effects of bubble size on gas hold-up and liquid velocity were examined experimentally using flights of bubbles produced from the three different spargers with different steady-state gas flow rates. The flights of bubbles were photographed with a high ISO setting on a Nikon D40x lens, 18 – 55mm (e.g., Figure 5.6). For each photograph, areas of up to 25 bubbles were measured using the open access software ImageJ v 1.47 (NIH) (Softonic International, 2014) and used to calculate average equivalent bubble diameters (referred to simply as bubble diameters in this study). This sample size gave an approximate 28% precision with a measured mean variance 0.2 mm and for 95% confidence level, according to the sample size estimation by Reckhow and Chapra (1983). The probabilities, p, that the shown effects of repeat measurements are attributable to random error, were determined based on a 1-way ANOVA. An effect is generally considered as statistically significant when $p < 0.05$. The p values between the different bubbles measured for the two runs were 0.19 and 0.74; therefore, only one measurement from each condition was used for the calculations in this paper.

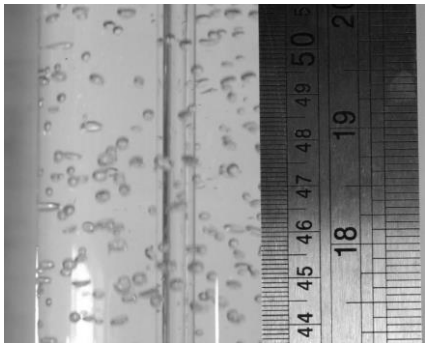

Figure 5.6. Example photograph of riser section of the photobioreactor used to measure bubble size.

To determine whether the size of the bubbles changed as a function of the height of the PBR, bubbles were measured at the bottom, middle and top of the riser, at 0.1 m, 0.5 m and 0.9 m, respectively, for the three spargers in PBR R1. Bubbles were then measured at the heights 0.1 m, 0.9 m and 1.9 m, for the three spargers in another PBR with double height, but with the same diameter and geometry (PBR R2). In both PBRs, sparger D1 showed monotonically increasing bubble diameter with increasing gas flow rate and height (Figure 5.7). Sparger D2 also shows an increase in bubble diameter with increasing gas flow rate and riser height, but with a shallower slope. However, for sparger D3 there was a slight decrease in bubble diameter with increasing height, which could be due to bubbles splitting during their rise in high turbulence. The performance of the three spargers shows that, in both PBRs, sparger D1 gives the

lowest bubble diameter output followed by sparger D2 and sparger D3. The mean bubble sizes and average standard deviations for the sparger measurements in the two set-ups (R1 and R2) are shown in Table 5.3.

The results of a 3-way ANOVA were approximated by the use of a regression equation with three factors in Excel. The probabilities p that the effect of the sparger and the gas flow rate on the bubble size is attributable to random error were 2.1×10^{-15} and 0.015 for PBR R1, respectively, and 5.3×10^{-6} and 0.16 for PBR R2. However, the effect of the height in the PBR on the bubbles is statistically insignificant as the probability was 0.961 and 0.334 for PBRs R1 and R2, respectively. To simplify calculations, the variation of the bubble diameter as a function of the gas flow rate was not taken into account in the validation of the model, and bubble diameters of 2.2, 3.3, 4.6 mm (average values between the two PBRs from Table 5.3) were used in the model.

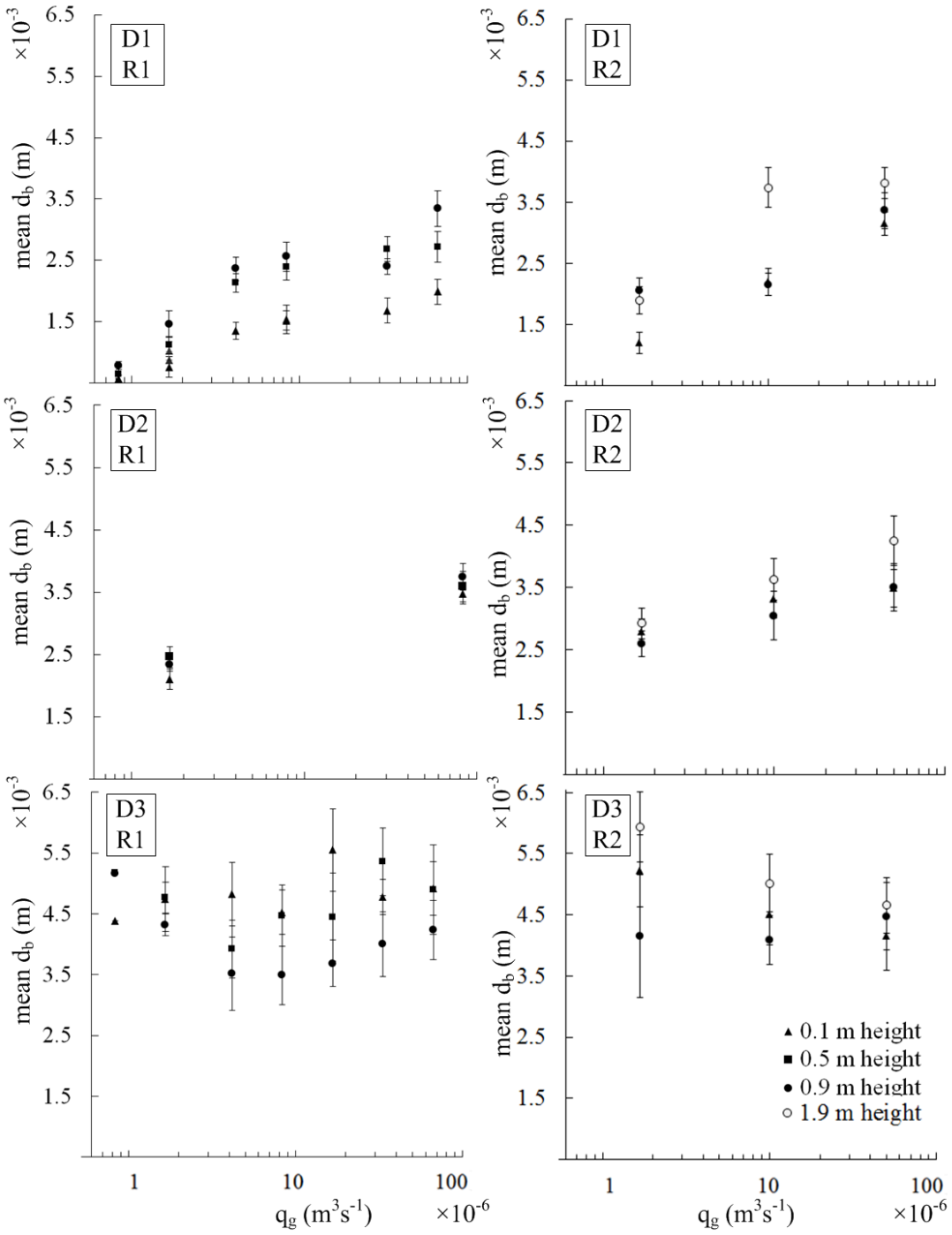

Figure 5.7. Bubble diameter measured at different heights of the riser as a function of gas flow rate for the three spargers (D1, D2 and D3) in the photobioreactor configurations R1 (left) and R2 (right) along with the 95% confidence intervals calculated from the standard deviation and the sample mean.

Table 5.3. Bubble diameters for different spargers.

Sparger	Measurements for PBR R1		Measurements for PBR R2	
	Mean bubble diameter (mm)	Standard deviation (mm)	Mean bubble diameter (mm)	Standard deviation (mm)
D1	1.8	0.5	2.6	0.7
D2	3.3	0.5	3.3	0.7
D3	4.4	0.6	4.7	1.0

5.3.3 Gas hold-up and liquid velocity measurement

Gas hold-up was measured using a U-bend manometer as suggested by Molina et al. (2001). Liquid circulation velocity was measured following the bubble measurements using a tracer injection of 0.8 mM acetic acid, detected by a pH probe (Jenway). The water was renewed after each measurement of velocity. The recirculation time was determined as the average duration between 3 peaks and between three troughs of the pH. The liquid circulation velocity was calculated by dividing the length of the PBR loop by the average recirculation time. One to three replicates were undertaken for each experimental condition to examine the repeatability of the method. The average standard errors among the average velocities for different gas flow rates were 0.0176 ms^{-1}, 0.0095 ms^{-1} and 0.0091 ms^{-1} for spargers D1, D2 and D3, respectively. ANOVA indicated probabilities p that the effect of the sparger or the gas flow rate on the liquid velocity are attributable to random error were greater than 0.95.

5.4 Results and discussion

5.4.1 Basic model validation for gas hold-up results

Figure 5.8 to 9 show measurements of the gas hold-up in the riser as a function of the gas flow rate, compared with predictions for the two modelling approaches. Figure 5.8 examines the influence of bubble diameter. Results from the model developed, using the parameter values from Table 5.1 and Table 5.2, are presented as different solid lines for the three bubble diameters (spargers) in PBR R1, while results from Chisti's model, which is independent of $\mathrm{d_b}$, are shown with a dashed line. Results for riser gas hold-up from Chisti's model are closer to the results from the model developed for $d_b = 3.3\,mm$, which suggests that bubbles of this size might have been

used for the development of the empirical Eq.6 in Chisti's model. The model developed shows that gas hold-up in the riser decreases with increasing bubble diameter, as drag coefficient and bubble slip velocity increase and thus less gas is retained in the PBR at a particular time. However, this is not validated by the experimental data. The dependence of the measured gas hold-up on bubble diameter appears to be minor in this figure.

Figure 5.9 shows the influence of riser diameter with $d_b = 4.6\,mm$ in the developed model and experiments. The selected limits used for the riser diameter are typical of the literature. The influence of the riser height is shown in Figure 5.10, again with $d_b = 4.6\,mm$ in this study's model and experiments. Similar behaviour and figures (not shown) were obtained for the other two spargers. The two models give similar gas hold-up results for all gas flow rates. In all cases, the models overestimate the gas hold-up, relative to the experiments, with an average relative error between the developed model and the experimental data measured of 59%, whereas the average relative error between Chisti's model and the experimental data is 93%.

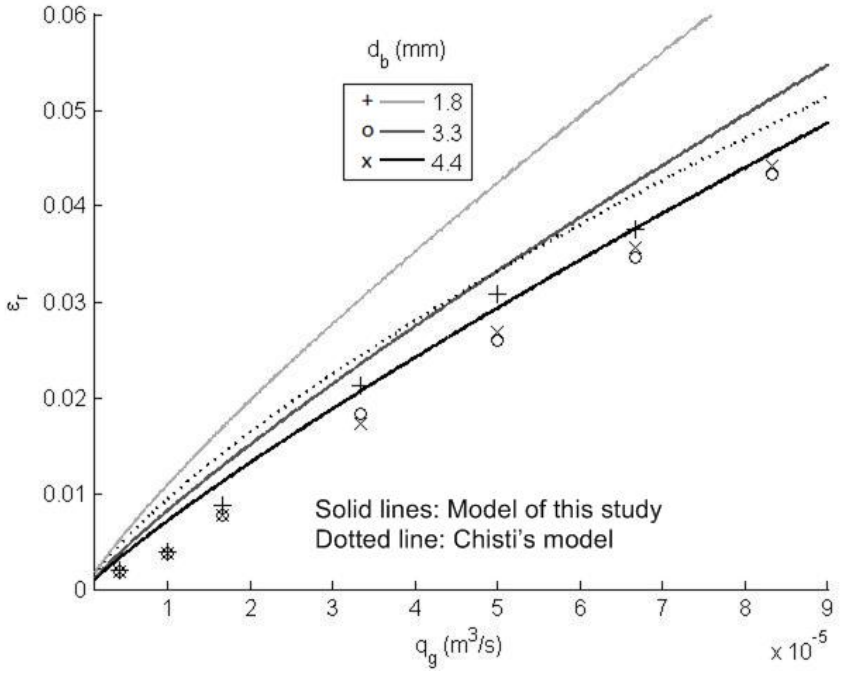

Figure 5.8. Measurements of gas hold-up as a function of the gas flow rate in photobioreactor R1 for the bubble diameters indicated, compared with predictions from the models.

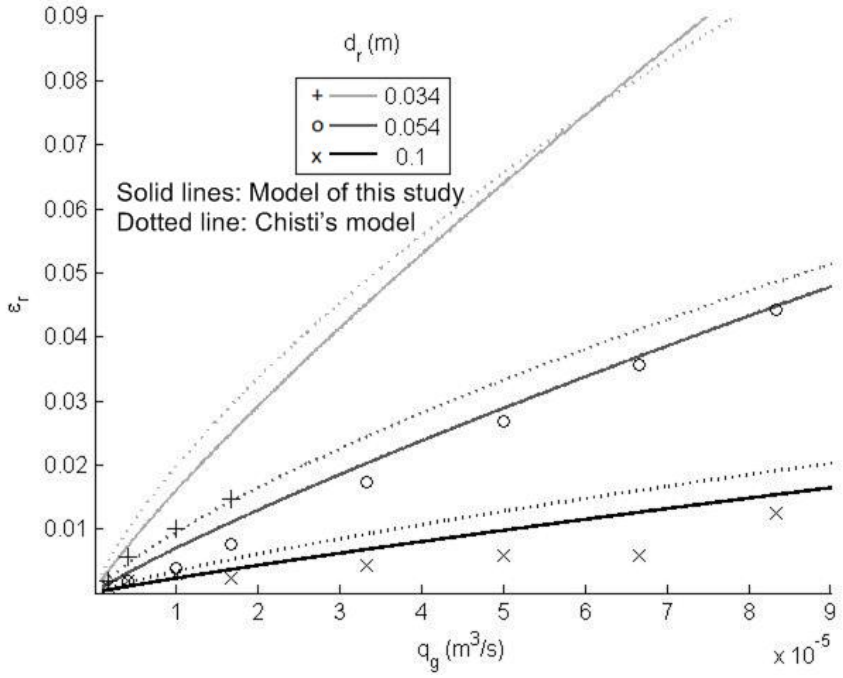

Figure 5.9. Measurements of gas hold-up as a function of gas flow rate in photobioreactors R1, R4 and R5, for the three different riser diameters indicated and using sparger D3, compared with predictions from the models.

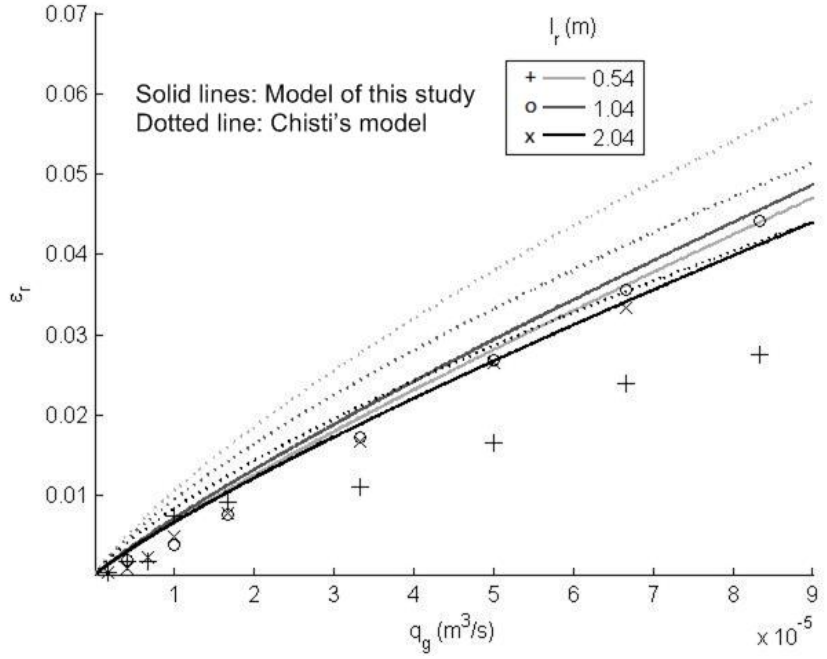

Figure 5.10. Measurements of gas hold-up as a function of the gas flow rate in photobioreactors R1, R2 and R3, for the three different riser heights indicated and using sparger D3, compared with predictions from the models.

5.4.2 Basic model validation for liquid circulation velocity results

The results for the bubbles slip velocity predicted by the developed model are in agreement with Chisti's (1989), and the assertion by Molina et al. (2001) that bubble slip velocities tend to range from 0.2 – 0.4 ms^{-1}. Figure 5.11 to Figure 5.13 show measurements of liquid circulation velocity as a function of the gas flow rate, examining the influence of bubble diameter, riser diameter and riser length, respectively. Both modelling approaches predict that the liquid circulation velocity increases with gas flow rate, which accords with experiment results. The average relative error between the developed model and set of experimental data measured for the liquid velocity is 31%, whereas the average relative error between Chisti's model and the experimental data of this work is 11%.

Moreover, the models were also compared to experimental data for various bubble diameters of two studies from the literature (Camarasa et al. 2001; Marquez et al. 1999) in Figure 5.14 to Figure 5.16. The fit to the model developed is better apart from the liquid velocity data in Figure 5.16, but there is a lack of literature measurements of liquid velocities for different bubble sizes, to verify this observation.

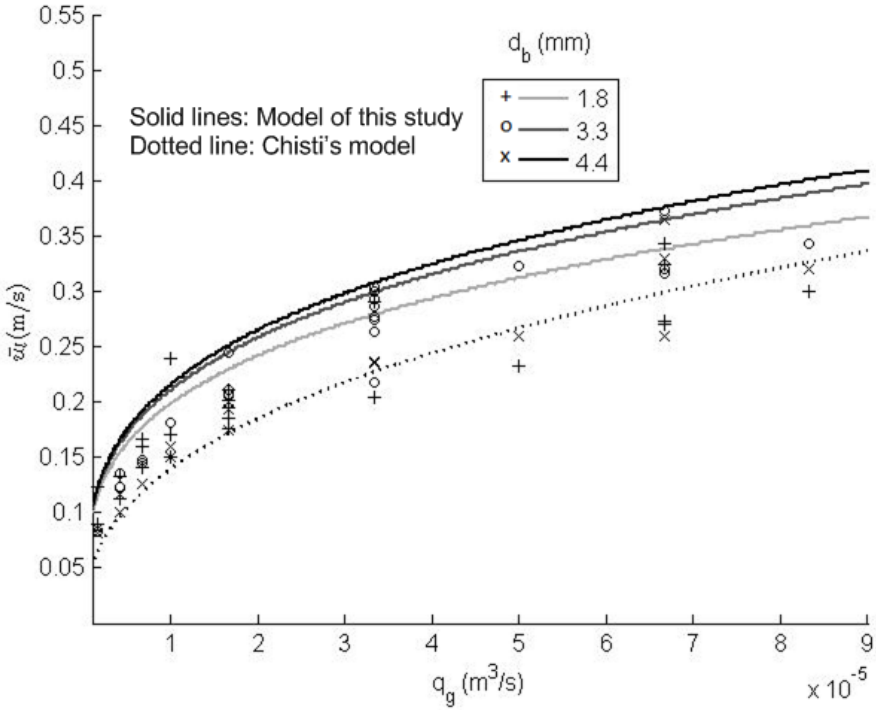

Figure 5.11. Measurements of liquid circulation velocity as a function of the gas flow rate in photobioreactor R1 for the three bubble diameters indicated, compared with predictions from the models.

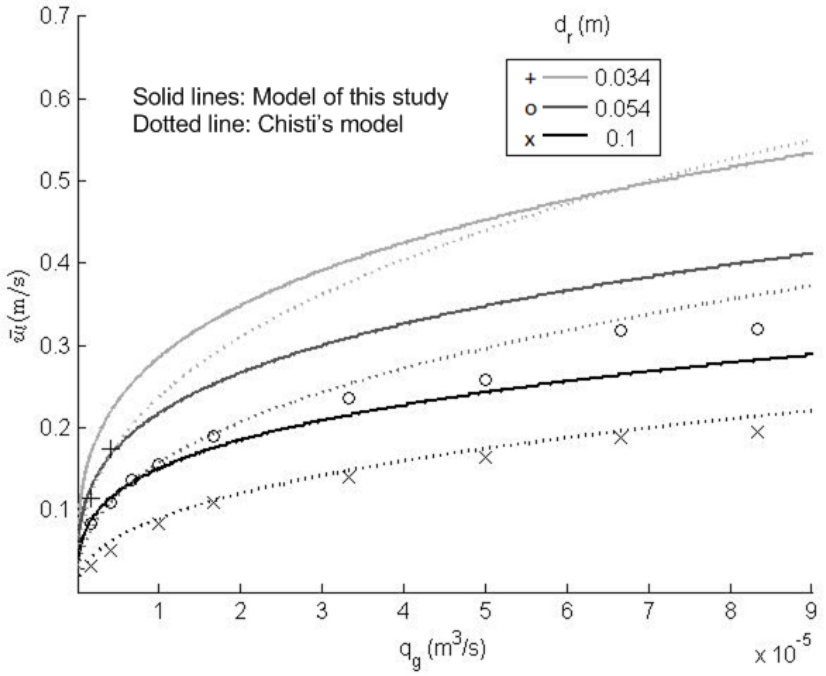

Figure 5.12. Measurements of liquid circulation velocity as a function of the gas flow rate in photobioreactors R1, R4 and R5, for the three different riser diameters indicated and using sparger D3, compared with predictions from the models.

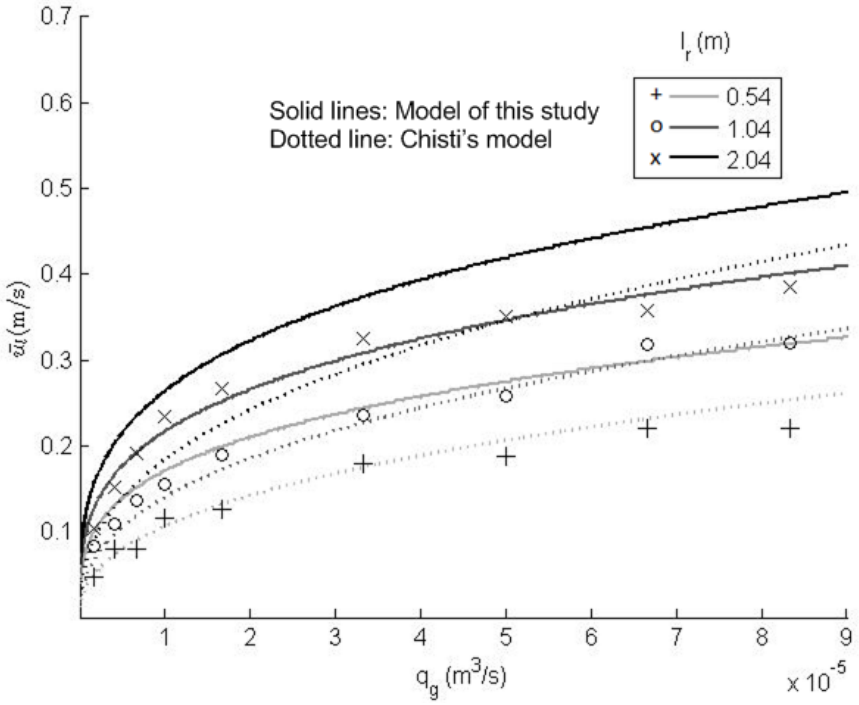

Figure 5.13. Measurements of liquid circulation velocity as a function of the gas flow rate in photobioreactors R1, R2 and R3, for the three different riser heights indicated and using sparger D3, compared with predictions from the models.

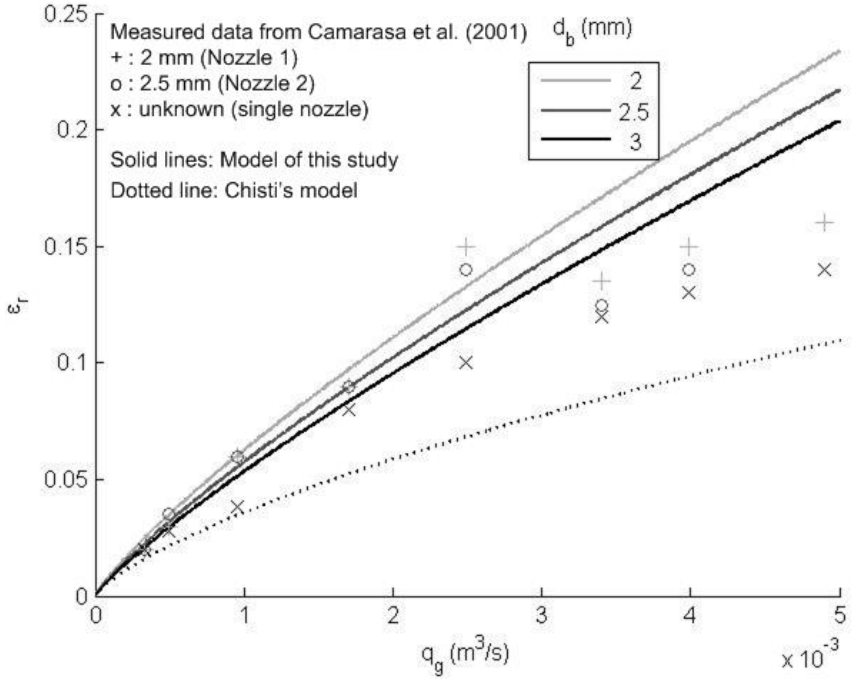

Figure 5.14. Measurements of gas hold-up by Camarasa et al. (2001) in an airlift photobioreactor with a riser diameter of 0.23 m and riser length of 3.50 m as a function of the gas flow rate, compared to predictions from the models.

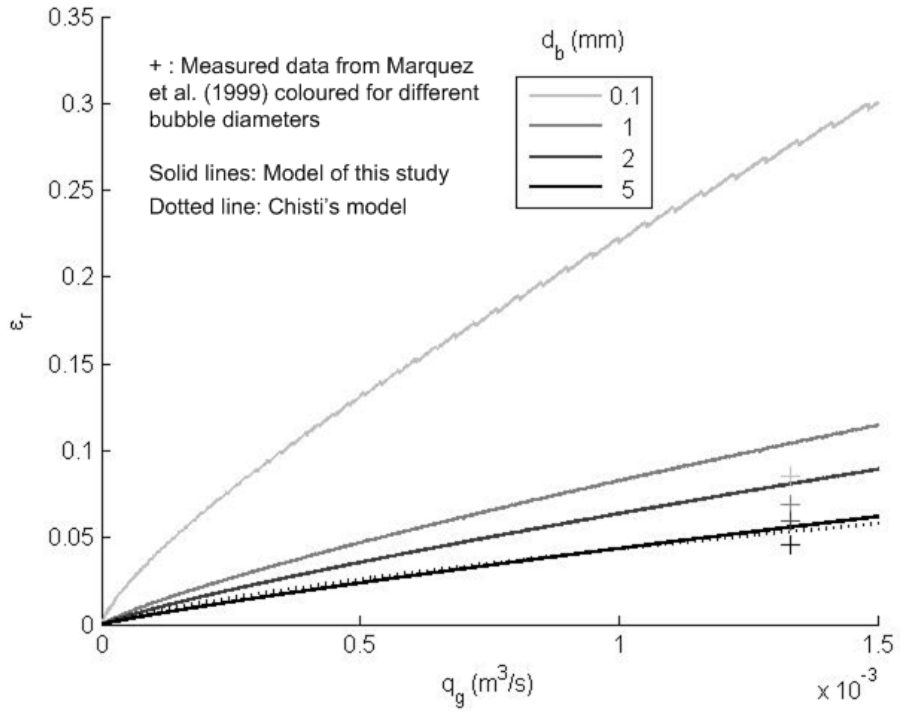

Figure 5.15. Measurements of gas hold-up by Marquez et al. (1999) in an airlift photobioreactor with a riser diameter of 0.19 m and riser length of 1.56 m as a function of gas flow rate, compared to predictions from the models.

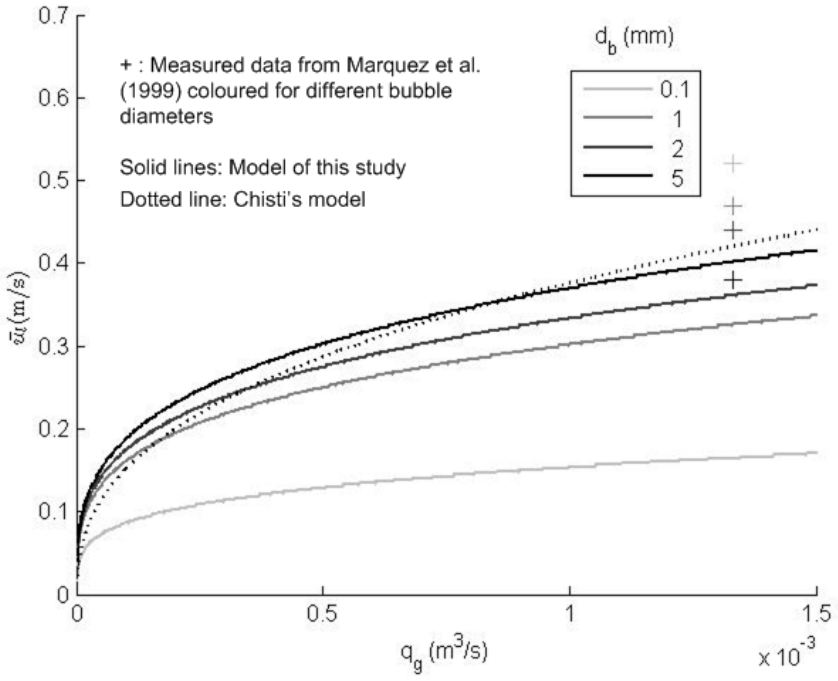

Figure 5.16. Measurements of liquid circulation velocity by Marquez et al. (1999) in an airlift photobioreactor with a riser diameter of 0.19 m and riser length of 1.56 m as a function of gas flow rate, compared to predictions from the models.

5.4.3 Model uncertainty and experimental errors

Uncertainties associated with the developed model include the assumptions of negligible bubble recirculation, spherical bubbles, and negligible friction of bubble wakes. There may be significant interfacial forces that are not considered. Overall, the model takes into account the integration of the main forces applied within the system and does not consider the micro-scale forces. Compared to Chisti's model, it uses fewer algorithm steps, achieving results comparable to the developed own and other experiments, it is based on a simple consideration of explicit hydrodynamic factors and involves the minimal possible reliance on empirical equations that could limit the range of the model applicability. The fact that the measurements and the model give comparable results indicates that the major part of the involved physics has been adequately accounted for.

Differences between model predictions and experimental results could be caused by either model or experimental inadequacies. Gas hold-up is overestimated by both models compared to this study's experiments, which may be caused by the assumption taken of a single bubble diameter, whereas bubble size distribution has been shown to

affect both the average gas hold-up and the distribution of gas within the PBR (Law & Battaglia, 2013). Also, the possible change in volumetric gas flow rate due to the temperature difference between the heated compressed gas and the bubbles after cooling by the water was not taken into account.

The results for the liquid velocity are likewise overestimated by the developed model compared to the experimental measurements, which may be attributable to the energy loss from turbulence produced by the bubbles and to small quantities of stagnant gas observed in the downcomer, especially at higher gas flows. Also, the surface tension developed upon addition of the acetic acid may have influenced the liquid velocity experiments. On the other hand, Chisti's model appears to underestimate liquid circulation velocity at lower gas flow rates, as his model incorporates more friction forces.

Figure 5.8 and Figure 5.11 show that the sensitivity of the gas hold-up and the liquid circulation velocity to the bubble diameter is lower than expected by the predictions. A clear order of the liquid circulation velocity output from the different spargers used is difficult to distinguish in Figure 5.11, which could probably be due to the sensitivity of the repeat measurements to factors such as the purity of the water and the gas flow meter adjustments. In addition, the influence of the drag coefficient on the liquid velocity is discussed below (5.4). The impression that the bubble size does not contribute as significantly as the gas flow rate to the liquid velocity could be further investigated using a targeted series of experiments, e.g., with a wider range of bubble sizes.

5.4.4 Effect of different drag coefficient correlations

The differences between the model developed and experimental data were greater when other drag coefficients for spherical shapes were used. For example, the correlations given by McCabe et al. (1956) (used by Chisti, 1989), Khan and Richardson (Sáez et al., 1998), Karamanev and Nikolov (1992) and Morisson (2013) gave errors in the gas hold-up of 72%, 66%, 150% and 67%, respectively; and in the liquid circulation velocity of 36%, 30%, 27% and 30%, respectively. As suggested by Sáez et al. (1998), these findings suggest that using an improved drag coefficient correlation could give better model fit. However, the use of different existing correlations did not lead to significant convergence of the models' curves, or give

outputs that matched the order of the experimental data in Figure 5.8. Bubbles with 1 – 10 mm diameter are ellipsoidal, lacking symmetry and oscillating in shape. Also, especially for air bubbles in water, their slip velocity is sensitive to the presence of surfactants (Clift et al., 1978). Curves given by Gaudin (1957) for distilled water and water with surfactants do not converge for ellipsoidal bubbles where surface tension forces are important (Clift et al. 1978; Gaudin 1957).

There is a need to determine a correlation for bubbles of size range where their shape and flow regime change from spherical to ellipsoid shapes. Various published results for air bubbles in water do not show good agreement, mostly due to differences in water purity, wall effects and measurement techniques (Clift et al. 1978; Gaudin 1957; McCabe et al. 1956). When data for correlation of bubble size to bubble rise velocity from experiments by Baker and Chao in McCabe et al. (1956), Taylor in Gaudin's work (1957), and Clift et al. (1978) were used in this model, gas hold-up estimation errors were found to be 95%, 100% and 100%, respectively; and liquid circulation velocity estimation errors were 28%, 28% and 28%, respectively. Apart from the small differences in errors, the data gave different orders in the curves for the different bubble diameters and only Baker and Chao's data gave the same order found in this study's experiments in (Figure 5.8). Therefore, the development of an appropriate new drag coefficient correlation for bubbles in the examined flow regime may substantially improve fluid dynamic models for airlift PBRs. Also, well defined bubble shapes and optimally spherical bubbles would not only follow the current model better but would also give higher liquid circulation velocities, though this may be hard to influence.

5.5 Conclusions

This chapter presented a novel approach for the estimation of the liquid circulation velocity in a vertical airlift PBR. The model developed was validated by comparison both to experiments conducted in this study and other experimental results, and with the results from Chisti's well-known semi-empirical model (1989). The model developed has a purely theoretical basis, allowing calculation of liquid velocity without the need for empirical expression for the gas hold-up. Thus, it is useful for estimation of gas hold-up and liquid velocity, and calculating optimal airlift PBR geometry, in applications where the conditions deviate from assumptions associated with the empirical formulae. A shipboard application would benefit from this model, as the estimation of liquid velocity can affect the estimation of heat loss on board. Importantly,

this model differs from Chisti's in that it shows the potential impact that the bubble diameter can have on gas hold-up and liquid velocity.

Predictions for gas hold-up and liquid circulation velocity from this model were comparable to experimental results over a range of values of gas flow rate, riser diameter, riser height, and bubble diameter, though the effect of varying the bubble diameter could not always be distinguished experimentally. Different drag coefficient correlations clearly affected model predictions and errors relative to the experimental data; improvement of the drag coefficient estimation is therefore recommended for good model fit.

6 Model of algal growth kinetics with variable light, temperature and nutrients

6.1 Introduction

A model of the effects of light intensity, temperature and nutrient concentrations on algal growth was developed to enable optimisation of the PBR operating conditions with respect to these variables (see 2.3.6.1). In general, the fit of algal growth models to data tends to be poor, as there is no clearly stated standard experimental approach for the cultivation of algae, and algal growth kinetics studies from the literature apply to different conditions (e.g., culture volumes and nutrient compositions) (Costache et al., 2013; Derakhshan et al., 2014; Gonçalves et al., 2014). Nevertheless, an attempt was made to calibrate the model developed here with experimental measurements from laboratory cultivation of the fast growing species *Chlorella sorokiniana* in small multi-well plates (Figure V.1 of Appendix V). This species was selected for the experiments here to speed up the experimental timeframe, though different shipboard applications could benefit from different wild algae (2.3.2.1 and 4.5).

The attempted calibration of the model by non-linear regression estimated the values of the growth parameters for the specific species used in the experiments. The model used a single substrate term for the effect of nutrients (as in Eq.27) and the generic form of the Arrhenius equation (Eq.29) for the temperature effect. A more complex form of the model developed counted the nutrients, nitrates, phosphates and CO_2, separately, and used the Arrhenius equation for the enzyme-mediated reactions of microorganisms (Eq.36). However, the increase in the number of parameters of the complex model form resulted in poor fit and estimated parameter values that were outside their natural bounds. Therefore, literature parameter values were used in a semi-continuous simulation of the model to predict optimal control variable values for some case studies of a shipboard PBR. These different case runs of the model addressed different objective functions: maximisation of the biomass concentration, of the productivity, and minimisation of the PBR volume.

6.2 Model development

The simultaneous effects of multiple growth inhibiting factors on the growth rate calculation has been previously examined not only for two different nutrients (Xin et al., 2010), but also for the effect of other types of factors, such as light and temperature under non-limiting nutrient supply (Bernard & Rémond, 2010). In the first case, the individual maximum growth rates for saturated nitrate and phosphate concentrations were determined experimentally in two different series of experiments where the concentration of the non-limiting nutrient factor was kept constant in each case. Then, since the data were in accordance with Monod's model, its integrated form was given (Eq.57) by using an overall maximum growth rate (at optimal nitrates and phosphates together), multiplied by the two different efficiency factors for nitrates and phosphates, respectively (Xin et al., 2010).

$$\mu_r = \mu_{max}\varphi(N)\varphi(P) = \mu_{max}\frac{C_N}{K_N + C_N}\frac{C_P}{K_P + C_P} \quad (57)$$

In Bernard and Rémond's (2010) study the same integrating method for the growth rate calculation was used under the hypothesis that the efficiency factor for temperature does not depend on irradiance. However, it has been stated that few models consider the simultaneous effect of more than two environmental factors on the growth (Zonneveld, 1998). For instance, Geider et al. (1997) have described the growth under the limitation of light, nutrients and temperature factors by considering the maximum growth rate as a multiplicative function of temperature and nutrient availability. They used the light utilisation factor of Van Oorschot (2.3.6.3.2), an Arrhenius equation and the Monod equation to describe the temperature dependence of the maximum growth rate and the nutrient limitation respectively (Geider et al., 1997).

Contrary to this approach, Arrigo and Sullivan (1994) described the effect of light and nutrients with the Monod equation and compared the growth under light-limited and under nutrient-limited conditions. However, this case considers exclusive limitation of one of the two factors, as one of the two variables is limited each time, according to the lowest growth rate. The maximum growth rate is also considered to be dependent on temperature. Response of algae species that grow in long-lasting ice fields to changes in four factors, temperature, irradiance, concentrations of nutrients and salinity was also presented.

In this study, the growth rate was estimated simultaneously, considering all of the main growth influencing factors (substrate, temperature, irradiance), by multiplying the maximum growth rate at the optimal values for the three factors with the different efficiency factors. Integrating the utilisation factors, the biomass concentration dynamic behaviour takes the form of Eq.58:

$$\frac{dC_b}{dt} = C_b\left[\mu_{max}\varphi(S)\varphi\left(C_{CO_2}\right)\varphi(I)\varphi(T) - m_a - D\right] \quad (58)$$

Monod's model was used with a space-averaged light intensity. Space-averaged light intensity is commonly used to substitute intensity in Eq.26 and to define a space-averaged growth rate in each time interval. It has been calculated in a plate PBR by integrating Eq.26 over z (depth) in Cartesian coordinates as shown in Eq.59 (Fernandez et al., 2001; Quinn et al., 2011).

$$I_{av} = I_0\frac{1 - exp(-K_a C_b d)}{K_a C_b d} \quad (59)$$

where d is the depth of the culture. Other approaches have discretised light intensity and growth rate along the different PBR layers and estimated the growth rate in each region to yield an average, as it was argued that this discretisation results in better accuracy (Huesemann et al., 2013; Kim et al., 2002).

Accurate predictions of the lag phase are very difficult to obtain and an empirical term was used that includes both influencing factors (temperature, culture history and pH), as in Koutsoumanis et al. (2000). In this model, the Arrhenius form of Eq.36, was used to represent the effect of temperature in a way that facilitates calibration.

The nutrients considered are nitrates, phosphates and CO_2. Their effects were simulated as separate Monod terms. Monod's model has been used to represent the effect of the CO_2 concentration on the growth (Cheenkachorn et al., 2011; Pegallapati & Nirmalakhandan, 2012). The dissolved CO_2 was computed in Eq.2 and Eq.3 in 2.3.2.4.Thus, the biomass concentration dynamic behaviour calculation used for the simulation of the process will have the form of Eq.60.

$$\frac{dC_b}{dt} = C_b[\mu_{max}\varphi(N)\varphi(P)\varphi(CO_2)\varphi(I_{av})\varphi(T) - m_a - D] =$$

$$C_b\left\{\mu_{max}\frac{C_N}{K_N + C_N}\frac{C_P}{K_P + C_P}\frac{C_{CO_2 l}}{K_{CO2} + C_{CO_2 l}}\frac{I_{av}}{K_I + I_{av}}\frac{2exp\left[\frac{E_a}{RT}\frac{(T - T_{opt})}{T_{opt}}\right]}{1 + exp^2\left[\frac{E_a}{RT}\frac{(T - T_{opt})}{T_{opt}}\right]} - m_a - D\right\} \quad (60)$$

where the nitrate and phosphate concentrations are computed from the following equations (see 2.3.6.3.3):

$$\frac{-dC_N}{dt} = \frac{1}{Y_{b/N}}\frac{dC_b}{dt} + m_{s/N}C_b - \frac{1}{Y_{b/N}}D(C_{N,0} - C_N) \quad (61)$$

$$\frac{-dC_P}{dt} = \frac{1}{Y_{b/P}}\frac{dC_b}{dt} + m_{s/P}C_b - \frac{1}{Y_{b/P}}D(C_{P,0} - C_P) \quad (62)$$

The parameter estimation was also applied to the simplified model (Eq.63), where the nitrates and phosphates were merged into a single substrate Monod term and the CO_2 Monod term was excluded, as CO_2 is assumed constant with time. Also, the temperature term was replaced by the simple Arrhenius equation in order to minimise the interdependent parameters for their estimation (Eq.29). The maximum growth rate term was integrated into the Arrhenius equation, with consistency units, as used in the literature when temperature was considered as single limiting factor (Eq.29).

$$\frac{dC_b}{dt} = C_b\left(k_0 e^{(-\frac{E_a}{RT})}\frac{C_S}{K_S + C_S}\frac{I_{av}}{K_I + I_{av}} - m_a - D\right) \quad (63)$$

where the substrate concentration is computed by Eq.64 and Eq.65.

$$C_S = C_N + C_P \quad (64)$$

$$\frac{-dC_S}{dt} = \frac{1}{Y_{b/S}}\frac{dC_b}{dt} + m_{s/S}C_b - \frac{1}{Y_{b/S}}D(C_{S,0} - C_S) \quad (65)$$

The assumptions made for the modelling and its calibration are the following.

a. The Cartesian-averaged intensity is used in the calibration and fit of the model for consistency with the validation experimental set-up.
b. Photoinhibition is not taken into account, to reduce the number of parameters to be estimated, and because it appears at irradiances over 1,000 lEm^{-2}s^{-1} in most strains (and in some cases at lower irradiances down to 300 μEm^{-2}s^{-1})

(Acién Fernández et al., 2013), while lower intensities were used in the experiments.

c. The function $\varphi(I)$ would have to be experimentally determined at a specific temperature (Huesemann et al., 2013), but it is assumed independent of temperature. Also, all rate parameters are assumed to be temperature independent.
d. The nutrient concentrations of the model represent the extracellular concentration. The metabolism of the uptake is not considered in the model and the uptake is assumed to be instantaneous.
e. N and P where combined in a single substrate term, although they play different roles (2.3.2.4) and have different metabolic functions.
f. Supply of the CO_2 in the gas fed is higher than its uptake by algae. Immediate dissolution is assumed and constant dissolved concentration for a given temperature and partial pressure.
g. The utilisation factor for temperature does not depend on irradiance.
h. Light scattering is not considered.
i. The nutrient concentration is not high enough to inhibit growth.
j. As individual cells mix in different discretisation layers within the culture, they immediately adjust to the light conditions of the new layer, expressing the growth rate that is experimentally determined at the local light intensity. This assumption has been previously made and it has been verified that changes in light intensity immediately change the photosynthetic O_2 evolution rate (Huesemann et al., 2013).
k. There is adequate mixing, so the liquid phases and algae cells are homogeneously distributed inside the PBR.
l. Sampling procedure and duration do not affect growth, as the sampling/growth time ratio was lower than 1/48.
m. Growth yield over the nitrates and phosphates is assumed stable and independent of the nutrient concentrations, contrary to the literature (van Bodegom, 2007).
n. All cultures in the beginning of each experiment are assumed to have the same age.
o. No growth inhibition by the reactions products is considered.
p. Dilution rate is zero as the calibration experiments are run in batches.

6.3 Model calibration and application – Methods

6.3.1 Experimental design

Experiments were conducted with the help of the 3rd year undergraduate students Rena Seyidova and Michael Gonzalez (Seyidova & Gonzalez, 2015), to investigate the growth conditions for *Chlorella sorokiniana* and the effects of the four factors discussed; CO_2 concentration in the surrounding gas phase, nutrient concentration, light intensity and temperature. The species was used due to its wide use and tolerance to CO_2 (2.3.2.1), as well as its easy access within the lab.

A set of factorial experiments (Box et al., 2005) – of the level 2x2x3 – was conducted using two different light intensities tested for two temperatures and three levels of nutrients. The CO_2 concentration fed was selected as that which gave the highest productivity in a series of preliminary experiments with three concentrations. The preliminary and factorial experiments were both conducted using multi-well plates where each well had a culture growing in different media dilution. The biomass and the nutrient concentrations were measured during the experiments.

Small multi-well plates have been used by others to examine the effects of different compounds on algae (Safonova et al., 2007), because they facilitate multiple measurements of cellular responses to various conditions (Tschumperlin et al., 2014). They have been used for studies of algal growth kinetics, though they are reported to be less accurate than cultures of large volume in measuring the strain-specific maximum specific growth rate (Van Wagenen et al., 2014), which is most likely due to the fast evaporation (Safonova et al., 2007).

In biological experiments, including algal studies, responses over time are often studied by repeated sampling from the same culture (e.g., Belanger, 1997). This popular method, termed “temporal pseudoreplication” or resampling, avoids the effort of preparation of numerous identical cultures and was followed in this experiment. However, this technique leads to a potential dependence of subsequent measurements on previous measurements. Therefore, this experiment ran a parallel series of wells under identical conditions, with sacrificial sampling over time, i.e., the culture in each well had grown independently from the start of the experiment until it was sacrificed to sampling (sacrificial replication). Only one resampling well was used for each nutrient dilution of the experimental condition tested, a specific volume of which was engaged to be measured on each measuring day.

Convergence on a global optimum is often difficult in non-linear regression (Demidenko, 2013). Regarding the number of measurements needed for the model calibration, an arbitrary number of required data points to adequately fit a non-linear model's curve is six, whereas in the existing experiments only four were taken (Illinois State University, 2014). In most real life studies in microorganisms, general conclusions are difficult, due to problems including pseudoreplication and confounding factors which are almost impossible to control (Azarbad et al., 2013). One of the solutions suggested in the literature when measurements are not accurate enough, would be for each data point used to make the plot to be averaged over numerous observations (Illinois State University, 2014).

The strain of *Chlorella sorokiniana* (UTEX1230) was provided by fellow doctoral student Alessandro Marco Lizzul who obtained it from the Culture Collection of Algae from the University of Texas, Austin, USA. The culture was maintained in the laboratory in 1 L bottles filled with deionised water and 20 mL/L of the Bold Modified Basal Freshwater Nutrient Solution. Samples of this broth were obtained and centrifuged in 2 mL cells using an Acotlab Microcentaur centrifuge at 6,500 rpm for 45 seconds, so that the sediment of the necessary number of cells when obtained and poured in each well would make up the desired initial biomass concentration of 0.06 g/L. The Bold media dilutions in deionised water used during each experiment in the wells were 5 mL/L, 10 mL/L and 20 mL/L (dilution factors will be used in the remaining text as shown in Table 6.1, with the theoretical concentrations estimated from Table V.1 of Appendix V). Each experiment ran under the constant CO_2, light and temperature conditions.

Table 6.1. Dilution factors and theoretical concentrations of the nutrients used in each series of experiments.

Media diluted in water (mL/L)	Dilution factor	Theoretical concentration of nitrate (g/L)	Theoretical concentration of phosphate (g/L)
5	1:200	0.193	0.163
10	1:100	0.386	0.326
20	1:50	0.772	0.653

6.3.2 Experimental set-up

Four wells were allocated for each nutrient dilution in each experimental series; 3 sacrificial wells and 1 resampling well. The volume was selected to minimise the space

requirements and duration of the experiments, as it provided thin culture depth with high light absorption. The plates used for the preliminary experiments (well height 12 mm, volume 12 mL) were transparent acrylic with ventilated lid, whereas the one used for the factorial experiments was a dark non-transparent silicon tray (well height 13 mm, volume 16 mL). The silicon trays allowed greater volume cultivation, sterilisation between the different experimental series, and illumination only from the top of the well as assumed by the model (pictures of both types of wells are shown in Figure V.1 of Appendix V). One of the sacrificial wells was sampled, measured and disposed of on the 1st, 2nd, 3rd and 5th day, at the same time as 2 mL were collected and measured from the resampling wells.

The experiments were conducted inside a greenhouse box (Heated Vitopod Propagator by Greenhouse Warehouse shown in Figure V.2 of Appendix V) to avoid contamination from airbourne particles and to control the desired CO_2 concentration during the cultivation. Illumination was provided by 15W LED rods, placed appropriately to illuminate all wells evenly. The cultivation plates were placed on a shaker turning at 130 rpm and a glass bead of 1 cm diameter was immersed in each well to facilitate mixing. The CO_2 fed to the greenhouse box was transported through flexible airline pipes from a 100% CO_2 cylinder and laboratory air at an ambient temperature of 20 °C was fed with a compressor Hailea AC0-009E 112W. The outlet was vented to a fume cupboard via an identical compressor. The two gases were not premixed before entering the box, but were placed away from the outflow pipe and the wells in order to have enough space to mix and maintain the desired concentration within the box space. The experimental set-up is shown in Figure 6.1.

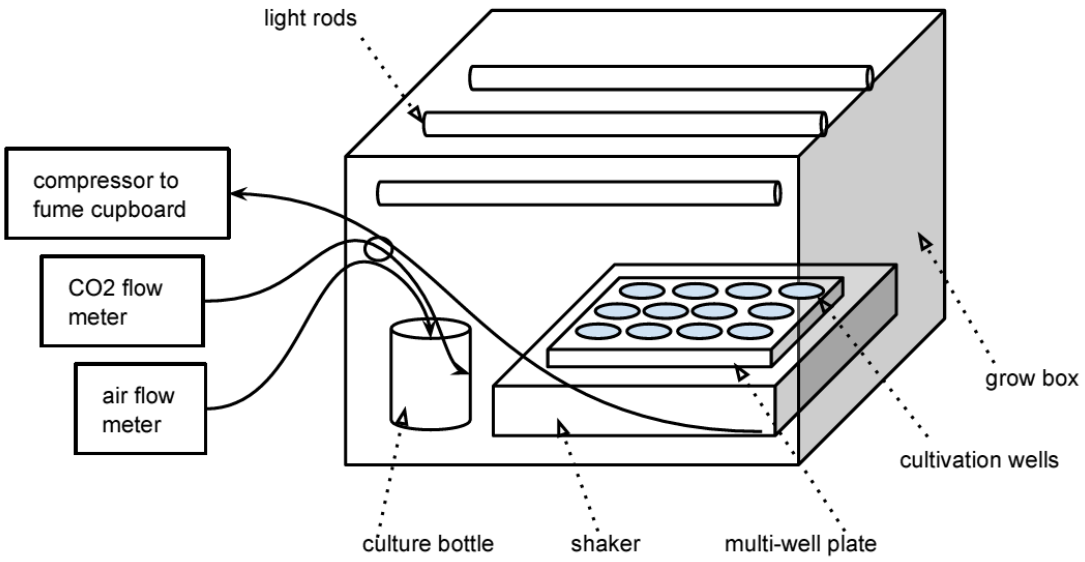

Figure 6.1. Schematic of the experimental set-up used during the CO_2 and the factorial experiments.

6.3.3 Experimental method

6.3.3.1 Preliminary CO_2 experiments

CO_2 was investigated at three distinct levels (700, 4,300 and 50,000 mg/kg). Four wells (three sacrificial ones and one resampling) were assigned for each of three nutrient concentrations, dilutions of 1:200, 1:100 and 1:50 of nutrient medium. A temperature of 30 °C and light intensity of 150 µmol/m^2/s were used. The flow rates and CO_2 concentrations measured for each experiment are shown in Table 6.2. Theoretical CO_2 concentrations computed are higher than the ones measured (24%), which might be attributed to need for calibration of the equipment, or to faster leakage of the CO_2 from uneven mixing of the two gases inside the box.

Table 6.2. Flow rates of the gas inlets and CO_2 concentration in the greenhouse box used during the CO_2 experiments.

Experiment	Air flow rate (cm^3/min)	CO_2 flow rate (cm^3/min)	Measured CO_2 concentration (mg/kg)	Theoretical CO_2 concentration (mg/kg)
1	300	0	700	1,150
2	1,000	2.5	4,300	4,930
3	1,000	42.5	50,000	62,960

6.3.3.2 Factorial experiments

The factorial experiments were conducted with a CO_2 concentration of 4,300 mg/kg selected based on the results of the preliminary experiments. Light intensities tested were 100 and 150 μmol/m^2/s with a photoperiod 24:0 h. The temperatures used were 22 – 25 °C and 34 – 37 °C. Table 6.3 shows the conditions used in each experiment. The high light intensity 150 μmol/m^2/s was achieved with an extra fluorescent rod. The lower temperature 22 – 25 °C was obtained by using an in-house designed water bath as shown in Figure 6.2. The temperature of the tap water used for cooling was approximately 16 °C and the flow rate was approximately 110 cm^3/min and it was achieved by the use of a Watson-Marlow H.R. peristaltic pump to overcome piping frictions. Duplicate samples (A and B) were taken from some sacrificial samples and Series 1 and 2 were repeated, to examine the methodological errors of the ion chromatography procedure. The second trials from Series 1 and 2 were used for the calibration, as they run for longer period, which would include cells dead phase and facilitate calibration of the corresponding parameter. Evaporation of the medium from the wells in Series 2 and 3 (6.4.1.2) was resolved by dilution of the wells after every measurement back to their initial volume.

6.3.3.3 Description of measurements

Optical density is the most common way to measure biomass concentration as it provides an immediate result. The optical densities of the samples taken each day were measured immediately, and then the samples were refrigerated until determination of anions by ion chromatography (IC) at the end of each series.

The optical densities of 2 mL biomass samples in cuvettes were measured with a Camspec M550 Double Beam Scanning UV/Visible Spectrophotometer. The calibration

curve for these sample measurements used 100 mL algae samples which corresponded to optical density readings of around 0.2, 0.5, 0.6, 1.2 and 2, and had been cultivated in 1 L bottle. Following measurement of their optical density, the calibration samples were filtered in a vacuum filter using a 1.5 μm pore-sized filter, and then the net mass of biomass was determined after oven drying at 105 °C to constant mass.

Table V.2 of Appendix V shows the results of the calibration measurements. Absorption was measured at a wavelength of 750 nm, as it is out of the visible light range, it does not interfere with the wavelength emitted by variable chlorophyll levels throughout the cells' lifetime (e.g., issues of absorbance higher than expected at low densities, due to high levels of chlorophyll grown at a point with low biomass concentration) and is that selected in most literature methods (Gonçalves et al., 2014; Quinn et al., 2011). More details of the calibration process are analysed in Appendix V.

Nitrate, phosphate and other ion (fluoride, F^-, chloride, Cl^-, nitrite, $NO_2{}^-$, bromide, Br^-, and sulphate, $SO_4{}^{2-}$) concentrations were measured in all of the samples by ion chromatography using the ICS 1100 Dionex IC system with AS-DV autosampler. The anion system's characteristics were: IonPac AS23 4mm analytical column, IonPac AG23 guard column, AMMS 300 4 mm suppressor, 30 ˚C Column temperature, 4.5mM Na_2CO_3 + 0.8mM $NaHCO_3$ Eluent, 1ml/min flow rate, conductivity detector, 25 μL injection volume. The samples collected over each series were filtered through a 0.45 μm syringe filter. 1 mL of each sample was placed in an ion chromatography sample tube and diluted with 4 mL of Milli-Q water, to keep anion concentrations in 1:100 and 1:50 nutrient dilutions within the detectable range (<200 mg/L) by the ion chromatography system.

Light intensity was determined using a conventional Hansatech Quantitherm Light Meter. Air temperature of the area around the wells inside the greenhouse box was measured to be the same (± 2 °C) as the temperature of the liquid algal cultures, using an H_2O Glass Thermometer. pH was not measured for all experiments as it was not used in the model, but it generally ranged between 6 and 8. CO_2 exposure was measured using a Fluke 975 Airmeter. Since the highest concentration used in the CO_2 experiments exceeded the upper detection limit of the meter, a 60 mL sample was taken from the greenhouse box air with a syringe and was injected into a sealable vessel (shown in Figure V.5 of Appendix V) of volume 10.750 L to dilute it for measurement.

6.3.3.4 Statistical analysis

Statistical analysis to examine the significance of the effects of the different factors tested in the CO_2 and the factorial experiments and their potential interaction was conducted in Excel. A t-test was done to compare the average results from the sacrificial and resampling measurements of biomass and nutrient concentrations. The 1-way ANOVA of the CO_2 experiments examined the effect of CO_2 concentration on biomass growth and substrate depletion, by taking into account only the 4,300 mg/kg and 50,000 mg/kg CO_2 levels, as the 700 mg/kg level did not have all of its measurements taken at similar times with the 4,300 mg/kg and 50,000 mg/kg levels. The 1-way ANOVA of the factorial experiments examined the effect of the initial nutrient concentration. The 2-way ANOVA of the factorial experiments examined the effect of temperature and initial nutrient concentration as well as their interaction. The regression was done each time by using the measurements of one time, to inspect the effect of each factor without the influence of time on each experiment. Specifically for the case of the CO_2 experiments, this was done by testing all three CO_2 experiments together at the 1st measurement (time 0), then testing the 2nd with the 50,000 mg/kg CO_2 experiments at the 2nd measurement, the 1st with the 4,300 mg/kg CO_2 experiments at the 3rd measurement and the 1st with the 50,000 mg/kg CO_2 experiments at the 4th measurement.

Plots of interactions between the variables were also created to show the effects of CO_2 concentration, nutrient dilution, temperature and light intensity on the productivity of the experiments in an illustrative way (see 6.4.1.2). The productivity was computed for the first 3 measurements of the experiments, which correspond to approximately 90 hours duration for the CO_2 experiments and 43 hours for the factorial ones, to avoid including the start of cell death and to use times that were tested in all experiments. For simplification purposes, the production of these plots used average values between the sacrificial and resampling measurements, and the expected (not measured) initial nutrient dilutions.

Table 6.3. Conditions used on each factorial experiment.

	Date	Nutrient dilution	CO_2 concentration (mg/kg)		Temperature range (°C)		Light Intensity (µmol/m^2/s)	
			Target	Measured	Target	Measured	Target	Measured
Series 1, Try 1	01/12/14–05/12/14	1:200 1:100 1:50	4,300	4,700	34 – 37	34.2	150	140
Series 2, Try 1	19/01/15–23/01/15	1:200 1:100 1:50	4,300	4,023	22 – 25	22.8	150	139
Series 3	26/01/15–02/02/15	1:200 1:100 1:50	4,300	4,400	22 – 25	23.5	100	84
Series 4	02/02/15–06/02/15	1:200 1:100 1:50	4,300	4,060	34 – 37	33	100	87
Series 1, Try 2	09/02/15–13/02/15	1:200 1:100 1:50	4,300	4,700	34 – 37	36.8	150	129
Series 2, Try 2	25/02/15–02/03/15	1:200 1:100 1:50	4,300	5,006	22 – 25	23.1	150	130

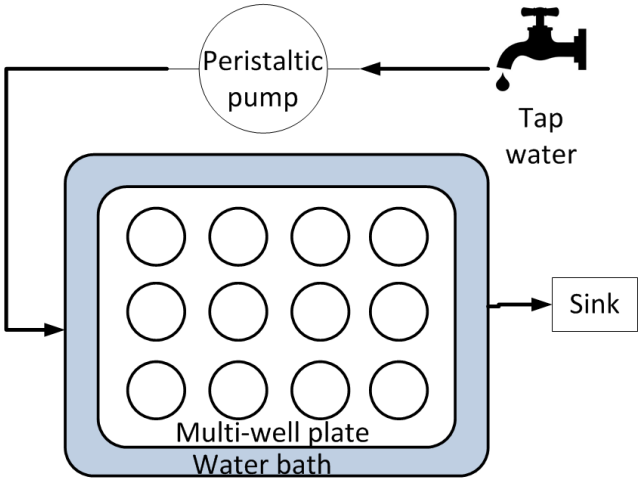

Figure 6.2. Schematic of the water bath used for Series 2 and 3.

6.3.4 Model calibration

6.3.4.1 Method

Fitting of the model parameters to the experimental data was conducted using an iterative procedure in gPROMS 3.7.1, one of the leading software platforms for this task. The process used a standard mathematical mixed-integer non-linear programming fitting solver called MAXLKHD. The convergence criterion used for the solution tolerance is:

$$\frac{1}{|\Phi^*|+1}\left(\left|\sum_j \frac{\partial \Phi^*}{\partial \theta_j}\delta\theta_j\right| + \sum_j |\mu_j| max(0, \theta_j^L - \theta_j^*, \theta_j^* - \theta_j^U)\right) \quad (66)$$

$$\sum_j max(0, \theta_j^L - \theta_j^*, \theta_j^* - \theta_j^U) \leq OptTol \quad (67)$$

where; θ_j is the j^{th} parameter to be estimated (including both model parameters and variance model parameters; θ_j^* is the final value of that parameter; θ_j^L is the lower bound imposed on the parameter; θ_j^U is the upper bound imposed on the parameter; Φ^* is the final value of the maximum likelihood objective function; $\delta\theta_j$ is the step taken in the parameter at the last iteration of the parameter estimation calculation; and μ_j is the Lagrange multiplier that corresponds to the bound constraints imposed on the parameter. The code used by the model is shown in Appendix V.

The following criteria were applied to govern successful parameter estimation in gPROMS, though they were not always achievable in this problem due to its complexity and the numerous unknown parameters:

1. An individual 95% t-value should be larger than the reference t-value.
2. The standard deviation of each model parameter should be much lower than its individual 95% t-value.
3. The values of the diagonal of the correlation matrix should be close to zero.
4. The weighted residual should be less than the -χ^2value to indicate an adequate model construct.

A constant relative variance model was selected from the four different variance models provided (constant variance, constant relative variance, heteroscedastic and linear variance). A parameter space had to be searched for the optimal solutions to be found. The initial guesses selected for each parameter as well as the parameters

selected to be first estimated had an influence on the estimated values. Multiple trials of initial guesses of each parameter within its bounds were needed to estimate a local minimum of the objective function.

6.3.4.2 Simplified model

The difficulty in satisfying the parameter estimation requirements and finding a satisfying fit between the measurements and the predictions of the calibrated model led to an attempt to calibrate a simpler form of the model. The calibration technique in this case used the same solver as described in 6.3.4.1, and treated the two differential equations of the model (Eq.63 and Eq.65) independently. The biomass growth and substrate depletion measurements for the sacrificial samples were described in Excel by the lowest order polynomials that gave the best fit. 3rd order polynomials were selected for all biomass curves, as they all gave R^2=1.0. Regarding the substrate curves, given the low values of the substrate concentrations and that some polynomials were predicting negative values, the polynomials that gave R^2>0.9 and no negative values for the examined range were selected. These polynomials replaced the biomass concentration in Eq.65 and the substrate concentration in Eq.63. The polynomial parameter values were fixed at the beginning of the estimation process, until the final step of the process.

First, the calibration of the model was completed for each experiment separately by using different polynomials for the three initial substrate concentrations tested. This was done for all four experimental series. Then, the four different pair combinations of the four series were each calibrated simultaneously. The parameters related to illumination were estimated for the series conducted at the same temperature, whereas the temperature parameters were estimated for the series with the same illumination intensity. Finally, parameter estimation was carried out using all four series simultaneously, excluding the use of the polynomials and relating the two equations to one another. The script of the final stage is shown in Appendix V.

6.3.4.3 Full model

The initial bounds used for the parameters during the calibration process were taken from the upper and lower values found in the literature (shown in Table V.5 and Table V.6 in Appendix V). Simultaneous estimation of the 13 parameters was not possible due to the interactions between them. Therefore, the estimation process was divided in

stages. In the first stage, the model included only the utilisation factors of the nutrients (nitrates and phosphates), assuming the remaining utilisation factors to be equal to their maximum value of 1. Parameter estimation was performed on all of the process entities that correspond to the conditions of each experiment conducted. Then, the model was gradually built up by using the values estimated in the previous stage as initial guesses. The 5 stages are summarised in Table 6.4. The 6th stage attempted to exclude the Monod term for nitrates. It was not used for the final results, just to examine the effect of this on the fit (as the nitrates depleted first in the measurements, causing the interruption of growth in the model).

Table 6.4. Stages of the parameter estimation for the full model.

Calibration stage	**Parameters included in the calibrated model**	**Experiment used**
1st stage	K_N, K_P	factorial experiments
2nd stage	K_N, K_P, K_I	factorial experiments
3rd stage	K_N, K_P, K_I, E_a, $T_{opt}K_{CO_2}$	CO_2 experiments
4th stage	K_N, K_P, K_I, E_a, $T_{opt}K_{CO_2}$	factorial experiments (fixed parameters from the previous stage)
5th stage	K_N, K_P, K_I, E_a, $T_{opt}K_{CO_2}$	factorial experiments (unfixed parameters)
6th stage	K_P, K_I, E_a, $T_{opt}K_{CO_2}$	1:100 Series 3 of the factorial experiment

The parameter estimation included the following steps:

1. Initial conditions for biomass and substrate concentrations were given.
2. The parameters of depth and incident light on the surface of the PBR were fixed at all times for the parameter estimation runs. The rest of the parameters were gradually unfixed as calibration passed to the next stages.
3. Initial parameter estimation in each model was done based only on the measurements of the biomass concentration. When a good fit was achieved (checked with the lack of fit test), with small confidence intervals for the estimated parameters, the parameter estimation was repeated by adding the measurements for the substrate concentration.
4. The previous step was repeated but with loose parameter bounds.
5. The model was selected according to its fit and its statistical summary.
6. Parameter estimation was repeated for the selected model but with the use of all measurements with all different initial conditions.

Also:

- The CO_2 experiments were excluded from the final parameter estimation for the full model, as the 700 mg/kg level for 1:100 and 1:50 nutrient dilutions gave initial nitrate and phosphate measured concentrations (see Table V.7 of Appendix V) that deviated substantially from their expected values (Table V.1 of Appendix V).
- An inhibition half saturation constant for the CO_2 depletion was used in its Monod term, as used by He et al. (2012).
- The average nutrient values measured in sacrificial samples A and B were used.
- The initial conditions of the sacrificial samples were used for the parameter estimation in each model entity, as they gave better predictions of both measurements (the sacrificial and the resampling ones).
- The initial guesses of the parameters in each estimation run, together with their bounds, strongly affected the final results, a fact which could be attributed to the number of local optima for estimation of the multiple parameters. The validity of the results could be greatly affected by this. Hence, the model had to be simplified to reduce the number of parameters. Various initial guesses were tried in the different runs to examine if they gave similar results.
- The constant relative variance used for the estimation was 0.1 for both biological variable (biomass and substrate concentration) measurements, in order to avoid over-parameterising the problem. The actuall overall uncertainty of the measuring methods was not known, but the average discrepancy between the nutrient measurements and their theoretically expected values was 0.15 (6.5.1).

The weakness in this method is that subsequent fits depend on previous fits. The overall purpose of this estimation approach is the development of a semi-empirical approach to help in the better fit of the model to the measurements and subsequently the optimal design of the reactor.

6.3.5 Model application for design of the photobioreactor

To maintain wild algae in shipboard PBRs in the exponential growth phase, avoiding long lag periods (especially in the winter period, 4.5.3) and the toxic effect of NO (4.3), a shipboard PBR can be operated semi-continuously (where a fixed biomass volume is removed at regular time intervals, and an equal volume of fresh medium is instantaneously added, increasing nutrient concentrations and diluting biomass concentration). By gradual dilutions, the biomass concentration would be maintained within levels that facilitate fast growth (e.g., as used in studies such as Sánchez et al., 2002; Ribeiro et al., 2008). The model was used to design the dilution regime to maximise biomass production. This study used the full model for the simulation of a semi-continuous PBR design in gPROMS (6.2). The simulations used the fixed parameters from Table 6.6, which came from values used in the literature and shown in Table V.5 of Appendix V (given that the estimated parameters in 6.4.2 exceeded their physically meaningful bounds). Optimisation of flue gas utilisation by algae has been previously simulated in an operation where CO_2 is fed in a semi-continuous mode, but other nutrients and temperature were not taken into account (He et al., 2012).

Three different simulations were performed using an iterative procedure, for three different objective functions: the dynamic maximisation of the biomass concentration, of the productivity (P_V), and the dynamic minimisation of the PBR volume. The control variables used in both case study simulations were depth, temperature and illumination intensity, as time invariant control types, and the CO_2, nitrate and phosphate concentrations and dilution rate as piecewise constant control types (Table 6.5). The initial guesses used for the above control variables, as well as the values of the fixed parameters, are the same as those given in Table 6.6. The time horizon used for all case studies was 350 hours.

Table 6.5. Control variables and types.

Variable	Control type	Allowable values	Initial guess	Lower bound	Upper bound
d [m]	Time-invariant	Continuous	0.12	0.03	0.20
I_0 [μE/m^2/sec]	Time-invariant	Continuous	90	0	180
T [K]	Time-invariant	Continuous	298	0	320
D [1/h]	Piecewise-constant	Continuous	0.0027	0.0000	0.1000
$C_{N,0}$ [g/L]	Piecewise-constant	Continuous	0.3	0.0	0.9
$C_{P,0}$ [g/L]	Piecewise-constant	Continuous	0.09	0	0.9
C_{CO2} [L/L]	Piecewise-constant	Continuous	0.005	0	0.2

Table 6.6. Parameter values used for the fed-batch simulation in gPROMS.

Parameters	Value
d [m]	0.12
I_0 [µE/m^2/sec]	90
T [K]	298
R [J/mol/K]	8.314
D [1/h]	0.0027
$C_{b,0}$ [g/L]	0.06
$C_{N,0}$ [g/L]	0.3
$C_{P,0}$ [g/L]	0.09
C_{CO2} [L/L]	0.01
μ_{max}[1/h]	0.1
m_a [1/h]	0.002
$m_{s/N}$[gnitrates/g cells/h]	0.0001
$m_{s/P}$[gphosphates/g cells/h]	0.0001
K_I [µE/m^2/sec]	100
K_a [m^2/g]	0.05
K_N [mol/m^3]	0.05
K_P [mol/m^3]	0.0027
K_{CO2} [m^3/m^3]	0.0000073
$Y_{b/N}$ [-]	0.5
$Y_{b/P}$ [-]	4
E_a [J/mol]	100,000
T_{opt} [K]	303

6.4 Model calibration and application – Results

6.4.1 Experimental results

6.4.1.1 Determination of optimal carbon dioxide concentration

Results of the preliminary CO_2 experiments are shown in Figure 6.3. Of the three different CO_2 concentrations, 4,300 mg/kg was shown to give higher growth than 700 mg/kg and 50,000 mg/kg. In contrast, the literature suggests that the optimal concentration is around 50,000 mg/kg (Myers, 1953; Nagaich et al., 2014; Nakano et al., 1996). The highest biomass concentration and productivity were reached with the 1:100 and 1:50 nutrient dilutions.

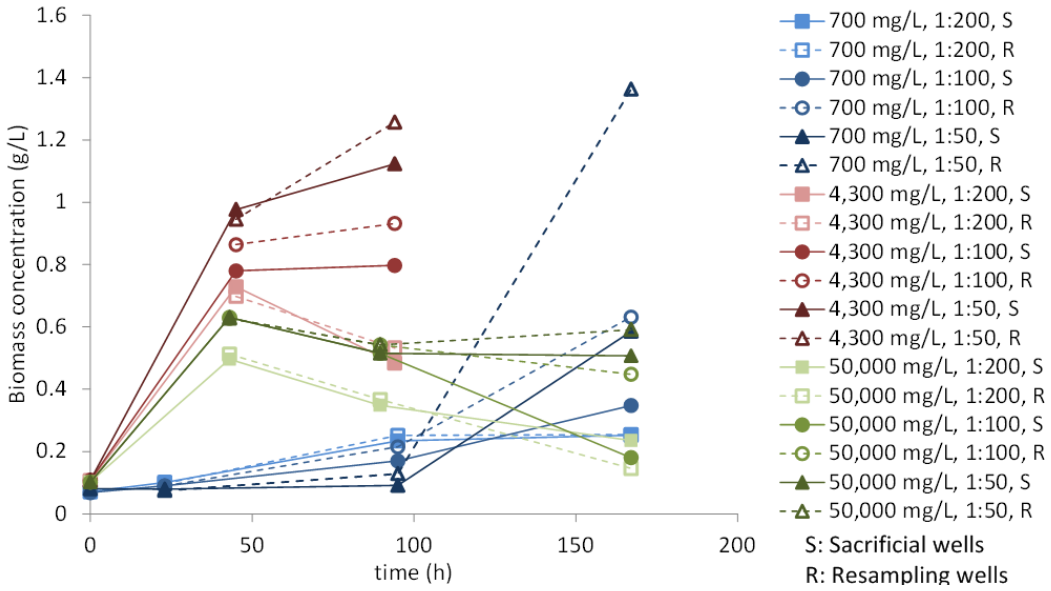

Figure 6.3. Results for the growth of *Chlorella sorokiniana* sacrificial and resampling plates under three different dilutions of the media (1:200, 1:100, 1:50) and three different CO_2 concentrations (700, 4,300, 50,000 mg/kg).

6.4.1.2 Factorial experiments

The growth rate was best for the highest nutrient dilution tested, 1:5, the lower temperature tested, 22 – 25 °C, and the higher light intensity tested, 150 µmol/m^2/s (Series 2). The nutrient removal rates for nitrates and phosphates were 97% and 37%, respectively. Uptake of nitrates was very rapid, with most series of the 1:200 and 1:100 dilutions experiments showing complete depletion of nitrate by the second measurement (Figure 6.5). It should be noted that results for biomass and nutrient concentrations may be overestimated due to the evaporation of the medium from the wells (e.g., up to 8 – 10 mL/day during Series 4), which meant that resampling wells contained a reduced volume at the end of the series of experiments.

Experimental data corresponding to CO_2 and factorial experiments are shown in Table V.7 and Table V.8 of Appendix V. The outcomes mentioned are also verified in Figure 6.7, showing the plots of interaction between the variables, CO_2 concentration, nutrient dilution, temperature and light intensity, on the productivity of the experiments. The effect of the CO_2 concentration at its two low values tested is greater than the effect of the initial nutrient dilution, as shown in plot A of Figure 6.7. Plot B shows no interaction between temperature and light intensity, though a slightly greater effect of temperature than light intensity. Plots C to D also confirm the greater effect of

temperature compared to light intensity and show a slightly greater interaction between the nutrient dilution and temperature, compared to nutrient dilution with light intensity.

The factorial experimental measurements are similar to the Blair et al. (2014) study, which used the same nutrients and genus, but flasks rather than plates. The fact that a significant effect of nutrient concentration and light on growth was found in their study, using similar nutrient concentrations, temperature and light intensities – although they obtained a much lower growth rate with the flasks – indicates that illumination and nutrients are simultaneously limiting factors and they are well taken into account for the model development.

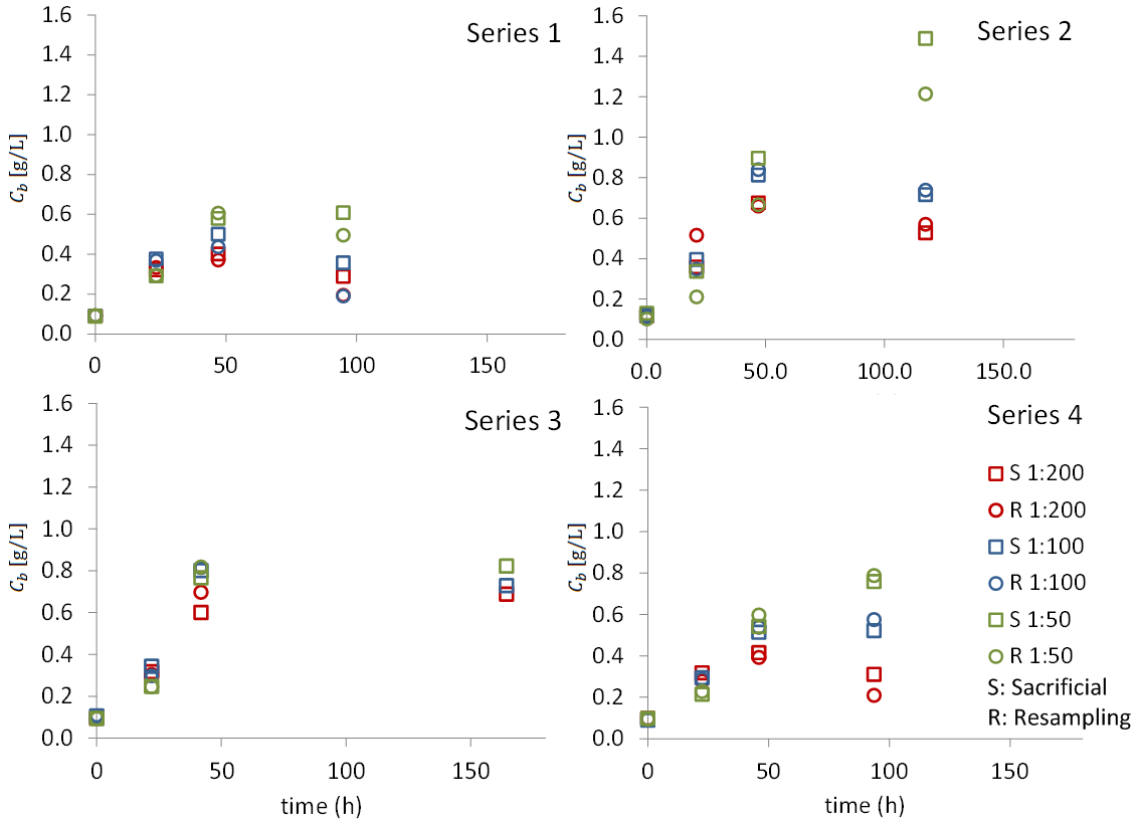

Figure 6.4. Biomass concentration measured for the four factorial experimental series.

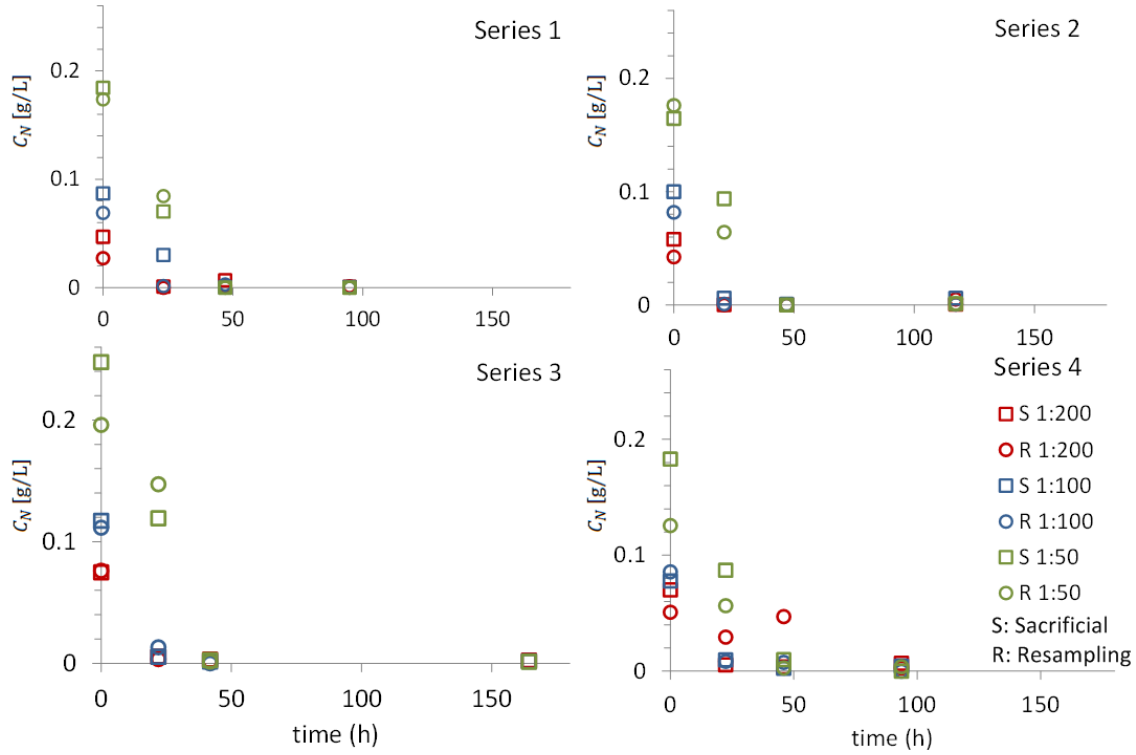

Figure 6.5. Nitrate concentrations measured for the four factorial experimental series.

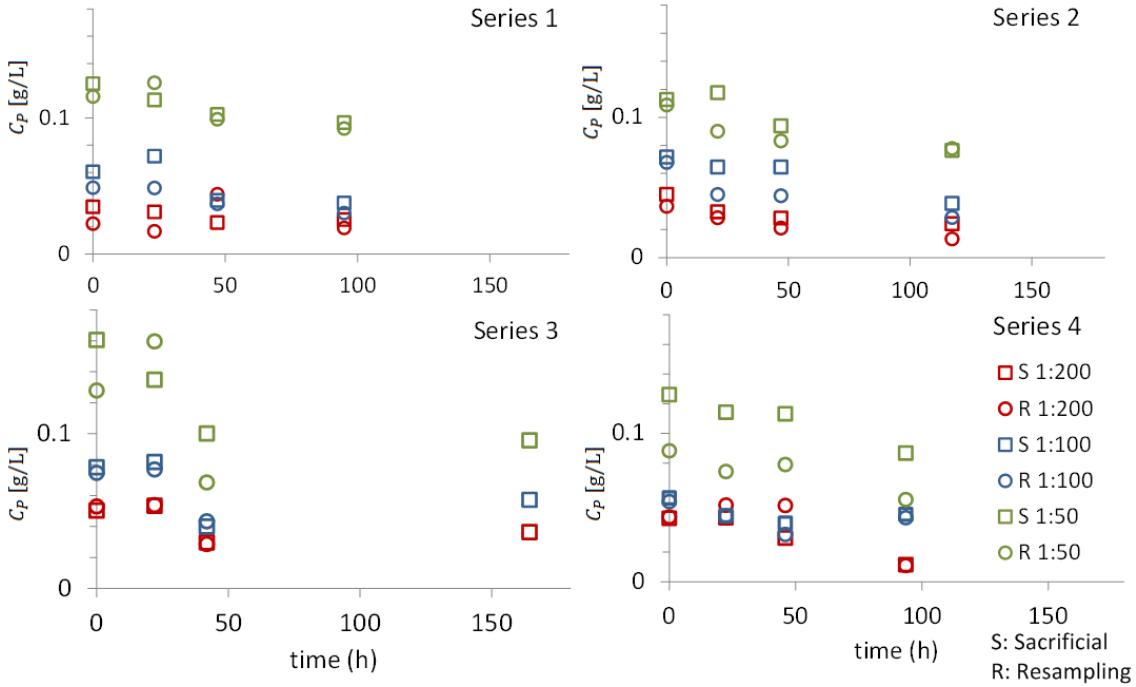

Figure 6.6. Phosphate concentrations measured for the four factorial experimental series.

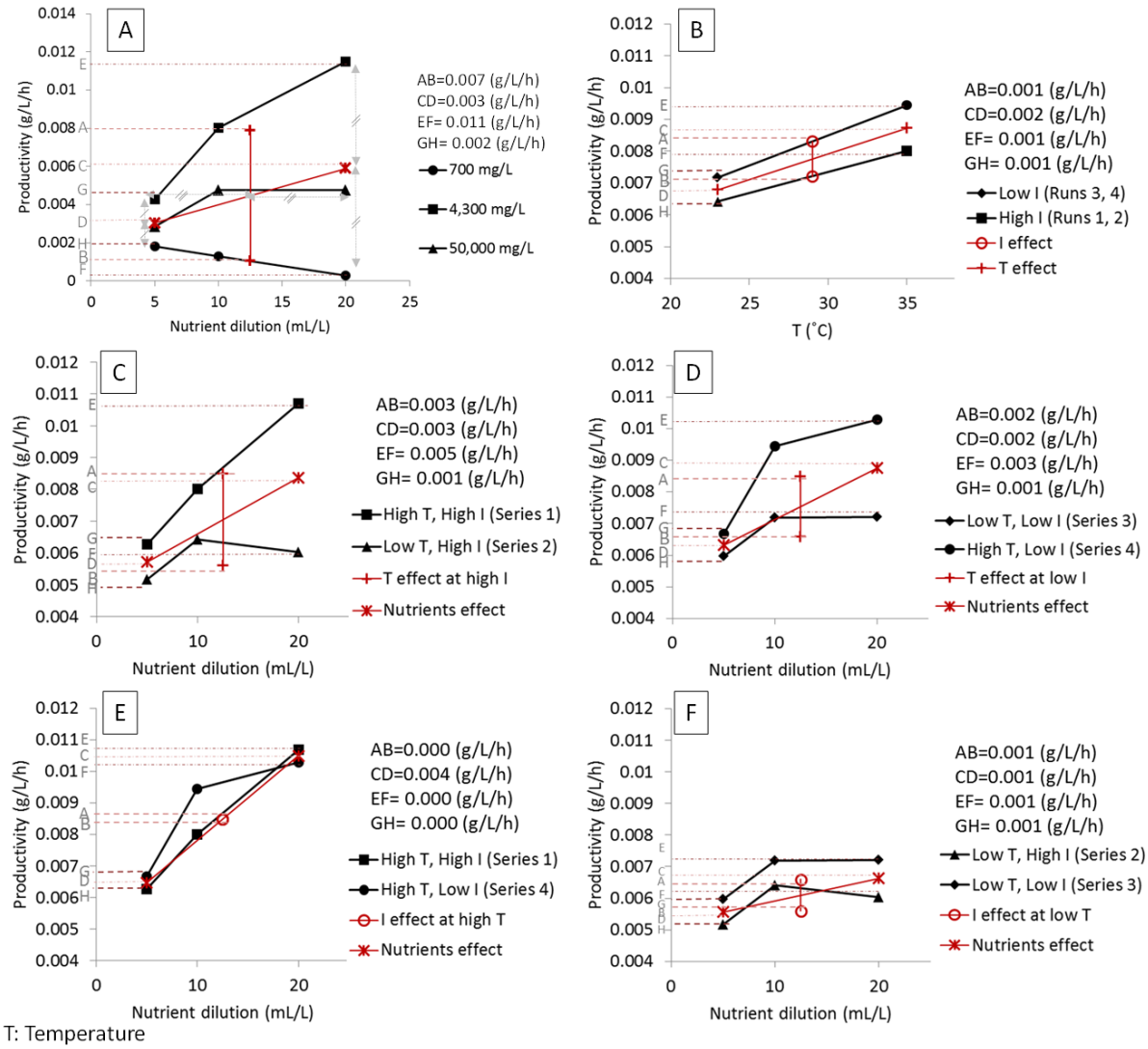

T: Temperature
I: light intensity
A: CO_2 experiments
B: Interaction between T and I
C: Interaction between T and nutrients, high I
D: Interaction between T and nutrients, low I
E: Interaction between I and nutrients, high T
F: Interaction between I and nutrients, low T

Figure 6.7. Interaction between the CO_2 concentration, nutrient dilution, temperature (T) and light intensity (I) on the productivity of the CO_2 experiments (I) and the factorial experiments (II-VI).

6.4.1.3 Statistical analysis

The P-values of the statistical analysis (6.3.3) are shown in Table 6.7 and Table 6.8. The t-test values from the average results from the sacrificial and resampling measurements of biomass and nutrient concentrations in the CO_2 experiments showed an insignificant effect of the difference between the sampling methods. The 1-way

ANOVA results showed an insignificant effect for both the CO_2 and initial nutrient concentration factors and no interaction between them. The regression P-values from the 1st measurement showed that the methodological measuring errors did not have significant effect on the initial values measured. The rest of the tests show that CO_2 concentration has a significant effect on the biomass concentration at the 2nd and 3rd measurements, whereas initial nutrient concentration becomes a significant factor at the 4th measurement. Finally, the two factors do not have a significant effect on the nitrates and phosphates at measurement time, which shows that better experimental design and appropriate frequency of measurement could detect differences for the different nutrient concentrations used. The high F-values of almost all tests imply insufficient evidence to prove a significant effect of the factors on growth.

Regarding the factorial experiments, t-tests for the effect of sacrificial samples A and B, taken at each ion chromatography measurement on Trials 2 of Series 1 and 2, showed no significant difference between the two replicates, thus their average values were used for the model's parameter estimation. Similarly, the average of sacrificial measurements from Series 1 and 2 and sacrificials of the rest of the experiments did not show a great difference from three variables measured in the resampling wells. Finally, Trials 1 and 2 for Series 1 and 2 did not show significantly different results either. The 1-way ANOVA of the effect of initial nutrient concentrations in each experiment showed an insignificant effect on biomass and nitrates, but significant on the phosphates in all experiments. The 2-way ANOVA showed an insignificant effect of the temperature on the biomass and nitrates and no interaction between temperature and initial nutrient concentrations in any of the experiments. Regression showed that illumination had a significant effect on the biomass only at the second and third measurements. Both nitrates and phosphates are shown to be significantly affected by the initial nutrient concentrations, which is more rational than the 1-way ANOVA result, due to independence from the different times. Also, temperature and illumination appeared to be important to the nutrient concentrations but their effect was lost after time zero, which would imply that this outcome is just an expression of possible measurement errors.

Table 6.7. P-values of the statistical tests of the CO_2 experiments. Shaded boxes indicate significant effect from P-values < 0.05.

Statistical test	Factor		Biomass	Nitrates	Phosphates
Paired two-tailed t-test	Sacr-Resamp		0.467	0.278	0.496
1-way ANOVA	700 mg/kg CO_2		0.77	0.28	0.09
	4,300 mg/kg CO_2		0.71	0.57	0.41
	50,000 mg/kg CO_2		0.58	0.66	0.33
2-way for 4,300 and 50,000 CO_2	CO_2		0.24	0.32	0.34
	Nutrients		0.63	0.61	0.34
	Interaction		0.87	0.51	0.41
Regression	1st measurement	Nutr	0.81	0.24	0.23
		CO_2	0.29	0.33	0.33
	2nd measurement	Nutr	0.052	0.45	0.28
		CO_2	0.013	0.50	0.75
	3rd measurement	Nutr	0.35	0.67	0.017
		CO_2	0.041	0.014	0.12
	4th measurement	Nutr	0.35	0.054	0.09
		CO_2	0.085	0.19	0.38

Table 6.8. P-values of the statistical tests of all the factorial experimental series. Shaded boxes indicate significant effect from P-values < 0.05.

Statistical test	Factor		Biomass	Nitrates	Phosphates
Paired two-tailed t-test	SacrA&B (Series 1&2 Try2)		-	0.51	0.46
	Sacr-Resamp		0.40	0.49	0.32
	Try 1&2 (for Series 1)		0.59	0.41	0.19
	Try 1&2 (for Series 2)		0.29	0.49	0.59
1-way ANOVA	Effect of nutr. Series 1 Try 2		0.64	0.45	0.000006
	Effect of nutr. Series 2 Try 1		0.70	0.68	0.02
	Effect of nutr. Series 3		0.98	0.40	0.003
	Effect of nutr. Series 4		0.65	0.57	0.005
2-way for Series 1,2,3,4 and effect of Nutrients, Temperature, Illumination	Series 1 & 2 (high I)	Temperature	0.13	0.69	0.52
		Nutrients	0.72	0.34	0.000006
		Interaction	0.66	0.89	0.34
	Series 3 & 4 (low I)	Temperature	0.98	0.68	0.036
		Nutrients	0.76	0.23	0.000003
		Interaction	0.91	0.84	0.61
	Series 2 & 4 (low T)	Temperature	0.15	0.76	0.14
		Nutrients	0.70	0.28	0.00006
		Interaction	0.69	0.80	0.37
	Series 1 & 3 (high T)	Temperature	0.69	0.77	0.86
		Nutrients	0.44	0.26	0.00000004
		Interaction	0.95	0.94	0.60
Regression	1^{st} measurement	Nutrinets	0.72	0.000002	0.000001
		Temperature	0.065	0.027	0.054
		Illumination	0.14	0.074	0.043
	2^{nd} measurement	Nutrinets	0.11	0.0015	0.0013
		Temperature	0.10	0.67	0.51
		Illumination	0.0005	0.25	0.09
	3^{rd} measurement	Nutrinets	0.049	0.24	0.00001
		Temperature	0.18	0.89	0.79
		Illumination	0.008	0.80	0.94
	4^{th} measurement	Nutrinets	0.54	0.27	0.08
		Temperature	0.060	0.23	0.32
		Illumination	0.50	0.79	0.60

6.4.2 Attempted model calibration

The results of the simplified model calibration are shown in Table 6.9, and the predictions of the calibrated simplified model (6.3.4.2) are shown along with the measurements in Figure 6.8 to Figure 6.11. The deviations are presented in Table 6.10 to show the individual actual over- or under-estimations of the model. t-test values between the experimental results and predictions for the different measurements of each experimental series are also given to assess the dependence of deviation on the measurement progress. The root mean square errors of the predicted variables were 36.7% and 9.5% for the biomass and substrate, respectively. Parameters K_a, K_I, K_S and m_S hit their bounds, as given in the literature, and the confidence intervals were not possible to estimate. Estimation of $Y_{C/S}$ was in agreement with its expected value according to grams of substrate uptaken for the measured grams of biomass produced. A test parameter estimation done for Series 1 using the normalised Arrhenius equation gave the same fit, implying that the Arrhenius equation does not influence the calibration much at this stage. The results of the attempt to calibrate the full model (6.3.4.3) are shown in Table V.9 to Table V.14 and Figure V.6 to Figure V.13 of Appendix V.

Table 6.9. Values of the estimated parameters from the calibration of the simplified model.

Parameter	Optimal Estimate	Initial Guess	Lower Bound	Upper Bound	95% confidence interval
E_a	27606	27312	20000	40000	5089
k_0	4001126	4001160	3000000	4100000	8090000
K_a	4	4	1	4	42
K_I	800	800	500	800	9003
K_S	3.000	2.862	2.000	3.000	5.589
m_S	0	5E-09	0	0.0004	-
m_a	0	0.003	0	0.08	0.0006
$Y_{C/S}$	2.3392	2.7808	1.0000	4.0000	0.1006

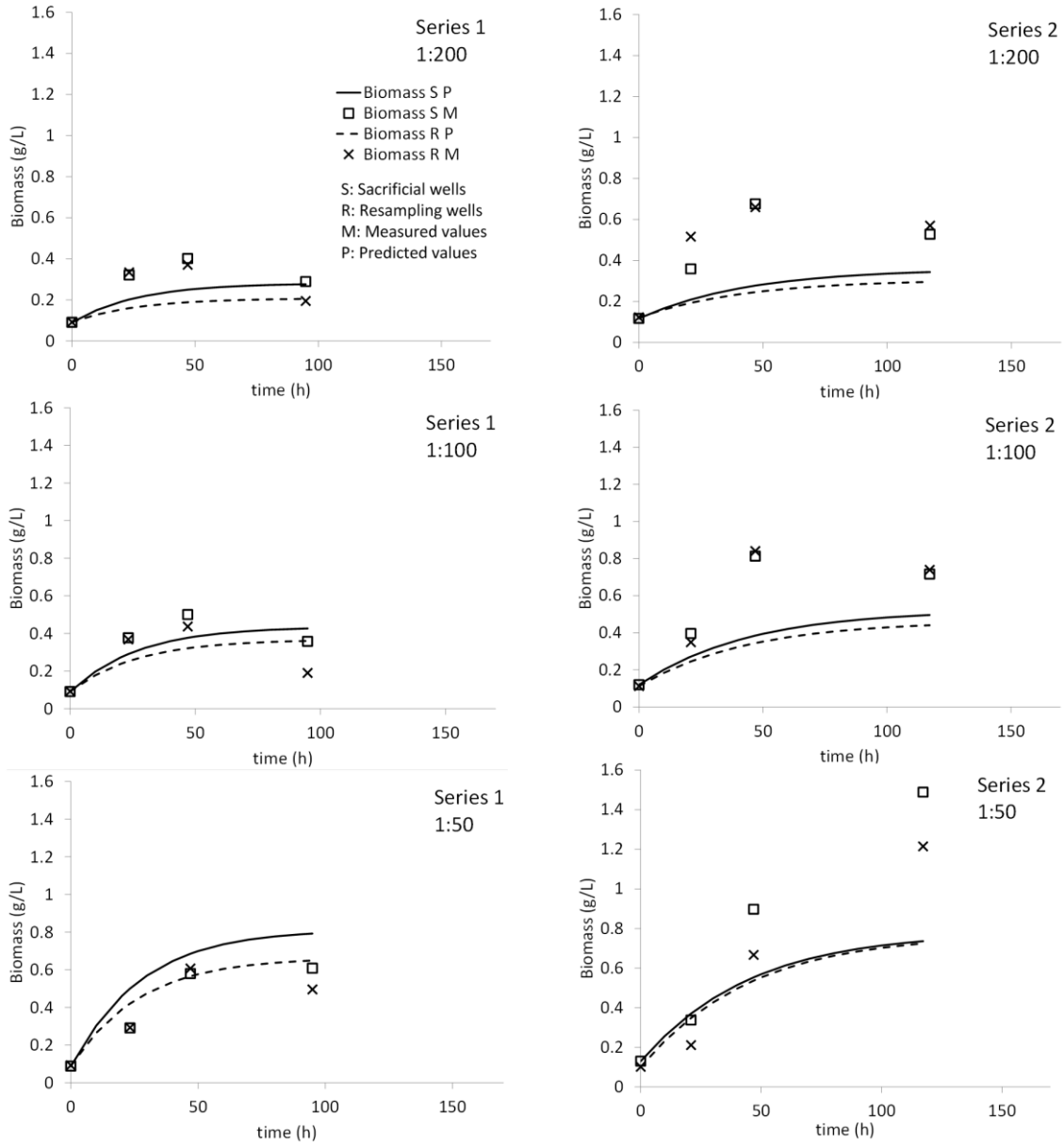

Figure 6.8. Biomass concentrations measured and predicted with the calibrated simplified model for Series 1 and 2 and the different nutrient dilutions.

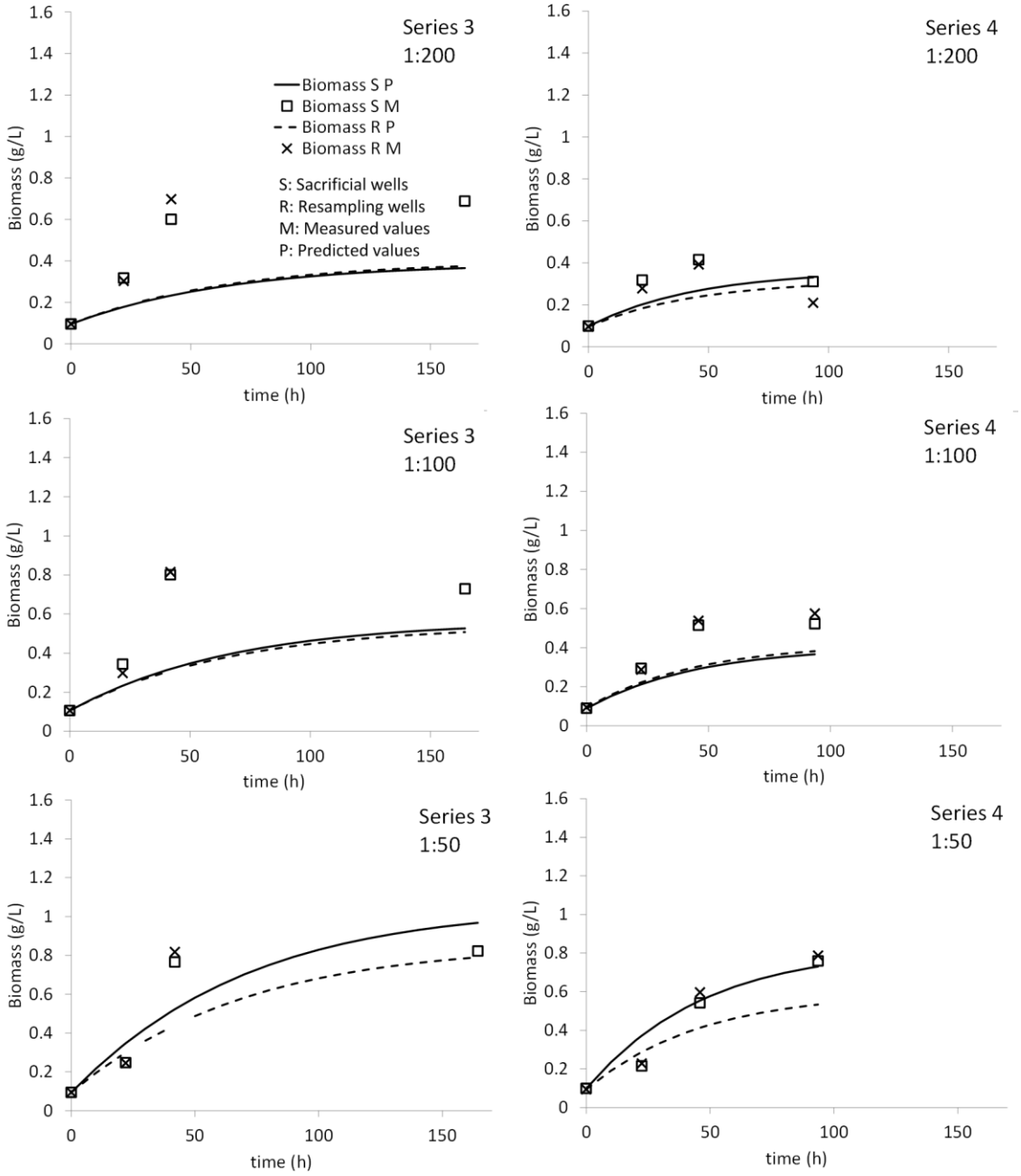

Figure 6.9. Biomass concentrations measured and predicted with the calibrated simplified model for Series 3 and 4 and the different nutrient dilutions.

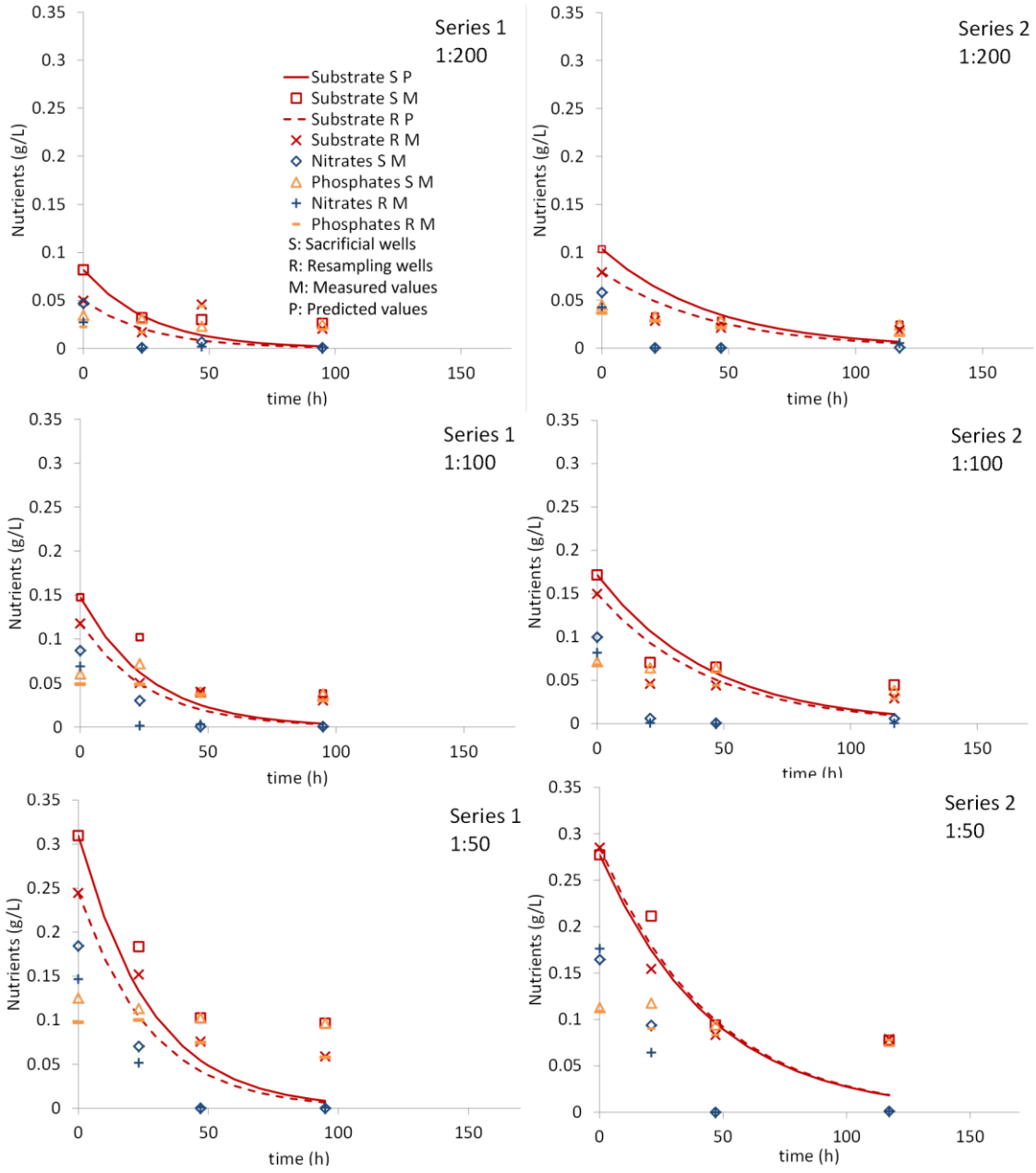

Figure 6.10. Substrate concentrations measured and predicted with the calibrated simplified model for Series 1 and 2 and the different nutrient dilutions.

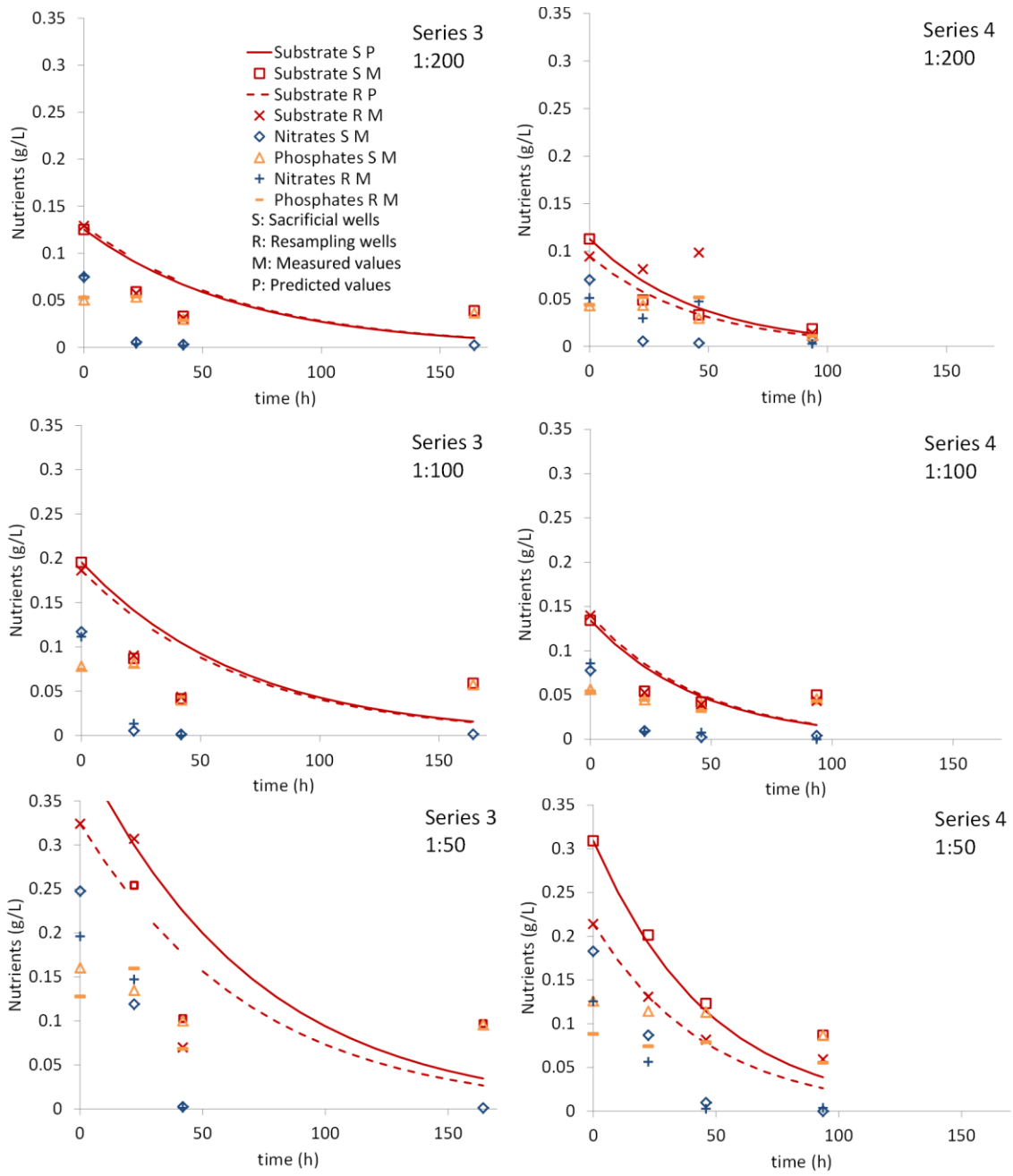

Figure 6.11. Substrate concentrations measured and predicted with the calibrated simplified model for Series 3 and 4 and the different nutrient dilutions.

Table 6.10. Average deviation percentage between the variables predicted by the calibrated simplified model and the measurements of the factorial experiments (the 1:200, 1:100, 1:50 nutrient dilutions for the sacrificial (S) and resampling (R) wells are shown; N/M are missing measurements).

	Series 1		Series 2		Series 3		Series 4	
	average % deviation	t-test	average % deviation	t-test	average % deviation	t-test	average % deviation	t-test
C_b (1:200R)	31.9	0.208	57.8	0.014	50.6	0.058	11.5	0.512
C_b (1:200S)	26.4	0.154	45.2	0.088	M/M	M/M	21.8	0.256
C_b (1:100R)	-10.5	0.850	43.1	0.118	40.0	0.141	33.2	0.084
C_b (1:100S)	9.4	0.509	38.3	0.103	M/M	M/M	33.7	0.064
C_b (1:50R)	-22.5	0.320	-1.7	0.469	-8.7	0.997	12.4	0.314
C_b (1:50S)	-40.1	0.033	26.4	0.259			-23.9	0.494
C_S (1:200R)	50.8	0.280	-7.6	0.724	-27.0	0.618	37.7	0.239
C_S (1:200S)	46.5	0.241	-13.7	0.701	M/M	M/M	-12.3	0.404
C_S (1:100R)	47.3	0.178	-16.5	0.621	-47.4	0.543	-9.0	0.085
C_S (1:100S)	55.6	0.059	11.7	0.947	M/M	M/M	0.6	0.998
C_S (1:50R)	54.8	0.016	13.7	0.834	-24.3	0.578	20.0	0.370
C_S (1:50S)	55.2	0.041	30.6	0.259			22.3	0.230

6.4.3 Model-based photobioreactor design and operation

The dynamic behaviours of the key variables in the case studies with the different objective functions to maximise biomass concentration and productivity and minimise PBR volume are shown in Figure 6.12. The corresponding time series of the control variable values required by the different case studies are presented in Figure 6.13. The case studies based on the different objective functions gave different results to the variables computed. PBR diameter is limited by light penetration, a fact which would result in a greater surface required per PBR volume and, hence, in high material requirements and large additional weight for a large-scale shipboard PBR. However,

PBR diameter was not used as a control variable as weight minimisation or constraint was not required by the current case studies, as it is shown by the results (Figure 6.3 and Figure 6.4) to be long enough for the growth and algae cell death.

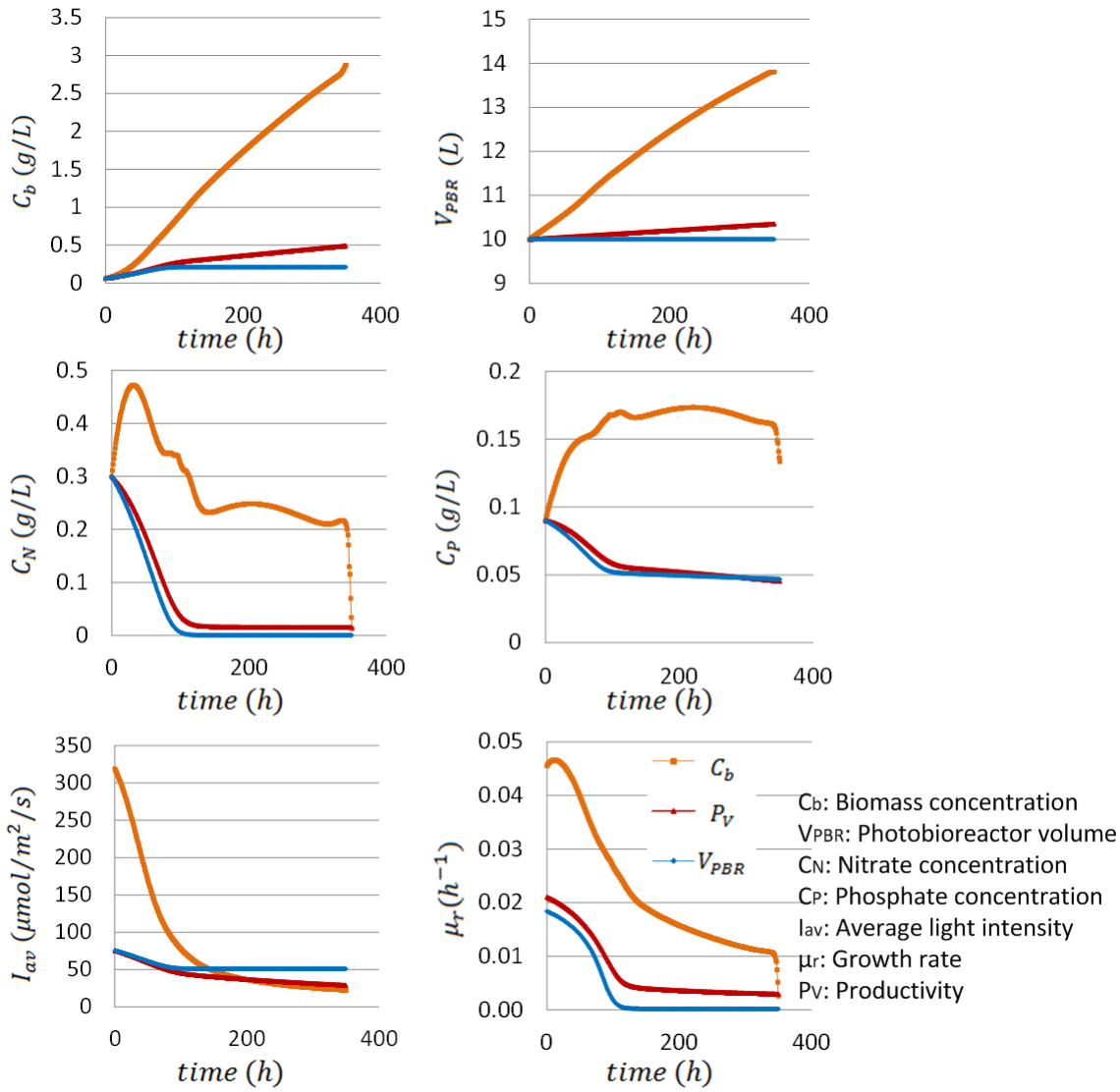

Figure 6.12. Time series of the key variables (biomass concentration, culture volume, nutrient concentrations, average light intensity, growth rate) for a time horizon of 350 hours, for the case studies that focused on optimising the biomass concentration, productivity and photobioreactor volume optimisation.

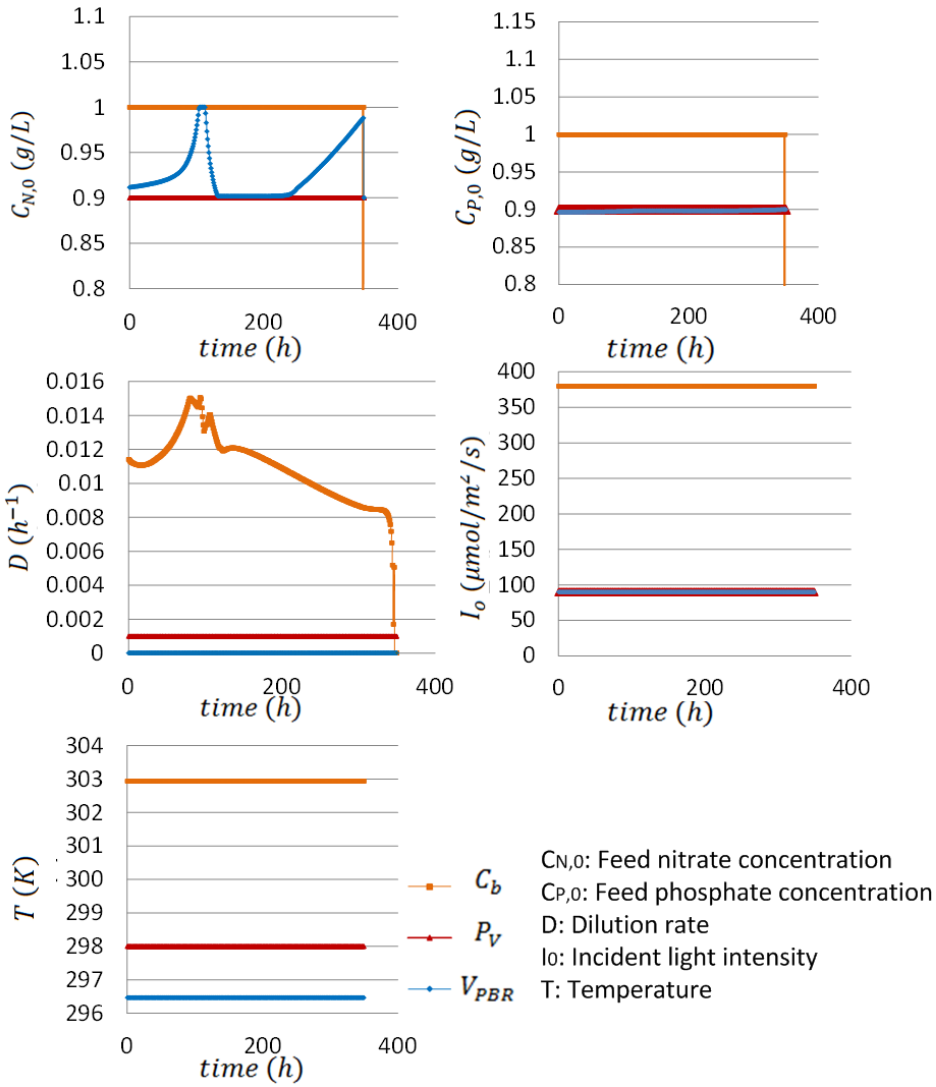

Figure 6.13. Time series of the control variables (i.e., nutrient feed concentrations, dilution rate, instant illumination intensity, temperature) for a time horizon of 350 hours, for the case studies that focused on optimising the biomass concentration, productivity and photobioreactor volume optimisation.

6.5 Model calibration and application – Discussion

6.5.1 Critical appraisal of the experimental approach

The experimental procedure had several limitations, as presented in the paragraphs below, potentially giving rise to errors in the results. The limitations were also responsible for the unclear significance of the factors' effects on the three variables.

Low frequency of measurements. More frequent measurements were needed for a more valid calibration using an average of the measurements. The fact that the four

phases of the growth are not identifiable in the plots of the experimental data illustrates that there are insufficient data points (6.3.1) to describe the expected features of the growth curve l, such as the lag phase described by the Arrhenius term.

Biomass precipitation before OD readings. Optical density readings had to be taken in the first minute after shaking of the sampling cuvette, while the algae remained suspended. However, the optical density fluctuated for the first few minutes, due to algae settling. Consequently, initial biomass optical density measured at time 0 was not the same for all experiments as expected (standard deviation 0.012 g/L). This could also be attributed to the loss of biomass during transportation (e.g., from the cuvette to the well).

Initial cultures of different age. There was a difficulty in maintaining a culture of the same age for the beginning of each experimental series. Incubating a new culture before the beginning of each experimental series would be time consuming; hence, the same cultivation bottle was used for each series and was diluted every time the broth volume was depleting. The difference in the culture age at the beginning of each experiment series influences the growth rate. This would result in some parameters of the model, such as specific maintenance rate, to actually be different from those estimated in the different experimental series.

Initial conditions. The lack of good fit of the model to the resampling measurements when using the sacrificial measurements for its calibration indicated the considerable effect of the failure in keeping the initial conditions used on the estimated growth curve stable among the different measurements, due to measurement errors.

Inadequate calibration curve. A complete calibration curve was not achieved. calibration of the spectrophotometer without the dilution of samples with optical densities greater than 0.8 reduced the accuracy of the measurements of the higher biomass concentrations as higher concentrations approach the detection limits of the instrument (see Figure V.3, Table V.2 and Table V.3 of Appendix V). Furthermore, the expired calibration of the Thermo Electron UV/Vis Spectrophotometer might have caused significant errors (measurements and description of the calibration curves are shown in Figure V.4 and Table V.4 of Appendix V).

Dilution of IC samples. The samples of 1:50 nutrient dilution at time 0 gave an IC measurement which exceeded the upper detection limit (200 mg/L) of the chromatograph. Consequently, all samples had to be diluted, which decreased accuracy for the samples of 1:200, as they approached the lower detection limits. A large discrepancy (of around 5% for nitrates and 25% for phosphates measured in the

main experiments) at time 0 was shown when comparing the initial nutrient concentration values measured with the ones estimated according to the media specification sheet (estimation shown in Table V.1 of Appendix V). This could be partially attributed to the fast nutrient uptake, but also to unfamiliarity with the ion chromatography method, as the nutrients were not only underestimated. A greater number of experiments could provide better estimation of the model parameters and a better fit of the model (see errors of the predictions in 6.5.2).

Also, a stop in growth (e.g., Series 1 1:50 in Figure 6.8 and Figure 6.10, and Series 3 1:50 in Figure 6.9 and Figure 6.11) shown in the experiments after the depletion of nitrates or phosphates did not occur in all series of experiments (e.g., Series 2 1:100 and 1:50 in Figure 6.8 and Figure 6.10, and Series 3 1:100 in Figure 6.9 and Figure 6.11). A possible error in the experimental method that could be responsible for this is non-detectable minor concentrations of nitrates and phosphates.

Evaporation of the medium. Evaporation of the medium from the wells (6.4.1.2) was a serious issue as it affects the optical density and ion chromatography results.

Inadequate illumination intensity measurements. There was variability of illumination intensity distribution from the light rods to the different wells, depending on their position on the plate (±20 μmol/m^2/s).

Gas leakage. Gas leakage from the greenhouse box may have resulted in variable CO_2 concentrations over time and within the box.

Extra problems during the CO_2 experiments. Additional problems arose which resulted in greater errors. First, the non-fully-transparent acrylic lids used might have blocked light and mass transfer. Second, CO_2 may have leaked from the chamber, where the 50,000 mg/kg CO_2 concentration was monitored. Also, the lower initial biomass concentration for the 700 mg/kg CO_2 level used might have caused a longer adaptation period. Finally, ion chromatography sample dilution was omitted during those experiments at that time due to unfamiliarity with the method. This fact may have led to inaccuracy of the nutrient concentrations measurements at time 0 (especially for the 1:50 dilution), which is revealed by their great difference from the rest of the measurements at time 0 in the CO_2 experiments (Table V.1 of Appendix V).

If each data point that was used to draw the plots (Figure 6.4 to Figure 6.6) had been the average over numerous observations, the results might have had a better fit (6.3.1).

6.5.2 Attempted model calibration

As expected by Demidenko (2013) (6.3.1), convergence on a global optimum was difficult to obtain in this non-linear regression, and the goal in this calibration was adapted from identifying a global optimum to finding a local optimum that estimates all parameter values within the range used in the literature. The experiments did not follow the same assumptions (e.g. consideration of chlorophyll to carbon ratio, see 2.3.6.3.3) used by the model (Zonneveld, 1998). Also, they were not designed according to the Xin et al. (2010) method (concentration of the non-limiting nutrient factor constant in each case, hence, data to be in accordance with Monod's model) and Bernard and Rémond (2010) method (temperature efficiency factor using cardinal temperature, see 6.2) for estimation of various limiting factors' parameters. The optimal values of each variable were not known, thus, the estimation of the model parameters using experiments where only one limiting factor acted each time was impossible.

Root mean square errors of the predictions were 36.7% and 9.5% for the biomass and substrate, respectively (6.4.1.2), which was comparable to the average analytical error of the initial substrate concentrations (6.5.1).

The model has a great number of parameters. A large deviation (Table V.12 of Appendix V) was observed in the estimated values of the parameters across the different stages of the calibration (Table 6.4). This fact could be attributed to the crucial consequences of the full model's complexity or to the calibration method. This was solved by stage-wise calibration, which had as a main problem the consideration of the N and P nutrient concentrations in a single substrate term in the model. Problems with the experiments (6.5.1) led to additional problems. The fact that the optimal estimations of the parameters did not give a good fit to the measurements with the model, could be a consequence of the number of stages of the calibration and of the errors in the measurements. The following observations were made regarding the estimated parameters.

Parameters outside meaningful bounds. Another problem encountered was that several parameters fell close to or outside one of their meaningful bounds. The inclusion of multiple factors in the biomass concentration formula – hence, multiplication with more values that are lower than 1 – does not allow the maximum growth rate to reach as a high peak value as it would have with fewer limiting factors. Therefore, during the calibration process, the half saturation constant values (K_I, K_N, K_P, K_{CO_2}) had to decrease to levels outside their lower bound reported in the literature, in order to increase the corresponding utilisation factors. The model itself however is

able to show the stages of the typical microbial growth curve (Figure 2.12), when the parameters are not limited to their physically meaningful bounds. One of the best fits of the full model (Eq.60) is shown in Figure 6.14, the parameter values of which are presented in Table V.16 of Appendix V.

No consideration of metabolism in the model. Due to the rapid uptake of the nitrates measured (6.4.1.2), the models (simplified and full one) predicted an early stop to growth. The most limiting factor in the given experimental conditions seems to be the nitrate concentrations, which is also verified by the fact that the yield over phosphates, $Y_{b/P}$, is estimated with a higher value than the yield over nitrates, $Y_{b/N}$. In some of the modelled biomass growth curves, a sudden decrease is shown instead of the smooth peak before apoptosis, due to the very low values taken by the nitrates efficiency factor in Eq.60 when nitrates deplete completely. In reality, as shown by the experiments in most plots (Figure 6.4 and Figure 6.5), even after the extracellular nitrates take values of zero, there is still growth. This indicates that metabolic characteristics and intracellular nitrate concentrations play a significant role in growth. When nitrates are excluded in stage 6, in order to show the detrimental effect of including the nitrate factor without including metabolism, there was a better fit (Table V.15 and Figure V.14 of Appendix V). This was the reason for the simplified model calibration attempt where the two nutrients were combined in one term as a substrate, regardless the fact that N and P have different roles and metabolic functions (2.3.2.4). Another way to overcome this, instead of including metabolic factors in the formulae, would be to measure the internal nutrient concentration experimentally.

Non-detectable nutrient concentration. Sometimes phosphates were not depleted in the model because biomass stopped growing in the model due to the nitrate depletion used from the experimental results. Thus, the parameter estimation process predicted higher values of the maintenance supply rate of minimum phosphates consumption to maintain cells, m_P values, which also happened to be partially determined by the random selection of the initial guesses. However, since there is inconsistent stop in growth shown after the depletion of nitrates or phosphates among the different series of experiments (6.5.1), it is not only the model that has an error but also the experimental method. This is supported by the fact that there is better fit at high (1:50) nutrient levels (measurements at low ion chromatography were not accurate enough to calibrate model).

Lag phase: Given that some of the factors that influence lag behaviour are culture temperature and pH history (2.3.6.3.4), the fact that the cultures of the different

experimental series had a different age might have influenced the differentiated results across the series of experiments. It might have been more accurate if an empirical term was used in the model that includes both factors (as cited in 6.2).

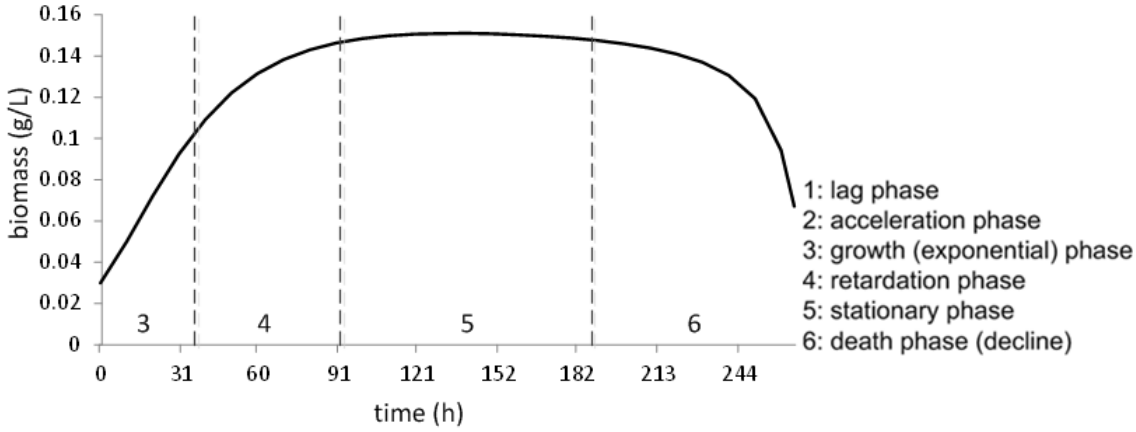

Figure 6.14. Stages of a typical microbial curve, as indicated in Figure 2.12, demonstrated by the full model.

Modelling also yielded several interesting observations regarding the role of nitrogen and phosphorous in the real and modelled algal systems:

Sensitivity to the half saturation constant for nitrates. A high sensitivity of the biomass concentration to the half saturation constant for nitrates, K_N, parameter was observed during the calibration of the full model. Also, the sudden stop of growth shown in Figure V.8 – Figure V.11 in Appendix V proved to be sometimes very sensitive to certain parameters, such as the half saturation constant for phosphates, K_P.

Maintenance coefficient. Very low values (≤2 × 10^{-4} g.substrate/g.cells/h in all cases, as in Ruiz et al., 2011) were predicted of the maintenance coefficient, m_S (2.3.6.3.3), which could be due to the fact that nitrogen and phosphorus are not elements essential for cell maintenance, unlike carbon (Ruiz et al., 2011).

6.5.3 Optimisation of the photobioreactor using the model

Figure 6.3 shows that all the control variables used in the case studies examined (6.4.3), nitrate and phosphate feed concentrations, dilution rate, instant light intensity and temperature, were computed to be higher in the case study that focused on optimising biomass concentration, rather than productivity or reactor volume. This fact

was responsible for the highest growth rate in this study among the rest of the case studies. Also, as expected, the case study that focused on minimisation of the PBR volume did not predict any requirement for dilution as this would increase the PBR volume. Temperature was also predicted to be lower in this case study, compared to the other two. Sharp changes in the feed nitrate concentration values predicted when the dilution rate was zero (in the volume minimisation process) are possibly an error deriving from the computational method.

Biomass concentration showed a continuous increase in all case studies, regardless of the dilutions occurring, which could be due to the low dilution rates proposed. The volume of the PBR and nutrient concentrations were predicted to be 40% higher for the case study that focused on optimising the biomass concentration rather than productivity or reactor volume, due to the dilutions occurring. A faster increase in the growth rate occurred after each dilution, due to better light penetration, as well as the high concentration, and thus faster depletion, of nutrients. Such a use of objective functions could minimise costs related to excessive nutrient supply, as the dilution rate is predicted to be low enough to avoid any excess of nutrients and consequent deceleration of growth, but at the same time high enough to accelerate growth by increasing the nutrient supply and light penetration. Average light intensity was significantly higher at the beginning of the biomass concentration optimisation case study, due to the high instant light intensity supplied, but it later decreased to the same range of values as in the other two case studies, due to the light inhibition caused by the high biomass concentration grown. It should be mentioned that since the Cartesian-averaged intensity is used in the calibration and the case studies of the model for consistency with the validation experimental set-up, more accurate results would have been obtained if cylindrical coordinates had been used in the optimization of the tubular PBR considered.

6.5.4 Improving the experimental design and set-up

Illumination and nutrients are simultaneously limiting factors and were both taken into account for the development of the model of algal growth kinetics. It was experimentally demonstrated that the effect of the difference between the sampling methods and of the methodological measuring errors on the measurements was insignificant. It was also shown that the effect of the CO_2 and initial nutrient concentration on biomass concentration was significant at only some of the measurements, whereas the effect of increase in biomass concentration due to

increase in temperature was slightly greater than that due to increase in illumination. No significant interaction between the factors was observed, but a slightly greater interaction was noted between the nutrient dilution and temperature compared to nutrient dilution with light intensity.

Non-linear regression of the growth model proved to be very complex, due to the large number of parameters. The fact that the optimal values of each variable were not known for the given set-up, made it more difficult to estimate the model's parameters. The calibration results implied model complexity, inadequate fit, a strong effect of the fit on the initial conditions of the experiment, an effect from the culture age, a need for larger volume of the vessels where the culture grows, the decisive influence of the initial guesses on the calibration, the estimations approaching given bounds, and a need for the inclusion of metabolism in the model. Also, better experimental design and a more appropriate frequency of measurement may enable the detection of a difference between the growth under the nutrient concentrations used. The case studies with the different objective functions gave different results for the variables investigated. The use of the objective functions presented here could minimise costs related to excessive nutrient supply.

7 Practical aspects of the shipboard integration of the photobioreactor

7.1 Introduction

In designing a shipboard PBR for waste processing, a key consideration is the location and method for storing a potentially large body of liquid with microorganisms. The design aspect becomes more challenging if the bioreactor is to have a minimal impact on the ships primary trading role, be it carrying cargo or passengers. Therefore, design and integration of a shipboard PBR facility should take into consideration existing ship systems such as ballast tanks for storage and growth of microorganisms and the engines of the ship for heat generation and nutrient supply via the flue gas. However, extensive modifications to the overall ship design may prove to be unavoidable, given the complex and multiple requirements of the PBR system.

Through the use of preliminary models, this chapter starts (7.2) by examining the availability of space for a PBR within the ballast system of different ship types and sizes, to treat gas emissions. The second part of this chapter (7.3) briefly examines the potential of a generic shipboard WHR system – which would apply to any ship size – to use the heat of the flue gas produced in a ship and store heated water in the ballast tank (or a storage tank) to be used for the PBR and other heating requirements. Different cases of operating conditions are examined for a ship of similar size as Tamesis in Appendix VI. Finally, the heating rate output from the flue gas of each ship of the current tankers and ferries fleet is computed, to examine the generic potential of onboard WHR systems to be used for PBRs.

The adaption of the PBR to the temperature conditions inside ships is examined in the third part (7.4) of this chapter. As mentioned in 2.3.2.3 and 2.2.3, the average temperature range tolerated by algae is 15 – 40 °C and the average flue gas temperature is 380 °C. For the case where a PBR is installed on the deck with an average ambient temperature around 10 °C, temperature control of the PBR becomes a vital issue. The need for heating is irrespective of the PBR position within the ship, as heat is lost either to the ambient air or the ballast's surrounding water. A system for the temperature control of the PBR developed in Chapter 4 is demonstrated and examined in this chapter. The suggested design would allow the PBR to be integrated into a WHR system on board a ship without requiring major modification to the PBR or

decreasing significantly its photosynthetic efficiency. The heat exchange structure is designed for tubular PBRs in general, hence, it is suited to small scale applications that do not treat the total ship emissions.

7.2 Availability of space for implementation of a photobioreactor in different ship types

7.2.1 Introduction

Ballast tanks offer space for microorganisms to grow but would require artificial light to support growth of photosynthetic organisms. On the other hand, an external installation (on deck) would benefit from direct access to natural light but would be more susceptible to climatic factors, temperature control, and be associated with reduced stability and possibly interfere with routine shipping activity. A combined system is imagined, in which the ballast tanks are used along with externally mounted PBRs so that the algal culture can be circulated from the large ballast volume to an external PBR, allowing for growth in light and dark cycles.

The main purpose of the ballast tank is to provide stability during material transfer and while underway. Surrounding water is typically used for ship ballast, due to its ready accessibility and is kept separate from the cargo and passenger space, so that safety and environmental risks can be better managed. Ballast water is pumped in and out and can be moved around various chambers to maintain safe operating conditions throughout a voyage. The dynamic nature of the marine environment poses a challenge for provision of optimal algal growth conditions and is also associated with potential safety, economic and environmental implications.

7.2.2 Materials and methods

A fundamental model has been developed, making use of Clarkson's World Fleet Register database (Clarkson Research Services Limited, 2011), and using inputs such as specific fuel consumption, engine power, ship size and growth rate in the PBR. The model estimates the total emissions and PBR water needs for a variety of tankers and ferries with different ballast capacities and engine sizes. The calculations are based on the widely accepted method of Moreno-Gutierrez et al. (2007). The fuel consumption is estimated according to Eq.68.

$$F_{fuel} = P_{ME} \times LF_{ME} \times S_{fp,ME} \times 24 \times r_{oper} \quad (68)$$

where P_{ME} is horsepower, LF_{ME} the load of the engine, $S_{fp,ME}$ specific fuel consumption per power unit and r_{oper} the day operation ratio. The model focuses on the main engine and assumes that the auxiliary engine emissions would either have a separate system or can be considered negligible relative to the main engine's emissions.

The fuel flow rate during the operating hours, the CO_2 flow rate and the PBR water requirements to treat the CO_2 produced are computed by Eq.69 – Eq.71, respectively:

$$F_f = \frac{F_{fuel}}{24 \times r_{oper}} \quad (69)$$

$$F_{CO_2} = F_f \times C_f \quad (70)$$

$$V_{PBR} = \frac{tpd \times C_f \times f_{scr} \times 1000}{Pr_{PBR} \times f_{fix}} \quad (71)$$

where C_f is the carbon emission factor, Pr_{PBR} is the productivity of the PBR, f_{scr} is the ratio of CO_2 fixed and f_{fix} is the CO_2 fixation factor.

The assumptions used are:

1. Load: the engine is operated at 0.75 of its maximum power output (Lloyd's Register Marine Services, 2008; Saborido et al., 2007).
2. Specific Fuel Consumption of the engine: 190 g/kWh (Lloyd's Register Marine Services, 2008; Saborido et al., 2007)
3. C_f (Carbon Emission Factor): 3.17. CO_2 emissions do not depend on the type of the fuel used or the engine type (2.2.1.1). The total bunker consumption (in tonnes/day) is simply multiplied by a factor of 3.17 in order to estimate the CO_2 emissions (in tonnes/day) (Psaraftis & Kontovas, 2008).
4. CO_2 concentration in flue gas: 5.2% (Cooper, 2003; Nishida et al., 1998; West, 2009).
5. Daily operation time (hours working per hours of the day) of the tankers is 1 (Chevron Shipping Co, 1995), and of the ferries is 0.45 (Mossey, n.d.; Nexus, 2010), although a rate of 0.8 for tankers and 0.3 for ferries minimised the deviation between the estimated and given fuel consumption values.
6. Ballast capacity: approximately 37% of the deadweight tonnage as justified in 2.2.2. This is a conservative assumption, as some data suggest a larger capacity (even double) (Clarkson Research Services Limited, 2011).
7. Proportion of the CO_2 captured: 39% of the flue gas is captured (Doucha et al., 2005), as mentioned in 2.3.5.2.

8. CO_2 fixation factor: 1.88 g/g of dry algae produced (derived from the molecular formula of algal biomass CO0.48H1.83N0.11P0.01) (Seambiotic Ltd., 2008; Van Den Hende et al., 2012).
9. Average productivity of the PBR: 1 g/L/day (Douskova et al., 2009).
10. The biomass grows all day although it is fed with the CO_2 only during the operating hours.
11. For simplicity, only fuel consumption during full load operation is considered (idling and manoeuvring are not explicitly considered), since this dominates the operating profile in terms of CO_2 produced.
12. 1 L of broth equals 1 kg broth

7.2.3 Results and discussion

The total water mass requirements for the treatment of the total flue gas emissions of each ship were computed. As shown in the Figure 7.1 and Figure 7.2, many tanker ballast tanks would be able to store sufficient water mass for the operation of a PBR that treats the total amount of their engines' emissions. The potential is lower for ferries, because of their high fuel consumption and low availability of space. This implementation is therefore feasible for the treatment of only a small part of the emissions, especially if the ballast is also expected to accommodate hot water from the WHR system for the heating of the PBR. Therefore, analysis of space availability for a PBR shows the implementation to be feasible in many cases, but it is also shown to be a big issue in many cases and ways to improve efficiency of the absorption need to be found. Actual results might be more promising in reality, as the ballast capacity ratio is actually larger than the one used for the calculations, according to some data.

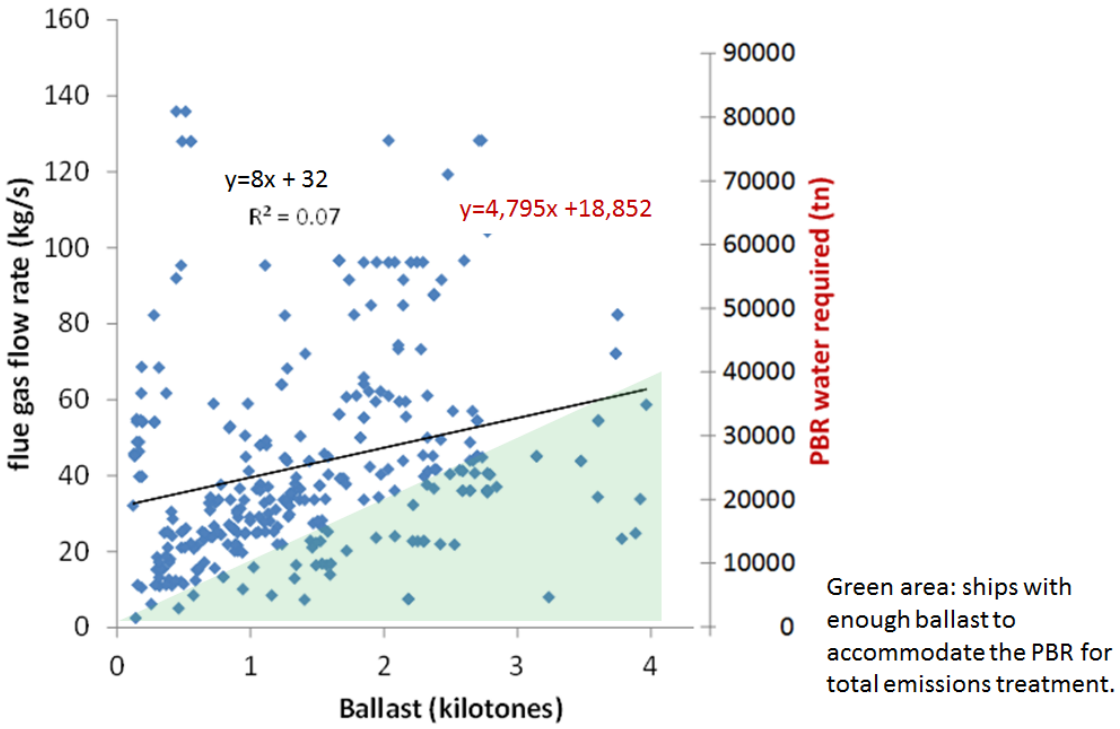

Figure 7.1. Ballast capacity computed for various ferries along with their estimated flue gas flow rates and the water requirements of a PBR to treat the total amount of emissions.

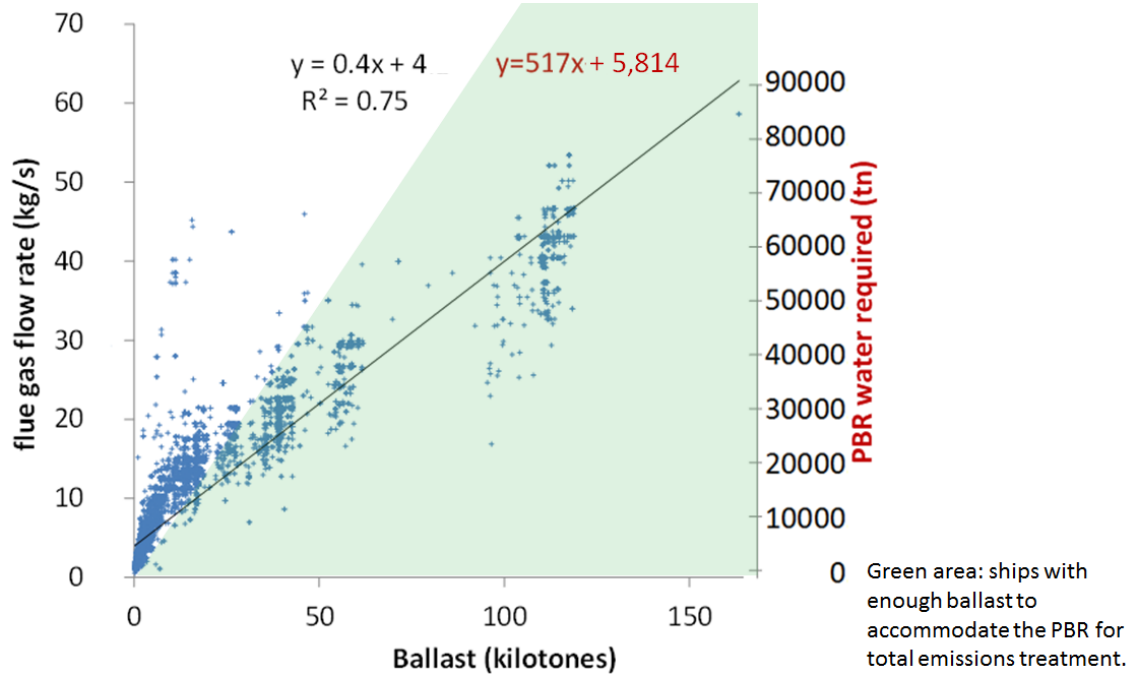

Figure 7.2. Ballast capacity computed for various tankers along with their estimated flue gas flow rates and the water requirements of a PBR to treat the total amount of emissions.

Apart from the ship type, its age plays a contributing role for the potential of the installation. It is less likely that older vessels would be able to repay the investment of either a scrubber or a PBR installation before the end of their commercial use. However, many newer vessels could save money by installing scrubbers or carbon capture and storage methods if taxation is imposed. Future work on this model would include energy requirements of the different modules, energy penalty and net CO_2 avoidance.

7.3 Use of ballast tanks for waste heat recovery

7.3.1 Introduction

Heating of ballast water to 37 – 38 °C using waste heat in tankers has been investigated for destruction of non-indigenous species before offloading of ballast water (Prince William Sound Regional Citizens' Advisory Council, 2005). In this case, heated ballast water could be used for heating of the spaces or the PBR during non-operating hours, minimizing the operating costs for heating. However, thermal treatment of ballast water is difficult to retrofit on old ships because of safety problems with expansion or corrosion (Prince William Sound Regional Citizens' Advisory Council, 2005). Extraction of the heat of the flue gas or the engine to the cooling water is one of the ways to thermally treat ballast water. The ability to couple algal growth with the ship engines, machinery, emissions and water use and to use low grade heat from the engine and cold water from the seawater or river water would make a technological advance that would bring emissions and costs down.

Some of the ships shown in 7.2 with enough storage to accommodate a PBR on board could have potential to also accommodate a WHR that facilitates the PBR heating overnight during non-operating hours, as well as the heating requirements for other utilities, by using the heat of the engine or the flue gas. The goal would be to simultaneously fit both the PBR system and the water tank for the WHR system into the ballast tanks. This section examines a whole ship WHR system design for a case ship of size similar to that of the Tamesis vessel.

Water stored at different temperatures in different compartments would supply thermostatically mixed water to the PBR, whereas the other compartment at higher temperature would supply the series of radiators working on the ship, and another would store hotter water overnight for the continuous operation of the PBR (3.2). In the current model a single compartment is examined.

7.3.2 System description and flowsheet development

The diagram in Figure 7.3 represents the central cooling system suggested for a WHR system on a ship of similar size to the Tamesis vessel, with a PBR (3.2). The storage tank supplies water heated from the flue gas to the series of radiators working on the ship and to the PBR continuously, by storing hot water without additional heating overnight. The water streams that would require management and integration with a WHR system are indicated with red and blue arrows. The flue gas would be cooled in a HE that heats up water taken from the sea or the river. For ships with big engines, a series of HE might be needed in order to cool the flue gas adequately. The cooled flue gas would have to pass through an open cycle SO_x scrubber before supply to the PBR. The PBR can either be based on the deck if it is small and treats a part of the emissions, or in the ballast tank, in a different compartment from the one where the hot water is stored.

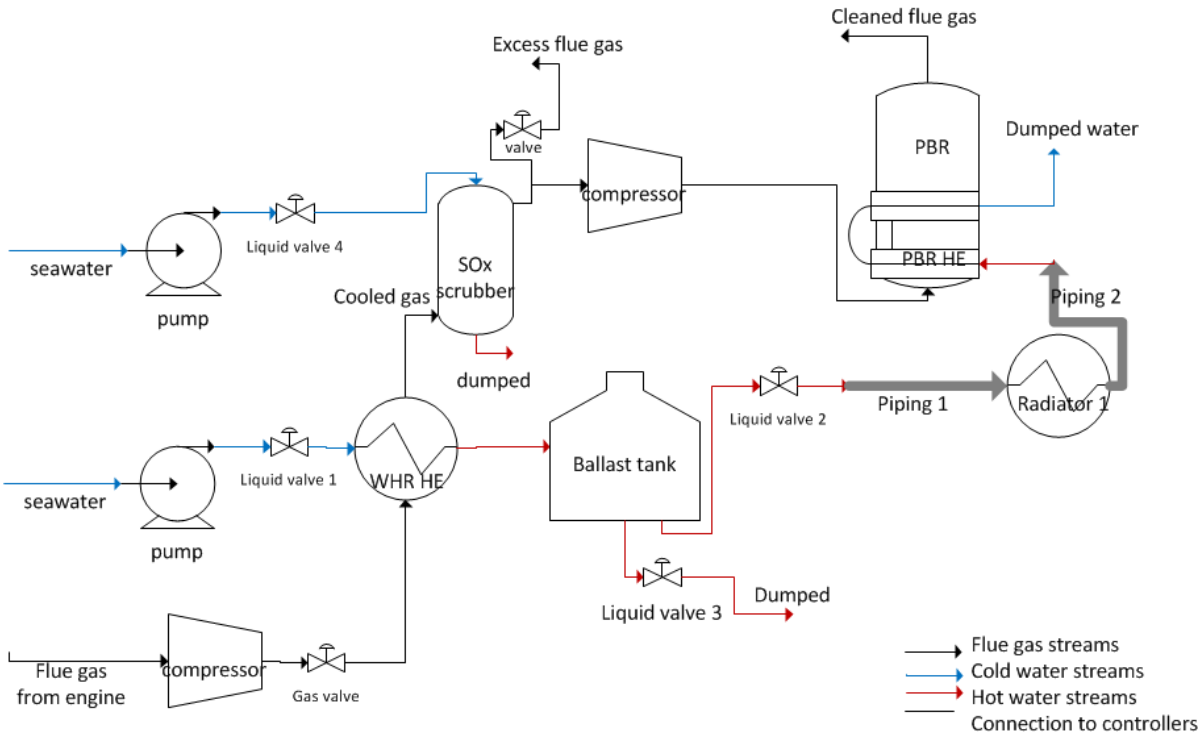

Figure 7.3. Flow diagram of the photobioreactor and waste heat recovery system on board.

In general, the WHR and PBR systems would have to be integrated into the ballast water management decision support systems, as ballast is not always allowed to be

filled. It is recognized that, in practice, the ship will not always be in an operating condition, where it can carry a large quantity of ballast water, according to the ballast water discharge assessment decision model by David and Gollasch (2015). Also, Tamesis does not need to comply with ballast water regulations, but tankers will do, therefore some considerations may work or may not work depending on the case.

A preliminary quantitative study with specific values of inlet and outlet temperatures and water flow rates of three HEs (two radiators and one for the PBR control) was conducted using a gPROMS flowsheet model (software introduced in 6.3.4), to verify the feasibility of the scenarios mentioned later in the present section. The first case considered a low flue gas flow rate (corresponding to approximately 0.2 tonnes/day fuel consumption engine if considered for a ferry), a small water storage capacity (40 tonnes) and two radiators on board. The objective was to first examine a case where one HE is enough to recover the heat from the whole flue gas produced by the engine. Sources, sinks, pumps, compressors, valves, tanks, pipes, heat pipes, coolers and HEs, as well as level and temperature controller component models of the software were used to construct the flowsheet (actual flow chart shown in Figure VI.1 of Appendix VI). Each gPROMS component model features an equations system. The flowsheet model method, the assumptions taken and the results are presented in Table VI.1 to Table VI.4, Figure VI.2 and Figure VI.3 and the text of Appendix VI. This design assumes the following:

1. A HE is retrofitable to the exhaust system of the ship.
2. A ship has sufficient space to accommodate the required storage tanks; implementation in the ballast tanks was not specifically considered.
3. All equipment (storage and distribution) is ideally insulated – i.e., no heat is lost except through radiators.
4. The issues of freight increase and cargo load from the ballast water mass required for the heating is not taken into account as the case ship is moored.

The main variables that affect the performance of a continuous WHR system on board like the one in Figure 7.3 are:

1. Flow rate of the flue gas into the HE F_g
2. Flue gas temperature
3. Heat transfer area of the HE
4. Flow rate of water into the HE $F_{w,1}$
5. Flow rate of water out of the tank $F_{w,2}$

6. Storage capacity
7. Ambient temperature
8. Heating rate required by the PBR and the radiator

Three constraints need to be fulfilled:

1. The heating rate of all the radiators and the PBR HE must satisfy the heating requirements of the ship (this is considered to be fulfilled when the temperature at the exit of the heater 3 is always higher than 28 °C),
2. The stored water mass is enough to last until the end of the night when the engine starts to operate again and heat up new hot water,
3. There is no overflow of the storage tank to cause flooding.

For the fulfilment of the above constraints, and for the given flue gas flow rate and storage capacity, the flow rates of the water through the liquid valves 1 and 2 needed to be adjusted simultaneously. In the model, this was done by the following control variables: Centrifugal pump flow rate, valve liquid 2 leakage fraction and flow coefficient, PID controller 2 max output. Five cases were examined for this ship example, where according to their water flow rates, different combinations of existence of (i) overflow, (ii) enough storage tank capacity and (iii) fulfilment of heating requirements were tested. The values of the control variables for the five cases are shown in Table VI.3 of Appendix VI and the outcomes regarding the constraints are presented in Table 7.1. Some of the variables were kept constant, whereas some were being adjusted to examine different scenarios for the gas and water transient flow rates and temperatures as well as the tank level (results are shown in Figure VI.2 and Figure VI.3 of Appendix VI).

Table 7.1. Constraints fulfilled for the cases examined (for a given storage capacity, given number of radiators and heat transfer areas of the heat exchangers and given flow rate and temperature of the flue gas).

	Case 1	Case2	Case 3	Case4	Case 5
Water flow rate at valve 1	$> F_{w1,p}$ and $<F_{w1,o}$	$>F_{w1,p}$ and $>F_{w1,o}$	$>F_{w1,p}$ and $>F_{w1,o}$	$<F_{w1,p}$, $<F_{w1,o}$ and $<F_{w1,b}$	$<F_{w1,p}$, $<F_{w1,o}$ and $>F_{w1,b}$
Water flow rate at valve 2	$<F_{w2,b}$	$<F_{w2,b}$	$>F_{w2,b}$	$>F_{w2,b}$	$<F_{w2,b}$
Overflow	No	Yes	Yes	No	No
Enough storage (when $F_{w2} \leq F_{w2,b}$)	Yes	Yes	No	No	Yes
Heating rate needs fulfilled (when $F_{w1} \leq F_{w1,p}$ and $F_{w2} \geq F_{w2,h}$)	No	No	No	Yes	Yes

7.3.3 Discussion for the different cases examined

For a given ship of the existing fleet, its flue gas temperature and flow rate, its storage capacity, the ambient temperature during its journey and its heating rate requirements are set variables that cannot be adjusted. Therefore, assuming that the heat transfer area of the HE is the maximum possible that can be implemented on the smokestack without causing considerable pressure drop, the only variables that can control the performance of the WHR system are the flow rates of the water, $\mathrm{F_{w,1}}$ and $\mathrm{F_{w,2}}$. The objective is to use the minimal possible pumping energy requirements while fulfilling the constraints mentioned in 7.3.2.

When the water flow rate through valve 1, $\mathrm{F_{w1}}$, is higher than a threshold value, $\mathrm{F_{w1,p}}$, it is not heated up adequately to provide the required heat rate to the radiators. If it is higher than a value, $\mathrm{F_{w1,o}}$, it leads to overflow of the tank for a given storage capacity. However, if it is below a value, $\mathrm{F_{w1,b}}$, it is not enough to fill up the required volume for the heating water of the radiators during the non-operating hours. When the water flow rate through valve 2, $\mathrm{F_{w2}}$, is higher than a threshold value, $\mathrm{F_{w2,b}}$, it empties the storage tank earlier than the beginning of the next day when the engine starts again. However, if it is below a value, $\mathrm{F_{w2,h}}$, it does not provide the required heat rate to the radiators. Therefore, the storage of a specific ship has enough volume when $\mathrm{F_{w2} \geq F_{w2,b}}$. Also, the heating rate needs are satisfied when $\mathrm{F_{w1} \leq F_{w1,p}}$ and $\mathrm{F_{w2} \geq F_{w2,h}}$.

Figure 7.4 and Figure 7.5 summarise the dependence of the objectives (vertical axes) on the two control variables (horizontal axes). The boundary values of the objectives in these figures are the constraints mentioned in 7.3.2. The optimal values of the two flow rates, F_{w1} and F_{w2}, to satisfy both objectives of the multiobjective optimisation would be the intersection of the two curves in both plots. The values, shapes and inclinations of the two curves depend on each specific occasion and the ship characteristics. However, the problem is more complex, as the two curves in each plot change depending on the value of the flow rate selected in the other plot, hence, there are many pairs of solutions. According to Figure 7.4 and Figure 7.5 and the corresponding pumping requirements for the five cases presented in Table VI.4 Appendix VI, the energy requirements for pumping are minimised when the lowest possible water flow rate is selected. However, this flow rate needs to be above a value, $F_{w1,b}$, that is enough to fill up a volume which will keep the heating overnight. Among the five cases examined, Case 5 is the best as it fulfils the heating rate needs, provides enough water volume without causing overflow or wasting pumping energy.

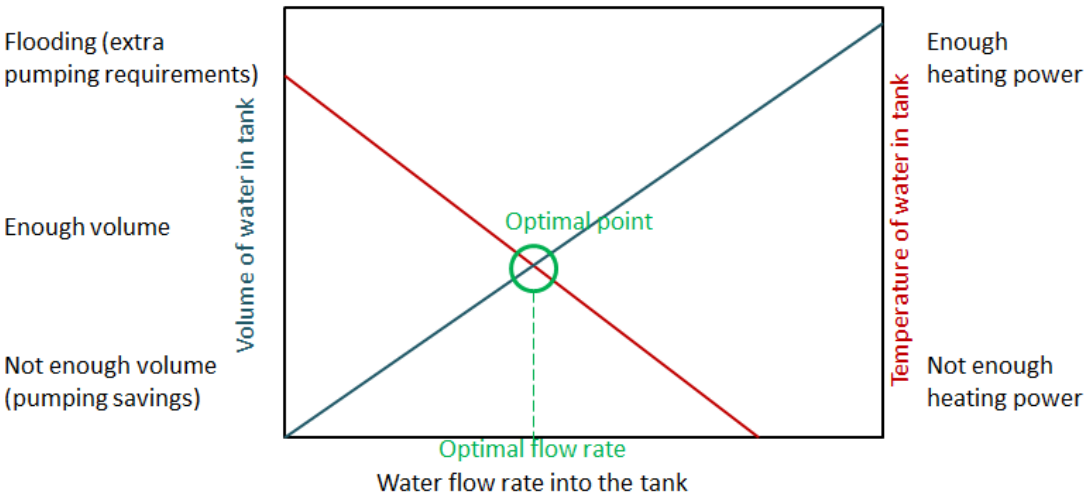

Figure 7.4. Objective functions versus the water flow rate into the tank.

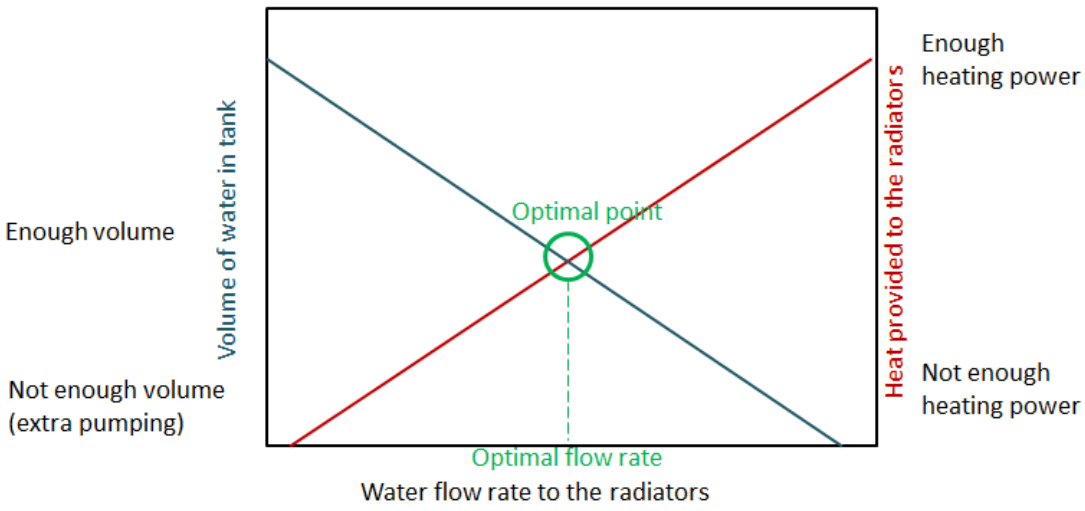

Figure 7.5.Objective functions versus the water flow rate into the radiators and the photobioreactor heat exchanger.

A proposed method to select the control variable values in the investigated problem would be to first assume a maximum temperature that can be reached by the heating water after losing heat in the tank, and subsequently use it to estimate the minimum possible flow rate $F_{w,2}$ which could be used to make this water stream reach its lowest allowed value at its exit from the heaters (temperature of the PBR plus 10 °C). The flow rate required passing through HE1 and flow into the tank can be computed – using the discharge rate from the tank – in order to fill just the volume needed by the time the engine of the ship stops. Finally, the heat loss of this water volume in the tank needs to be checked to see whether it results in the same temperature with the one assumed in the beginning. If it does not satisfy this check, a lower temperature needs to be assumed and the estimation steps need to be repeated. This approach would give the optimal water flow rates that correspond to the minimal possible pumping energy requirements in the existing problem. However, when the problem includes the cooled flue gas cleaning through the PBR and scrubber, then the low water flow rates selected from the proposed approach would not provide sufficient cooling to the flue gas to enter the scrubber or PBR, thus a higher rate should be selected.

7.3.4 Heating rate output to be stored in the ballast of tankers and ferries

Different pairs of ballast capacities and flue gas flow rates of existing ships of the current fleet can be implemented in this flowsheet model to reach outcomes about the heat rate that can be provided by each ship type and size. The great number of ferries and tankers data processed by the Clarkson's World Fleet Register (Clarkson Research Services Limited, 2011), is associated with wide range of ballast capacities, engine sizes and fuel flow rates. The computations developed in 7.2.2 were used to estimate flue gas flow rate and the potential of the different ship types and sizes for the implementation of a WHR system.

To simplify the selection of the set variable pairs of the WHR system (ballast capacity and flue gas flow rate), ships of different ballast capacities and main engine fuel consumptions were plotted in Figure 7.6 and Figure 7.7 and their trendlines were computed. The heating requirements of each ship are different and unknown, thus the output of the model was selected to be the heating rate provided by the hot water. For the given gas flow rates and the corresponding ballast mass, the maximum heating rate output from the heat exchange system of the WHR was computed from Eq.72, and results are shown on the same figures.

$$q_{max} = F_g c_{p,g} (T_{g,in} - T_{g,out}) \tag{72}$$

The assumptions used were the same as the ones stated in 7.2.2 plus that temperature of the flue gas is 380 °C (according to 2.2.3), its outlet's from the HE is 80 °C and heat capacity of flue gas: 1,012 J/K/kg.

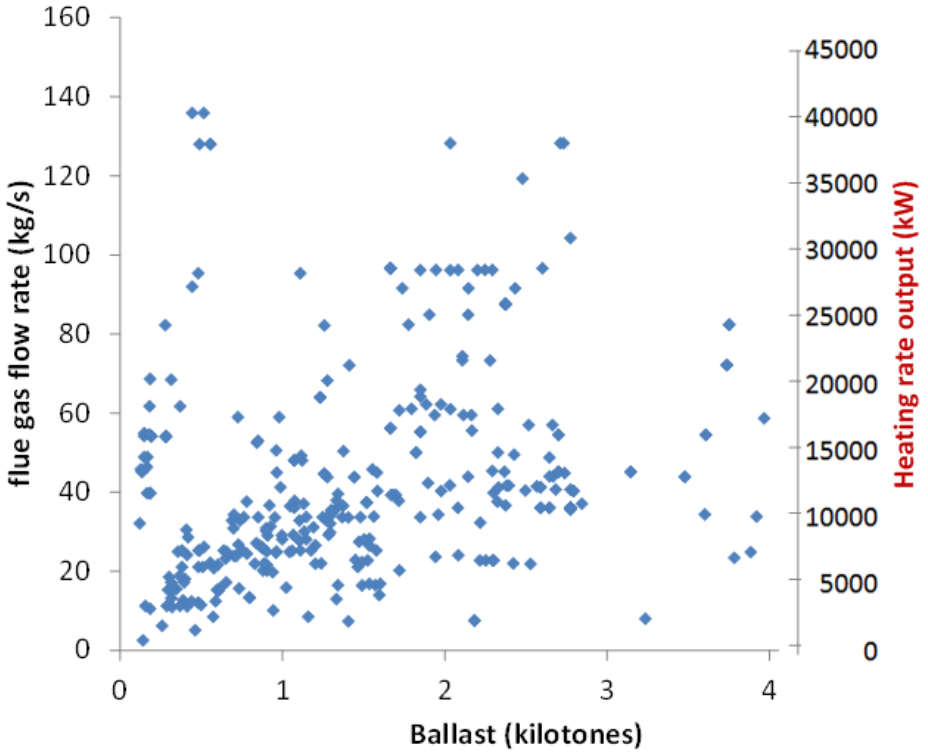

Figure 7.6. Ballast capacity computed for various ferries along with their estimated flue gas flow rates and their maximum heating output produced for the waste heat recovery system.

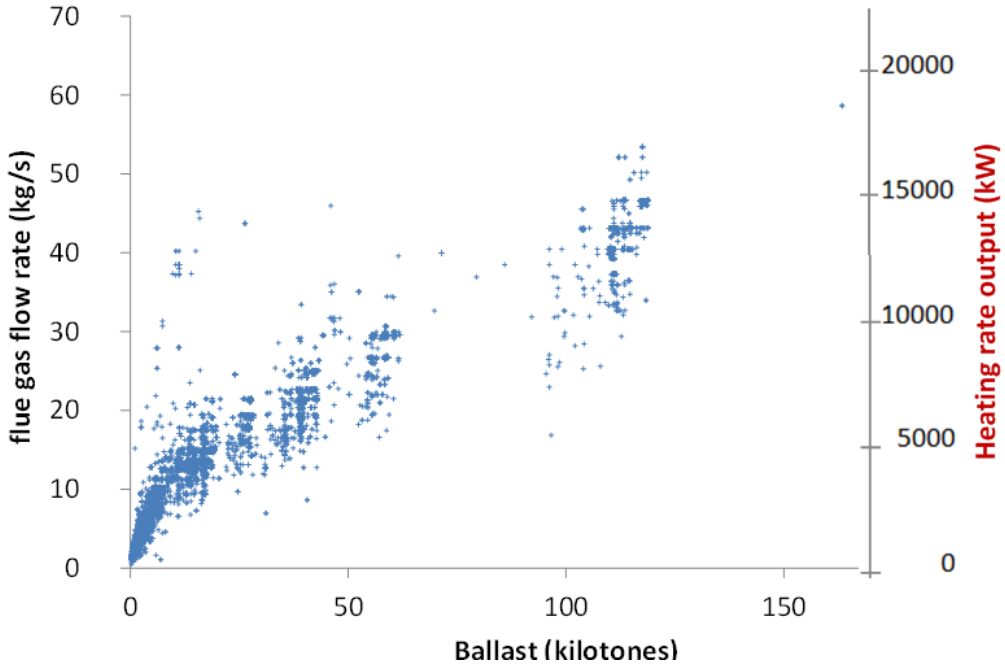

Figure 7.7. Ballast capacity computed for various tankers along with their estimated flue gas flow rates and their maximum heating output produced for the waste heat recovery system.

Some pairs of ballast capacities with the flue gas flow rates of different ferries and tankers can be selected in order to examine representative cases and draw conclusions about the WHR system implementation on the total fleet. The flowsheet would need to be modified, as for the high flow rates of flue gas, one HE and one compressor is not enough to provide the required cooling. The summary of the pumping requirements could then be linked to the results and cases where ships can store both a WHR system and a PBR in the ballast.

An alternative implementation would be to use a WHR predominantly to extract kinetic energy from the exhaust gas (e.g. using a steam Rankine cycle, like the case of Maersk mentioned in 2.2.3), before SO_x scrubbing and use of exhaust in a PBR. Then, the use any low grade waste heat from the WHR or engine jacket cooling water could be used for the purposes of PBR thermal management. The kinetic energy could either be used to supplement propulsion power or provide electrical energy (via a generator). The appropriate solution (kinetic or heat recovery) will depend on the specifics of wider energy demands of the ship and the cost and efficiency of the different technologies.

7.4 Waste heat recovery for temperature control of the photobioreactor

7.4.1 Introduction

As shown in Figure 7.8, there are two sources of heat added to the PBRs in general, the heat from the hot flue gas and the radiation energy from the illumination. Some part of this energy is consumed by the endothermic photosynthesis and another part is lost to the environment (either by conduction and convection or by radiation). During hot periods a heat exchanger (HE) can be added to cool the PBR. In the case of a shipboard PBR placed on the deck of Tamesis, there could be a need either for heating, due to the low ambient temperature in London (the example city of this case study), or for cooling – through a cold water reservoir – in the case of heat conduction through the metal of the shell if the PBR is placed above water level.

Figure 7.8. Heat absorbed and emitted by the photobioreactor.

The design of the temperature control structure for an algal PBR adds several constraints regarding its efficient operation, including reduction in light penetration and increase of the system's weight. Temperature control methods used in algal PBRs for cooling or heating include water baths, immersed water tubes, water spraying, shading with tubes of dark plastic and immersed heating/cooling coils (Carvalho et al., 2006; Jeffryes & Agathos, n.d.). All of them add operating cost as well as significant weight to the system, an important parameter for the case of an onboard application. Systems that require a heating structure to be installed would show a trade-off between the cost (capital and operating) of the heating structure and potential thermal design of the system instead. However, in the case of PBRs, where wall transparency is a crucial point, insulation becomes difficult. The case of controlling the temperature with adjusting the temperature of the sparged gas has been examined for bubble columns, but not for the case of airlifts or PBR materials with simultaneous heat loss through the wall (Komarov & Sano, 1998).

This section presents a heat transfer model that provides an estimate of the heating requirements of a shipboard PBR, and the possible solutions that could meet these requirements. The model estimates the required temperature of the sparged gas, $\mathrm{T_{g_{in}}}$, to maintain the mixture's steady state temperature range within the culture's tolerance limits along the whole length of the PBR. Liquid velocity computed in Chapter 5 was used as an input here, for the estimation of the necessary temperature of the mixture in the entrance of the riser, $T_{m_{in}}$. The effect of the riser diameter, gas flow rate, wall thermal conductivity, wall thickness, ambient temperature and heat transfer coefficient is presented.

The second part of this section presents an alternative suggestion for temperature control. A double pipe HE is suggested to replace part of the downcomer, where the passing broth restores its required temperature (shown also in Figure 7.9 below). The high conductivity part of the downcomer used for the double pipe could be positioned at the junction between the end of the downcomer and the entrance of the riser. This novel method proposed is shown in this chapter to be a feasible way of temperature control for the ship PBR. The fluid medium in the temperature regulation circuit could be designed to switch between hot and cold coolant streams, adding the flexibility to use the same circuit for cooling if necessary, as in Zimmerman et al. (2008), depending on the engine mode and the weather conditions. The two models developed in this section can be applied to outdoor or indoor external loop airlift tubular PBRs with spatially stable external temperature and fed with a gas.

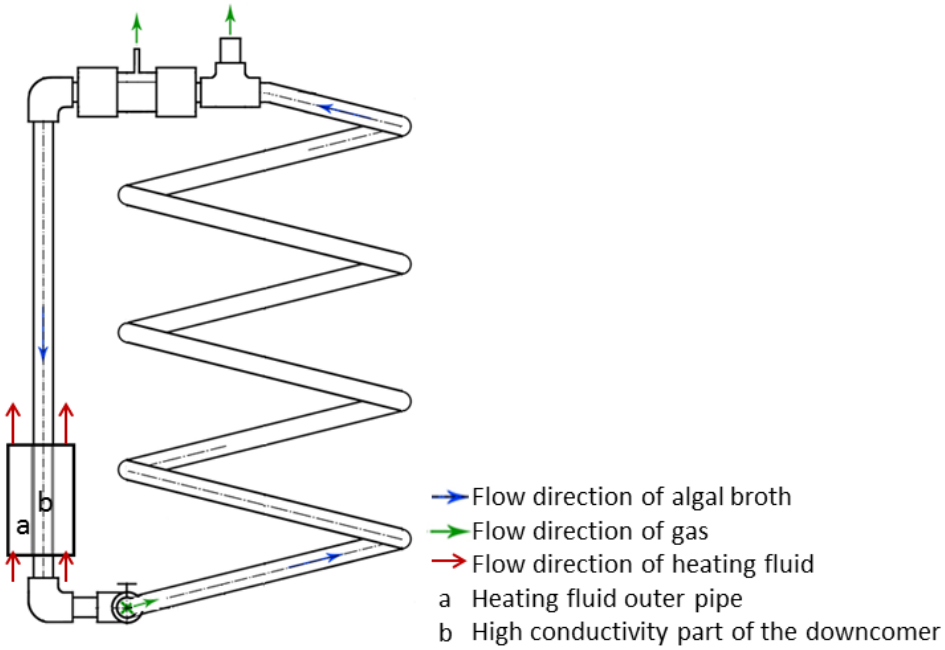

Figure 7.9. The double pipe heat exchanger concept to control the photobioreactor's temperature.

7.4.2 Method

7.4.2.1 Equations

The heat provided by the hot gas sparged to the mixture is lost through the wall after its propagation for a certain distance in the PBR, especially when ambient temperature is low. The mixture is recirculating from the end of the PBR downcomer back to its riser with the liquid velocity computed in Chapter 5. It can be hypothesised that by its entrance into the riser and after its contact with the sparged gas, the mixture obtains a required temperature, $T_{m_{in}}$, which after the heat loss at the end of the loop ends up to be equal to the culture's optimal temperature, $T_{m_{out}}$ (temperatures shown in Figure 7.10). The sparged gas should heat the liquid sufficiently to maintain the temperature in the PBR within the permitted range so as not to harm the algae.

The necessary temperature of the flue gas sparged, $T_{g_{in}}$, to maintain the temperature required by the culture along the PBR until the end of the loop, $T_{m_{out}}$, is estimated at steady state. The PBR tube is considered for the simulation as a single cylinder tube-shell HE assuming the stable ambient temperature as the shell fluid temperature. The temperature differences appearing within the system at steady-state are the following (also indicated in Figure 7.10):

i. Temperature difference in the mixture along the tube (driven by the convective and conductive heat flux)

ii. Temperature difference on wall along the tube (conductive heat loss due to the difference of the temperatures out of the tube, T_e, and in the tube, T_m)

iii. Radial temperature difference in the mixture

Taking into account the first two heat transfers (full list of assumptions shown in 7.4.2.2), the energy conservation equation requires the heat flux in the mixture with axial temperature variation dT to be equal to the heat loss to the environment.

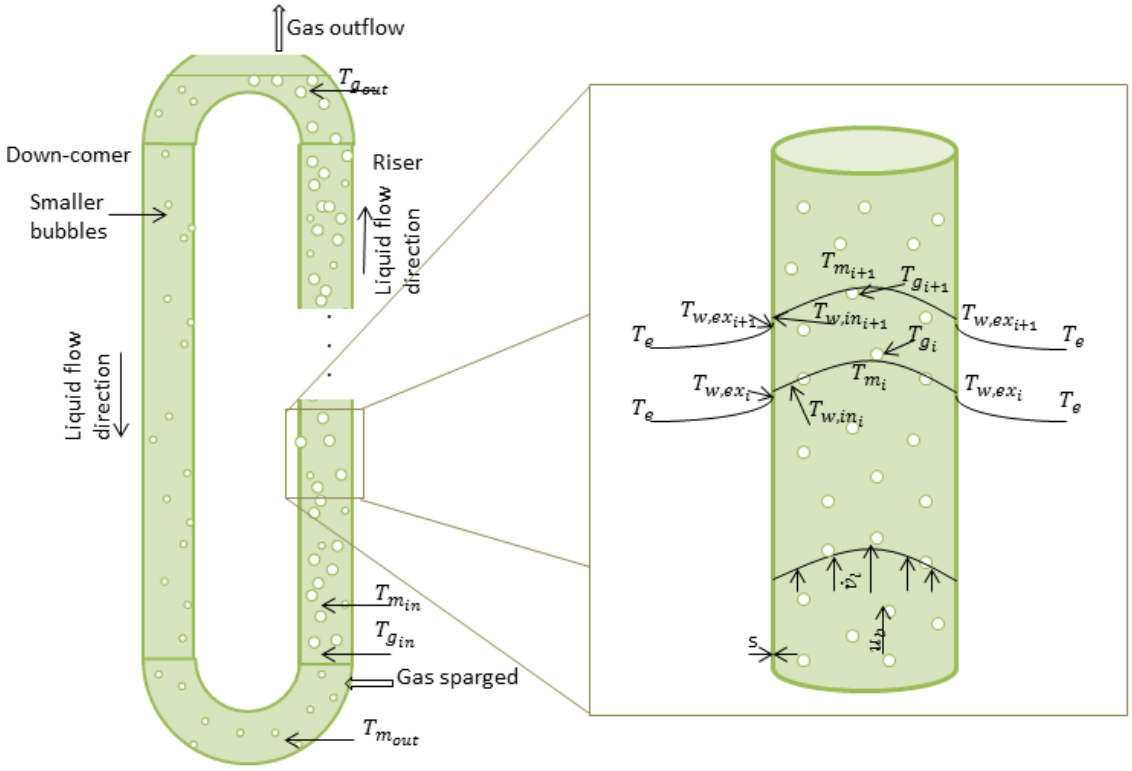

Figure 7.10. Illustration of mixture temperatures distributed along the tube (left image) and across the tube radius (right image).

Regarding the heat transfer within the mixture of the PBR, the conservation of energy can be written in the form of Eq.73, taking the form of Eq.74 at a steady one dimensional flow field in cylindrical coordinates without heat sources (Lienhard Iv & Lienhard, 2008; Perry et al., 1999).

$$\underset{energy\ storage}{\rho c_p \cdot \left(\frac{\partial T}{\partial t} + \vec{u} \cdot \nabla T\right)} \underset{enthalpy\ convection}{} = \underset{heat\ conduction}{k\nabla^2 T} + \underset{heat\ generation}{q} \tag{73}$$

$$\frac{\partial T_m}{\partial z} = \frac{k_m}{\rho_m c_{pm}} \left(\frac{1}{r} \frac{\partial}{\partial r} r_t \frac{\partial T_m}{\partial r} + \frac{\partial^2 T_m}{\partial z^2} \right) \tag{74}$$

where T_m the temperature of the broth, z the longitudinal dimension, k_m the thermal conductivity of the mixture, ρ_m the density of the mixture, c_{pm} the specific heat capacity of the mixture, and r the tube radius.

The heat loss through the walls can be estimated from Fourier's Law for heat conduction as in Eq.75, where k_t coefficient is the thermal conductivity of the tube wall. The average heat transfer coefficient of the ambient air medium around the outside of the tube is $\overline{h_e}$. Special attention should be paid to the assumption of its value (discussed in the Assumption list, 7.4.2.2), which is greatly influenced by the weather (e.g., wind speed and rain). According to Newton's law Eq.76 gives the cooling formula in steady state for the radial dimension and for a tube of uniform longitudinal temperature. This equation can be rewritten in Eq.77 in terms of $q_{loss} = q_{radial}(2\pi r l)$ for a cylinder of length l. Eq.77 is analogous to Ohm's law where the denominator is the sum of two thermal resistances (i.e., the convection through the boundary layer of air outside the tube and the conduction through the wall), as would be in the case of a series circuit (Lienhard Iv & Lienhard, 2008; Perry et al., 1999). The heat lost through the wall varies along the tube, as it is indirectly dependent on the difference between the mixture temperature and the ambient temperature, $T_m - T_e$, and because T_m changes along the tube.

$$\vec{q} = -k_t \nabla T \tag{75}$$

$$q_{convection} = q_{conduction} \Rightarrow \overline{h_e}(T_w - T_e)_{r_t = r_e} = -k_t \frac{dT}{dr}\Big|_{r_t = r_e} \tag{76}$$

$$q_{loss} = \frac{T_{w_{in}} - T_e}{\frac{1}{\overline{h_e} 2\pi r_e l} + \frac{ln(\frac{r_e}{r_i})}{2\pi k_t l}} = \frac{T_{w_{in}} - T_e}{R_{t_{conv}} - R_{t_{cond}}} \tag{77}$$

where k_t the thermal conductivity of the tube walls, T_w and $T_{w_{in}}$ the wall and the inner wall temperature, r_e and r_i the external and internal radius, $R_{t_{conv}}$ and $R_{t_{cond}}$ the thermal resistance by convection and conduction.

Given that only the temperature of the PBR fluid needs to be estimated, the heat transfer wall surface is considered as a single cylinder tube-shell HE, along which the fluid in the shell maintains stable temperature. The equations for heat transfer in HEs

by Lienhard Iv and Lienhard (2008) (chapter 2 & 7) and Perry et al. (1999) are used. The difference of the heat in the mixture, between its entrance and exit (of its recirculation path) is given by Eq.78, where $\dot{m}$ is given by Eq.79, with u_m being the velocity of the mixture (considered as the linear liquid velocity, $\bar{u}_l$). The heat exchanged through the wall of the tube per differential length is given by Eq.80, which after axial integration and replacement of the overall heat transfer coefficient, U, and logarithmic mean temperature difference, $LMTD$, relations, results in Eq.81, where $\overline{h_m}$ is the average heat transfer coefficient of the mixture. According to energy equilibrium, the heat in Eq.78 should equal the heat found in Eq.81, and thus $T_{m_{in}}$ can be computed, as shown in Eq.82. Prandtl (Pr), Graetz (Gz) and Nusselt ($\overline{Nu_d}$) numbers and $\overline{h_m}$ are computed as shown in Appendix VI.

$$q = \dot{m} c_{p_m} \left(T_{m_{out}} - T_{m_{in}}\right) \tag{78}$$

$$\dot{m} = \rho_m u_m a \tag{79}$$

$$dq = dA \cdot U \cdot LMTD \tag{80}$$

$$q = \frac{1}{\frac{1}{h_m \pi d_r l} + \frac{ln\left(\frac{d_o}{d_r}\right)}{2k_t \pi l} + \frac{1}{h_e \pi d_o l}} \frac{\left(T_{m_{out}} - T_e\right) - \left(T_{m_{in}} - T_e\right)}{ln\left(\frac{T_{m_{out}} - T_e}{T_{m_{in}} - T_e}\right)} \tag{81}$$

$$T_{m_{in}} = \frac{\left(T_{m_{out}} - T_e\right)}{exp\left(-4\left\{\rho_m u_m \pi d_r^2 c_{p_m}\left[\frac{1}{h_m \pi d_r l} + \frac{ln\left(\frac{d_o}{d_r}\right)}{2k_t \pi l} + \frac{1}{h_e \pi d_o l}\right]\right\}^{-1}\right)} + T_e \tag{82}$$

where $\frac{1}{h_m \pi d_r l} = R_{t_m}$, $\frac{s}{k_t \pi \frac{d_r + d_o}{2} l} = R_{t_t}$, $\frac{1}{h_e \pi d_o l} = R_{t_e}$ are the absolute thermal resistances by convection in the mixture, by conduction in the tube and by convection in the ambient air. Finally, for the approximation of the quantities $\mu_m, k_m, c_{p_m}, \rho_m$ the following equations are used, in combination with the gas hold-up estimated from Chapter 5.

$$\mu_m = \mu_g \varepsilon_r + \mu_l (1 - \varepsilon_r) \tag{83}$$

$$k_m = k_g \varepsilon_r + k_l (1 - \varepsilon_r) \tag{84}$$

$$c_{p_m} = c_{p_g} \varepsilon_r + c_{p_l} (1 - \varepsilon_r) \tag{85}$$

$$\rho_m = \rho_g \varepsilon_r + \rho_l (1 - \varepsilon_r) \tag{86}$$

The temperatures mentioned are mean temperatures after thermal quasi-equilibrium between the liquid and the bubbles in each fractional differential volume. Bubbles come in a thermal quasi-equilibrium with the liquid after their propagation through a certain length, which is assumed to be minor compared to the total reactor length. The required temperature of the gas to enter the PBR in order to heat up the mixture from $T_{m_{out}}$ to $T_{m_{in}}$ will be $T_{g_{in}}$, which is found by the mass and energy equilibrium of the mixing at the entrance of the PBR expressed in Eq.87. The computed temperature can be tested whether it is within the tolerable range allowed by the algae grown in the PBR and the range provided by the hot flue gas.

$$q_g \rho_g c_{p_g} \left(T_{g_{in}} - T_{m_{in}}\right) = q_l \rho_l c_{p_l} (T_{m_{in}} - T_{m_{out}}) \tag{87}$$

$$\Rightarrow T_{g_{in}} = T_{m_{in}} + \frac{\dot{v}_l (1 - \varepsilon_r) \pi \frac{d_r^2}{4} c_{p_l} \rho_l}{q_g c_{p_g} \rho_g} (T_{m_{in}} - T_{m_{out}})$$

Regarding the second temperature control method suggested (double pipe HE), the temperature ($T_{hf_{in}}$) and flow rate of the heating fluid (q_{hf}) in the design proposed (Figure 7.9), and the required length of the HE (l_{HE}) are calculated similarly. The variables of the shell fluid in Eq.82 are replaced by the variables of the heating fluid, after computation of $T_{m_{in}}$ from Eq.82, and thus Eq.88 is solved with trial and error.

$$\rho_{hf} q_{hf} c_{p_{hf}} \left(T_{hf_{out}} - T_{hf_{in}}\right) = \frac{1}{\frac{1}{h_m \pi d_r l_{HE}} + \frac{ln\left(\frac{d_o}{d_r}\right)}{2 k_t \pi l_{HE}} + \frac{1}{h_{hf} \pi d_o l_{HE}}} \frac{\left(T_{m_{out}} - T_{hf_{out}}\right) - \left(T_{m_{in}} - T_{hf_{in}}\right)}{ln\left(\frac{T_{m_{out}} - T_{hf_{out}}}{T_{m_{in}} - T_{hf_{in}}}\right)} \tag{88}$$

7.4.2.2 Assumptions

1. The mixture is incompressible with negligible density changes, as more than 90% of the mixture is water (gas hold-up estimated in 5.4).

2. Pressure variations in the flow are not large enough to affect k and h values and the thermodynamic properties.
3. The viscous stresses do not dissipate enough energy to warm the fluid significantly.
4. No consideration of the enthalpy of photosynthesis and other reactions.
5. Steady state flow and quasi-equilibrium conditions.
6. No consideration of heat transfer through radiation from the sun and emittance to the environment. An approximate tube wall temperature was estimated from the sunlight absorptance and emittance equation (Eq.89) and using the assumptions in Lienhard Iv and Lienhard (2008). Heat loss from the wall to the mixture inside will reduce the wall temperature, but is assumed zero for this estimation due to lack of information on the heat loss. Assuming average global sunlight intensity over the year, q_{solar}, is 235 W/m^2, a maximum ambient air temperature of 30 °C and sky temperature 15 °C, emittance, ε_{IR}, 0.92 (0.937 degrees for glass (Perry et al., 1999) and plastic 0.91 (The Engineering Toolbox, n.d.)), absorptance, a_{solar}, 0.6 for greens-red-blue colours (The Engineering Toolbox, n.d.), then temperature of the external tube wall is estimated to be 25.5 °C, which is not of great difference from the one assumed without radiation.

$$a_{solar}q_{solar} + \varepsilon_{IR}\sigma T_{sky}^4 = h_e\left(T_{w,ex} - T_e\right) + \varepsilon_{IR}\sigma T_{w,ex}^4 \quad (89)$$

7. Bubbles reach thermal equilibrium with the liquid after a length from their introduction which is very small compared to the total length of the tube.
8. No consideration of dirt and scale thermal resistances on the wall of the tube.
9. No friction generated heat from the liquid contact with the inner tube walls.
10. No axial heat transfer along the tube wall.
11. Uniform distribution of the temperature of the mixture across each fractional cross section of the tube (due to the adequate mixing induced in an airlift).
12. For the velocity of the mixture it is assumed that $u_m = \bar{u}_l$.
13. $d_d = d_r$
14. T_e constant along the tube and during time.
15. The physical properties of the mixture (e.g., μ_m, k_m, c_{p_m}) are constant along the whole tube, even for the part of the downcomer (which occupies a small part of the PBR in our case) where most of the bubbles have already been degassed.
16. Prandtl (Pr) number can be found from Eq.92 by using the properties of the mixture for simplification, although it is related to the properties of the continuous phase in a more complex way (Brennen, 2005).

17. $\mu, k, \rho, c_{p_l} = \mu, k, \rho, c_{p_{water}}$ and $\mu, k, \rho, c_{p_g} = \mu, k, \rho, c_{p_{air}}$
18. For the estimation of the physical and thermal properties of the tube, it is assumed that it is made of a fluoropolymer, such as fluorinated ethylene-propylene.
19. For the temperature and flow situations encountered here, a simple proportionality with a constant coefficient is usually adequate. The heat transfer coefficient of the ambient air by free convection (by warming or cooling of the air) is in the range of 3 to 25 W/m²K and by forced convection (by wind) within the range of 10 to 200 W/m²K (MediaWiki, 2008; The Engineering Toolbox, n.d.). It is assumed that the surface of the tube does not get wet by rain or surrounding water sprayed. Its value is taken as a first approximation equal to 12 W/m^{2}K.
20. Mass inflow of the sparged gas equals its outflow and only the inflow's heat input is considered, as the outflow is assumed to have equal temperature with the mixture.
21. Range of temperatures tolerated by algae: 15 – 40 °C (2.3.2.3).
22. Range of ambient temperatures that are likely to be encountered: -5 – 20 °C. The case where ambient temperature is above the temperature of the PBR is not examined, as it is hardly reached in London where the examined reactor is based in. However, chilling of the PBR could be realized by the use of the same HE and jacket water before its entrance to the engine.
23. Range of the flue gas temperature: 120 – 720 °C (2.2.3).

Additionally, for the double pipe HE system, the following assumptions are considered:

24. Counter current flow HE.
25. The outer HE pipe is perfectly insulated.
26. The temperature difference between the inlet temperature of the mixture and the exit temperature of the heating fluid is 10 K, which is suggested as the minimum value allowed for the greater temperature difference within the heat exchanger (MacKetta, 1992).
27. The heat transfer coefficient of the heating fluid is 200 Wm^{-2}K^{-1} for the case of air and 300 Wm^{-2}K^{-1} for the case of water (The Engineering Toolbox, n.d.).
28. The high conductivity tube part length estimated to replace or be added to the downcomer is not taken into account in the initial estimation of the heat loss from the entire PBR.
29. Range of the heating fluid temperatures: less than 80 – 85 °C when water is used (which is the jacket cooling water outflow as mentioned in 2.2.3), and less than 720 °C when flue gas is used (2.2.3).

7.4.2.3 Computation, parameters and variables

Calculation of the heat loss through the PBR walls to the ambient and of the mixture temperature at the entrance of the loop for a given temperature at its exit is realised by use of the equations shown in the following algorithm. The Matlab code developed for the computations is presented in Appendix VI.

Algorithm

1. Set the parameters given in Table 7.2. Compute $\dot{v}_l$ and ε_r from Chapter 5
2. Compute Re from Eq.55.
3. Compute $\mu_m, k_m, c_{p_m}, \rho_m$ from Eq.83 – 86.
4. Compute Pr from Eq.92.
5. Compute Nu :

   If laminar: compute Gz from Eq.93, then compute $\overline{Nu_{d_{laminar}}}$ from Eq.94.

   If transition: compute $Nu_{d_{transition}}$ from Eq.95.

   If turbulent: compute $Nu_{d_{turbulent}}$ from Eq.96.
6. Compute $\mathrm{h_m}$ from Eq.1.
7. Compute $\mathrm{T_{m_{in}}}$ from Eq.82.
8. Compute $\mathrm{T}_{g_{in}}$ from Eq.87.

Table 7.2. Parameters and variables used for the estimation of the temperature distribution.

Parameters	Values
d_r	0.060
d_b	0.005
l_d	1.50
q_g	0.00004
l_r	6.00
ν_l	0.801×10^{-6}
μ_l	0.798×10^{-3}
μ_g	1.983×10^{-5}
ρ_l	1000
ρ_g	1.225
c_{p_l}	4,181.3
c_{p_g}	1,012
π	3.142
K_l	1.5
g	9.810
k_t	0.195
k_l	0.55
k_g	0.027
s	0.002
h_e	12.00
$T_{m_{out}}$	296 (23 °C)
T_e	283 (10 °C)
ε	0.0000025

The parameters and variables used for the computations and their interrelation according to the two models developed (the hydrodynamic model and the heat transfer model) is shown in Figure 7.11. The inputs and outputs of the models could be modified according to the needs of each problem. Some examples of different combinations are shown in Table 7.3.

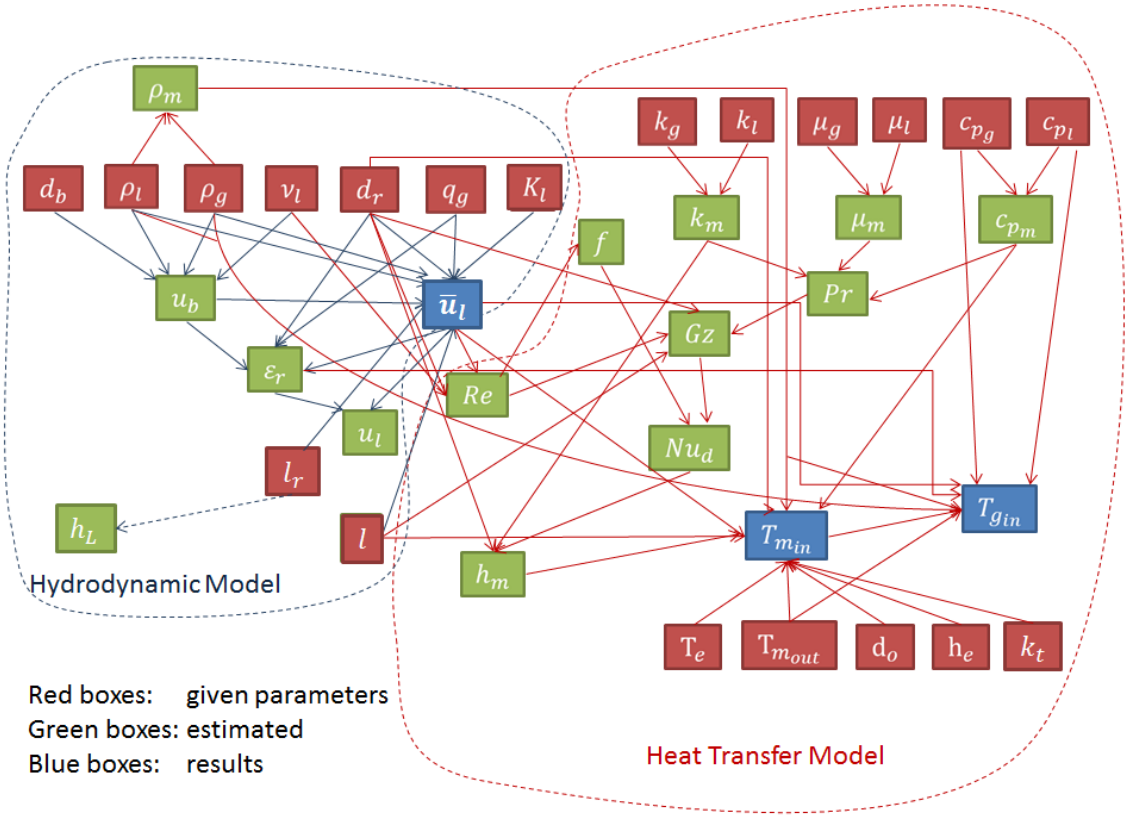

Figure 7.11. The interrelation amongst the airlift photobioreactor's parameters and variables according to the two models developed.

Table 7.3. Various combinations for inputs and outputs when using a modified script for the hydrodynamic and the heat transfer model.

Inputs	Outputs
$\boldsymbol{d_b, d_r, q_g, l_r, s, T_{m_{out}}}$	$\bar{u}_l, \varepsilon_r, T_{g_{in}}, q_{loss}$
$\boldsymbol{d_b, d_r, q_g, l_r, s, T_{g_{in}}}$	$\bar{u}_l, \varepsilon_r, T_{m_{out}}, q_{loss}$
$\boldsymbol{d_b, l_r, q_g, s, T_{g_{in}}, T_{m_{out}}}$	$\bar{u}_l, \varepsilon_r, d_r, q_{loss}$

7.4.3 Results and discussion

The computed values of the variables are shown in Table 7.4 and the effect of the parameters of riser diameter, gas flow rate, wall thermal conductivity, wall thickness, ambient temperature and heat transfer coefficient is presented in Figure 7.12 to Figure 7.18. According to the results in Table 7.4 the heat loss from the wall is minimal during one loop through the reactor, requiring the mixture to enter the riser at a temperature just 0.2 K higher than the exit temperature (all values shown in Figure

7.12). However, because of the great difference in heat capacity of the gas sparged and the liquid broth in the PBR, the required temperature for the gas inflow, $T_{g_{in}}$, would be much higher (more than 3,000 K) than the actual temperature of the flue gas. Besides, this temperature is too high for the algae to tolerate. Therefore, temperature control would be impossible by just using the hot flue gas sparging. The temperature along the PBR is within the temperature limits tolerated by most strains. However, if no temperature control is used, then the temperature of the broth would gradually drop down after several recirculations to the ambient temperature (computed equal to T_e for the parameter values shown in the case of Table 7.2), which can be too low for the culture.

Figure 7.12 shows the temperature of the mixture, $\mathrm{T_{m_{in}}}$, required to maintain $\mathrm{T_{m_{out}}}$ at 23 °C, as a function of $\mathrm{q_g}$, and $\mathrm{d_r}$ as the third dimension. The heat loss through the walls and the temperature of the sparged gas required to increase the temperature of the recirculated mixture from $\mathrm{T_{m_{out}}}$ to $\mathrm{T_{m_{in}}}$, are shown in Figure 7.13 and Figure 7.14 respectively. For the production of these plots, all other parameters, except those used as the third dimension in each case, have the values given in Table 7.2.

Figure 7.12 verifies that, $T_{m_{in}}$ decreases with an increase in q_g because of the higher heat added by the larger gas mass and because of the shorter duration that the mixture is in contact with the cooled tube before each recirculation. Nevertheless, there is an increase for a small range of very low q_g which might be caused due to the low u_l produced and the higher time of recirculation that leaves the mixture exposed to heat loss for longer.

Figure 7.14 shows the $T_{g_{in}}$ required for the entering sparged gas. Here, q_g plays a much more important role than the d_r to the heat loss (also shown in Figure 7.13). However, even with very high q_g values, the $T_{g_{in}}$ required is much higher than the temperature of the flue gas and, hence, the temperature control with the sparged hot gas does not seem possible. Heat loss through the entire wall of the PBR has a range of 130 to 320 W (Figure 7.13) which is not too high to be easily compensated for with another method. Heat loss in the PBR decreases with q_g increase, because the mixture recirculation velocity increases too (according to the findings of Chapter 5) and the time needed for one loop is shorter.

Figure 7.15 to Figure 7.18 demonstrate the heat loss with various parameters as a third dimension (i.e., $s,\ \mathrm{k_t}, \mathrm{h_e}, \mathrm{T_e}$, respectively). It is shown that for the range of the values of the parameters used in PBRs, wall thickness, s, and thermal conductivity, k_t,

(Figure 7.15 and Figure 7.16), do not play an important role for the heat loss relative to the other parameters examined. Heat loss – and consequently $T_{m_{in}}$ – is more sensitive to h_e and to T_e (Figure 7.17 and Figure 7.18), but the heat loss still results in $T_{m_{in}}$ less than 0.5 °C higher than the $T_{m_{out}}$. The sensitivity to h_e is very important for the actual operating conditions of the PBR, because it means that for low q_g values, the heat loss depends on the airflow around the PBR and also means that rainy weather and wet surface of the walls due to river water sprayed on them would also increase heat loss significantly.

Table 7.4. Results for the variables when the model uses the parameters and variables shown in Table 7.2.

Variables	Values estimated
$\boldsymbol{u_b}$	0.392
$\boldsymbol{\bar{u}_l}$	0.517
$\boldsymbol{Re_l}$	38743
$\boldsymbol{\varepsilon_r}$	0.016
$\boldsymbol{c_{p_m}}$	4,132
$\boldsymbol{r_e}$	0.032
$\boldsymbol{f}$	0.001
$\boldsymbol{Nu_d}$	21.62
$\boldsymbol{Pr}$	5.99
$\boldsymbol{h_m}$	195.25
$\boldsymbol{k_m}$	0.5419
$\boldsymbol{\mu_m}$	7.85 x10^{-4}
$\boldsymbol{q_m}$	0.00008
$\boldsymbol{q_{loss}}$	198
$\boldsymbol{T_{m_{in}}}$	296.03
$\boldsymbol{T_{g_{in}}}$	4327

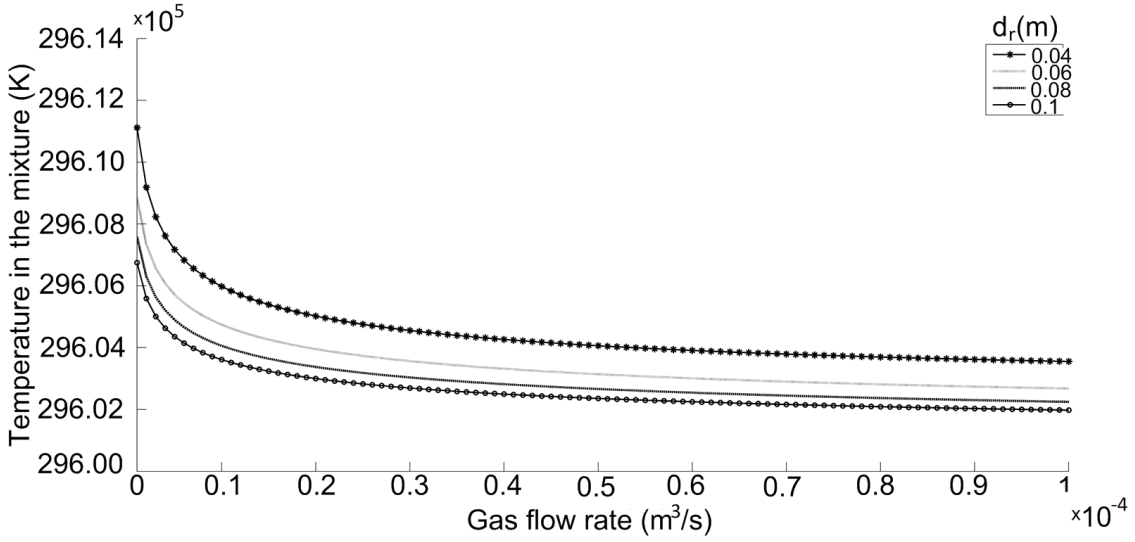

Figure 7.12. Temperature of the mixture required at the entrance of the riser to maintain at 23°C at the exit, as a function of gas flow rate and for various riser diameters.

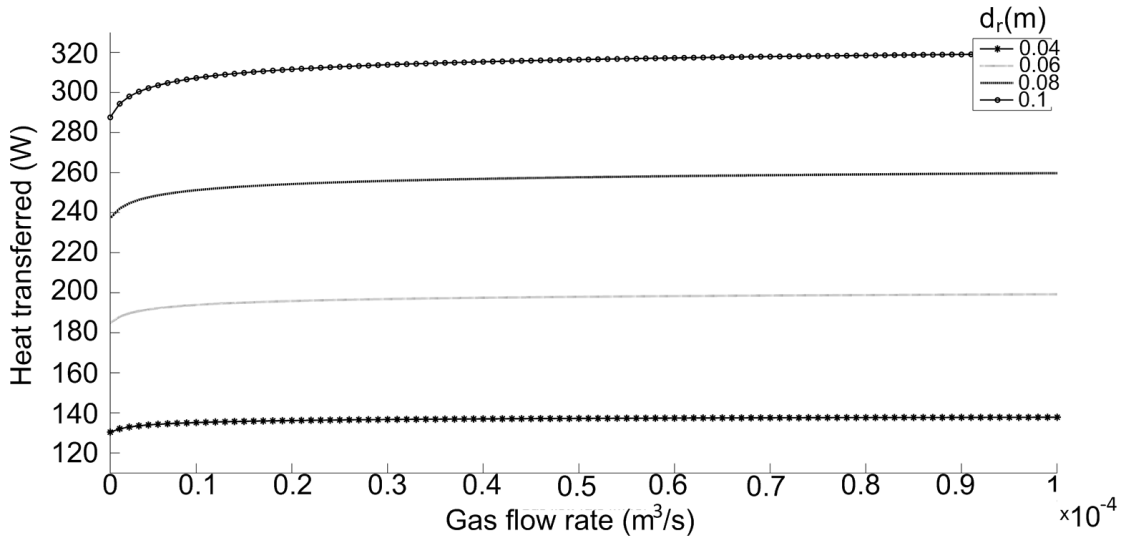

Figure 7.13. Heat loss through the walls of the photobioreactor when ambient temperature is 10°C and the temperature of the mixture at the end of the tube is maintained at 23°C, as a function of gas flow rate and for various riser diameters.

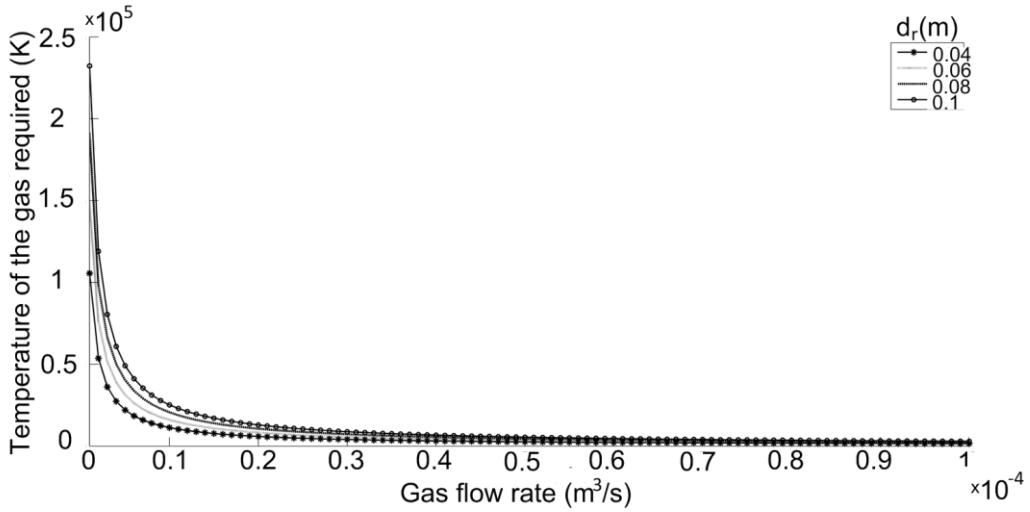

Figure 7.14. Temperature of the sparged gas required at the entrance of the riser to maintain the mixture at 23°C at the exit, as a function of gas flow rate and for various riser diameters.

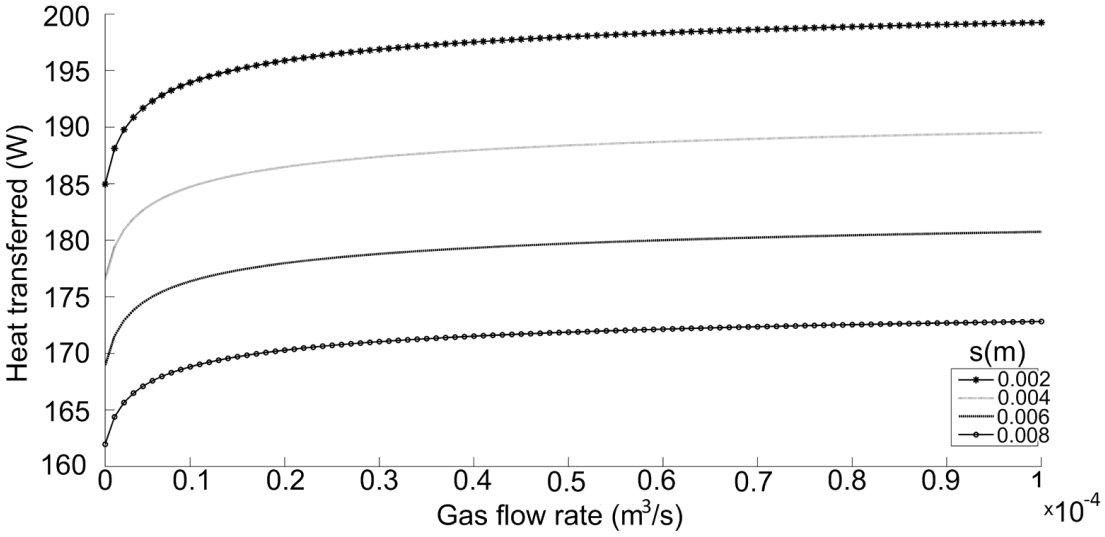

Figure 7.15. Heat loss through the walls of the photobioreactor when ambient temperature is 10°C and the temperature of the mixture at the end of the tube is maintained at 23°C, as a function of gas flow rate and for various wall thicknesses, s.

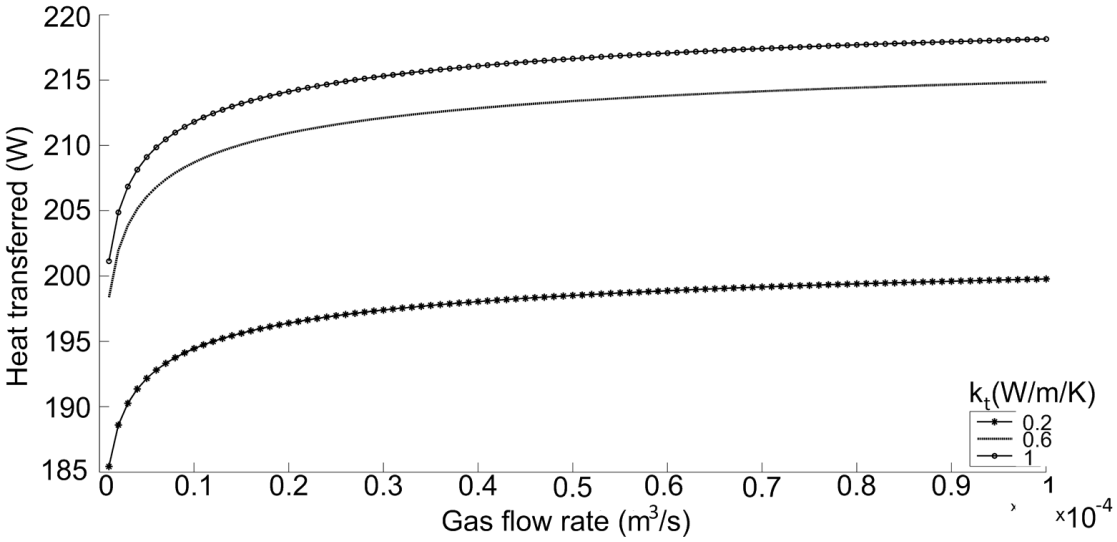

Figure 7.16. Heat loss through the walls of the photobioreactor when ambient temperature is 10°C and the temperature of the mixture at the end of the tube is maintained at 23°C, as a function of gas flow rate and for various wall thermal conductivities, k_t (0.1 for fluorinated ethylene-propylene and 1 for glass).

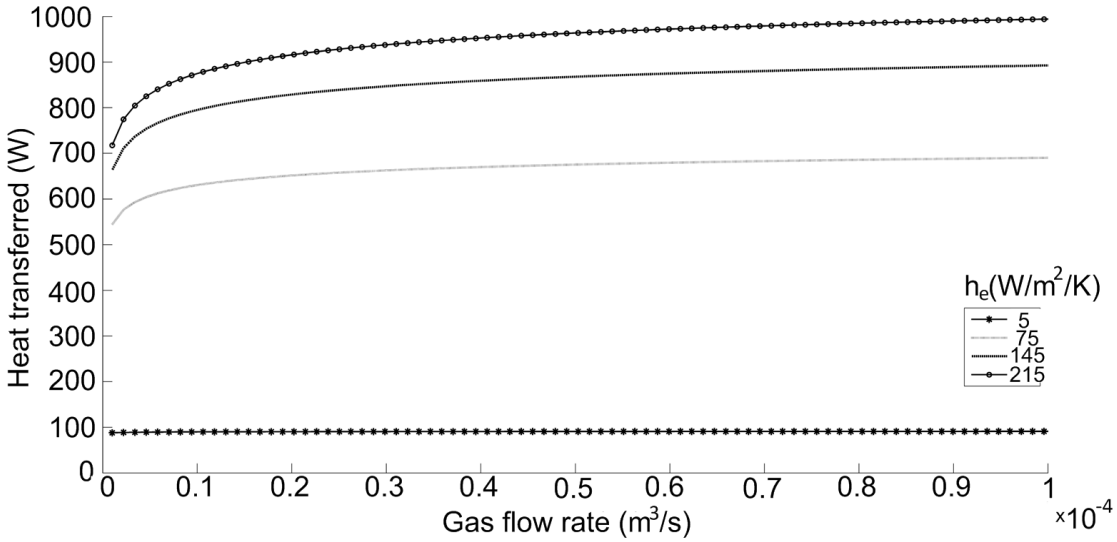

Figure 7.17. Heat loss through the walls of the photobioreactor when ambient temperature is 10°C and the temperature of the mixture at the end of the tube is maintained at 23°C, as a function of gas flow rate and for various wall heat transfer coefficients of the ambient air, h_e.

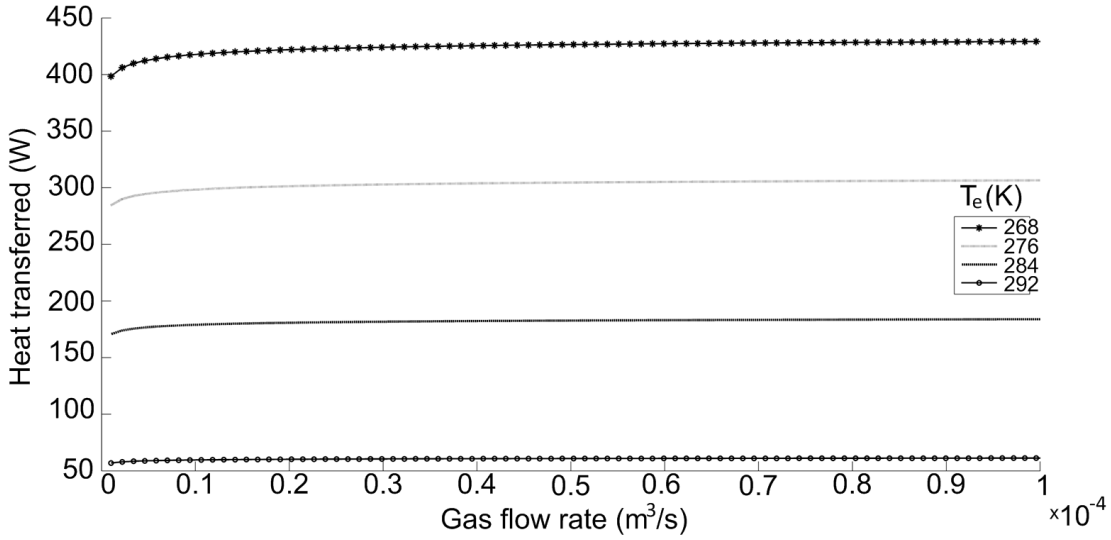

Figure 7.18. Heat loss through the walls of the photobioreactor when ambient temperature is 10°C and the temperature of the mixture at the end of the tube is maintained at 23°C, as a function of gas flow rate and for various ambient temperatures, T_e.

A double pipe HE is suggested to replace part of the downcomer (shown in Figure 7.9), where the passing broth is restored to the required temperature, before entering the riser for the next recirculation. This would not require a great mass of heating fluid to surround the PBR and consequently minimises the impact on light absorption into the PBR. Either hot water or the actual flue gas could be used as the heating fluid, as water is a commonly used WHR system fluid (7.3), and flue gas is supplied in abundance on the ship, respectively. The temperature of the mixture would increase from $T_{m_{out}}$ to $T_{m_{in}}$ as it passes through this system, because of the high thermal conductivity of the tube and the high flow rates of the heating gas, or the high heat capacity and heat transfer coefficient of the water. Temperature required for the heating fluid or this design and the length of the high conductivity tube part are important parameters to be considered. It is important for the temperature of the heating fluid not to exceed the upper limit of temperature tolerated by the specific algae strain. Therefore, instead of using too high temperatures of the heating fluid, a longer high-conductivity part could be added to allow lower heating fluid temperatures for adequate heating of the PBR.

The HE characteristics for a case study of the PBR designed in 4.2 and liquid velocity 0.3 m/s are shown in Figure 7.19. Length and flow rate requirements for this temperature control are also shown. When gas is used as the heating fluid, high flow

rates are needed due to the low heat capacity, and they correspond to high volumes. Hence, the feasibility of this heating method depends on the mass of the available flue gas and its ability to cool the PBR size implemented in each case. This suggestion for temperature control does not require the whole PBR to be immersed in a temperature control bath. It only requires a replacement of a small part of the plastic PBR with a high conductivity part, e.g., stainless steel with k_t = 16 $Wm^{-1}K^{-1}$ (The Engineering Toolbox, n.d.) (full list of parameter values used is shown in Table VI.5 of Appendix VI), surrounded by an outer insulated pipe.

According to Figure 7.19, if water is used as the heating fluid, and its inlet temperature is around 358 K (which is the maximum temperature maintained by the jacket cooling water outflow as mentioned in 2.2.3), less than 70 cm of the downcomer would need to be replaced by the high conductivity tube part and less than 10 g/s mass flow rate of the water is needed. Similar curves are shown for the case where flue gas is used as the heating fluid, though higher flow rates and longer HE tubes are needed. It has to be noted that if the high conductivity tube part replaces part of the downcomer, then the heat loss at the reduced length is less than initially estimated and the actual length replacement required has to be corrected. Likewise, in the case that the high conductivity part does not replace part of the downcomer, but adds length to it, then the initially used liquid velocity changes slightly and a corrected heat loss needs to be computed.

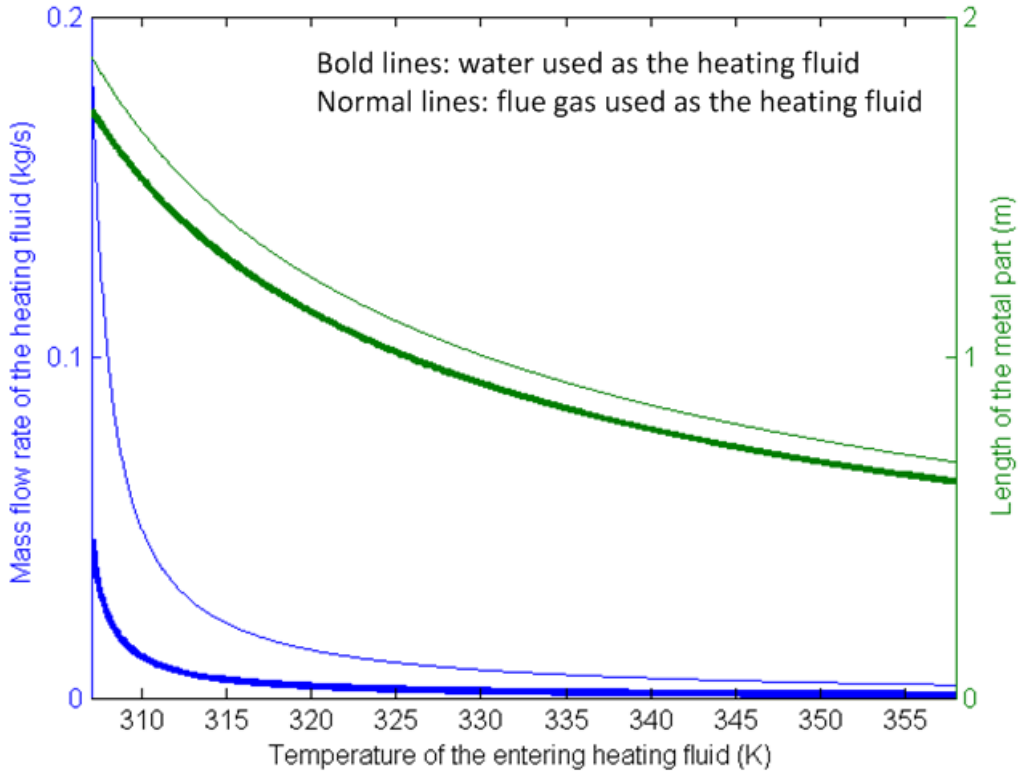

Figure 7.19. Mass flow rate of the heating fluid and length of the high conductivity part of the downcomer required in order for the heat exchanger to raise the temperature of the mixture at the entrance to $T_{m,in}$ as shown in Table 7.4.

7.5 Conclusions

Water mass requirements computed for the treatment of the total flue gas emissions of each ship suggest that many tankers would have the storage capacity in the ballast tanks for the operation of such PBRs (at least when they are operated in the ballast condition and so can use the ballast tank's capacity). The high fuel consumption and low space availability of ferries make them less appropriate for this implementation. Even for the ferries, a portion of the emissions can still be fixed, but space is a crucial issue and would require significant developments in the design of the ship, logistics or PBR efficiency.

A generic WHR system was proposed, which uses the flue gas to heat a PBR and fulfils the heating requirements of the utilities of the ship. The control variables of the system and the constraints to be fulfilled were discussed. A WHR for a case ship of similar size as Tamesis was run with the gPROMS flowsheet model. The influence of

the water flow rates on the fulfilment of the discussed constraints (i.e., fulfilment of the heating rate needs, with overflow avoidance and enough storage capacity) was demonstrated. Finally, heating output from potential WHR systems for the existing ferry and tanker fleets was computed, in order to pair the flue gas heating output to the ballast capacities of each ship and examine a broader feasibility of this implementation.

Finally, a heat transfer model was developed to estimate the heat loss through the walls of a PBR based on the deck of a ship, for various ranges of parameters. If no temperature control is used, the temperature reaches the ambient temperature, which can be too low for the culture. The temperature variation along the PBR is not high and it is within the temperature limits tolerated by most strains. However, temperature control using the sparged gas was found to be infeasible, due to the great difference in heat capacity of the gas sparged and the broth in the PBR. It was also shown that the inlet temperature of the mixture, and consequently heat loss and inlet temperature of the gas, was not sensitive to parameters like the thermal conductivity of the walls, wall thickness and gas flow rate, over the ranges considered, but was very sensitive to riser diameter, heat transfer coefficient of the air and ambient temperature. A second temperature control method was therefore proposed, consisting of a double pipe HE occupying a small portion of the PBR downcomer, made of a high conductivity tube. Even minor lengths of the high conductivity tube part were found to be enough to control the temperature of the PBR, using allowable ranges of the heating fluid flow rate and temperature. This HE design could be a solution that could be used in combination with the WHR system of the ship for an experiment pilot installation. However, a different design would be more appropriate to generalise across full installations in large ships, where the PBR is not necessarily tubular and, hence, the double pipe HE does not apply.

8 Conclusions and future work

8.1 Thesis summary

The research in this thesis has developed new scientific and technological knowledge related to the development of a shipboard PBR for the capture of CO_2 from flue gas. A variety of important issues regarding implementation, both in a broad shipping fleet and in a specific vessel (Tamesis), were considered. Several related aspects were explored using the existing literature across multiple disciplines and a research scope was developed in compliance with available resources, combining experimental and modelling approaches.

This thesis has investigated shipping emissions and waste streams, the existing regulations regarding pollutants and methods to decrease shipping pollution. The algal cultivation systems and factors affecting their growth were then analysed. From this, a PBR design for a small ship was identified that would capture some of the broad challenges required for both computational and experimental modelling. This included developing a simple theoretical hydrodynamic model to compute liquid velocity and gas hold-up in airlift PBRs, according to bubble size and reactor dimensions, and a model of algal kinetics, based on the simultaneous effects of multiple factors.

Modelling was conducted in the MATLAB and gPROMS environments, to address:

1. The hydrodynamics of the gas-liquid mixture recirculating in airlift PBRs. The model is applicable to outdoor or indoor external loop airlift tubular PBRs;
2. The kinetics of algae growth process in relation to light intensity, temperature and nutrient concentrations;
3. The space requirements estimations for the PBR implementation on different ship sizes and types;
4. The space requirement for the storage of water was found to be approximately 0.6 times the ballast capacity of the tankers and approximately 30 times the ballast capacity of the ferries, recovering 100% of the flue gas waste heat to continuously provide the required heat to the PBR and other utilities;
5. The heat transfer between the PBR and a suggested HE design. The model is applicable to tubular PBRs fed with a gas and with spatially stable

external temperature, estimating the effect of the ambient temperature on the temperature of the liquid along the PBR tube.

Some of the models developed can be integrated together so that the outputs of one feed the inputs of a subsequent model, according to the needs of the problem under consideration. For instance, the hydrodynamic model can provide the results for liquid velocity and gas holdup to be used in the heat transfer model, which can estimate the temperature in the PBR. The temperature can then be used to estimate the growth rate.

At an experimental level, a hybrid helical airlift PBR was designed and assembled. It was a challenging design on which to test theoretical models. There is plenty of scope to improve the design and assembly of the reactor for carbon capture and to further test the reactor on an operating vessel.

Wild algae samples were collected from fresh water sources to compare the growth characteristics with *Chlorella sorokiniana*, obtained from the laboratory based within the CEGE department of UCL.

8.2 Concluding remarks

Overall conclusions drawn from this research can be summarised as follows:

1. Shipboard PBRs are a means to assist in partial CO_2 capture and can feasibly be incorporated into the systems onboard a ship. However, the technical feasibility of the implementation would potentially require complex modifications of the whole design of the ship storage spaces, machinery, fluid transport and control systems.
2. The dependence of the algae growth on poly-parametric factors and its sensitivity to environmental and other conditions on ships do not permit the determination of standard procedures and steps for PBR system operation, leaving areas open for further research and optimisation in this regard.
3. The need for a large water mass and for high gas absorption efficiency limit this application as far as the percentage of CO_2 captured is concerned. One hundred percent capture with respect to the total emissions of many ship types, as they are currently designed, would be likely to be too energy consuming.
4. The ability to robustly couple algal growth with the ship engines, machinery, emissions and water use and to use low grade heat from the engine and cold water from the ambient seawater or river water, would constitute a technological advance that would bring emissions and wasted energy down. An algal PBR might

contribute not only to CO_2 fixation but also to reduction of the NO_x and particulate matter in the exhaust of the ships.

5. One of the outputs of a PBR – cultivating algae – has a variety of uses both as a biomass and energy commodity which could potentially be used onboard, or transferred to land and further production processes. These uses could create a revenue stream that could help to offset some of the costs associated with an onboard PBR.

Summarising the answers to the research questions of this work (3.1), regarding research question 1; a helical airlift design was tested and proved to face the issue of bubble coalescence, concentration of ship NO_x and SO_x have potential for toxic effect on algal growth, whereas cultivation of wild algae showed significant delay compared to the commercial species. Regarding research question 2, the hydrodynamic model developed has less reliance on empirical expressions and helped for dimensioning of the PBR, depending on the required operating conditions. Research question 3 was answered through the experiments of growth under different conditions and their use in the calibration of the model developed that used various factors. Difficulties in the calibration were analysed and predictions of the growth was examined to optimise the PBR requirements in material and energy inputs. Finaly, regarding research question 4; potential of different ships to accommodate the treatment of the total amount of emissions was estimated and revealed the appropriate ships, heat loss of the examined PBR design was estimated for different flow rates, the adjustment of flue gas temperature was shown to be inadequate to control PBR temperature, whereas the suggested HE design and WHR system were evaluated under different flow rates. In detail, this first study on the capture of ship CO_2 emissions using shipboard PBRs revealed the following:

1. Some key practical challenges of PBR system integration include the viability with respect to ship-specific conditions (research question 1, 3.1), the most important of which are high NO_x and SO_x concentrations (1500 mg/kg and 600 mg/kg, respectively, as presented in 4.3), the high temperature of the flue gas (380 °C, as stated in 2.2.3) and the varying salinity of the surrounding water supplied to each ship. SO_x scrubbers would be needed before the flue gas entrance to the PBR. Salinity, however, did not appear to be a serious obstacle for many algal species (12 – 40 g/L, as shown in 4.4). Thus, seawater could be used for PBR operation as far as algae growth is concerned.

2. Initial findings suggest that raw sample collections grow better under air with 10% CO_2 concentration, compared to ambient air (research question 1, 3.1). However, their growth rate was slower when compared with *Chlorella sorokiniana* which took 1 day to reach exponential growth, contrary to the other samples which took 7 days approximately. Consequently, raw samples would benefit from pre-treatment. In addition, tests of the fluid dynamics in PBRs and of the algal growth kinetics were completed to validate and calibrate the models developed, using *Chlorella sorokiniana*.
3. A hybrid helical airlift PBR was suggested and constructed as a potentially optimal design for small and medium-scale implementations on ships, as it provides high gas absorption efficiency, good light absorption and low hydrostatic pressure. The main problem faced by the PBRs constructed is bubble coalescence (research question 1, 3.1). According to the lab measurements, the optimal inclination was suggested to be approximately 40°, which would avoid bubble coalescence and optimise gas retention time.
4. The hydrodynamic model developed and validated in this research work, calculating the liquid velocity without the need for empirical expression of the gas hold-up (contrary to other models in the literature), can evaluate optimal PBR geometries for given problems. The model also revealed the impact that the bubble diameter can have on gas hold-up and liquid velocity (research question 2, 3.1).
5. Results from the preliminary CO_2 experiments using *Chlorella sorokiniana* revealed that of the three different CO_2 concentrations tested, 4,300 mg/kg resulted in a higher growth rate than 700 mg/kg or 50,000 mg/kg, although the literature suggests that the latter is optimal. The growth rate was best at the highest nutrient concentration tested, 1:50, the lower temperature tested, 22 – 25 °C, and the highest light intensity tested, 150 μmol/m^2/s. Further improvement of growth rate is possible at higher nutrient concentrations and light intensities. The nutrient removal rates for nitrates and phosphates were 97% and 37%, respectively (research question 3, 3.1).
6. The non-linear growth model is difficult to calibrate and the inclusion of many factors in the biomass concentration formula leads to the estimation of extreme parameter values and the maximum growth rate predictions were not always in a good fit with the experiments. Experiments for the calibration of the model showed no significant interaction between the factors, but a slightly greater interaction was noted between the nutrient dilution and temperature compared to nutrient dilution

with light intensity. The growth model was simulated for different case studies based on three different objective functions using parameter values from the literature and the different results of the predicted key variables and the suggested control variables were discussed. The optimisation of productivity using the dilution rate as a control variable could also save significant needs related to excessive nutrient supply (research question 3, 3.1).

7. The specifics of the machinery installed (e.g., engine power and therefore emissions outputs), the operating hours of the ships and their empty space available are chiefly what determine whether an algal PBR system has potential for emission reduction (research question 4, 3.1). The ballast tanks of many tankers would be able to store a sufficient mass of water for the operation of a PBR that could treat the total mass of their engines' emissions. The potential is lower for ferries, because of their high fuel consumption and low availability of space.
8. A PBR placed on a ship would, depending on its area of operation, face significant heat loss and so may require heating in order to maintain its temperature within the range tolerated by algal cultures.
    a. A solution for heating of the PBR was proposed, with the integration of a WHR system and the use of a double pipe HE (research question 4, 3.1). The suggested design would require a significantly smaller mass of water to surround the PBR and would also maintain the light penetration compared to other temperature controlling methods used by PBRs. Finally, the importance of the water flow rates for the efficiency of the system was discussed, to minimise the respective power consumption and energy penalty. This optimisation would require the minimum possible flow rate of the heating water that could be used to make this water stream reach its lowest allowed value at its exit from the heaters. The WHR and PBR systems have to be integrated into the ballast water management decision support systems, to optimise space use and balance, as well as to prevent transfer of harmful aquatic organisms and pathogens.
    b. The proposal to provide heating with the use of the hot flue gas straight from the engine was examined. An extremely high gas temperature would be required due to the wide difference in heat capacity between the gas and liquid and the low gas volume sparged in the given liquid mass (research question 4, 3.1). The model showed that the temperature required for the flue gas was sensitive to the PBR diameter, the gas flow rate and the ambient temperature

and the ambient air heat transfer coefficient, but not to the thermal conductivity and the width of the PBR tube for the parameter ranges used in PBRs.

8.3 Recommendations for further work

Further research is recommended in the following directions:

1. The effect of the helix inclination on the bubble coalescence needs to be verified with the use of a helix PBR, in addition to the straight tube used in this study. Also, other PBR designs would need to be considered for a shipboard PBR, to find the most appropriate choice.
2. The effect of the NO_x and SO_x concentrations on the growth rate and the lipid productivity depends on the algal species, but the concentration range of the flue gas of ships has not yet been tested on algae. Hence, experimental testing of algae tolerance to these levels would provide knowledge about the specific gas cleaning pretreatment required before the PBR.
3. Improvement of the drag coefficient estimation is recommended for the good fit of the hydrodynamic models, simulating bubbles of the size range used in PBRs. Different drag coefficient correlations clearly affected model predictions and errors relative to the experimental data.
4. Also, experimental work in which the models would be tested more rigorously within real conditions of the examined environment is required. Making available a range of modelling approaches will help in understanding complex processes that will ultimately allow for deriving values such as the biomass productivity.
5. Estimation of the pumping needs in the case of inclined tube PBRs would be useful in order to evaluate the energy savings from the lower hydrostatic pressures and consider them with respect also to the possible increase in gas retention time and absorption efficiency.
6. The scale-up of the pilot plant and design of a PBR system for the treatment of larger gas volumes is essential for the commercialisation of this waste bioremediation system. A larger scale in the appropriate ships could also increase efficiency and CO_2 fixation potential and thereby reduce the respective energy penalty.
7. More frequent measurements are needed in order to calibrate a growth model that includes several factors, as the four phases of the growth are not identifiable with the existing measurement data. Also, a growth model that takes into account metabolism in combination with kinetics would reveal the actual relation of algae

growth with the extracellular nitrate concentrations, as the current kinetics model gives phase input to the growth model and simulates an early stop of growth.

8. Inclusion of the heat produced by the photosynthesis and the heat introduced in the PBR by radiation into the heat transfer model that simulates the proposed novel heat exchange device would be useful in order to provide more accurate results, if their effect proves to be significant.
9. Algal species capable of growing under minimal air and CO_2 supply might be needed, to maintain the PBR during the non-working hours of the engine, avoiding the use of storage tank for CO_2 provision during those hours. Algae should also be able to adapt to changes in temperature that may occur during a journey crossing many lines of latitude. Influence of changes in light conditions that occur at different times of the day and in PBR mass distribution between deck and holds would facilitate optimisation of the pumping flow rate of PBR water from holds to deck for a continuous flow. The influence of medium-duration light/dark cycles is not clear (2.3.5.3.1), so experiments with intermittent illumination of the order of a few minutes will supplement the literature with cycles of this range. While sunlight provision on the deck would save illumination energy requirements, the placement of the PBR close to the waterline would help improve ship stability. Continuous provision of light to the PBR using sunlight is crucial to save energy requirements. Further work is needed in stress response to introduce a better understanding of the adaption mechanisms as a result of various stress responses appearing on board a ship.

9 References

Aaron, D., & Tsouris, C. (2005). Separation of CO_2 from Flue Gas: A Review. *Separation Science and Technology*, *40*(1-3), 321–348. doi:10.1081/SS-200042244

Abatzoglou, N., & Boivin, S. (2009). A review of Biogas Purification Processes. *Biofuels Bioproducts & Biorefining*, *3*, 42–71. doi:10.1002/bbb

Abdel-Basset, R. (1993). Role of Calcium and Calmodulin Antagonist in Photosynthesis and Salinity Tolerance in *Chlorella Vulgaris*. *Biologia Plantarum*, *35*(August 1993), 237–244.

Acién Fernández, F. G., Fernández Sevilla, J. M., & Molina Grima, E. (2013). Photobioreactors for the Production of Microalgae. *Reviews in Environmental Science and Biotechnology*, (12), 131–151. doi:10.1007/s11157-012-9307-6

Acien Fernandez, F. G., Garcia Camacho, F., Sanchez Perez, J. A., Fernandez Sevilla, J. M., & Molina Grima, E. M. (1998). Modeling of Biomass Productivity in Tubular Photobioreactors for Microalgal Cultures: Effects of Dilution Rate, Tube Diameter, and Solar Irradiance. *Biotechnology and Bioengineering*, *58*(6), 605–16. Retrieved from http://www.ncbi.nlm.nih.gov/pubmed/10099298

Aitken, D., & Antizar-Ladislao, B. (2012). Achieving a Green Solution: Limitations and Focus Points for Sustainable Algal Fuels. *Energies*, *5*(5), 1613–1647. doi:10.3390/en5051613

Alabi, A. O., Tampier, M., & Bibeau, E. (2009). *Microalgae Technologies & Processes for Biofuels / Bioenergy Production in British Columbia: Current Technology, Suitability & Barriers to Implementation*. *Current*. Retrieved from http://www.fao.org/uploads/media/0901_Seed_Science_-_Microalgae_technologies_and_processes_for_biofuelsbioenergy_production_in_British_Columbia.pdf

Alexandrov, G. A., & Yamagata, Y. (2007). A Peaked Function for Modeling Temperature Dependence of Plant Productivity. *Ecological Modelling*, *200*(1-2), 189–192. doi:10.1016/j.ecolmodel.2006.07.012

Algal Biomass Organisation. (2012). Algae Biomass Organisation Hails New UCSD Study Showing Saltwater Algae Viable For Biofuels. Retrieved March 14, 2013, from http://www.algaebiomass.org/algae-biomass-organization-hails-new-ucsd-study-showing-saltwater-algae-viable-for-biofuels/

Alias, A. Z. (1988). Effect of Salinity and Light Intensity on the Growth of *Chlorella-Virginica*. *Pertanika*, *11*(3), 469–474. Retrieved from http://apps.webofknowledge.com/full_record.do?product=UA&search_mode=GeneralSearch&qid=1&SID=S27hiFGmOgNlDOhA4Kd&page=4&doc=36&cacheurlFromRightClick=no

Alwi, S. I. S., Algaetech Group of Companies, K. L. M., Rahman, R. A., & Norsham Bin Che Yahya, M. (2010). Advance Emission Control & Precision Agriculture; CO_2 Sequestration Using Algae Integrated Management System. In *International*

Conference on Chemistry and Chemical Engineering (ICCCE) (pp. 350–353). IEEE Conference Publications. doi:10.1109/ICCCENG.2010.5560415

Alyabyev, A. J., Loseva, N. L., Gordon, L. K., Andreyeva, I. N., Rachimova, G. G., Tribunskih, V. I., Ponomareva, A. A., & Kemp, R. B. (2007). The Effect of Changes in Salinity on the Energy Yielding Processes of *Chlorella Vulgaris* and *Dunaliella Maritima* Cells. *Thermochimica Acta*, *458*(1-2), 65–70. doi:10.1016/j.tca.2007.03.003

Aníbal, J., Madeira, H. T., Carvalho, L. F., Esteves, E., Veiga-Pires, C., & Rocha, C. (2014). Macroalgae Mitigation Potential for Fish Aquaculture Effluents: an Approach Coupling Nitrogen Uptake and Metabolic Pathways Using *Ulva Rigida* and *Enteromorpha Clathrata*. *Environmental Science and Pollution Research International*, *21*(23), 13324–34. doi:10.1007/s11356-013-2427-x

Anish. (2011). Marine Insight. *Why 2-stroke Engines are Used More commonly than 4-stroke on Ships?* Retrieved August 25, 2015, from http://www.marineinsight.com/tech/auxiliary-machinery/why-2-stroke-engines-are-used-more-commonly-than-4-stroke-on-ships/

Araújo, O. Q. F., Gobbi, C. N., Chaloub, R. M., & Coelho, M. A. Z. (2009). Assessment of the Impact of Salinity and Irradiance on the Combined Carbon Dioxide Sequestration and Carotenoids Production by *Dunaliella Salina*: A Mathematical Model. *Biotechnology and Bioengineering*, *102*(2), 425–35. doi:10.1002/bit.22079

Arrigo, K. R., & Sullivan, C. W. (1994). A High Resolution Bio-Optical Model of Microalgal Growth : Tests Using Sea-Ice Algal Community Time-Series Data. *Limnology and Oceanography*, *39*(3), 609–631.

Asenjo, J. A. (1995). Bioreactor System Design. In J. A. Asenjo & J. C. Merchuk (Eds.), *Bioreactor System Design*. U.S.A.: Marcel Dekker Inc. Retrieved from http://books.google.co.uk/books?id=jM2jhnWZjhEC&printsec=frontcover&source=gbs_ge_summary_r&cad=0#v=onepage&q&f=false

Ashokkumar, V., Rengasamy, R., Deepalakshmi, S., Sivalingam, A., & Sivakumar, P. (2014). Mass Cultivation of Microalgae and Extraction of Total Hydrocarbons: A Kinetic and Thermodynamic Study. *Fuel*, *119*(2014), 308–312.

Atkins, M. (2010). Atkins Researched Proposal, (202).

Ayub, A. (2009). *Marine Diesel Engines* (CRC Press., pp. 1–194). Delhi, India: Ane Books Pvt. Ltd. Retrieved from http://books.google.co.uk/books?id=_SILMwAACAAJ&source=gbs_similarbooks

Azarbad, H., Niklińska, M., van Gestel, C. A. M., van Straalen, N. M., Röling, W. F. M., & Laskowski, R. (2013). Microbial Community Structure and Functioning along Metal Pollution Gradients. *Environmental Toxicology and Chemistry / SETAC*, *32*(9), 1992–2002. doi:10.1002/etc.2269

Baird, C., & Cann, M. (2012). *Environmental Chemistry* (5th ed.). New York: W. H. Freeman and Company.

Barbosa, M. J., Janssen, M., Ham, N., Tramper, J., & Wijffels, R. H. (2003). Microalgae Cultivation in Air-Lift Reactors: Modeling Biomass Yield and Growth Rate as a

Function of Mixing Frequency. *Biotechnology and Bioengineering*, *82*(2), 170–9. doi:10.1002/bit.10563

Becker, E. W. (1994). *Microalgae: Biotechnology and Microbiology*. Cambridge University Press.

Belanger, S. E. (1997). Literature Review and Analysis of Biological Complexity in Model Stream Ecosystems : Influence of Size and Experimental Design. *Ecotoxicology and Environmental Safety*, *36*, 1–16.

Bernard, O., & Rémond, B. (2010). Validation of a Simple Model Accounting for Light and Temperature Effect on Microalgal Growth. *Bioresource Technology*, *123*(2012), 520–527. doi:10.1016/j.biortech.2012.07.022

Bitog, J. P., Lee, I.-B., Lee, C.-G., Kim, K.-S., Hwang, H.-S., Hong, S.-W., Seo, I. H., Kwon, K. S. & Mostafa, E. (2011). Application of Computational Fluid Dynamics for Modeling and Designing Photobioreactors for Microalgae Production: A Review. *Computers and Electronics in Agriculture*, *76*(2), 131–147. doi:10.1016/j.compag.2011.01.015

Blair, M. F., Kokabian, B., & Gude, V. G. (2014). Light and Growth Medium Effect on *Chlorella Vulgaris* Biomass Production. *Journal of Environmental Chemical Engineering*, *2*(1), 665–674. doi:10.1016/j.jece.2013.11.005

Bochum, R. U. (n.d.). H2 design. *Vision: Regenerative, C-Free Energy*. Retrieved October 12, 2015, from http://www.ruhr-uni-bochum.de/h2design/profile/main.de.html

Borgvang, S. A. (2011). International Workshop on Algae Technology, Hydrogen Production and Use of Algae Biomass. In S. A. Borgvang (Ed.), *Bioforsk Fokus* (Vol. 6). Kolkata, India: Bioforsk.

Borkenstein, C. G., Knoblechner, J., Frühwirth, H., & Schagerl, M. (2011). Cultivation of *Chlorella Emersonii* with Flue Gas Derived from a Cement Plant. *Journal of Applied Phycology*, 131–135. doi:10.1007/s10811-010-9551-5

Borowitzka, M. A. (n.d.). Topic 8 : Algal Culture and Biotechnology. In *BIO301*.

Borowitzka, M. A., & Borowitzka, L. J. (1988). *Micro-algal Biotechnology*. (Michael A. Borowitzka & L. J. Borowitzka, Eds.). Cambridge: Cambridge University Press.

Bosch Gmbh, R. (2003). *Diesel Engine Management: An Overview: Bosch Technical Instruction* (Paperback.). Robert Bosch GmbH. Retrieved from http://isbndb.com/d/book/diesel_engine_management_an_overview.html

Bowes, M. J., Gozzard, E., Johnson, a C., Scarlett, P. M., Roberts, C., Read, D. S., Armstrong, L. K., Harman, S. A., & Wickham, H. D. (2012). Spatial and Temporal Changes in Chlorophyll-a Concentrations in the River Thames Basin, UK: are Phosphorus Concentrations Beginning to Limit Phytoplankton Biomass? *The Science of the Total Environment*, *426*, 45–55. doi:10.1016/j.scitotenv.2012.02.056

Box, G. E. P., Hunter, J. S., & Hunter, W. G. (2005). *Statistics for Experimenters: Design, Innovation, and Discovery (Wiley Series in Probability and Statistics)* (2nd Editio.). Wiley-Blackwell.

Brennan, L., & Owende, P. (2010). Biofuels from Microalgae — A Review of Technologies for Production, Processing, and Extractions of Biofuels and Co-Products. *Renewable and Sustainable Energy Reviews*, *14*(2), 557–577. doi:10.1016/j.rser.2009.10.009

Brennen, C. E. (2005). *Fundamentals of Multiphase Flows*. California Institute of Technology, Pasadena CA: Cambridge University Press.

Briassoulis, D., Panagakis, P., Chionidis, M., Tzenos, D., Lalos, A., Tsinos, C., Berberidis, K., & Jacobsen, A. (2010). An Experimental Helical-Tubular Photobioreactor for Continuous Production of *Nannochloropsis sp*. *Bioresource Technology*, *101*(17), 6768–6777.

Brindley, C., Acién Fernández, F. G., & Fernández-Sevilla, J. M. (2011). Analysis of Light Regime in Continuous Light Distributions in Photobioreactors. *Bioresource Technology*, (102), 3138–48. doi:10.1016/j.biortech.2010.10.088

Buhr, H. O., & Miller, S. B. (1983). A Dynamic Model of the High-rate Algal-Bacterial Wastewater Treatment Pond. *Water Res.*, *17*, 29–37.

Busciglio, A., Grisafi, F., Scargiali, F., & Brucato, A. (2013). On the Measurement of Local Gas Hold-up, Interfacial Area and Bubble Size Distribution in Gas–Liquid Contactors via Light Sheet and Image Analysis: Imaging Technique and Experimental Results. *Chemical Engineering Science*, *102*(2013), 551–566. doi:10.1016/j.ces.2013.08.029

Cabello, J., Morales, M., & Revah, S. (2014). Dynamic Photosynthetic Response of the Microalga *Scenedesmus Obtusiusculus* to Light Intensity Perturbations. *Chemical Engineering Journal*, (252), 104–111. doi:10.1016/j.cej.2014.04.073

Camarasa, E., Carvalho, E., Meleiro, L. a. ., Maciel Filho, R., Domingues, A., Wild, G., Poncin, S., Midoux, N., & Bouillard, J. (2001). Development of a Complete Model for an Air-Lift Reactor. *Chemical Engineering Science*, *56*(2), 493–502. doi:10.1016/S0009-2509(00)00253-0

Carvalho, A. P., Meireles, L. a, & Malcata, F. X. (2006). Microalgal Reactors: a Review of Enclosed System Designs and Performances. *Biotechnology Progress*, *22*(6), 1490–506. doi:10.1021/bp060065r

Castenholz, R. W., & Utkilen, H. C. (1984). Physiology of Sulfide Tolerance in a Thermophilic *Oscillatoria*. *Arch Microbiol*, *138*, 299–305.

Chang, Y.-C., Tseng, R.-S., Chen, G.-Y., Chu, P. C., & Shen, Y.-T. (2013). Ship Routing Utilizing Strong Ocean Currents. *Journal of Navigation*, *66*, 825–835. doi:10.1017/S0373463313000441

Cheenkachorn, K., Choosri, N., Chutrapukdeekul, A., & Kangsadan, T. (2011). Computational Modeling of Microalgae Culture Using a Helical Photobioreactor. In *9th IASME / WSEAS International Conference on Fluid Mechanics and Aerodynamics (FMA '11)* (Vol. 2, pp. 300–305). Florence, Italy.

Chevron Shipping Co. (1995). Chevron Shipping Co. and Marine Engineers Beneficial Association, District No. 1-Pacific Coast District. Case 32–UC–292. *NLRB*, *53*, 379–382.

Chiang, C.-L., Lee, C.-M., & Chen, P.-C. (2011). Utilization of the *Cyanobacteria Anabaena sp. CH1* in Biological Carbon Dioxide Mitigation Processes. *Bioresource Technology*, *102*(9), 5400–5. doi:10.1016/j.biortech.2010.10.089

Chisti, Y. (1989). *Airlift Bioreactors* (p. 353). Elsevier Applied Science Ltd.

Chisti, Y. (2007). Biodiesel from Microalgae. *Biotechnology Advances*, *25*(3), 294–306. doi:10.1016/j.biotechadv.2007.02.001

Chiu, S.-Y., Kao, C.-Y., Chen, C.-H., Kuan, T.-C., Ong, S.-C., & Lin, C.-S. (2008). Reduction of CO_2 by a High-Density Culture of *Chlorella sp*. in a Semicontinuous Photobioreactor. *Bioresource Technology*, *99*(9), 3389–96. doi:10.1016/j.biortech.2007.08.013

Chiu, S.-Y., Kao, C.-Y., Huang, T.-T., Lin, C.-J., Ong, S.-C., Chen, C.-D., Chang, J. S., & Lin, C. (2011). Microalgal Biomass Production and On-Site Bioremediation of Carbon Dioxide, Nitrogen Oxide and Sulfur Dioxide from Flue Gas Using *Chlorella sp*. Cultures. *Bioresource Technology*, *102*, 9135–9142. doi:10.1016/j.biortech.2011.06.091

Chiu, S.-Y., Tsai, M.-T., Kao, C.-Y., Ong, S.-C., & Lin, C. (2009). The Air-Lift Photobioreactors with Flow Patterning for High-Density Cultures of Microalgae and Carbon Dioxide Removal. *Eng. Life Sci.*, *9*(3), 254–260. doi:10.1002/elsc.200800113

Cho, S. H., Ji, S.-C., Hur, S. B., Bae, J., Park, I.-S., & Song, Y.-C. (2007). Optimum Temperature and Salinity Conditions for Growth of Green Algae *Chlorella Ellipsoidea* and *Nannochloris Oculata*. *Fisheries Science*, *73*(5), 1050–1056. doi:10.1111/j.1444-2906.2007.01435.x

Choptiany, J. M. H., Pelot, R., & Sherren, K. (2014). An Interdisciplinary Perspective on Carbon Capture and Storage Assessment Methods. *Journal of Industrial Ecology*, *18*(3), 445–458. doi:10.1111/jiec.12121

Christenson, L., & Sims, R. (2011). Production and Harvesting of Microalgae for Wastewater Treatment, Biofuels, and Bioproducts. *Biotechnology Advances*, *29*(6), 686–702. doi:10.1016/j.biotechadv.2011.05.015

Chung, Y.-C., Ho, K.-L., & Tseng, C.-P. (2003). Hydrogen Sulfide Gas Treatment by a Chemical-Biological Process: Chemical Absorption and Biological Oxidation Steps. *Journal of Environmental Science and Health. Part. B, Pesticides, Food Contaminants, and Agricultural Wastes*, *38*(5), 663–79. doi:10.1081/PFC-120023522

Clarkson Research Services Limited. (2011). Clarksons Research World Fleet Register. Retrieved August 21, 2015, from http://wfr.clarksons.net/wfr/Login.aspx?ReturnUrl=/wfr/

Clift, R., Grace, J., & Weber, M. (1978). *Bubbles, Drops and Particles* (pp. 169–180). Academic Press.

Concas, A., Lutzu, G. A., Pisu, M., & Cao, G. (2012). Experimental Analysis and Novel Modeling of Semi-Batch Photobioreactors Operated with *Chlorella Vulgaris* and Fed

with 100% (v/v) CO_2. *Chemical Engineering Journal*, *213*(2012), 203–213. doi:10.1016/j.cej.2012.09.119

Conde, L., Travieso, L., & Leiva, A. (1993). Biogas Purification Process Using Intensive Microalgae Cultures. *Biotechnology Letters*, *15*(3), 317–320.

Cooper, D. (2003). Exhaust Emissions from Ships at Berth. *Atmospheric Environment*, *37*(27), 3817–3830. doi:10.1016/S1352-2310(03)00446-1

Cooper, David. (2002). Representative Emission Factors for Use in Quantification of Emissions from Ships Associated with Ship Movements between Port in the European Community ". *Environmental Research*, 1–44.

Costache, T. A., Acién Fernández, F. G., Morales, M. M., Fernández-Sevilla, J. M., Stamatin, I., & Molina, E. (2013). Comprehensive Model of Microalgae Photosynthesis Rate as a Function of Culture Conditions in Photobioreactors. *Applied Microbiology and Biotechnology*, *97*(17), 7627–37. doi:10.1007/s00253-013-5035-2

Cuaresma, M., Janssen, M., Vílchez, C., & Wijffels, R. H. (2009). Productivity of Chlorella Sorokiniana in a Short Light-Path (SLP) Panel Photobioreactor under High Irradiance. *Biotechnology and Bioengineering*, *104*(2), 352–9. doi:10.1002/bit.22394

David, M., & Gollasch, S. (2015). *Global Maritime Transport and Ballast Water Management - Issues and Solutions*. (M. David & S. Gollasch, Eds.) (Invading N.). New York.

De Morais, M. G., & Costa, J. A. V. (2007). Carbon Dioxide Fixation by *Chlorella Kessleri, C. Vulgaris, Scenedesmus Obliquus* and *Spirulina sp*. Cultivated in Flasks and Vertical Tubular Photobioreactors. *Biotechnology Letters*, *29*(9), 1349–52. doi:10.1007/s10529-007-9394-6

De Rosa, F., & Holtshausen, C. (2011). Cargill. *Cargill Propels Shipping Forward with Largest Kite-Powered Vessel*. Retrieved June 18, 2013, from http://www.cargill.com/news/releases/2011/NA3040908.jsp

Defra. (2010). *Defra UK Ship Emissions Inventory* (pp. 1–268). Crown Copyright.

Delwiche, C. F., Kuhsel, M., & Palmer, J. D. (1995). Phylogenetic Analysis of tufA Sequences Indicates a Cyanobacterial Origin of All Plastids. *Molecular Phylogenetics and Evolution*, *4*(2), 110–128.

Demidenko, E. (2013). *Mixed Models - Theory and Application with R* (2nd ed.). New Jersey: Wiley Series in Probability and Statistics.

Derakhshan, M. V., Nasernejad, B., Dadvar, M., & Hamidi, M. (2014). Pretreatment and Kinetics of Oil Extraction from Algae for Biodiesel Production. *Asia-Pacific Journal of Chemical Engineering*, *9*, 629–637. doi:10.1002/apj

DNV. (2008). *Marpol 73/78 Annex VI - Regulations of Air Polution from Ships - Technical and Operational Implications*. *Fuel* (pp. 1–32).

Doucha, J., Straka, F., & Lívanský, K. (2005). Utilization of Flue Gas for Cultivation of Microalgae *Chlorella sp*. in an Outdoor Open Thin-Layer Photobioreactor. *Journal of Applied Phycology*, *17*(5), 403–412. doi:10.1007/s10811-005-8701-7

Douskova, I., Doucha, J., Livansky, K., Machat, J., Novak, P., Umysova, D., Zachleder, V., & Vitova, M. (2009). Simultaneous Flue Gas Bioremediation and Reduction of Microalgal Biomass Production Costs. *Applied Microbiology and Biotechnology*, *82*(1), 179–85. doi:10.1007/s00253-008-1811-9

Dubyne, D. (2015). Oil Seed Crops Food and Energy. *Algae*. Retrieved October 12, 2015, from http://www.oilseedcrops.org/algae/

Edwards, M. (2009). *The Algal Industry Survey*.

Electric, G. (2013). GE Power and Water, Water & Process Technologies. *Membrane Bioreactor (MBR)*. Retrieved October 12, 2015, from http://www.gewater.com/products/membrane-bioreactor-mbr.html

Entec. (2002). *Ship Emissions Final Report - Quantification of Ship Emissions*. *Ship Emissions Final reeport* (pp. 3–48). Entec.

Entec. (2010). *Defra UK Ship Emissions Inventory* (pp. 1–268). Crown Copyright.

European Federation for Transport and Environment, A. (2011). Transport & Environment. *Shipping and Climate Change*. Retrieved July 12, 2013, from http://www.transportenvironment.org/what-we-do/shipping/shipping-and-climate-change

Fathom. (2011). *Ship Efficiency The Guide*.

Fathom Shipping. (2013). Clean Technology Intelligence for the Maritime Sector. *Power From Exhaust Gas: The Paybacks Of Waste Heat Recovery Systems*. Retrieved February 19, 2015, from http://fathom-ctech.com/whos-doing-what-item/the-paybacks-of-waste-heat-recovery-systems/08-02-2013/53/

Fernandez, F., Camacho, F., Perez, J., Sevilla, J., & Grima, E. (1998). Modeling of Biomass Productivity in Tubular Photobioreactors for Microalgal Cultures: Effects of Dilution Rate, Tube Diameter, and Solar Irradiance. *Biotechnology and Bioengineering*, *58*(6), 605–16. Retrieved from http://www.ncbi.nlm.nih.gov/pubmed/10099298

Fernandez, F. G., Sevilla, J. M., Perez, J. A., Molina Grima, E., & Chisti, Y. (2001). Airlift-Driven External-Loop Tubular Photobioreactors for Outdoor Production of Microalgae: Assessment of Design and Performance. *Chemical Engineering Science*, *56*, 2721–2732.

Figueroa, J. D., Fout, T., Plasynski, S., McIlvried, H., & Srivastava, R. D. (2008). Advances in CO_2 Capture Technology—The U.S. Department of Energy's Carbon Sequestration Program. *International Journal of Greenhouse Gas Control*, *2*(1), 9–20. doi:10.1016/S1750-5836(07)00094-1

Fischer, H. (2011). Fischer Group - Triple Yield Trigeneraton on the AIDA Cruise Ship. *F.E.R. Fischer Edelstahlrohre GmbH*. Retrieved February 25, 2012, from http://www.fischer-group.com/en/fischer_companies/fischer_eco_solutions/trigeneration.php?navanchor=2110107

Fishman, D., Majumdar, R., Morello, J., Pate, R., & Yang, J. (2010). *National Algal Biofuels Technology Roadmap*. *Renewable Energy*. Maryland.

Florin, N., & Fennell, P. (2010). *Review of Advanced Carbon Capture Technologies* (pp. 1–28). London. Retrieved from www.avoid.uk.net

Francisco, É. C., Neves, D. B., Jacob-Lopes, E., & Franco, T. T. (2010). Microalgae as Feedstock for Biodiesel Production: Carbon Dioxide Sequestration, Lipid Production and Biofuel Quality. *Journal of Chemical Technology & Biotechnology*, *85*(3), 395–403. doi:10.1002/jctb.2338

García-Calvo, E., Rodríguez, A., Prados, A., & Klein, J. (1999). A fluid dynamic model for three-phase airlift reactors. *Chemical Engineering Science*, *54*, 2359–2370.

Gardner, M. (2011). *The Effectiveness of Hollow Fibre Membranes in Transferring Flue Gas into Microalgal Culture for Sequestration Purposes*. *Test*. Dalhousie University Halifax, Nova Scotia.

Gaudin, A. M. (1957). *Flotation* (Second., pp. 350–351). McGraw-Hill.

Geider, R. J., MacIntyre, H. L., & Kana, T. M. (1997). Dynamic model of phytoplankton growth and acclimation: responses of the balanced growth rate and the chlorophyll a:carbon ratio to light, nutrient-limitation and temperature. *Marine Ecology Progress Series*, *148*, 187–200.

Giannuzzi, L., Pinotti, A., & Zaritzky, N. (1998). Mathematical modelling of microbial growth in packaged refrigerated beef stored at different temperatures, *39*, 101–110.

Girdhari, R. S. K. (2011). *Systems and Control Modelling of energy consumption for algae photo bioreactors in various scenarios*. Wageningen University.

Gonçalves, A. L., Simões, M., & Pires, J. C. M. (2014). The Effect of Light Supply on Microalgal Growth, CO_2 Uptake and Nutrient Removal from Wastewater. *Energy Conversion and Management*, *85*, 530–536.

González López, C. V., Acién Fernández, F. G., Fernández Sevilla, J. M., Sánchez Fernández, J. F., Cerón García, M. C., & Molina Grima, E. (2009). Utilization of the Cyanobacteria *Anabaena sp. ATCC 33047* in CO_2 Removal Processes. *Bioresource Technology*, *100*(23), 5904–5910. doi:http://dx.doi.org/10.1016/j.biortech.2009.04.070

Goulielmos, A. M., Giziakis, K. V., & Christodoulou, A. (2011). A Future Regulatory Framework for CO_2 Emissions of Shipping in the Mediterranean Area. *Indian Journal of Engineering and Materials Science*, *4*(1), 39–60.

Gouveia, L., & Oliveira, A. C. (2009). Microalgae as a Raw Material for Biofuels Production. *Journal of Industrial Microbiology & Biotechnology*, *36*(2), 269–74. doi:10.1007/s10295-008-0495-6

Greenway, H., & Setter, T. L. (1979). Na^+, C^{1-} and K^+ Concentrations in *Chlorella Emersonii* Exposed to 100 and 335 mM NaCl. *Australian Journal of Plant Physiology*, *6*, 61–67.

Han, G. B., Lee, J. G., Lee, B. H., & Lee, Y. W. (2006). Development of Soil-Covered SBR Process for Small Scale Sewage Treatment. *Environmental Technology*, *27*(7), 715–22. doi:10.1080/09593332708618684

Hanagata, N., Takeuchi, T., Fukuju, Y., Barnes, D. J., & Karube, I. (1992). Tolerance of Microalgae to High CO_2 and High Temperature. *Phytochemistry*, *31*(10), 3345–3348.

Harrould-Kolieb, E., & Savitz, J. (2010). *Shipping Solutions: Technological and Operational Methods Available to Reduce CO_2*. Retrieved from www.oceana.org

He, L. (2014). *Construction of a Ship-board Algae Reactor*. University College London.

He, L., Subramanian, V. R., & Tang, Y. J. (2012). Experimental Analysis and Model-based Optimization of Microalgae Growth in Photo-bioreactors Using Flue Gas. *Biomass and Bioenergy*, *41*(314), 131–138. doi:10.1016/j.biombioe.2012.02.025

Henley, W. J., Major, K. M., & Hironaka, J. L. (2002). Response to Salinity and Heat Stress in Two Halotolerant *Chlorophyte* Algae. *Journal of Physiology*, *766*, 757–766.

Hillebrand, M., Pflugmacher, S., & Hahn, A. (2016). Toxicological Risk Assessment in CO_2 Capture and Storage Technology. *International Journal of Greenhouse Gas Control*, *55*, 118–143. doi:10.1016/j.ijggc.2016.10.014

Hiremath, S., & Mathad, P. (2010). Impact of Salinity on the Physiological and Biochemical Traits of *Chlorella*. *J. Algal Biomass Uthln.*, *1*(2), 51–59.

Huang, J., Li, Y., Wan, M., Yan, Y., Feng, F., Qu, X., Wang, J., Shen, G., Li, W., Fan, J., & Wang, W. (2014). Novel Flat-plate Photobioreactors for Microalgae Cultivation with Special Mixers to Promote Mixing along the Light Gradient. *Bioresource Technology*, *159*(2014), 8–16. doi:10.1016/j.biortech.2014.01.134

Huang, L., Hwang, A., & Phillips, J. (2011). Effect of Temperature on Microbial Growth Rate -Mathematical Analysis: the Arrhenius and Eyring-Polanyi Connections. *Journal of Food Science*, *76*(8), E553–60. doi:10.1111/j.1750-3841.2011.02377.x

Huesemann, M. H., Van Wagenen, J., Miller, T., Chavis, A., Hobbs, S., & Crowe, B. (2013). A Screening Model to Predict Microalgae Biomass Growth in Photobioreactors and Raceway Ponds. *Biotechnology and Bioengineering*, *110*(6), 1583–94. doi:10.1002/bit.24814

Hutto, L. B. (2001). A Comprehensive Guide to Shipboard Waste Management Options. In *Oceans MTS/IEEE Conference and Exhibition* (pp. 295–301).

Illinois State University. (2014). How Many Data Points are Enough? *Department of Physics*. Retrieved September 30, 2015, from http://www2.phy.ilstu.edu/~wenning/slh/How_Many_Data_Points.pdf

Illman, A., Scragg, A., & Shales, S. (2000). Increase in *Chlorella* Strains Calorific Values when Grown in Low Nitrogen Medium. *Enzyme and Microbial Technology*, *27*(8), 631–635. Retrieved from http://www.ncbi.nlm.nih.gov/pubmed/11024528

IMO. (2009). *Second IMO GHG Study 2009*. *Reproduction* (p. 220). London.

IMO. (2011). IMO International Maritime Organisation - Marine Environment Protection Committee (MEPC) – 62nd session: 11 to 15 July 2011. *Mandatory Energy Efficiency Measures for International Shipping Adopted at IMO Environment Meeting*. Retrieved from http://www.imo.org/MediaCentre/PressBriefings/Pages/42-mepc-ghg.aspx

IMO - Marine Environmental Protection Committee. (2014). *Third IMO GHG Study*. London.

Indiamart. (2015). *Biotech Laboratory Equipments - Autoclavable Benchtop Photobioreactor*. Retrieved October 12, 2015, from http://www.indiamart.com/napro-scientific/biotech-laboratory-equipments.html

Ishii, M., & Zuber, N. (1979). Drag Coefficient and Relative Velocity in Bubbly, Droplet or Particulate Flows. *American Institute of Chemical Engineers Journal*, *25*(5), 843–855.

Janssen, M. (2002). *Cultivation of Microalgae: Effect of Light/Dark Cycles on Biomass Yield*. Wageningen University, The Netherlands.

Janssen, M., Kuijpers, T. C., Veldhoen, B., Ternbach, M. B., Tramper, J., Mur, L. R., & Wijffels, R. H. (1999). Specific Growth Rate of *Chlamydomonas Reinhardtii* and *Chlorella Sorokiniana* under Medium Duration Light/Dark Cycles: 13–87 s. *Journal of Biotechnology*, *70*(1-3), 323–333. doi:10.1016/S0168-1656(99)00084-X

Jean, H. (2013). Average Light Intensity Inside a Photobioreactor. *Undergraduate Journal of Mathematical Modeling: One + Two*, *4*(1), 1–7. doi:10.5038/2326-3652.4.1.9

Jeffryes, C. S., & Agathos, S. N. (n.d.). Algae as a Frontier in Bioprocessing: Technical and Economic Challenges. Unit of Bioengineering Faculty of Bioengineering, Agronomy & Environment, Université Catholique de Louvain, Belgium: CERTH. Retrieved from http://www.certh.gr/dat/0D92D187/file.pdf

Jones, A. P. (1999). Indoor Air Quality and Health. *Atmospheric Environment*, *33*, 4535–4564.

Juneja, A., Ceballos, R., & Murthy, G. (2013). Effects of Environmental Factors and Nutrient Availability on the Biochemical Composition of Algae for Biofuels Production: A Review. *Energies*, *6*(9), 4607–4638. doi:10.3390/en6094607

Kageson, P. (2009). Transport for a Global Economy, Challenges and Opportunities in the Downturn, Environmental Impacts of International Transport, Making International Transport Pay Its Climate Bill. In *International Transport Forum* (pp. 1–16). Leipzig: International Transport Forum. Retrieved from http://www.transportenvironment.org/sites/te/files/media/KAGESON_W5_Aviation_and_shipping.pdf

Kalesh, N. S., & Nair, S. M. (2005). The Accumulation Levels of Heavy Metals (Ni, Cr, Sr, & Ag) in Marine Algae from Southwest Coast of India. *Toxicological & Environmental Chemistry*, *87*(2), 135–146. doi:10.1080/02772240400029744

Kalinkina, L. G., & Naumova, T. G. (1992). The Content of Free Amino Acids in Sea and Fresh-water *Chlorella* Cells under Saline Conditions in the Presence of the Inhibitors of Glycolate Pathway. *Fiziologiya Rastenii*, *39*(3), 559–569. Retrieved from http://apps.webofknowledge.com/full_record.do?product=UA&search_mode=GeneralSearch&qid=1&SID=S27hiFGmOgNlDOhA4Kd&page=4&doc=35&cacheurlFromRightClick=no

Kapdi, S. S., Vijay, V. K., Rajesh, S. K., & Prasad, R. (2005). Biogas Scrubbing, Compression and Storage: Perspective and Prospectus in Indian Context. *Renewable Energy*, *30*(8), 1195–1202. doi:10.1016/j.renene.2004.09.012

Karamanev, D. G., & Nikolov, L. N. (1992). Free Rising Spheres Do Not Obey Newton's Law for Free Settling. *American Institute of Chemical Engineers Journal*, *38*(11), 1843–1846.

Kastánek, F., Sabata, S., Solcová, O., Maléterová, Y., Kastánek, P., Bránykiková, I., Kuthan, K., & Zachleder, V. (2010). In-field Experimental Verification of Cultivation of Microalgae *Chlorella sp*. Using the Flue Gas from a Cogeneration Unit as a Source of Carbon Dioxide. *Waste Management & Research: The Journal of the International Solid Wastes and Public Cleansing Association, ISWA*, *28*(11), 961–6. doi:10.1177/0734242X10375866

Kim, N.-J., Suh, I. S., Hur, B.-K., & Lee, C.-G. (2002). Simple Monodimensional Model for Linear Growth Rate of Photosynthetic Microorganisms in Flat-Plate Photobioreactors. *J. Microbiol. Biotechnol.*, *12*, 962–971.

Kirst, G. O. (1989). Salinity Tolerance of Eukaryotic Marine Algae. *Annu. Rev. Plant. Mol. Biol.*, *40*, 21–53.

Knudsen, O. (2010). Exhaust Gas Cleaning. Aalborg Industries.

Koberg, M., Cohen, M., Ben-Amotz, A., & Gedanken, A. (2011). Bio-diesel Production Directly from the Microalgae Biomass of *Nannochloropsis* by Microwave and Ultrasound Radiation. *Bioresource Technology*, *102*(5), 4265–9. doi:10.1016/j.biortech.2010.12.004

Komarov, S. V., & Sano, M. (1998). Bubble Behavior and Heat Transfer in Preheated Gas injection into Liquid Bath. *ISIJ International*, *38*(10), 1045–1052. Retrieved from https://www.jstage.jst.go.jp/article/isijinternational1989/38/10/38_10_1045/_pdf

Konopkat, A., & Brock, T. D. (1978). Effect of Temperature on Blue-Green Algae (Cyanobacteria) in Lake Mendota. *Applied and Environmental Microbiology*, *36*(4), 572–576.

Koutita, K., Lizzul, A. M., Campos, L. C., Rai, N., Smith, T. W. P., & Stegemann, J. A. (2015). A Theoretical Fluid Dynamic Model for Estimation of the Hold-up and Liquid Velocity in an External Loop Airlift Bioreactor. *International Journal of Applied Science and Technology*, *5*(4), 11–29. Retrieved from http://www.ijastnet.com/journals/Vol_5_No_4_August_2015/3.pdf

Koutita, K., Stegemann, J. A., Smith, T. W. P., & Rai, N. (2013a). Development of a Ship-board Algal Bioreactor. In *Thames Estuary Partnership Summer Networking*. University College London, UK.

Koutita, K., Stegemann, J. A., Smith, T. W. P., & Rai, N. (2013b). Ship-board Bioreactors for Algae Production. In *Sustainable Chemicals from Microalgae Encompassing Biocrude Through to Fine Chemicals*. Royal School of Chemistry, Burlington House, London.

Koutita, K., Stegemann, J. A., Smith, T. W. P., & Rai, N. (2014). Transient Modelling of Algal Growth in Semi-continuous Photobioreactors and the Effect of an Integrated

Heat Exchanger on Biomass Productivity. In *4th international Conference on algal Biomass, Biofuels and Bioproducts*. Santa-Fe Convention Centre, New Mexico, USA.

Koutsoumanis, K. P., Taoukis, P. S., & Drosinos, E. H. (2000). Applicability of an Arrhenius Model for the Combined Effect of Temperature and CO_2 Packaging on the Spoilage Microflora of Fish. *Applied and Environmental Microbiology*, *66*(8), 3528–3534.

Kuiper, G. (2010). Physics of Cavitation: Gas Content and Nuclei. In *Cavitation on Ship Propellers* (pp. 9–79). Delft: TU Delft.

Kumar, A., Yuan, X., Sahu, A. K., Dewulf, J., Ergas, S. J., & Langenhove, H. V. (2010). A Hollow Fiber Membrane Photo-bioreactor for CO_2 Sequestration from Combustion Gas Coupled with Wastewater Treatment: a Process Engineering Approach. *Journal of Chemical Technology Biotechnology*, *85*(3), 387–394. doi:10.1002/jctb.2332

Kumar, Amit, Ergas, S., Yuan, X., Sahu, A., Zhang, Q., Dewulf, J., Malcata, F. X., & van Langenhove, H. (2010). Enhanced CO_2 Fixation and Biofuel Production via Microalgae: Recent Developments and Future Directions. *Trends in Biotechnology*, *28*(7), 371–80. doi:10.1016/j.tibtech.2010.04.004

Kumar, K., Dasgupta, C. N., Nayak, B., Lindblad, P., & Das, D. (2011). Development of Suitable Photobioreactors for CO_2 Sequestration Addressing Global Warming Using Green Algae and Cyanobacteria. *Bioresource Technology*, *102*(8), 4945–53. doi:10.1016/j.biortech.2011.01.054

Kunjapur, A. M., & Eldridge, R. B. (2010). Photobioreactor Design for Commercial Biofuel Production from Microalgae. *Industrial & Engineering Chemistry Research*, *49*(8), 3516–3526. doi:10.1021/ie901459u

Kunze, C., & Spliethoff, H. (2012). Assessment of Oxy-fuel, Pre- and Post-combustion-based Carbon Capture for Future IGCC Plants. *Applied Energy*, *94*, 109–116. doi:10.1016/j.apenergy.2012.01.013

Kuramochi, T., Ramírez, A., Turkenburg, W., & Faaij, A. (2012). Comparative Assessment of CO_2 Capture Technologies for Carbon-intensive Industrial Processes. *Progress in Energy and Combustion Science*, *38*(1), 87–112. doi:10.1016/j.pecs.2011.05.001

Kurano, N., Ikemoto, H., Miyashita, H., Hasegawa, T., Hata, H., & Miyachi, S. (1995). Fixation and Utilization of Carbon Dioxide by Microalgal Photosynthesis. *Energy Conservation Management*, *36*(6), 689–692.

Lane, C., Surman-Lee, S., Sellwood, J., & Lee, J. V. (2007). *The Thames Recreational Users Study - Final Report 2007*. London. Retrieved from http://www.hpa.org.uk/webc/HPAwebFile/HPAweb_C/1194947405865

Langer, J. (1969). Handbook of Microalgal Culture. *Annals of Physics*, *54*(2).

Lavens, P., & Sorgeloos, P. (1996). *Manual on the Production and Use of Live Food for Aquaqulture*. (P. Lavens & P. Sorgeloos, Eds.) (p. 295). Rome.

Law, D., & Battaglia, F. (2013). Numerical Simulations for Hydrodynamics of Air-Water External Loop Airlift Reactor Flows With Bubble Break-Up and Coalescence Effects. *Journal of Fluids Engineering*, *135*(8), 081302. doi:10.1115/1.4024396

LEAP. (n.d.). LEAP Micro AD Closed Loop Recycling. *The Pilot System*. Retrieved March 26, 2016, from http://communitybydesign.co.uk/

Lee, J. N., Lee, J. S., Shin, C. S., Park, S. C., & Kim, S. W. (2000). Methods to Enhance Tolerances of *Chlorella KR-1* to Toxic Compounds in Flue Gas. *Applied Biochemistry and Biotechnology*, *84-86*(x), 329–42.

Lee, Y., Ding, S., Low, C., Chang, Y., Forday, W. L., & Chew, P. (1995). Design and Performance of an a-Type Tubular Photobioreactor for Mass Cultivation of Microalgae. *Journal of Applied Phycology*, *7*(1), 47–51.

Leigh-Jones, C. (1998). A practical Guide to Marine Oil Handling. In IMarEST (Ed.), *Time* (pp. 1–121). MEP series - Marine Engineering Practice. Retrieved from http://eshop.imarest.org/mep-series-volume-3-part-19-a-practical-guide-to-marine-oil-fuel-handling.html

Levin, G. V, Clendenning, J. R., Gibor, A., & Bogar, F. D. (1962). Harvesting of Algae by Froth Flotation. *Applied Microbiology*, *10*, 169–75. Retrieved from http://www.pubmedcentral.nih.gov/articlerender.fcgi?artid=1057831&tool=pmcentrez&rendertype=abstract

Li, S., & Li, W. (2011). Physiological and Biochemical Responses of Antarctic Microalga *Chlorella sp NJ-18* to Salinity Stress. *Fresenius Environmental Bulletin*, *20*(6), 1346–1351. Retrieved from http://apps.webofknowledge.com/full_record.do?product=UA&search_mode=GeneralSearch&qid=1&SID=S27hiFGmOgNlDOhA4Kd&page=2&doc=15&cacheurlFromRightClick=no

Li, X. Z., Hauer, B., & Rosche, B. (2013). Catalytic Biofilms on Structured Packing for the Production of Glycolic Acid. *Journal of Microbiology and Biotechnology*, *23*(2), 195–204. Retrieved from http://www.ncbi.nlm.nih.gov/pubmed/23412062

Li, Y., Horsman, M., Wang, B., Wu, N., & Lan, C. Q. (2008). Effects of Nitrogen Sources on Cell Growth and Lipid Accumulation of Green Alga *Neochloris Oleoabundans*. *Applied Microbiology and Biotechnology*, *81*(4), 629–36. doi:10.1007/s00253-008-1681-1

Liang, Y., Sarkany, N., & Cui, Y. (2009). Biomass and Lipid Productivities of *Chlorella Vulgaris* Under Autotrophic, Heterotrophic and Mixotrophic Growth Conditions. *Biotechnology Letters*, *31*(7), 1043–9. doi:10.1007/s10529-009-9975-7

Liang, Z., Rongwong, W., Liu, H., Fu, K., Gao, H., Cao, F., Zhang, R., Sema, T., Henni, A., Sumon, K., Nath, D., Gelowitz, D., Srisang, W., Saiwan, C., Benamor, A., Al-marri, M., Shi, H., Supap, T., Chan, C., Zhou, Q., Abu-zahra, M., Wilson, M., Olson, W., Idem, R., & Tontiwachwuthikul, P. (2015). Recent Progress and New Developments in Post-Combustion Carbon-capture Technology with Amine Based Solvents. *International Journal of Greenhouse Gas Control*, *40*, 26–54.

Lienhard IV, J. H., & Lienhard V, J. H. (2008). *A Heat Transfer Textbook* (3rd ed.). Massachusetts: Phlogiston Press Cambridge Massachusetts.

Liu, W., Au, D. W. T., Anderson, D. M., Lam, P. K. S., & Wu, R. S. S. (2007). Effects of Nutrients, Salinity, pH and Light:Dark Cycle on the Production of Reactive Oxygen Species in the Alga *Chattonella Marina*. *Journal of Experimental Marine Biology and Ecology*, *346*(1-2), 76–86. doi:10.1016/j.jembe.2007.03.007

Lloret, J., Bolanos, L., Mercedes, L. M., Peart, J. M., Brewin, N. J., Bonilla, I., & Rivilla, R. (1995). Ionic Stress and Osmotic Pressure Induce Different Alterations in the Lipopolysaccharide of a *Rhizobium Meliloti* Strain. *Applied and Environmental Microbiology*, *61*(10), 3701–3704. doi:0099-2240/95

Lloyd, G., & Veritas, D. N. (2006). Greenhouse Gas Emissions for Shipping and Implementation Guidance for the Marine Fuel Sulphur Directive. *Solutions*.

Lloyd's Register Marine Services. (2008). *Container Ship Speed Matters*.

Loubiere, K., Pruvost, J., Aloui, F., & Legrand, J. (2011). Investigations in an External-loop Airlift Photobioreactor with Annular Light Chambers and Swirling Flow. *Chemical Engineering Research and Design*, *89*(2), 164–171. doi:10.1016/j.cherd.2010.06.001

MacKetta, J. J. (1992). *Heat Transfer Design Methods*. (J. J. MacKetta, Ed.) (p. 105). New York: Marcel Decker Inc. Retrieved from https://books.google.gr/books?id=U96_KxIOz-EC&pg=PA105&lpg=PA105&dq=maximum+allowable+temperature+difference+between+fluids+in+heat+exchanger&source=bl&ots=Y8bbTAhpKK&sig=GGBdGvUS57RWzPgcsK-E0OFsMz4&hl=en&sa=X&ved=0ahUKEwiZ5pDT0a_LAhVKAxoKHQXZAhYQ6AEILDAD#v=onepage&q=maximum allowable temperature difference between fluids in heat exchanger&f=false

Maeda, K., Owadai, M., Kimura, N. K., & Karubd, I. (1995). CO_2 Fixation from the Flue Gas on Coal-fired Thermal Power Plant by Microalgae. *Energy Conversion Management*, *36*(6), 717–720. Retrieved from ftp://138.96.0.43/biocore/OBERNARD/articles/sdarticle(2).pdf

Maersk. (n.d.). Constant Care for the Environment. *Environmental Management*. Maersk Line. Retrieved from maerskline.com

Makarevičienė, V., Andrulevičiūtė, V., Skorupskaitė, V., & Kasperovičienė, J. (2011). Cultivation of Microalgae *Chlorella sp*. and *Scenedesmus sp*. as a Potentional Biofuel Feedstock. *Environmental Research, Engineering and Management*, *3*(3), 21–27.

Mallick, N. (2002). Biotechnological Potential of Immobilized Algae for Wastewater N, P and Metal Removal: a Review. *Biometals*, *15*(4), 377–90. Retrieved from http://www.ncbi.nlm.nih.gov/pubmed/12405533

MAN Diesel. (2008). *Quality Requirements of Operating Supplies* (pp. 3–23).

Mandeno, G., Craggs, R., Tanner, C., Sukias, J., & Webster-Brown, J. (2005). Potential Biogas Scrubbing Using a High Rate Pond. *Water Science Technology*, *51*(12), 253–6. Retrieved from http://www.ncbi.nlm.nih.gov/pubmed/16114691

Mann, G., Schlegel, M., & Sakalauskas, R. S. A. (2009). Biogas-Conditioning with Microalgae. *Agronomy Research*, *7*(1), 33–38.

MarineLog. (2013). EC Seeks Ship CO_2 Monitoring and Reporting Requirement. Retrieved June 10, 2015, from http://www.marinelog.com/index.php?option=com_k2&view=item&id=4276:ec-seeks-ship-co2-monitoring-and-reporting-requirement&Itemid=231

Markl, H. (1977). CO_2 Transport and Photosynthetic Productivity of a Continuous Culture of Algae. *Biotechnology and Bioengineering*, *XIX*, 1851–1862.

Marquez, M. A., Saez, A. E., Carbonell, R. G., & Robert, G. W. (1999). Coupling of Hydrodynamics and Chemical Reaction in Gas-Lift Reactors. *American Institute of Chemical Engineers Journal*, *45*(2).

Martinez, M. E., Jimnez, J. M., & Yousfi, F. E. (1999). Influence of Phosphorus Concentration and Temperature on Growth and Phosphorus Uptake by the Microalga *Scenedesmus Obliquus. Bioresource Technology*, *67*, 233–240.

Mata, T. M., Martins, A. A., & Caetano, N. S. (2010). Microalgae for Biodiesel Production and other Applications: A Review. *Renewable and Sustainable Energy Reviews*, *14*(1), 217–232. doi:10.1016/j.rser.2009.07.020

Matsumoto, H., Shioji, N., Hamasaki, A., Ikuta, Y., Fukuda, Y., Sato, M., Endo, N., & Tsukamoto, T. (1995). Carbon Dioxide Fixation by Microalgae Photosynthesis Using Actual Flue Gas Discharged from a Boiler. *Applied Biochemistry and Biotechnology*, *51/52*, 681–692.

McCabe, W. L., Smith, J. C., & Harriot, P. (1956). *Unit Operations of Chemical Engineering* (6th ed., pp. 150–185). Mc Graw Hill International Edition.

MediaWiki. (2008). Heat Transfer Coefficients and Resistances. *Wufi Pro 2D Plus*. Retrieved December 14, 2012, from http://www.wufi-wiki.com/mediawiki/index.php5/Details:HeatTransfer

Mehta, R., & Hawxby, K. (1977). Use of Ultravioilet Radiation to Achieve Bacteria-Free Algal Culture. *Proceedings of the Oklahoma Academy of Science*, *60*(Table 1), 54–60.

Merchuk, J. (2003). Airlift Bioreactors: Review of Recent Advances. *The Canadian Journal of Chemical Engineering*, *81*(June-August), 324–337.

Merchuk, J., & Siegel, M. (1988). Air-lift Reactors in Chemical and Biological Technology. *Journal of Chemical Technology & Biotechnology*, *41*, 105–120.

Miyairi, S. (1995). CO_2 Assimilation in a Thermophilic Cyanobacterium. *Energy Conversion and Management*, *Vol.36(6-9*, pp. 763–766. Retrieved from http://www.sciencedirect.com/science/article/pii/019689049500116U

Molina, E., Fernández, J., Acién, F. G., & Chisti, Y. (2001). Tubular Photobioreactor Design for Algal Cultures. *Journal of biotechnology*, *92*(2), 113–31. Retrieved from http://www.ncbi.nlm.nih.gov/pubmed/11640983

Molina Grima, E., Acien, F. G., Garcia Camacho, F., & Chisti, Y. (1999). Photobioreactors: Light Regime, Mass Transfer, and Scaleup. *Biotechnology*, *70*, 231–247.

Molina Grima, E., Garcia Camacho, F., Sgnchez Perez, J. A., Acien Fernandez, F. G., & Fernandez Sevilla, J. M. (1997). Evaluation of Photosynthetic Effiency in Microalgal Cultures Using Averaged Irradiance. *Enzyme and Microbial Technology*, *0229*(97), 375–381.

Molina Grima, E., Garcia Carnacho, F., Sanchez Perez, J. A., Fernandez Sevilla, J. M., Acien Fernandez, F. G., & Contreras Gomez, A. (1994). A Mathematical Model of Microalgal Growth in Light-Limited Chemostat Culture. *Journal of Chemical Technology and Biotechnology*, *61*, 167–173.

Molina Grima, E., Sanchez Perez, J. A., Garcia Camacho, F., Fernandez Sevilla, J. M., & Acien Fernandez, F. G. (1996). Productivity Analysis of Outdoor Chemostat Culture in Tubular Air-lift Photobioreactors. *Journal of Applied Phycology*, (8), 369–380.

Mondal, M. K., Balsora, H. K., & Varshney, P. (2012). Progress and Trends in CO_2 Capture / Separation Technologies: A Review. *Energy*, *46*, 431–441.

Monod, J. (1949). The Growth of Bacterial Cultures. *Annual Review of Microbiology*, *3*, 371–394.

Moo-Young, M., & Chisti, Y. (1994). Bioreactor Applications in Waste Treatment. *Resources, Conservation and Recycling*, *11*, 13–24.

Moreno-Gutierrez, J., Calderay, F., Saborido, N., Boile, M., Valero, Valero, R. R., & Duran-Grados, V. (2007). Methodologies for Estimating Shipping Emissions and Energy Consumption: A Comparative Analysis of Current Methods. *Energy*, *86*(2015), 603–616.

Mori, K., Ohya, H., Matsumoto, K., & Furune, H. (1987). Sunlight Supply and Gas Exchange Systems in the Microalgal Bioreactor. *Advances in Space Research: the Official Journal of the Committee on Space Research (COSPAR)*, *7*(4), 47–52. Retrieved from http://www.ncbi.nlm.nih.gov/pubmed/11537269

Morisson, F. A. (2013). *An Introduction to Fluid Mechanics* (p. 625). New York: Cambridge Universitty Press.

Morita, M., Watanabe, Y., & Saiki, H. (2000). Investigation of Photobioreactor Design for Enhancing the Photosynthetic Productivity of Microalgae. *Biotechnology and Bioengineering*, *69*(6), 693–8. Retrieved from http://www.ncbi.nlm.nih.gov/pubmed/10918145

Mossey, B. (n.d.). *Regular Maintenance of Marine Diesel Engines is Key to More Uptime and Lower Life-cycle Costs* (pp. 1–6). Retrieved from www.mtu-online.com

Muñoz, R., & Guieysse, B. (2006). Algal–bacterial Processes for the Treatment of Hazardous Contaminants: A Review. *Water Research*, *40*(15), 2799–2815. doi:10.1016/j.watres.2006.06.011

Myer, R. (2006). Trial Plant to Transform Emissions into Biofuels. *The Age*. Retrieved from http://www.theage.com.au/news/business/trial-plant-to-transform-emissions-into-biofuels/2006/11/12/1163266412354.html

Myers, J. (1953). Growth Characteristics of Algae in Relation to the Problem of Mass Culture. In J. S. Burlew (Ed.), *Algae Culture from Laboratory to Power Plant* (pp. 37–54). Washington, D.C.: Carnegie Institution of Washington.

Myers, J. A., Curtis, B. S., & Curtis, W. R. (2013). Improving Accuracy of Cell and Chromophore Concentration Measurements Using Optical Density. *BMC Biophysics*, *6*(4). doi:10.1186/2046-1682-6-4

Nagaich, V., Dongre, S. K., Singh, P., Yadav, M., & Tiwari, A. (2014). Maximum-CO_2 Tolerance in Microalgae: Possible Mechanisms and Higher Lipid Accumulation. *International Journal of Advanced Research*, *2*(5), 101–106.

Nagase, H., Eguchi, K., Yoshihara, K., Hirata, K., & Miyamoto, K. (1998). Improvement of Microalgal NOx Removal in Bubble Column and Airlift Reactors. *Journal of Fermentation and Bioengineering*, *86*(4), 421–423.

Nagase, H., Yoshihara, K., Eguchi, K., Okamoto, Y., Murasaki, S., Yamashita, R., Hirata, K., & Miyamoto, K. (2001). Uptake Pathway and Continuous Removal of Nitric Oxide from Flue Gas Using Microalgae. *Biochemical Engineering Journal*, *7*(3), 241–246. doi:10.1016/S1369-703X(00)00122-4

Nakano, Y., Miyatake, K., Okuno, H., Hamazaki, K., Takenaka, S., Honami, N., Kiyota, M., Aiga, I., & Kondo, J. (1996). Growth of Photosynthetic Algae *Euglena* in High CO_2 Conditions and its Photosynthetic Characteristics. *Acta Horticulturae*, *440*(9), 49–54.

Nexus. (2010). *Nexus Ferry Strategy* (pp. 1–53).

Nishida, O., Kiuchi, T., & Fujita, H. (1998). Marine NOx and COx Emissions under Various Operating Conditions. *MESJ*, *32*(1), 1–7.

Noüe, J., Laliberté, G., & Proulx, D. (1992). Algae and Waste Water. *Journal of Applied Phycology*, *4*(3), 247–254. doi:10.1007/BF02161210

Nyholm, N. (1977). Kinetics of Phosphate Limited Algal Growth. *Biotechnology and Bioengineering*, *XIX*, 467–492.

Octoply Ltd. (n.d.). Octoply Ltd. *Sound*. Retrieved from http://www.octoply.co.uk/sound.htm

Oilgae. (n.d.). *Capture of CO_2 Emissions Using Algae*. Retrieved from http://www.oilgae.com/ref/downloads/Analysis_of_CO2_Capture_Using_Algae.pdf

Oilgae. (2010). *Oilgae Guide to Algae-based Wastewater Treatment*.

Oilgae. (2011a). *The Comprehensive Guide for Algae-based Carbon Caprute*.

Oilgae. (2011b). *Oilgae Comprehensive Report*.

Olguín, E. J. (2012). Dual Purpose Microalgae-Bacteria-based Systems that Treat Wastewater and Produce Biodiesel and Chemical Products Within a Biorefinery. *Biotechnology Advances*, *30*(5), 1031–46. doi:10.1016/j.biotechadv.2012.05.001

Oneal, A. (2015). Mixer Direct. *The World of Algae*. Retrieved October 12, 2015, from http://www.mixerdirect.com/blog/the-world-of-algae/

Ono, E., & Cuello, J. L. (2001). Selection of Optimal Microalgae Species for CO_2 Sequestration. In *New Phytologist* (pp. 1–7).

Ota, M., Kato, Y., Watanabe, H., Watanabe, M., Sato, Y., Smith, R. L., & Inomata, H. (2009). Fatty Acid Production from a Highly CO_2 Tolerant Alga, *Chlorocuccum Littorale*, in the Presence of Inorganic Carbon and Nitrate. *Bioresource Technology*, *100*(21), 5237–42. doi:10.1016/j.biortech.2009.05.048

Packer, M. (2009). Algal Capture of Carbon Dioxide; Biomass Generation as a Tool for Greenhouse Gas Mitigation with Reference to New Zealand Energy Strategy and Policy. *Energy Policy*, *37*(9), 3428–3437.

Pearce, F. (2011). NewScientist. *Shipping Industry Agrees CO_2 Emission Standards*. Retrieved June 19, 2013, from http://www.newscientist.com/article/dn20713-shipping-industry-agrees-co2-emission-standards.html#.UcHpYufVDY8

Pedersen, M. F. (2011). DieselNet. *International: IMO Marine Engine Regulations*. Retrieved July 12, 2013, from http://www.dieselnet.com/standards/inter/imo.php

Pegallapati, A. K., & Nirmalakhandan, N. (2012). Bioresource Technology Modeling Algal Growth in Bubble Columns under Sparging with CO_2-enriched Air. *Bioresource Technology*, *124*, 137–145.

Pereira, D. A., José, N. M., Villamizar, S. M. G., Sales, E. A., & Perelo, L. W. (2014). Hollow Glass Microspheres for Temperature and Irradiance Control in Photobioreactors. *Bioresource Technology*, (158), 98–104. doi:10.1016/j.biortech.2014.01.143

Perry, R. H., Green, D. W., & Maloney, J. O. (Eds.). (1999). *Mcgraw-Hill - Perrys Chemical Engineers Handbook* (7th ed.). The McGraw-Hill Companies, Inc.

Petersen, E. E., & Margaritis, A. (2001). Hydrodynamic and Mass Transfer Characteristics of Three-Phase Gaslift Bioreactor Systems. *Critical Reviews in Biotechnology*, *1*(4), 233–294.

Posten, C. (2009). Design Principles of Photo-bioreactors for Cultivation of Microalgae. *Engineering in Life Sciences*, *9*(3), 165–177. doi:10.1002/elsc.200900003

Prince William Sound Regional Citizens' Advisory Council. (2005). Ballast Water Treatment Methods. *Technology Review*. Retrieved from http://www.pwsrcac.org/docs/d0017600.pdf

Psaraftis, H. N. (2012). Market-based Measures for Greenhouse Gas Emissions from Ships: a Review. *World Maritime University Journal of Maritime Affairs*.

Psaraftis, H. N., & Kontovas, C. A. (2008). *Ship Emissions Study* (pp. 1–44). Athens, Greece.

Quinn, J., de Winter, L., & Bradley, T. (2011). Microalgae Bulk Growth Model with Application to Industrial Scale Systems. *Bioresource Technology*, *102*(8), 5083–92. doi:10.1016/j.biortech.2011.01.019

Quintella, C. M., Hatimondi, S. A., Musse, A. P. S., Miyazaki, S. F., Cerqueira, G. S., & Moreira, A. D. A. (2011). CO_2 Capture Technologies: An Overview with Technology Assessment Based on Patents and Articles. *Energy Procedia*, *4*, 2050–2057. doi:10.1016/j.egypro.2011.02.087

Reckhow, K. H., & Chapra, S. C. (1983). Data Analysis and Empirical Modeling. In *Engineering Approaches for Lake Management*. Butterworth, Boston.

Resolution MEPC.184(59) Annex 9. 2009 Guidelines for Exhaust Gas Cleaning Systems., 184 In Situ 1–24 (2009). Retrieved from http://www.mardep.gov.hk/en/msnote/pdf/msin1003anx1.pdf

Ribeiro, R. L. L., Mariano, A. B., Souza, J. A., & Vargas, J. V. C. (2008). Transient Modeling and Simulation of Compact Photobioreactors. *Thermal Engineering*, *7*(2), 66–71.

Richmond, A. (2004). *Handbook of Microalgal Culture: Biotechnology and Applied Phycology*. Blackwell Science.

Rodolfi, L., Chini Zittelli, G., Bassi, N., Padovani, G., Biondi, N., Bonini, G., & Tredici, M. R. (2009). Microalgae for Oil: Strain Selection, Induction of Lipid Synthesis and Outdoor Mass Cultivation in a Low-cost Photobioreactor. *Biotechnology and Bioengineering*, *102*(1), 100–12. doi:10.1002/bit.22033

Rosenberg, J. N., Mathias, A., Korth, K., Betenbaugh, M. J., & Oyler, G. A. (2011). Microalgal Biomass Production and Carbon Dioxide Sequestration from an Integrated Ethanol Biorefinery in Iowa: A Technical Appraisal and Economic Feasibility Evaluation. *Biomass and Bioenergy*, *35*(9), 1–12. doi:10.1016/j.biombioe.2011.05.014

Ruangsomboon, S. (2011). Effect of Light, Nutrient, Cultivation Time and Salinity on Lipid Production of Newly Isolated Strain of the Green Microalga, *Botryococcus Braunii KMITL 2*. *Bioresource Technology*, 1–5. doi:10.1016/j.biortech.2011.07.025

Ruiz, J., Alvarez, P., Arbib, Z., Garrido, C., Barragán, J., & Perales, J. a. (2011). Effect of Nitrogen and Phosphorus Concentration on their Removal Kinetic in Treated Urban Wastewater by *Chlorella Vulgaris*. *International Journal of Phytoremediation*, *13*(9), 884–96. doi:10.1080/15226514.2011.573823

Ruse, L. E. S., & Love, A. (1997). Predicting Phytoplankton Composition in the River Thames, England. *Regulated Rivers: Research & Management*, *13*(January 1996), 171–183.

Sáez, A., Marquez, M., Roberts, G., & Carbonell, R. (1998). Hydrodynamic Model for Gas-lift Reactors. *American Institute of Chemical Engineers Journal*, *44*(6), 1413–1423.

Safonova, T. A., Aslamov, I. A., Basharina, T. N., Chenski, A. G., Vereschagin, A. L., Glyzina, O. Y., & Grachev, M. A. (2007). Cultivation and Automatic Counting of Diatom Algae Cells in Multi-Well Plastic Plates. *Diatom Research*, *22*(1), 189–195. doi:10.1080/0269249X.2007.9705703

Sánchez, A., Garc, M. C., Garc, F., Grima, E. M., & Chisti, Y. (2002). Growth and Biochemical Characterization of Microalgal Biomass Produced in Bubble Column

and Airlift Photobioreactors: Studies in Fed-batch Culture. *Enzyme and Microbial Technology*, *31*, 1015–1023.

Schaechter, M. (2009). Encyclopedia of Microbiology. In *Volume 1* (3rd ed., pp. 100–200). Elsevier Inc. Retrieved from https://books.google.co.uk/books?id=rLhdW5YzuO4C&pg=RA2-PA177&lpg=RA2-PA177&dq=autotrophic+heterotrophic+mixotrophic+taxonomy+algae&source=bl&ots=p_faqj0bUM&sig=Yum_2Nj6WuAw5WE_NL7szEADTfE&hl=en&sa=X&ved=0CC8Q6AEwAWoVChMI9Ov6lqaNxgIVhMcUCh3tTQCF#v=onepage&q=autotrophic heterotrophic mixotrophic taxonomy algae&f=false

Schlesinger, R. B., Kunzli, N., Hidy, G. M., Gotschi, T., & Jerrett, M. (2006). The Health Relevance of Ambient Particulate Matter Characteristics: Coherence of Toxicological and Epidemiological Inferences. *Inhalation Toxicology*, *18*, 95–125. doi:10.1080/08958370500306016

Schlink, U., Thiem, A., Kohajda, T., Richter, M., & Strebel, K. (2010). Quantile Regression of Indoor Air Concentrations of Volatile Organic Compounds (VOC). *Science of the Total Environment*, *408*, 3840–3851.

Scott, S. a, Davey, M. P., Dennis, J. S., Horst, I., Howe, C. J., Lea-Smith, D. J., & Smith, A. G. (2010). Biodiesel from Algae: Challenges and Prospects. *Current Opinion in Biotechnology*, *21*(3), 277–86. doi:10.1016/j.copbio.2010.03.005

Seambiotic Ltd. (2008). *Seambiotic Ltd. - Algae Pilot Plant* (pp. 1–9).

Seckbach, J., & Ikan, R. (1972). Sterols and Chloroplast Structure of Cyanidium caldarium. *Plant physiology*, *49*(3), 457–9. Retrieved from http://www.pubmedcentral.nih.gov/articlerender.fcgi?artid=365987&tool=pmcentrez&rendertype=abstract

Setter, T. L., & Kuo, H. G. (1982). Inhibition of Cell Division by High External NaCl Concentrations in Synchronized Cultures of *Chlorella Emersonii*. *Aust. J. Plant Physiol.*, *9*, 179–196.

Seyidova, R., & Gonzalez, M. (2015). *Effect of Temperature, Light Intensity and Nutrient Dilution on the Growth of Chlorella Sorokiniana* (pp. 1–81). London.

Shah, M. M. R., Alam, M. J., & Mia, M. Y. (2003). Chlorella sp.: Isolation, Pure Culture and Small Scale Culture in Brackish-water. *Bangladesh J. Sci. Ind. Res.*, *38*(3-4), 165–174.

Shah, Y., Kelkar, B., Godbole, S., & Deckwer, W.-D. (1982). Design Parameters Estimations for Bubble Column Reactors. *American Institute of Chemical Engineers Journal*, *28*(3), 353–379.

Shang, H., Scott, J. a., Shepherd, S. H., & Ross, G. M. (2010). A Dynamic Thermal Model for Heating Microalgae Incubator Ponds Using Off-gas. *Chemical Engineering Science*, *65*(16), 4591–4597. doi:10.1016/j.ces.2010.04.042

Sheehan, J., Dunahay, T., Benemann, J., & Roessler, P. (1998). A Look Back at the U.S. Department of Energy' s Aquatic Species Program: Biodiesel from Algae. *Renewable Energy*.

Sialve, B., Bernet, N., & Bernard, O. (2009). Anaerobic Digestion of Microalgae as a Necessary Step to Make Microalgal Biodiesel Sustainable. *Biotechnology Advances*, *27*(4), 409–16. doi:10.1016/j.biotechadv.2009.03.001

Sieg, D. (2008). *Making Algae Biodiesel At Home* (pp. 1 – 322).

Smith, T. (2014). Technical Energy Efficiency, its Interaction with Optimal Operating Speeds and the Implications for the Management of Shipping's Carbon Emissions. *Carbon Management*, *3*(6), 589–600. doi:10.4155/cmt.12.58

Smith, T., Newton, P., Winn, G., Grech, A., & La Rosa, A. G. (2013). Analysis Techniques for Evaluating the Fuel Savings Associated with Wind Assistance. In *Low Carbon Shipping Conference* (pp. 1–13). London.

Softonic International S.L. (2014). ImageJ. *Scriptable Java App for Scientific Image Processing*. Retrieved from http://imagej.en.softonic.com/download

Solomon, C., Casey, P., Mackne, C., & Lake, A. (1998). *Ultraviolet Disinfection* (pp. 1–4). National Small Flows Clearinghouse, Environmental Technology Initiative.

Solovchenko, A. E., Khozin-Goldberg, I., Didi-Cohen, S., Cohen, Z., & Merzlyak, M. N. (2007). Effects of Light Intensity and Nitrogen Starvation on Growth, Total Fatty Acids and Arachidonic Acid in the Green Microalga *Parietochloris Incisa*. *Journal of Applied Phycology*, *20*(3), 245–251. doi:10.1007/s10811-007-9233-0

South, D. B., & Somers, G. L. (n.d.). *Pseudoreplication - Part 1* (pp. 1–6).

Stephenson, A. L., Kazamia, E., Dennis, J. S., Howe, C. J., Scott, S. a., & Smith, A. G. (2010). Life-Cycle Assessment of Potential Algal Biodiesel Production in the United Kingdom: A Comparison of Raceways and Air-Lift Tubular Bioreactors. *Energy & Fuels*, *24*(7), 4062–4077. doi:10.1021/ef1003123

Sukenik, A., Bilanovic, D., & Shelef, G. (1988). Flocculation of Microalgae in Brackish and Sea Waters. *Biomass*, *15*(3), 187–199. doi:10.1016/0144-4565(88)90084-4

Swinnen, I. A. M., Bernaerts, K., Dens, E. J. J., Geeraerd, A. H., & Van Impe, J. F. (2004). Predictive Modelling of the Microbial Lag Phase: a Review. *International Journal of Food Microbiology*, *94*(2), 137–59. doi:10.1016/j.ijfoodmicro.2004.01.006

Tesař, V., & Bandalusena, H. C. H. (2010). Bistable Diverter Valve in Microfluidics. *Experiments in Fluids*, *50*(5), 1225–1233. doi:10.1007/s00348-010-0983-0

Thames Estuary Partnership Biodiversity Action Group. (n.d.). *Tidal Thames Habitat Action Plan*.

The Engineering Toolbox. (n.d.). The Engineering Toolbox. *Convective Heat Transfer*. Retrieved December 19, 2012, from http://www.engineeringtoolbox.com/convective-heat-transfer-d_430.html

The International Council on Clean Transportation. (2011). *Reducing Greenhouse Gas Emissions from Ships*. Retrieved from ww.theicct.org

Tredici, M., & Zittelli, G. (1998). Efficiency of Sunlight Utilization: Tubular Versus Flat Photobioreactors. *Biotechnology and Bioengineering*, *57*(2), 187–97. Retrieved from http://www.ncbi.nlm.nih.gov/pubmed/10099193

Tschumperlin, D., Liu, F., & Mih, J. (2014). Multi-well Culture Plate Comprising Gels with Different Shear Modulus - Patent No: US8871499 B2.

Ugwu, C. U., Aoyagi, H., & Uchiyama, H. (2008). Photobioreactors for Mass Cultivation of Algae. *Bioresource Technology*, *99*(10), 4021–8. doi:10.1016/j.biortech.2007.01.046

Ugwu, C. U., Ogbonna, J. C., & Tanaka, H. (2002). Improvement of Mass Transfer Characteristics and Productivities of Inclined Tubular Photobioreactors by Installation of Internal Static Mixers. *Applied Microbiology and Biotechnology*, *58*(5), 600–7. doi:10.1007/s00253-002-0940-9

Valdés, F. J., Hernández, M. R., Catalá, L., & Marcilla, A. (2012). Estimation of CO_2 Stripping/CO_2 Microalgae Consumption Ratios in a Bubble Column Photobioreactor Using the Analysis of the pH Profiles. Application to *Nannochloropsis Oculata* Microalgae Culture. *Bioresource Technology*, *119*, 1–6. doi:10.1016/j.biortech.2012.05.120

Van Bodegom, P. (2007). Microbial Maintenance: a Critical Review on its Quantification. *Microbial Ecology*, *53*(4), 513–23. doi:10.1007/s00248-006-9049-5

Van Den Hende, S., Vervaeren, H., & Boon, N. (2012). Flue Gas Compounds and Microalgae: (Bio-)Chemical Interactions Leading to Biotechnological Opportunities. *Biotechnology Advances*, *30*(6), 1405–24. doi:10.1016/j.biotechadv.2012.02.015

Van Wagenen, J., Løvstad Holdt, S., De Francisci, D., Valverde-Pérez, B., Gy Plósz, B., & Angelidaki, I. (2014). Microplate-based Method for High-throughput Screening of Microalgae Growth Potential. *Bioresource Technology*, (169), 566–572. doi:10.1016/j.biortech.2014.06.096

Vatopoulos, K., & Tzimas, E. (2012). Assessment of CO_2 Capture Technologies in Cement Manufacturing Process. *Journal of Cleaner Production*, *32*(2012), 251–261. doi:10.1016/j.jclepro.2012.03.013

Vejrazka, C., Janssen, M., & Streefland, M., (2011). Photosynthetic Efficiency of *Chlamydomonas Reinhardtii* in Flashing Light. *Biotechnology and Bioengineering*, 1–30. doi:10.1002/bit.

Vunjak-Novakovic, G., Kim, Y., Wu, X., Berzin, I., & Merchuk, J. C. (2005). Air-Lift Bioreactors for Algal Growth on Flue Gas: Mathematical Modeling and Pilot-Plant Studies. *Industrial & Engineering Chemistry Research*, *44*(16), 6154–6163. doi:10.1021/ie049099z

Wahal, S. (2010). *Nutrient Utilisation from Anaerobic Digester Effluent Through Algae Cultivation*. Utah State University.

Watanabe, Y., de la Noue, J., & Hall, D. O. (1995). Photosynthetic Performance of a Helical Tubular Photobioreactor Incorporating the Cyanobacterium *Spirulina Platensis*. *Biotechnology and Bioengineering*, *47*(2), 261–269.

Weisse, T., & Stadler, P. (2003). Effect of pH on Growth, Cell Volume, and Production of Freshwater Ciliates, and Implications for their Distribution. *Limnology and Oceanography*, *51*(4), 1708–1715.

Weissman, J. C., Goebel, R. P., & Benemann, J. R. (1988). Photobioreactor Design: Mixing, Carbon Utilization, and Oxygen Accumulation. *Biotechnology and Bioengineering*, *31*(4), 336–44. doi:10.1002/bit.260310409

West, M. (2009). EGCSA - Exhaust Gas Cleaning Systems Association. Retrieved February 18, 2012, from http://www.egcsa.com/index.php

Westerhoff, P., Hu, Q., Esparza-Soto, M., & Vermaas, W. (2010). Growth Parameters of Microalgae Tolerant to High Levels of Carbon Dioxide in Batch and Continuous-flow Photobioreactors. *Environmental Technology*, *31*(5), 523–32. doi:10.1080/09593330903552078

Wetherell, D. F. (1961). Culture of Fresh Water Algae in Enriched Natural Sea Water. *Physiol. Plant.*, *14*.

Wiscombe, T. (2010). Bluarchitecture. *Energy Flowers Helix Bioreactor*. Retrieved October 12, 2015, from http://bluarchitecture.blogspot.co.uk/2009/06/energy-flowershelix-bioreactor.html

Wolkers, H., Barbosa, M., Kleinergis, D., Bosma, R., & Wijffers, R. H. (2011). *Microalgae: the Green Gold of the Future? Large-scale Sustainable Cultivation of Microalgae for the Production of Bulk Commodities*. *algae.wur.nl*. Wageningen: © Wageningen UR.

Wu, S. Z. S., & Lee, X. M. (2014). *Preliminary Study for the Development of Algal Bioreactor for Cleaning of Anaerobic Digestion Biogas* (pp. 1–68). London.

Xin, L., Hu, H., Ke, G., & Sun, Y. (2010). Effects of Different Nitrogen and Phosphorus Concentrations on the Growth, Nutrient Uptake, and Lipid Accumulation of a Freshwater Microalga *Scenedesmus Sp*. *Bioresource Technology*, *101*(14), 5494–500. doi:10.1016/j.biortech.2010.02.016

Xiong, W., Li, X., Xiang, J., & Wu, Q. (2008). High-density Fermentation of Microalga *Chlorella Protothecoides* in Bioreactor for Microbio-diesel Production. *Applied Microbiology and Biotechnology*, *78*(1), 29–36. doi:10.1007/s00253-007-1285-1

Yanagi, M., Watanabe, Y., & Saiki, H. (1995). CO_2 Fixation by *Chlorella sp. HA-1* and its Utilization. *Energy Conversion and Management*, *36*(6-9), 713–716.

Yang, J., Cao, J., Xing, G., & Yuan, H. (2014). Lipid Production Combined with Biosorption and Bioaccumulation of Cadmium, Copper, Manganese and Zinc by Oleaginous Microalgae *Chlorella Minutissima UTEX2341*. *Bioresource Technology*, *175*, 537–544. doi:10.1016/j.biortech.2014.10.124

Yoshihara, K. (1996). Biological Elimination of Nitric Oxide and Carbon Dioxide from Flue Gas by Marine Microalga *NOA-113* Cultivated in a Long Tubular Photobioreactor. *Journal of Fermentation and Bioengineering*, *82*(4), 351–354. doi:10.1016/0922-338X(96)89149-5

Young, M., Carbonell, R., & Ollis, D. (1991). Airlift Bioreactors: Analysis of Local Two-phase Hydrodynamics. *American Institute of Chemical Engineers Journal*, *37*(3), 403–428.

Zeiler, K. G., Heacox, D. A., Toon, S. T., Kadam, K. L., & Brown, L. M. (1995). The use of Microalgae for Assimilation and Utilisation of Carbon Dioxide from Fossil Fuel-fired Power Plant Flue Gas. *Energy Conservation Management*, *36*(6-9).

Zemke, P. E., Wood, B., & Stucker, B. (2010). *Mathematical Modeling of Light Utilization and the Effects of Temperature Cycles on Productivity in a Steady-State Algal Photobioreactor*. Utah State University.

Zeng, X., Danquah, M. K., Chen, X. D., & Lu, Y. (2011). Microalgae Bioengineering: From CO_2 Fixation to Biofuel Production. *Renewable and Sustainable Energy Reviews*, *15*(6), 3252–3260. doi:10.1016/j.rser.2011.04.014

Zhang, K., Miyachi, S., & Kurano, N. (2001). Evaluation of a Vertical Flat-plate Photobioreactor for Outdoor Biomass Production and Carbon Dioxide Bio-fixation: Effects of Reactor Dimensions, Irradiation and Cell Concentration on the Biomass Productivity and Irradiation Utilization Efficiency. *Applied Microbiology and Biotechnology*, *55*(4), 428–433. doi:10.1007/s002530000550

Zhang, T., Wang, J., Wang, T., Lin, J., & Jin, Y. (2005). Effect of Internal on the Hydrodynamics in External-loop Airlift Reactors. *Chemical Engineering and Processing: Process Intensification*, *44*(1), 81–87. doi:10.1016/j.cep.2004.05.003

Zheng, M. (2004). Diesel Engine Exhaust Gas Recirculation—a Review on Advanced and Novel Concepts. *Energy Conversion and Management*, *45*(6), 883–900. doi:10.1016/S0196-8904(03)00194-8

Zheng-Rong, O., Xiao-Bin, W., Ya-Hong, G., Hong, M., Hong-Jun, H., Gui-Yan, Z., & Ye-Guang, L. (2010). The Effects of Light Intensities, Temperatures, pH and Salinities on Photosynthesis of *Chlorella*. *Journal of Wuhan Botanical Research Yanjiu*, *28*(1), 49–55. doi:10.3724/SP.J.1142.2010.10049

Zhou, P., & Wang, H. (2014). Carbon Capture and Storage—Solidification and Storage of Carbon Dioxide Captured on Ships. *Ocean Engineering*, *91*, 172–180. doi:10.1016/j.oceaneng.2014.09.006

Zijffers, J.-W. F., Schippers, K. J., Zheng, K., Janssen, M., Tramper, J., & Wijffels, R. H. (2010). Maximum Photosynthetic Yield of Green Microalgae in Photobioreactors. *Marine Biotechnology (New York, N.Y.)*, *12*(6), 708–18. doi:10.1007/s10126-010-9258-2

Zimmerman, W. B., Hewakandamby, B. N., Tesaĝ, V., Bandulasena, H. C. H., & Omotowa, O. A. (2009). On the Design and Simulation of an Airlift Loop Bioreactor with Microbubble Generation by Fluidic Oscillation. *Food and Bioproducts Processing*, *87*(C3), 215–227.

Zimmerman, W., Zandi, M., Bandulasena, H., Tesař, V., Gilmour, D., & Ying, K. (2011). Design of an Airlift Loop Bioreactor and Pilot Scales Studies with Fluidic Oscillator Induced Microbubbles for Growth of a Microalgae *Dunaliella Salina*. *Applied Energy*, *88*, 3357–3369.

Zonneveld, C. (1998). Light-limited Microalgal Growth: a Comparison of Modelling Approaches. *Ecological Modelling*, (113), 41–54. doi:10.1016/S0304-3800(98)00133-1

Appendix I. Background

Table I.1. Summary of pollutant quantities emitted by ships. Data taken from: [1]Lloyds Register Engineering Services emission factors in kg/hr (Loyds Register Engineering Services, 1995). P = engine power (kW) x engine load (85% maximum continuous rating of the engine), N = No of MEs, A = Total auxiliary power (kW), C = 1, 2, 3, 4 and 5 where vessel gross registered tonnage is < 1000, 1000 – 5000, 5000 – 10000, 10000 – 50000 and > 50000 respectively (David Cooper, 2002). [2]IPCC 2006 (IMO, 2009). [3]CORINAIR (IMO, 2009). [4]Non-regulated\ subject to IMO NO_x regulation (2007 average emission factor) (IMO, 2009). [5]* pre-2000 engine\post 2000\ fleet average (Defra, 2010). [6]NO_x (Entec, 2002).

Component	Kg/hr				g/kWh										Kg/tonne fuel	
					At sea 2007 [5]					Manoeuvring and at Berth 2007 [5]						
	ME medium speed [1]	ME slow speed [1]	AE (medium speed) [1]	Diesel Engines [1]	SSD Engine	MSD Engine	HSD Engine	GT Engine	ST Engine	SSD Engine	MSD Engine	HSD Engine	GT Engine	ST Engine	Diesel Engines[1]	2007 inventory
CO_2				660	MGO 588 MDO 588 RO 620	MGO 645 MDO 645 RO 677	MGO 645 MDO 645 RO 677	MGO 922 MDO 922 RO 970	MGO 922 MDO 922 RO 970	MGO 647 MDO 647 RO 682	MGO 710 MDO 710 RO 745	MGO 710 MDO 710 RO 745	MGO 1014 MDO 1014 RO 1067	MGO 1014 MDO 1014 RO 1067	3170	RFO 3,130 MDO 3,190 [2]
NO_x[6]	4.25 x 10^{-3} x $P^{1.15}$ x N	17.50x10^{-3}xPxN	4.25 x 10^{-3} x $A^{1.15}$	slow speed 17 medium speed 12	MGO 17\14.1\16 MDO 17\14.1\16 RO 18.1\15\17 *	MGO 13.2\11\12.4 MDO 13.2\11\12.4 RO 14\11.6\13.1 *	MGO 12\10\11.3 MDO 12\10\11.3 RO 12.7\10.5\11.9 *	MGO 5.7\4.7\5.3 MDO 5.7\4.7\5.3 RO 6.1\5.1\5.7 *	MGO 2\1.7\1.9 MDO 2\1.7\1.9 RO 2.1\1.7\2 *	MGO 13.6\11.3\12.8 MDO 13.6\11.3\12.8 RO 14.5\12\13.6 *	MGO 10.6\8.8\9.9 MDO 10.6\8.8\9.9 RO 11.2\9.3\10.5 *	MGO 9.6\8\9 MDO 9.6\8\9 RO 10.2\8.5\9.6 *	MGO 2.9\2.4\2.7 MDO 2.9\2.4\2.7 RO 3.1\2.6\2.9 *	MGO 1.6\1.3\1.5 MDO 1.6\1.3\1.5 RO 1.7\1.4\1.6 *	slow speed 87 medium speed 57	Slow-speed diesel 90\78(85) Medium-speed diesel 60\51(56) [4] Boilers 7
N_2O																0.08 [2,3]
SO_2	2.31 x 10^{-3} x P x N for engines < 2000 kW 12.47 x 10^{-3} x P x N for engines > 2000 kW	11.34x10^{-3}xPxN	2.36 x 10^{-3} x A x C	4.2 x S%	MGO 0.7 MDO 5.6 RO 10.5	MGO 0.8 MDO 6.2 RO 11.5	MGO 0.8 MDO 6.2 RO 11.5	MGO 1.2 MDO 8.7 RO 16.5	MGO 1.2 MDO 8.7 RO 16.5	MGO 0.8 MDO 6.2 RO 11.6	MGO 0.9 MDO 6.8 RO 12.7	MGO 0.9 MDO 6.8 RO 12.7	MGO 1.3 MDO 9.6 RO 18.1	MGO 1.3 MDO 9.6 RO 18.1	20 x S%	RFO (2.7 %) 54 MDO (0.5%) 10 [3]
CO	15.32 x 10^{-3} x $P^{0.68}$ x N	0.68 x 10^{-3} x $P^{1.08}$ x N	15.32 x 10^{-3} x $A^{0.68}$	1.6											7.4	7.4 [3]
HC	4.86 x 10^{-3} x $P^{0.69}$ x N	0.28 x 10^{-3} x P x N	4.86 x 10^{-3} x $A^{0.69}$	0.5											2.4	
NMVOC					0.6	0.5	0.2	0.1	0.1	1.8	1.5	0.6	0.5	0.3		2.4 [3]
CH_4																0.3 [2,3]
PM				1.5 fuel oil 0.2 gas oil	MGO 0.3 MDO 0.3 RO 1.7	MGO 0.3 MDO 0.4 RO 0.8	MGO 0.3 MDO 0.4 RO 0.8	MGO 0 MDO 0 RO 0.1	MGO 0.3 MDO 0.4 RO 0.8	MGO 0.9 MDO 1.2 RO 2.4	MGO 0.9 MDO 1.2 RO 2.4	MGO 0.9 MDO 1.2 RO 2.4	MGO 0.5 MDO 0.7 RO 1.5	MGO 0.9 MDO 1.2 RO 2.4	7.6 fuel oil 1.2 gas oil	RFO 6.7 MDO 1.1 [3]

CO is carbon monoxide, HC is hydrocarbons, CH4 is methane, PM is particulate matter, HFO is heavy fuel oil, MDO is marine diesel oil, MGO is marine gas oil, RO is residual oil and VOC is volatile organic compounds.

Table I.2. Critical variables for algal production systems, taken from the Algal Industry Survey (Edwards, 2009).

Critical system parameters	**World (importance factor)**
Algal species	4.1
Light penetration	4.0
Growing containers	3.9
Variable controls (temperature, pH)	3.6
Nutrient costs	3.2
Mixing methods	3.2
Monitors	2.9
Fouling	2.9

Table I.3. Comparison of algal cultivation systems for land based implementations. Data taken from: [1](Scott et al., 2010), [2](Kumar et al., 2011), [3](Chisti, 1989), [4](Molina et al., 2001), [5](Morita et al., 2000), [6](Watanabe, De la Noue & Hall, 1995), [7](Wolkers et al., 2011), [8](Tredici & Zittelli, 1998), [9](Posten, 2009), [10(]Lee et al., 1995), [11](Christenson & Sims, 2011), [12](Gardner, 2011), as well as (Brennan & Owende, 2010; Carvalho, Meireles & Malcata, 2006; Girdhari, 2011).

Design	Light utilisation	Gas retention	Mixing	Maintenance	Control	Stability	Energy requirement	Ground footprint	O_2 release	Sum
Raceway ponds[1]	Low	Low	Poor	Easy	Difficult	High	Low	Small	High	16
Bubble columns[2]	Medium	Medium	Medium	Difficult	Easy	Low	Low	Small	High	17
Airlifts[2,3,4]	Medium	High	Good	Difficult	Easy	Low	Low	Small	High	19
Helical[2,5,6]	High	High	Medium	Difficult	Easy	Medium	Low	Medium	Low	18
Flat panel[7]	High	Medium	Medium	Difficult	Difficult	Low	Low	Small	High	17
Horizontal tubular[2,8,9]	High	Low	Poor	Difficult	Easy	High	High	Big	Low	14
Inclined system[10]	High	Medium	Medium	Difficult	Easy	Low	Low	Medium	High	17
Stirred tank[2]	Low	Low	Good	Easy	Difficult	High	High	Small	High	17
Plastic bag[11]	High	Low	Medium	Difficult	Difficult	Medium	Low	Small	High	17
Hollow Fibre Membranes[12]	High	High	Good	Difficult	Easy	High	High	Medium	Low	19

Table I.4. Productivities of various photobioreactor designs.

Microalgal species	Mode of operation	PBR type	Volume (L)	Productivity ($gL^{-1}d^{-1}$)	Reference
Phaedoctylum tricornutum	Continuous	Tubular	200	1.9	(Molina et al., 2001)
Phaedoctylum tricornutum	Continuous	External loop airlift tubular	200	1.2	(Fernandez et al., 2001)
Arthrospira platensis M2	-	Coiled tubular	120	0.9	(Tredici & Zittelli, 1998)
Chlorella sorokiniana	Continuous	Flat panel	1.6	12.2	(Cuaresma et al., 2009)
		Raceway pond		0.5 - 1.5	(Rosenberg et al., 2011)
		Helical tubular		0.9 gL-2d-1	(Tredici & Zittelli, 1998)
		Horizontal manifold		1.3	(Tredici & Zittelli, 1998)
		Horizontal a-type manifold		72 gm-2d-1	(Lee et al., 1995)

Table I.5. Percentage of vessels ballast water capacity in relation to the ships deadweight tonnage (David & Gollasch, 2015).

Ship type/ deadweight tonnage	% of deadweight tonnage
Bulk carriers	33
Bulk carriers /250,000&70,000	30-45
Bulk carriers /35,000	33-57
Tankers	38
Tankers/100,000	40-45
Tankers/40,000	43
Cargo	35
Cargo/40,000	28-40
Cargo/17,000	35
Cargo/15,000	30
General Cargo	29
General Cargo/8,000	38
Passenger/ Roll-on-roll-off vessel	43
Average percentage	37

Appendix II. Characteristics of the ship

The Sound vessel was built by Asi-Verken A.S. of Amal, Sweden in 1959 as a car ferry. It has four 6-cylinder main engines Scania D11R 81 BT of 180 hp and two auxiliaries John Deere Generators (Powertech 4500) of 38 kW each. Images of the MV Sound, engine room and a part of the deck of the ship are shown in Figure II.1 to Figure II.3.

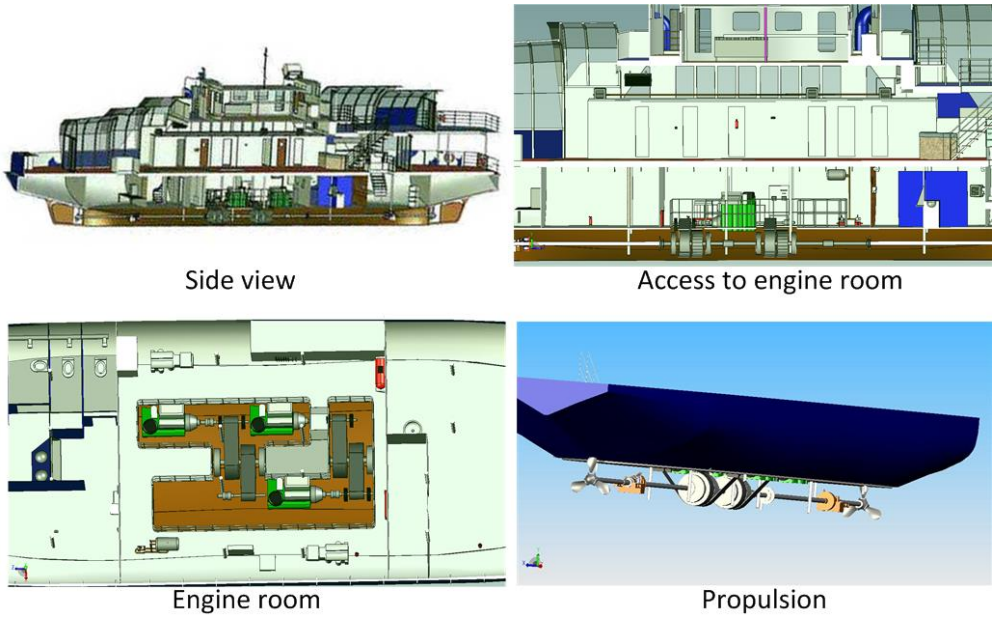

Figure II.1. Ship section and engine room drawings of motor vessel Sound by Octoply Ltd.(Octoply Ltd., n.d.).

Figure II.2. Engine room of motor vessel Sound by Octoply Ltd.

Figure II.3. Image of a deck area on motor vessel Sound by Octoply Ltd.

Appendix III. Photobioreactor design aspects

Reactor photos and inclination test

Figure III.1. Side view of the hybrid helical airlift photobioreactor constructed at the Camley Street Park.

Figure III.2. Side view of the hybrid helical airlift photobioreactor constructed onboard Tamesis (left picture) and its bottom connection (right picture).

Table III.1. Average bubble size (in mm) at the bottom and top positions of the column and their size difference for various gas flow rates and inclinations.

		Flow rates (L/min)					
Inclination	Position	0.1	0.4	0.6	0.8	1.0	1.5
20°	Bottom	0.97	2.15	2.31	2.83	2.90	3.00
	Top	6.05	9.28	10.09	9.74	7.20	5.60
	difference	5.08	7.13	7.78	6.91	4.30	2.60
30°	Bottom	1.17	1.50	1.56	2.09	2.23	2.75
	Top	5.14	5.75	6.43	5.16	4.91	5.19
	difference	3.97	4.25	4.87	3.07	2.68	2.44
40°	Bottom	0.89	1.38	1.61	1.80	2.35	2.40
	Top	4.84	5.12	4.57	4.50	4.50	3.72
	difference	3.95	3.74	2.96	2.70	2.15	1.32
50°	Bottom	0.78	1.20	1.89	2.01	2.42	2.71
	Top	4.75	4.85	4.38	4.68	4.55	4.55
	difference	3.97	3.65	2.49	2.67	2.13	1.84
60°	Bottom	0.79	1.07	1.56	2.10	2.44	2.62
	Top	4.81	4.69	4.58	4.61	4.25	4.58
	difference	4.02	3.62	3.02	2.51	1.81	1.96

Algae tolerance to SO_x, NO_x and salinity

Table III.2. CO_2, NO_x and SO_2 and temperature tolerance of various algal species (growth conditions not included) (Gardner, 2011; Kumar et al., 2011; Ono & Cuello, 2001).

Algal species	Maximum temperature tolerance (°C)	Maximum CO_2% (v/v) tolerance	Maximum SO_x (mg/kg) tolerance	Maximum NO_x (mg/kg) tolerance	Reference
Cyanidium caldarium	60	100	>200	-	(Ono & Cuello, 2001; Seckbach & Ikan, 1972)
Scenedesmus sp.	30	80	-	-	(Hanagata et al., 1992; Ono & Cuello, 2001)
Chlorococcun littorale	-	60 – 70	-	-	(Ota et al., 2009)
Synechococcus elongates	60	60	-	-	(Miyairi, 1995)
Euglena gracilis	-	45	-	-	(Nakano et al., 1996)
Chlorella sp.	45	40	-	-	(Hanagata et al., 1992; Ono & Cuello, 2001)
Chlorella sp. HA-1	-	15	-	100	(Yanagi et al., 1995)
Eudorina sp.	30	20	-	-	(Hanagata et al., 1992)
Dunalliela tertioleta	-	15	-	1000	(Nagase et al., 1998)
Nannochloris sp.	25	15	-	100	(Yoshihara, 1996)
Tetraselmis sp.	-	14	185	125	(Matsumoto et al., 1995)
Monoraphidium minutum	25	13.6	200	150	(Zeiler et al., 1995)
Spirulina sp.	-	12	-	-	(de Morais & Costa, 2007)
Chlorella sp. T-1	35	100	20	60	(Maeda et al., 1995)
Chlorella KR-1			150		(Lee et al., 2000)
Chlorella sp. MTF-7		<10	>90		(Chiu et al., 2011)

Table III.3. Optimal salinities for maximum productivity and salinities tolerated for some genera, species and strains which are widely used for carbon fixation.

	Salinity type	Examined Salinity suitable for growth [gL^{-1}]	Salinity for optimal growth [gL^{-1}]	Reference
Nannochloropsis	Artificial seawater from hypochlorite solution	20 – 40, 0 – 36	35	(Briassoulis et al., 2010)
Tetraselmis sp.	Total salinity		20 – 35	(Kunjapur & Eldridge, 2010)
Isochrysis sp.	Total salinity		25 – 35	(Kunjapur & Eldridge, 2010)
Porphyra umbilicalis	Control of NaCl or seawater	7 – 200	7 – 52	(Kirst, 1989)
Scenedesmus MJ11/18	Total salinity	2.5 – 20		(Borgvang, 2011)
Scenedesmus species	Total salinity	1.7 – 5.8	1.7	(Borgvang, 2011)
Botryococcus braunii KMITL 2	Addition of seawater	0 – 20	20	(Ruangsomboon, 2011)
Dunaliella salina	Addition of NaCl	3 – 290	180 – 220	(Araújo et al., 2009)
Dunaliella maritime	Addition of NaCl	29 – 87	87	(Alyabyev et al., 2007)
Spirulina-Spirulina	Addition of Seawater	1 – 270	20 – 70	(Oilgae, 2011b)

Table III.4. Tideway Salinity between Kew and Southend, March 2006. The changing levels of salinity in the Thames Tideway (Lane et al., 2007).

Location	**Salinity gL^{-1}**
Kew Bridge	0.37
Barnes Bridge	0.39
Vauxhall Bridge	0.40
Charring Cross Bridge	0.40
Tower Bridge	0.40
Putney Bridge	0.41
Greenwich	0.44
Charlton	0.61
Woolwich	1.06
Becton	1.56
Erith	6.21
Littlebrook	11.13
Gravesend	18.52
Southend (sample taken out of temporal context)	32

Wild algae samples experiments

Table III.5. Water quality of the samples taken from the six different sites.

Site\Parameter		Regent's Canal near Camley Street Natural Park	Indoor potted plant	Camley Street Natural Park pond	Boating Lake, Regent's Park	St James' s Park Lake	Serpentine Lake, Hyde Park
Date		41614	41659	41659	41659	41659	41659
Temperature (°C)		7.8		4.9	6.6	6.5	7.0
Dissolved Oxygen (mg/L)		9.23		3.83	4.68	9.19	7
Carbon	TOC (mg/L)	4.947	84.18	7.085	9.02	6.18	9.01
	TC (mg/L)	48.975	86.26	46.81	70.23	53.02	56.68
	IC (mg/L)	44.028	2.08	39.72	61.21	46.84	47.66
Ion Chromatography	Fluoride (mg/L)	0.80	-	1.03	1.76	1.10	10.39
	Chloride (mg/L)	76.41	-	63.65	58.15	94.83	575.35
	Nitrite (mg/L)	-	-	0.066	-	-	-
	Nitrate (mg/L)	10.71	-	3.20	6.88	8.00	11.10
	Phosphate (mg/L)	-	-	0.69	1.50	-	-
	Sulphate (mg/L)	84.24	-	52.08	117.77	91.58	941.61

Table III.6. Specification sheet of the Bold Modified Basal Freshwater Nutrient Solution (B 5282, pH 3.7 – 4.7, osmolality 556 – 604 mOs/kg) purchased from supplier Sigma-Aldrich.

Component	**Concentration (mg/L)**
Boric acid	11.42
Calcium chloride dihydrate	25.0
Cobalt nitrate • $6H_2O$	0.49
Cupric sulfate • $5H_2O$	1.57
EDTA (free acid)	50.0
Ferrous sulfate • $7H_2O$	4.98
Magnesium sulfate • $7H_2O$	75.0
Manganese chloride • $4H_2O$	1.44
Molybdenum trioxide	0.71
Nickel chloride • $6H_2O$	0.003
Potassium hydroxide	31.0
Potassium iodide	0.003
Potassium phosphate monobasic	175.0
Potassium phosphate dibasic	75.0
Sodium chloride	25.0
Sodium nitrate	250.0
Sodium selenite	0.002
Stannic chloride	0.001
Vanadium sulfate • $3H_2O$	0.0022
Zinc sulfate • $7H_2O$	8.82
Grams of powder to prepare 1L	n/a

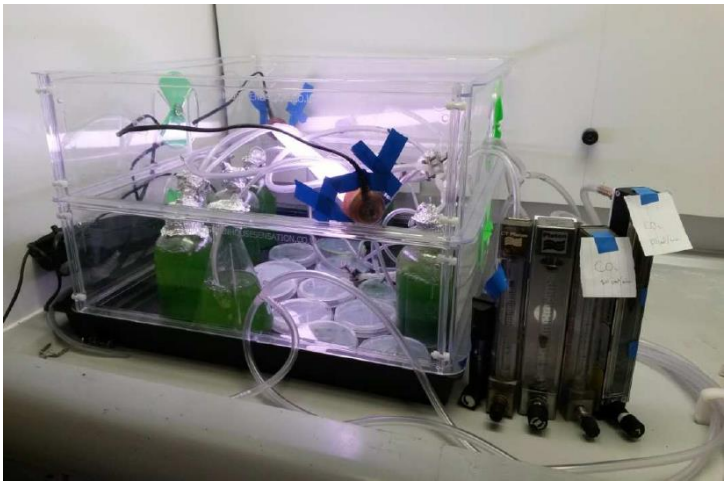

Figure III.3. Set-up of the cultivation of wild algae.

Table III.7. Data used for the production of the calibration curve of the wild algae.

Dilution	Optical density	Algal concentration (g/L)
1:0	0.966	0.492
1:1	0.575	0.228
1:2	0.391	0.161
1:3	0.299	0.119
1:4	0.174	0.068

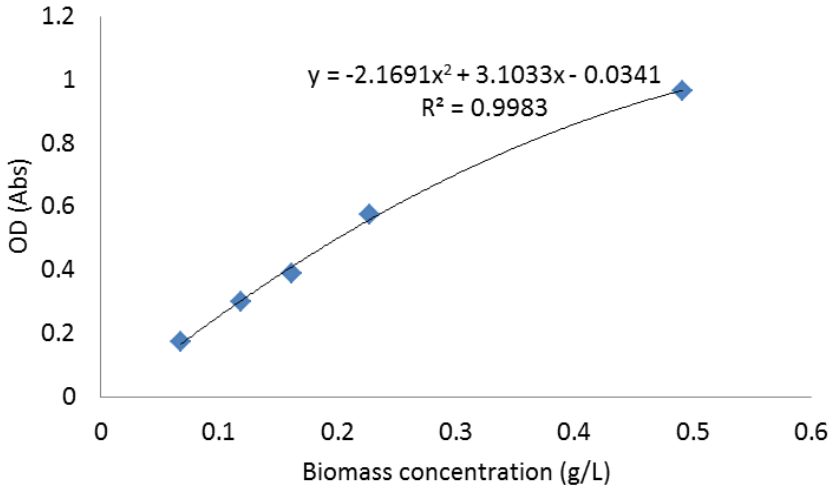

Figure III.4. Calibration curve for the cultivation experiments of wild algae.

The inverted formula used to convert from the optical density readings to biomass concentration was therefore:

$$C_b = 0.2948 \cdot OD^2 + 0.1897 \cdot OD + 0.0314 \quad (90)$$

Table III.8. Biomass concentration measurements (in g/L) for the four wild algae samples growth under normal conditions (no UV light or fed CO_2).

Day	RC22/1	PP	CSP	RP	SJP	HP	RC20/2	RC20/3	RC20/4	RC20/5
0	0.161	0.033	0.033	0.032	0.033	0.032	0.010	0.000	0.000	0.003
1	0.164	0.034	0.045	0.041	0.048	0.035				
5	0.240	0.040	0.035	0.042	0.039	0.034				
6	0.225	0.039	0.032	0.035	0.034	0.033				
7							0.027	0.037	0.017	0.020
8	0.254	0.043	0.032	0.033	0.034	0.032				
12	0.427	0.058	0.032	0.038	0.033	0.033				
13	0.400	0.075	0.043	0.062	0.044	0.043				
14		0.048	0.032	0.034	0.032	0.061	0.200	0.227	0.047	0.377
16		0.044	0.034	0.035	0.032	0.035				
19		0.050	0.039	0.039	0.034	0.036				
21		0.031	0.031	0.031	0.031	0.031	0.537	0.317	0.090	0.700
29		0.135	0.089	0.046	0.102	0.033	0.783	0.510	0.247	0.810
36							0.243	0.757	0.197	0.463
43							0.147	0.157	0.070	0.207
50							0.123	0.227	0.063	0.157
57							0.040	0.153	0.040	0.177
64							0.073	0.173	0.043	0.160

Table III.9. Biomass concentration measurements (in g/L) for the four wild algae samples RC5/1A – RC5/1D and RC24/1D1 – RC24/1D3.

Day	RC5/1A	RC5/1B	RC5/1C	RC5/1D	RC24/1D1	RC24/1D2	RC24/1D3
0	0.073	0.074	0.072	0.071	0.047	0.044	0.046
1					0.050	0.048	0.050
2	0.074	0.058	0.051	0.081	0.049	0.051	0.059
3					0.043	0.074	0.097
4					0.052	0.110	0.162
5	0.079	0.052	0.061	0.097			
9					0.085	0.306	0.648
14	0.112	0.104	0.072	0.156			

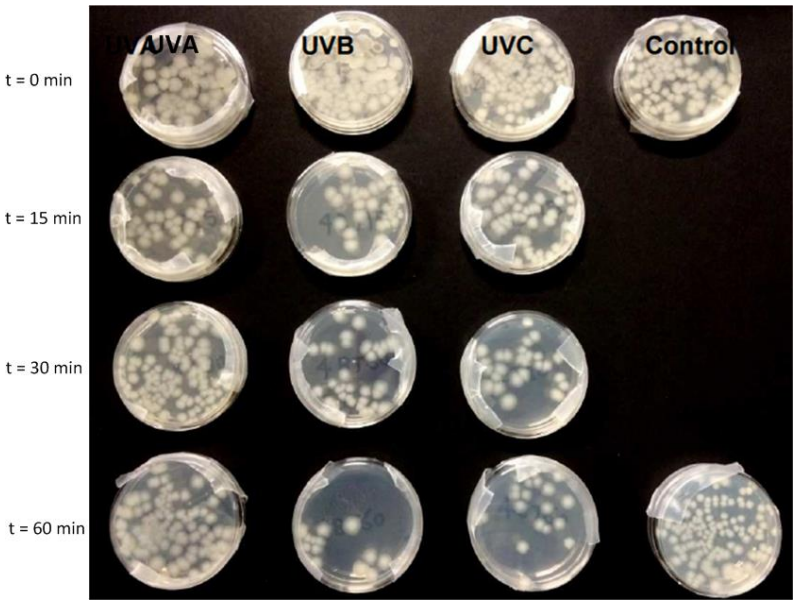

Figure III.5. Effect of UV wavelength and duration of exposure on the bacteria, grown in agar Petri dishes after the UV treatment.

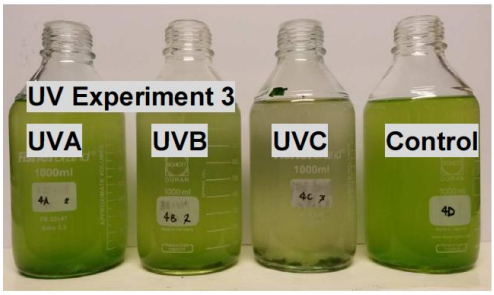

Figure III. 6. Cultivation bottles at the end of the growth monitoring of the UV effect experiments (Bottles RC5/1A – RC5/1D from left to right).

Table III.10. Possible identities of some algal species isolated from the wild algae samples.

Microscopy photo	Possible identity
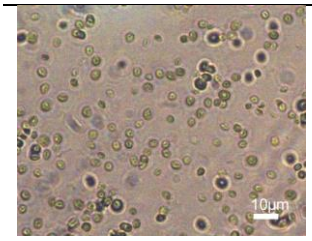	*Chlorella vulgaris*
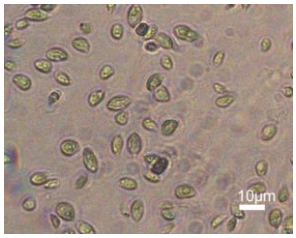	*Acutodesmus* genus
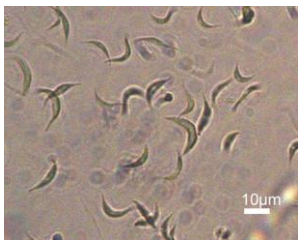	*Monoraphidium Contortum*
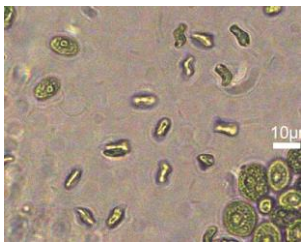	*Chlamydomonas* genus
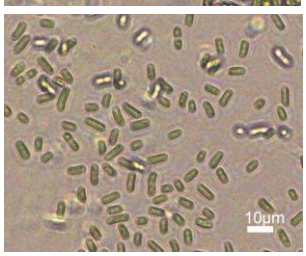	*Stichococcus* genus

Desmodesmus Abundans

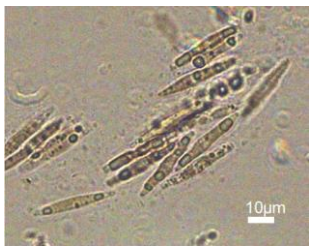

Navicula genus

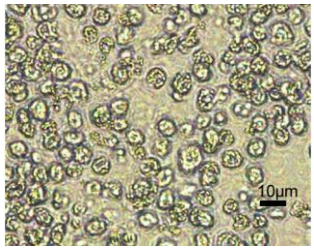

Chlamydomonas genus

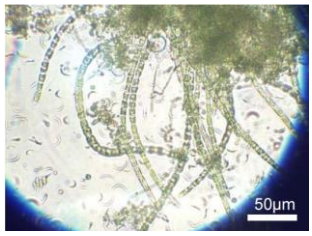

Anabaena genus

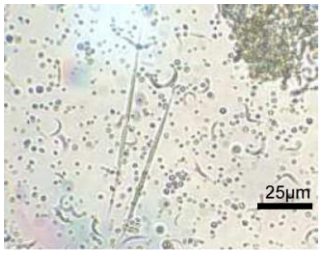

Ancistrodesmus genus

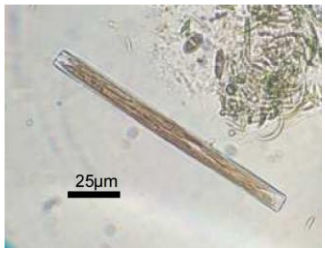

Sinedra genus

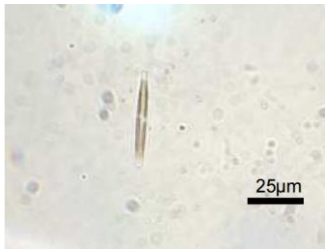

Nitzsechia genus

Appendix IV. MATLAB script of the hydrodynamic model

```
clear all; close all; clc;

%PARAMETERS
d_r=0.054; %[m] riser diameter
d_d=0.054; %[m] downcomer diameter
d_b=0.015; % [m] diameter of the sparger
d_contr=0.052; %[m](used for the 2.04 m long reactor to connect the pipes)
d_exp1=0.058; %[m](diameter of top and bottom middle fittings)
d_exp2=0.063; %[m](diameter of the four connecting curves on the corners)
a_r= pi*(d_r^2)/4; %[m^2] (cross section area of the riser)
a_d= pi*(d_d^2)/4; %[m^2] (cross section area of the downcomer)
a_b= pi*(d_b^2)/4; %[m^2] (cross section area of the sparger)
v_l=0.000000801; %[m2/s] (kinematic viscosity of the liquid)
m_l=0.000798; %[kg/m/s] (dynamic voscosity of the liquid)
p_l=1000; %[kg/m3] (density of the liquid)
p_g=1.225; %[kg/m3] (density of the gas)
l_r=1.04; %[m] (length of the riser)
l_d=l_r; %[m] (length of the downcomer
l=l_r+l_d+0.3; %[m] (total length of the reactor including the degasser and
botom zone)
h_L=l_r; %[m] (liquid dispersion height)
% k_B=5; %if we take it from table on page 209
% k_B=11.4*((a_d/a_b)^0.79); %[dimensionless] if we find it from eq.5.55 in
page 210
k_B=5; %taken from table 5.7 for external loops in Chisti
K_fit=(1.5+1.5+1.3+0.75); %[frictional loss, no of velocity heads]
n_contr1=2; %number of contraction fittings from d_exp2 to d_r
n_contr2=2; %number of contraction fittings from d_exp2 to d_exp1
n_contr3=0; %number of contraction fittings from d_r to d_contr m
n_expan1=2; % number of expansion fittings from d_r to d_exp2
n_expan2=2; % number of expansion fittigns from d_exp1 to d_exp2
n_expan3=0; % number of expansion fittings from d_contr to d_r
mid_fit=0; %it gets 1 later only when we have the 2 m long reactor with the
fittings in the middle of the tubes
K_contr=(n_contr1*0.5*(1-((d_r^2)/(d_exp2^2))))+(mid_fit*n_contr3*0.5*(1-
((d_contr^2)/(d_r^2))))+(n_contr2*0.5*(1-((d_exp1^2)/(d_exp2^2)))); % (K from
contractions in the loop)
K_exp=(mid_fit*n_expan3*((1-
((d_contr^2)/(d_r^2)))^2)*((d_r^2)/(d_contr^2)))+(n_expan1*((1-
((d_r^2)/(d_exp2^2)))^2)*((d_exp2^2)/(d_r^2)))+(n_expan2*((1-
((d_exp1^2)/(d_exp2^2)))^2)*((d_exp2^2)/(d_exp1^2))); %(K from expansions in
the loop)
K_avg=K_fit+K_contr+K_exp; % (all K values summed up for the case of the Power
balance model)
r=0.0000025; % [m](meann height of roughness)
pi=3.142;
g=9.81; %[m/s2]
n=1000; %linspace for the horizontal axis of the figures
d=0.5; %step for l_r when in z axis
z=30; %linspace for q_g 3D plot
vvm=1; %[volume gas/volume liquid/minute] (not needed)
q_g_examined=[0.00000167, 0.000004167, 0.000006667, 0.00001, 0.00001667,
0.000033333, 0.00005, 0.0000667, 0.00008333]; % [m^3/s] (gas flow rate the
values tested in lpm were; 0.1, 0.25, 0.4, 0.6, 1, 2, 3, 4, 5)
d_b_examined=[0.001, 0.0018, 0.0033, 0.0044, 0.005, 0.01]; %[m] (bubble
diameters, used for the z axis of figures)
l_r_row=[0.54,1.04,2.04];
x=size(q_g_examined,2); % linspace for q_g
b=size(d_b_examined,2); % linspace for d_b
d_r_examined=[0.034, 0.054, 0.1];
```

```
%ESTIMATION OF u_b
% The following part estimates the relative rising velocity of the bubbles in
a
% bubble column as a function of their diameter, by using the formula
% produced in the report which is derived by equating Buoyancy force with
% drag force from the water.

d_b = linspace(0.0001,0.01,n); %(for the x axis of figure 1)
s_d_b=size(d_b);
u_b = zeros(1,s_d_b(2));
Re=zeros(1,n);

for i=1:s_d_b(2);
    u_b_t=linspace(0.00005,2,n); %(vector used for the trial and error method)
    u_b_e_numerator=4*g*d_b(i).*(p_l-p_g); %
    u_b_e_denom_0 = 3*p_l;
    Re=u_b_t.*d_b(i)./v_l;
    u_b_e_denom_1 = 24./Re.*(ones(1,n)+0.1*(Re.^0.75));
    u_b_e = (u_b_e_numerator.*((u_b_e_denom_0.*u_b_e_denom_1).^(-1))).^0.5;
%[m/s]
    u_b_error = abs(u_b_e-u_b_t);
    u_b_rel_error=u_b_error./u_b_e;
    [inVal, position] =min(u_b_rel_error);
    u_b(i) = u_b_e(position);

end


% Approach Power Balance
vel_l_1=zeros(s_d_b(2),x);
q_g_row=q_g_examined;
q_g_col=reshape(q_g_row,x,1);

for m=1:s_d_b(2);
    for k=1:size(q_g_col,1);
        vel_l_1_t=linspace(0.00005,2,n);
        vel_l_1_e_1=(vel_l_1_t.^3).*(vel_l_1_t+u_b(m)*ones(1,n));
        vel_l_1_e_num1=8*g*(p_l-p_g)*u_b(m).*l_r.*q_g_col(k);
        vel_l_1_e_den1=pi*p_l*d_r;
        vel_l_1_e_den2=K_avg*d_r*ones(1,n);
        vel_l_1_e_den3=1;
        vel_l_1_e_den4=-
4*log((0.27*r/d_r).*ones(1,n)+((7*v_l./(vel_l_1_t.*d_r)).^0.9));

vel_l_1_e_2=(vel_l_1_e_num1./(vel_l_1_e_den1.*(vel_l_1_e_den2+vel_l_1_e_den3.*
(vel_l_1_e_den4.^(-2)))));
        vel_l_1_e_error = abs(vel_l_1_e_1-vel_l_1_e_2);
        vel_l_1_e_rel_error=abs(vel_l_1_e_error./vel_l_1_t);
        [inVal, position] =min(vel_l_1_e_rel_error);
        vel_l_1(m,k)=vel_l_1_t(position);
    end
end

% Approach Chisti's formula
u_g_2_col=q_g_col./(pi.*(d_r.^2)./4);
u_l_2=zeros(s_d_b(2),x);
vel_l_2=zeros(s_d_b(2),x);
u_l_2_er=zeros(s_d_b(2),x);

for v=1:s_d_b(2);
    for k=1:size(q_g_col,1);
        u_l_2_t=linspace(0.00005,2,n);
        u_l_2_er_e=
u_g_2_col(k)./(0.24*ones(1,n)+1.35*((u_g_2_col(k)*ones(1,n)+u_l_2_t).^0.93));
        u_l_2_ed=0; % (closer results to the experiments when e_d=0)
%         u_l_2_ed=0.46*u_l_2_er_e-0.024; %(from eq.5.59 in Chisti)
```

```
        e_mean=((a_r*u_l_2_er_e)+(a_d*u_l_2_ed))./(a_r+a_d);
        h_D=h_L./(1-e_mean);
        u_l_2_num=2*g*h_D.*(u_l_2_er_e-u_l_2_ed);
        u_l_2_den= k_B.*((1./((ones(1,n)-
u_l_2_er_e).^2))+((a_r/a_d).^2).*(1./((ones(1,n)-u_l_2_ed).^2)));
        u_l_2_e=(u_l_2_num./u_l_2_den).^(1/2);
        u_l_2_error=abs(u_l_2_t-u_l_2_e);
        u_l_2_rel_error=u_l_2_error./u_l_2_e;
        [inVal,position]=min(u_l_2_rel_error);
        u_l_2(v,k)=u_l_2_e(position);
        u_l_2_er(v,k)=u_l_2_er_e(position);
        vel_l_2(v,k)=u_l_2(v,k)./(1-u_l_2_er(v,k));
    end
end



%--------------------

    % x axis: q_g, z axis: d_b

% Approach Power Balance
q_g_row=linspace(0.0000001,0.00009,n);
s_q_g_row=size(q_g_row);
d_b_row=d_b_examined;
s_d_b_row=size(d_b_row);
d_b_col=reshape(d_b_row,b,1);
vel_l_1=zeros(b,n);

u_b_few = zeros(1,s_d_b_row(2)); % estimation of the u_b

for i=1:s_d_b_row(2);
    u_b_t=linspace(0.00005,2,n);
    u_b_e_numerator=4*g*d_b_row(i).*(p_l-p_g);
    u_b_e_denom_0 = 3*p_l;
    Re=u_b_t.*d_b_row(i)./v_l;
    u_b_e_denom_1 = 24./Re.*(ones(1,n)+0.1*(Re.^0.75));
    u_b_e = (u_b_e_numerator.*((u_b_e_denom_0.*u_b_e_denom_1).^(-1))).^0.5;
%[m/s]
    u_b_error = abs(u_b_e-u_b_t);
    u_b_rel_error=u_b_error./u_b_e;
    [inVal, position] =min(u_b_rel_error);
    u_b_few(i) = u_b_e(position);


end



for k=1:s_q_g_row(2); % estimation of the v_l
    for m=1:size(d_b_col,1);
        vel_l_1_t=linspace(0.00005,2,n);
        vel_l_1_e_1=(vel_l_1_t.^3).*(vel_l_1_t+u_b_few(m)*ones(1,n));
        vel_l_1_e_num1=8*g*(p_l-p_g)*u_b_few(m).*l_r.*q_g_row(k);
        vel_l_1_e_den1=pi*p_l*d_r;
        vel_l_1_e_den2=K_avg*d_r*ones(1,n);
        vel_l_1_e_den3=l;
        vel_l_1_e_den4=-
4*log((0.27*r/d_r)*ones(1,n)+((7*v_l./(vel_l_1_t.*d_r)).^0.9));

vel_l_1_e_2=vel_l_1_e_num1./(vel_l_1_e_den1.*(vel_l_1_e_den2+vel_l_1_e_den3.*(
vel_l_1_e_den4.^(-2))));
        vel_l_1_e_error = abs(vel_l_1_e_1-vel_l_1_e_2);
        vel_l_1_e_rel_error=vel_l_1_e_error./vel_l_1_e_2;
        [inVal, position] =min(vel_l_1_e_rel_error);
        vel_l_1(m,k)=vel_l_1_t(position);
    end
```

```
end


% Approach Chisti's formula
u_g_2_row=q_g_row./(pi.*(d_r.^2)./4);
u_l_2=zeros(b,n);
vel_l_2=zeros(b,n);
u_l_2_er=zeros(b,n);

for k=1:s_q_g_row(2);
    for v=1:size(d_b_col,1);
        u_l_2_t=linspace(0.00005,2,n);
        u_l_2_er_e=
u_g_2_row(k)./(0.24*ones(1,n)+1.35*((u_g_2_row(k)*ones(1,n)+u_l_2_t).^0.92));
        u_l_2_ed=0;
%         u_l_2_ed=0.46.*u_l_2_er_e-(0.024*ones(1,n));
        e_mean=((a_r*u_l_2_er_e)+(a_d*u_l_2_ed))/(a_r+a_d);
        h_D=h_L./(1-e_mean);
        u_l_2_num=2*g*h_D.*(u_l_2_er_e-u_l_2_ed);
        u_l_2_den= k_B.*((1./((ones(1,n)-
u_l_2_er_e).^2))+((a_r/a_d).^2).*(1./((ones(1,n)-u_l_2_ed).^2)));
        u_l_2_e=(u_l_2_num./u_l_2_den).^(1/2);
        u_l_2_error=abs(u_l_2_t-u_l_2_e);
        u_l_2_rel_error=u_l_2_error./u_l_2_e;
        [inVal,position]=min(u_l_2_rel_error);
        u_l_2(v,k)=u_l_2_e(position);
        u_l_2_er(v,k)=u_l_2_er_e(position);
        vel_l_2(v,k)=u_l_2(v,k)./(1-u_l_2_er(v,k));
    end
end



%-------------------

    % x axis: d_r, z axis: d_b
% Approach Power Balance

q_g_stable=0.00001667; % select a flow rate
d_r_row=linspace(0.03,0.1,n);
s_d_r_row=size(d_r_row);
d_b_row=d_b_examined;
s_d_b_row=size(d_b_row);
d_b_col=reshape(d_b_row,b,1);
vel_l_1=zeros(b,n);

for k=1:s_d_r_row(2);
    for m=1:size(d_b_col,1);
        vel_l_1_t=linspace(0.00005,2,n);
        vel_l_1_e_1=(vel_l_1_t.^3).*(vel_l_1_t+u_b_few(m)*ones(1,n));
        vel_l_1_e_num1=8*g*(p_l-p_g)*u_b_few(m).*l_r.*q_g_stable;
        vel_l_1_e_den1=pi*p_l*d_r_row(k);
        vel_l_1_e_den2=K_avg*d_r_row(k)*ones(1,n);
        vel_l_1_e_den3=l;
        vel_l_1_e_den4=-
4*log((0.27*r/d_r_row(k))*ones(1,n)+((7*v_l./(vel_l_1_t.*d_r_row(k))).^0.9));

vel_l_1_e_2=vel_l_1_e_num1./(vel_l_1_e_den1.*(vel_l_1_e_den2+vel_l_1_e_den3.*(
vel_l_1_e_den4.^(-2))));
        vel_l_1_e_error = abs(vel_l_1_e_1-vel_l_1_e_2);
        vel_l_1_e_rel_error=vel_l_1_e_error./vel_l_1_e_2;
        [inVal, position] =min(vel_l_1_e_rel_error);
        vel_l_1(m,k)=vel_l_1_t(position);
    end
end
```

```
% Approach Chisti's formula
u_g_2_row=q_g_stable./(pi.*(d_r_row.^2)./4);
u_l_2=zeros(b,n);
vel_l_2=zeros(b,n);
d_d_row=d_r_row;
a_r_row= pi*(d_r_row.^2)./4; %[m^2]
a_d_row= pi*(d_d_row.^2)./4; %[m^2]

for k=1:s_d_r_row(2);
    for v=1:size(d_b_col,1);
        u_l_2_t=linspace(0.00005,2,n);
        u_l_2_er=
u_g_2_row(k)./(0.24+1.35*((u_g_2_row(k)*ones(1,n)+u_l_2_t).^0.92));
        u_l_2_ed=0;
%         u_l_2_ed=0.46.*u_l_2_er-(0.024*ones(1,n));
        e_mean=((a_r.*u_l_2_er)+(a_d.*u_l_2_ed))./(a_r+a_d);
        h_D=h_L./(ones(1,n)-e_mean);
        u_l_2_num=2*g*h_D.*(u_l_2_er-u_l_2_ed);
        u_l_2_den= k_B.*((1./((ones(1,n)-
u_l_2_er).^2))+((a_r_row(k)./a_d_row(k)).^2).*(1./((ones(1,n)-u_l_2_ed).^2)));
        u_l_2_e=(u_l_2_num./u_l_2_den).^(1/2);
        u_l_2_error=abs(u_l_2_t-u_l_2_e);
        u_l_2_rel_error=u_l_2_error./u_l_2_e;
        [inVal,position]=min(u_l_2_rel_error);
        u_l_2(v,k)=u_l_2_e(position);
        u_l_2_er(v,k)=u_l_2_er(position);
        vel_l_2(v,k)=u_l_2(v,k)./(1-u_l_2_er(v,k));
    end
end




%-------------------

    % x axis: q_g, z axis: d_r

% Approach Power Balance
% d_b_stable=0.004; %u_b(292) will be used, since d_b(399)=0.004
q_g_row=linspace(0.0000001,0.00009,n);
s_q_g_row=size(q_g_row);
d_r_row=d_r_examined;
s_d_r_row=size(d_r_row);
d_r_col=reshape(d_r_row,s_d_r_row(2),1);
vel_l_1=zeros(s_d_r_row(2),n);

for k=1:s_q_g_row(2);
    for m=1:size(d_r_col,1);
        vel_l_1_t=linspace(0.00005,2,n);
        vel_l_1_e_1=(vel_l_1_t.^3).*(vel_l_1_t+u_b(453)*ones(1,n));
        vel_l_1_e_num1=8*g*(p_l-p_g)*u_b(453).*l_r.*q_g_row(k);
        vel_l_1_e_den1=pi*p_l*d_r_col(m);
        vel_l_1_e_den2=K_avg*d_r_col(m)*ones(1,n);
        vel_l_1_e_den3=l;
        vel_l_1_e_den4=-
4*log((0.27*r/d_r_col(m))*ones(1,n)+((7*v_l./(vel_l_1_t.*d_r_col(m))).^0.9));

vel_l_1_e_2=vel_l_1_e_num1./(vel_l_1_e_den1.*(vel_l_1_e_den2+vel_l_1_e_den3.*(
vel_l_1_e_den4.^(-2))));
        vel_l_1_e_error = abs(vel_l_1_e_1-vel_l_1_e_2);
        vel_l_1_e_rel_error=vel_l_1_e_error./vel_l_1_e_2;
        [inVal, position] =min(vel_l_1_e_rel_error);
        vel_l_1(m,k)=vel_l_1_t(position);
    end
end
```

```
% Approach Chisti's formula
q_g_mat=repmat(q_g_row,s_d_r_row(2),1);
d_r_mat=repmat(d_r_col,1,n);
u_g_2_mat=q_g_mat./(pi.*(d_r_mat.^2)./4);
u_l_2=zeros(s_d_r_row(2),n);
vel_l_2=zeros(s_d_r_row(2),n);
d_d_col=d_r_col+ones(s_d_r_row(2),1)*0.01;
a_r_col= pi*(d_r_col.^2)./4; %[m^2]
a_d_col= pi*(d_d_col.^2)./4; %[m^2]

for k=1:s_q_g_row(2);
    for v=1:size(d_r_col,1);
        u_l_2_t=linspace(0.0005,3,n);
        u_l_2_er=
u_g_2_mat(v,k)./(0.24.*ones(1,n)+1.35*((u_g_2_mat(v,k).*ones(1,n)+u_l_2_t).^0.
92));
        u_l_2_ed=0;
%         u_l_2_ed=0.46.*u_l_2_er-(0.024*ones(1,n));
        e_mean=((a_r.*u_l_2_er)+(a_d.*u_l_2_ed))./(a_r+a_d);
        h_D=h_L./(1-e_mean);
        u_l_2_num=2*g*h_D.*(u_l_2_er-u_l_2_ed);
        u_l_2_den= k_B.*((1./((ones(1,n)-
u_l_2_er).^2))+((a_r_col(v)./a_d_col(v)).^2).*(1./((ones(1,n)-u_l_2_ed).^2)));
        u_l_2_e=(u_l_2_num./u_l_2_den).^(1/2);
        u_l_2_error=abs(u_l_2_t-u_l_2_e);
        u_l_2_rel_error=u_l_2_error./u_l_2_e;
        [inVal,position]=min(u_l_2_rel_error);
        u_l_2(v,k)=u_l_2_e(position);
        u_l_2_er(v,k)=u_l_2_er(position);
        vel_l_2(v,k)=u_l_2(v,k)./(1-u_l_2_er(v,k));
    end
end


%-------------------------

    % x axis q_g, z axis: l_r

% Approach Power Balance
q_g_row=linspace(0.0000001,0.00009,n);
s_q_g_row=size(q_g_row);
l_d_row=l_r_row;
l_row=l_r_row+l_d_row;
s_l_r_row=size(l_r_row);
l_r_col=reshape(l_r_row,s_l_r_row(2),1);
vel_l_1=zeros(s_l_r_row(2),size(d_b_examined,2),n);

for k=1:s_q_g_row(2);
    for p=1:size(d_b_examined,2);
    for m=1:size(l_r_col,1);
        if m>=3;
        mid_fit=1;
        K_contr=(n_contr1*0.5*(1-
((d_r^2)/(d_exp2^2))))+(mid_fit*n_contr3*0.5*(1-
((d_contr^2)/(d_r^2))))+(n_contr2*0.5*(1-((d_exp1^2)/(d_exp2^2))));
K_exp=(mid_fit*n_expan3*((1-
((d_contr^2)/(d_r^2)))^2)*((d_r^2)/(d_contr^2)))+(n_expan1*((1-
((d_r^2)/(d_exp2^2)))^2)*((d_exp2^2)/(d_r^2)))+(n_expan2*((1-
((d_exp1^2)/(d_exp2^2)))^2)*((d_exp2^2)/(d_exp1^2)));
K_avg=K_fit+K_contr+K_exp;
        end

        if m<=1;
           d_r=0.058; %because the short reactor was a PVC non-transparent
tube with different thickness and ID
        else d_r=0.054;
        end
```

```
        vel_l_1_t=linspace(0.00005,2,n);
        vel_l_1_e_1=(vel_l_1_t.^3).*(vel_l_1_t+u_b_few(p)*ones(1,n));
        vel_l_1_e_num1=8*g*(p_l-p_g)*u_b_few(p).*l_r_row(m).*q_g_row(k);
        vel_l_1_e_den1=pi*p_l*d_r;
        vel_l_1_e_den2=K_avg*d_r*ones(1,n);
        vel_l_1_e_den3=l_row(m);
        vel_l_1_e_den4=-
4*log((0.27*r/d_r)*ones(1,n)+((7*v_l./(vel_l_1_t.*d_r)).^0.9));

vel_l_1_e_2=vel_l_1_e_num1./(vel_l_1_e_den1.*(vel_l_1_e_den2+vel_l_1_e_den3.*(
vel_l_1_e_den4.^(-2))));
        vel_l_1_e_error = abs(vel_l_1_e_1-vel_l_1_e_2);
        vel_l_1_e_rel_error=vel_l_1_e_error./vel_l_1_e_2;
        [inVal, position] =min(vel_l_1_e_rel_error);
        vel_l_1(m,p,k)=vel_l_1_t(position);
    end
    end
end

% Approach Chisti's formula
q_g_mat=repmat(q_g_row,s_l_r_row(2),1);
l_r_mat=repmat(l_r_col,1,n);
u_g_2_mat=q_g_mat./(pi.*(d_r.^2)./4);
u_l_2=zeros(s_l_r_row(2),n);
vel_l_2=zeros(s_l_r_row(2),n);
h_L_row=l_r_row;

for k=1:s_q_g_row(2);
    for v=1:size(l_r_col,1);
        if v<=1;
           d_r=0.058; %because the short reactor was a PVC non-transparent
tube with different thickness and ID
        else d_r=0.054;
        end

        u_l_2_t=linspace(0.00005,2,n);
        u_l_2_er=
u_g_2_mat(v,k)./(0.24.*ones(1,n)+1.35*((u_g_2_mat(v,k).*ones(1,n)+u_l_2_t).^0.
92));
        u_l_2_ed=0;
%         u_l_2_ed=0.46.*u_l_2_er-(0.024*ones(1,n));
        e_mean=((a_r.*u_l_2_er)+(a_d.*u_l_2_ed))./(a_r+a_d);
        h_D_row=h_L_row(v)./(1*ones(1,n)-e_mean);
        u_l_2_num=2*g*h_D_row.*(u_l_2_er-u_l_2_ed);
        u_l_2_den= k_B.*((1./((ones(1,n)-
u_l_2_er).^2))+((a_r./a_d).^2).*(1./((ones(1,n)-u_l_2_ed).^2)));
        u_l_2_e=(u_l_2_num./u_l_2_den).^(1/2);
        u_l_2_error=abs(u_l_2_t-u_l_2_e);
        u_l_2_rel_error=u_l_2_error./u_l_2_e;
        [inVal,position]=min(u_l_2_rel_error);
        u_l_2(v,k)=u_l_2_e(position);
        u_l_2_er(v,k)=u_l_2_er(position);
        vel_l_2(v,k)=u_l_2(v,k)./(1-u_l_2_er(v,k));
    end
end



%-------------------------

%ESTIMATION OF u_l

    % a axis q_g, z axis: d_b
% Approach Power Balance

d_r_stable=0.054;
```

```
q_g_row=linspace(0.000001,0.00009,n);
d_b_row=d_b_examined;
d_b_col=reshape(d_b_row,b,1);
vel_l_1_er=zeros(b,n);
e_r_1=zeros(b,n);
e_r_2=zeros(b,n);
u_g_2_row=q_g_row./(pi.*(d_r_stable.^2)./4);


for s=1:b;
    for t=1:n;
        vel_l_1_er_t=linspace(0.00005,2,n);
        vel_l_1_e_er_1=(vel_l_1_er_t.^3).*(vel_l_1_er_t+u_b_few(s)*ones(1,n));
        vel_l_1_e_er_num1=8*g*(p_l-p_g)*u_b_few(s).*l_r.*q_g_row(t);
        vel_l_1_e_er_den1=pi*p_l*d_r;
        vel_l_1_e_er_den2=K_avg*d_r*ones(1,n);
        vel_l_1_e_er_den3=1;
        vel_l_1_e_er_den4=-
4*log((0.27*r/d_r)*ones(1,n)+((7*v_l./(vel_l_1_er_t.*d_r)).^0.9));

vel_l_1_e_er_2=vel_l_1_e_er_num1./(vel_l_1_e_er_den1.*(vel_l_1_e_er_den2+vel_l
_1_e_er_den3.*(vel_l_1_e_er_den4.^(-2))));
        vel_l_1_e_er_error = abs(vel_l_1_e_er_1-vel_l_1_e_er_2);
        vel_l_1_e_er_rel_error=vel_l_1_e_er_error./vel_l_1_e_er_2;
        [inVal, position] =min(vel_l_1_e_er_rel_error);
        vel_l_1_er(s,t)=vel_l_1_er_t(position);
        e_r_1(s,t) =
(4*q_g_row(t))./(pi*(d_r_stable^2)*(u_b_few(s)+vel_l_1_er(s,t))) ;


    % Approach Chisti's formula

    u_l_2_t=linspace(0.00005,2,n);
    u_l_2_er=
u_g_2_row(t)./(0.24+1.35*((u_g_2_row(t)*ones(1,n)+u_l_2_t).^0.92));
    u_l_2_ed=0;
%     u_l_2_ed=0.46.*u_l_2_er-(0.024*ones(1,n));
    e_mean=((a_r.*u_l_2_er)+(a_d*u_l_2_ed))./(a_r+a_d);
    h_D=h_L./(1-e_mean);
    u_l_2_num=2*g*h_D.*(u_l_2_er-u_l_2_ed);
    u_l_2_den= k_B.*((1./((ones(1,n)-
u_l_2_er).^2))+((a_r./a_d).^2).*(1./((ones(1,n)-u_l_2_ed).^2)));
    u_l_2_e=(u_l_2_num./u_l_2_den).^(1/2);
    u_l_2_error=abs(u_l_2_t-u_l_2_e);
    u_l_2_rel_error=u_l_2_error./u_l_2_e;
    [inVal,position]=min(u_l_2_rel_error);
    u_l_2(s,t)=u_l_2_e(position);
    e_r_2(s,t)=u_l_2_er(position);
    end
end


%--------------------------------------------------------------------

    % x axis: d_r, z axis: db

% Power balance approach

q_g_stable=0.00001667;
d_r_row=linspace(0.03,0.1,n);
d_d_row=d_r_row;
d_b_row=d_b_examined;
d_b_col=reshape(d_b_row,b,1);
vel_l_1_er=zeros(b,n);
e_r_1=zeros(b,n);
u_l_2_e=zeros(1,s_d_b(2));
u_l_2_er=zeros(1,s_d_b(2));
```

```
e_r_2=zeros(b,n);
u_g_2_row=q_g_stable./(pi.*(d_r_row.^2)./4);
a_r_row= pi*(d_r_row.^2)./4; %[m^2]
a_d_row= pi*(d_d_row.^2)./4; %[m^2]

for s=1:b;
    for t=1:n;
        vel_l_1_er_t=linspace(0.00005,2,n);
        vel_l_1_e_er_1=(vel_l_1_t.^3).*(vel_l_1_t+u_b_few(s)*ones(1,n));
        vel_l_1_e_er_num1=8*g*(p_l-p_g)*u_b_few(s).*l_r.*q_g_stable;
        vel_l_1_e_er_den1=pi*p_l*d_r_row(t);
        vel_l_1_e_er_den2=K_avg*d_r_row(t)*ones(1,n);
        vel_l_1_e_er_den3=1;
        vel_l_1_e_er_den4=-
4*log((0.27*r/d_r_row(t))*ones(1,n)+((7*v_l./(vel_l_1_t.*d_r_row(t))).^0.9));

vel_l_1_e_er_2=vel_l_1_e_er_num1./(vel_l_1_e_er_den1.*(vel_l_1_e_er_den2+vel_l
_1_e_er_den3.*(vel_l_1_e_er_den4.^(-2))));
        vel_l_1_e_er_error = abs(vel_l_1_e_er_1-vel_l_1_e_er_2);
        vel_l_1_e_er_rel_error=vel_l_1_e_er_error./vel_l_1_e_er_2;
        [inVal, position] =min(vel_l_1_e_er_rel_error);
        vel_l_1_er(s,t)=vel_l_1_er_t(position);
        e_r_1(s,t) =
(4*q_g_stable)./(pi*(d_r_row(t)^2)*(u_b_few(s)+vel_l_1_er(s,t))) ;


        % Approach Chisti's formula

    u_l_2_t=linspace(0.00005,2,n);
    u_l_2_er=
u_g_2_row(t)./(0.24+1.35*((u_g_2_row(t)*ones(1,n)+u_l_2_t).^0.92));
    u_l_2_ed=0;
%     u_l_2_ed=0.46.*u_l_2_er-(0.024*ones(1,n));
    e_mean=((a_r.*u_l_2_er)+(a_d.*u_l_2_ed))./(a_r+a_d);
    h_D=h_L./(1-e_mean);
    u_l_2_num=2*g*h_D.*(u_l_2_er-u_l_2_ed);
    u_l_2_den= k_B.*((1./((ones(1,n)-
u_l_2_er).^2))+((a_r_row(t)./a_d_row(t)).^2).*(1./((ones(1,n)-u_l_2_ed).^2)));
    u_l_2_e=(u_l_2_num./u_l_2_den).^(1/2);
    u_l_2_error=abs(u_l_2_t-u_l_2_e);
    u_l_2_rel_error=u_l_2_error./u_l_2_e;
    [inVal,position]=min(u_l_2_rel_error);
    u_l_2(s,t)=u_l_2_e(position);
    e_r_2(s,t)=u_l_2_er(position);
    end
end



%-------------------------

    % x axis:q_g, z axis: d_r

    % Power balance approach
q_g_row=linspace(0.000001,0.00009,n);
s_q_g_row=size(q_g_row);
d_r_row=d_r_examined;
d_d_row=d_r_row;
s_d_r_row=size(d_r_row);
% d_b_stable=0.004; %u_b(292) will be used, since d_b(399)=0.004
d_r_col=reshape(d_r_row,s_d_r_row(2),1);
vel_l_1_er=zeros(s_d_r_row(2),n);
e_r_1=zeros(s_d_r_row(2),n);
e_r_2=zeros(s_d_r_row(2),n);
q_g_mat=repmat(q_g_row,s_d_r_row(2),1);
d_r_mat=repmat(d_r_col,1,s_q_g_row(2));
u_g_2_mat=q_g_mat./(pi.*(d_r_mat.^2)./4);
```

```
a_r_row= pi*(d_r_row.^2)./4; %[m^2]
a_d_row= pi*(d_d_row.^2)./4; %[m^2]

for k=1:s_q_g_row(2);
    for m=1:size(d_r_col,1);
        vel_l_1_er_t=linspace(0.00005,2,n);
        vel_l_1_e_er_1=(vel_l_1_er_t.^3).*(vel_l_1_er_t+u_b(453)*ones(1,n));
        vel_l_1_e_er_num1=8*g*(p_l-p_g)*u_b(453).*l_r.*q_g_row(k);
        vel_l_1_e_er_den1=pi*p_l*d_r_col(m);
        vel_l_1_e_er_den2=K_avg*d_r_col(m)*ones(1,n);
        vel_l_1_e_er_den3=1;
        vel_l_1_e_er_den4=-
4*log((0.27*r/d_r_col(m))*ones(1,n)+((7*v_l./(vel_l_1_t.*d_r_col(m))).^0.9));

vel_l_1_e_er_2=vel_l_1_e_er_num1./(vel_l_1_e_er_den1.*(vel_l_1_e_er_den2+vel_l
_1_e_er_den3.*(vel_l_1_e_er_den4.^(-2))));
        vel_l_1_e_er_error = abs(vel_l_1_e_er_1-vel_l_1_e_er_2);
        vel_l_1_e_er_rel_error=vel_l_1_e_er_error./vel_l_1_e_er_2;
        [~, position] =min(vel_l_1_e_er_rel_error);
        vel_l_1_er(m,k)=vel_l_1_er_t(position);
        e_r_1(m,k) =
(4*q_g_row(k))./(pi*(d_r_col(m)^2)*(u_b(453)+vel_l_1_er(m,k))) ;


        %Chisti's approach

    u_l_2_t=linspace(0.00005,2,n);
    u_l_2_er=
u_g_2_mat(m,k)./(0.24+1.35*((u_g_2_mat(m,k)*ones(1,n)+u_l_2_t).^0.92));
    u_l_2_ed=0;
%     u_l_2_ed=0.46.*u_l_2_er-(0.024*ones(1,n));

e_mean=((a_r_row(m).*u_l_2_er)+(a_d_row(m).*u_l_2_ed))./(a_r_row(m)+a_d_row(m)
);
    h_D=h_L./(1-e_mean);
    u_l_2_num=2*g*h_D.*(u_l_2_er-u_l_2_ed);
    u_l_2_den= k_B.*((1./((ones(1,n)-
u_l_2_er).^2))+((a_r_row(m)./a_d_row(m)).^2).*(1./((ones(1,n)-u_l_2_ed).^2)));
    u_l_2_e=(u_l_2_num./u_l_2_den).^(1/2);
    u_l_2_error=abs(u_l_2_t-u_l_2_e);
    u_l_2_rel_error=u_l_2_error./u_l_2_e;
    [inVal,position]=min(u_l_2_rel_error);
    u_l_2(m,k)=u_l_2_e(position);
    e_r_2(m,k)=u_l_2_er(position);


    end

end



%-------------------------

    % x axis: l_r, z axis: d_b

% Power balance approach
q_g_stable=0.00001667;
l_r_row=linspace(0.01,6,n);
l_d_row=l_r_row;
l_row=l_r_row+l_d_row;
h_L_row=l_r_row;
d_b_row=d_b_examined;
d_b_col=reshape(d_b_row,b,1);
vel_l_1_er=zeros(b,n);
e_r_1=zeros(b,n);
u_l_2_holdup=zeros(1,s_d_b(2));
```

```
u_l_2_holdup_er=zeros(1,s_d_b(2));
e_r_2=zeros(b,n);
u_g_2=q_g_stable./(pi.*(d_r.^2)./4);
a_r= pi*(d_r.^2)./4; %[m^2]
a_d= pi*(d_d.^2)./4; %[m^2]

for s=1:b;
    for t=1:n;
        vel_l_1_er_t=linspace(0.00005,2,n);
        vel_l_1_e_er_1=(vel_l_1_t.^3).*(vel_l_1_t+u_b_few(s)*ones(1,n));
        vel_l_1_e_er_num1=8*g*(p_l-p_g)*u_b_few(s).*l_r_row(t).*q_g_stable;
        vel_l_1_e_er_den1=pi*p_l*d_r;
        vel_l_1_e_er_den2=K_avg*d_r*ones(1,n);
        vel_l_1_e_er_den3=l_row(t);
        vel_l_1_e_er_den4=-
4*log((0.27*r/d_r)*ones(1,n)+((7*v_l./(vel_l_1_t.*d_r)).^0.9));

vel_l_1_e_er_2=vel_l_1_e_er_num1./(vel_l_1_e_er_den1.*(vel_l_1_e_er_den2+vel_l
_1_e_er_den3.*(vel_l_1_e_er_den4.^(-2))));
        vel_l_1_e_er_error = abs(vel_l_1_e_er_1-vel_l_1_e_er_2);
        vel_l_1_e_er_rel_error=vel_l_1_e_er_error./vel_l_1_e_er_2;
        [inVal, position] =min(vel_l_1_e_er_rel_error);
        vel_l_1_er(s,t)=vel_l_1_er_t(position);
        e_r_1(s,t) = (4*q_g_stable)./(pi*(d_r^2)*(u_b_few(s)+vel_l_1_er(s,t)))
;


        % Approach Chisti's formula
    u_l_2_t=linspace(0.00001,2,n);
    u_l_2_er= u_g_2./(0.24+1.35*((u_g_2*ones(1,n)+u_l_2_t).^0.92));
    u_l_2_ed=0;
%     u_l_2_ed=0.46.*u_l_2_er-(0.024*ones(1,n));
    e_mean=((a_r.*u_l_2_er)+(a_d*u_l_2_ed))./(a_r+a_d);
    h_D_row=h_L_row(t)./(1-e_mean);
    u_l_2_num=2*g*h_D_row.*(u_l_2_er-u_l_2_ed);
    u_l_2_den= k_B.*((1./((ones(1,n)-
u_l_2_er).^2))+((a_r./a_d).^2).*(1./((ones(1,n)-u_l_2_ed).^2)));
    u_l_2_e=(u_l_2_num./u_l_2_den).^(1/2);
    u_l_2_error=abs(u_l_2_t-u_l_2_e);
    u_l_2_rel_error=u_l_2_error./u_l_2_e;
    [inVal,position]=min(u_l_2_rel_error);
    u_l_2(s,t)=u_l_2_e(position);
    e_r_2(s,t)=u_l_2_er(position);
    end
end



%----------

    %x axis:q_g, z axis: l_r

% Power balance approach
q_g_row=linspace(0.0000001,0.00009,n);
s_q_g_row=size(q_g_row);
l_r_row=[0.54,1.04,2.04];
l_d_row=l_r_row;
l_row=l_r_row+l_d_row;
h_L_row=l_r_row;
s_l_r_row=size(l_r_row);
l_r_col=reshape(l_r_row,s_l_r_row(2),1);
vel_l_1_er=zeros(s_l_r_row(2),size(d_b_examined,2),n);
e_r_1=zeros(s_l_r_row(2),n);
e_r_2=zeros(s_l_r_row(2),n);
u_g_2_row=q_g_row./(pi.*(d_r.^2)./4);

for k=1:s_q_g_row(2);
```

```
    for p=4;
    for m=1:size(l_r_col,1);
        if m>=3;
        mid_fit=1;
        K_contr=(n_contr1*0.5*(1-
((d_r^2)/(d_exp2^2))))+(mid_fit*n_contr3*0.5*(1-
((d_contr^2)/(d_r^2))))+(n_contr2*0.5*(1-((d_exp1^2)/(d_exp2^2))));
K_exp=(mid_fit*n_expan3*((1-
((d_contr^2)/(d_r^2)))^2)*((d_r^2)/(d_contr^2)))+(n_expan1*((1-
((d_r^2)/(d_exp2^2)))^2)*((d_exp2^2)/(d_r^2)))+(n_expan2*((1-
((d_exp1^2)/(d_exp2^2)))^2)*((d_exp2^2)/(d_exp1^2)));
K_avg=K_fit+K_contr+K_exp;
        end

        if m<=1;
           d_r=0.058; %because the short reactor was a PVC non-transparent
tube with different thickness and ID
        else d_r=0.054;
        end

        vel_l_1_er_t=linspace(0.00005,2,n);
        vel_l_1_e_er_1=(vel_l_1_er_t.^3).*(vel_l_1_er_t+u_b_few(p)*ones(1,n));
        vel_l_1_e_er_num1=8*g*(p_l-p_g)*u_b_few(p).*l_r_row(m).*q_g_row(k);
        vel_l_1_e_er_den1=pi*p_l*d_r;
        vel_l_1_e_er_den2=K_avg*d_r*ones(1,n);
        vel_l_1_e_er_den3=l_row(m);
        vel_l_1_e_er_den4=-
4*log((0.27*r/d_r)*ones(1,n)+((7*v_l./(vel_l_1_t.*d_r)).^0.9));

vel_l_1_e_er_2=vel_l_1_e_er_num1./(vel_l_1_e_er_den1.*(vel_l_1_e_er_den2+vel_l
_1_e_er_den3.*(vel_l_1_e_er_den4.^(-2))));
        vel_l_1_e_er_error = abs(vel_l_1_e_er_1-vel_l_1_e_er_2);
        vel_l_1_e_er_rel_error=vel_l_1_e_er_error./vel_l_1_e_er_2;
        [inVal, position] =min(vel_l_1_e_er_rel_error);
        vel_l_1_er(m,k)=vel_l_1_er_t(position);
        e_r_1(m,k) = (4*q_g_row(k))./(pi*(d_r^2)*(u_b_few(p)+vel_l_1_er(m,k)))
;


        %Chisti's approach

    u_l_2_t=linspace(0.00001,2,n);
    u_l_2_er=
u_g_2_row(k)./(0.24+1.35*((u_g_2_row(k)*ones(1,n)+u_l_2_t).^0.92));
    u_l_2_ed=0;
%     u_l_2_ed=0.46.*u_l_2_er-(0.024*ones(1,n));
    e_mean=((a_r.*u_l_2_er)+(a_d*u_l_2_ed))./(a_r+a_d);
    h_D_row=h_L_row(m)./(1-e_mean);
    u_l_2_num=2*g*h_D_row.*(u_l_2_er-u_l_2_ed);
    u_l_2_den= k_B.*((1./((ones(1,n)-
u_l_2_er).^2))+((a_r./a_d).^2).*(1./((ones(1,n)-u_l_2_ed).^2)));
    u_l_2_e=(u_l_2_num./u_l_2_den).^(1/2);
    u_l_2_error=abs(u_l_2_t-u_l_2_e);
    u_l_2_rel_error=u_l_2_error./u_l_2_e;
    [inVal,position]=min(u_l_2_rel_error);
    u_l_2(m,k)=u_l_2_e(position);
    e_r_2(m,k)=u_l_2_er(position);


    end
    end
end
```

Appendix V. Growth kinetics

Estimation of the initial nutrient concentrations

Table V.1. Estimation of the nitrate and phosphate concentrations contained in the media.

Nutrient element contained	Component	Chemical formula	Quantity (mg/L)	Molecular weight (g/mol)	mol/L	Macronutrient quantity (g/L)	Total nitrates and phosphates (g/L)
N (Mr_{NO3-} = 62)	Cobalt nitrate • $6H_2O$	$Co(NO_3)_2$ • $6H_2O$	0.49	291	0.00000168	0.000104	0.19307
	EDTA (free acid)	$C_{10}H_{16}N_2O_8$	50.0	292	0.00017123	0.010616	
	Sodium nitrate	$NaNO_3$	250.0	85	0.00294118	0.182353	
P ($Mr_{(PO4)3-}$ = 95)	Potassium phosphate monobasic	KH_2PO4	175.0	136	0.00128677	0.122243	0.16319
	Potassium phosphate dibasic	K_2HPO_4	75.0	174	0.00043103	0.040948	

Pictures of the set-up

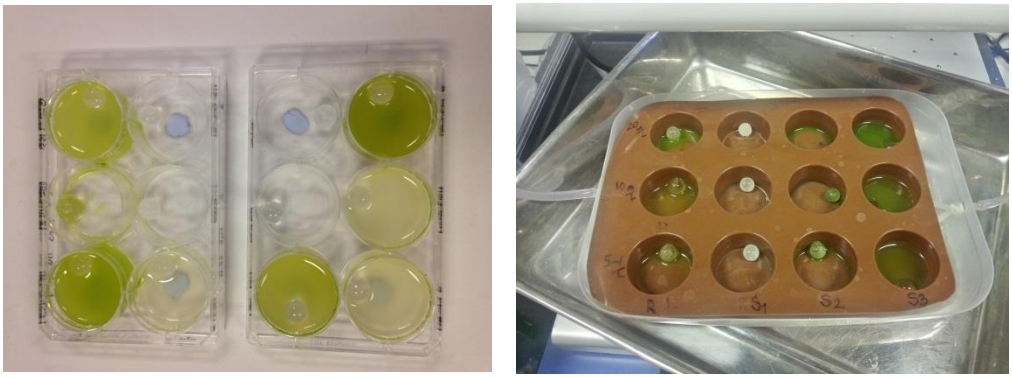

Figure V.1. Multi-well plates used for the experiments. Left: transparent plates from the CO2 preliminary experiments, Right: non-transparent silicon tray from the factorial experiments.

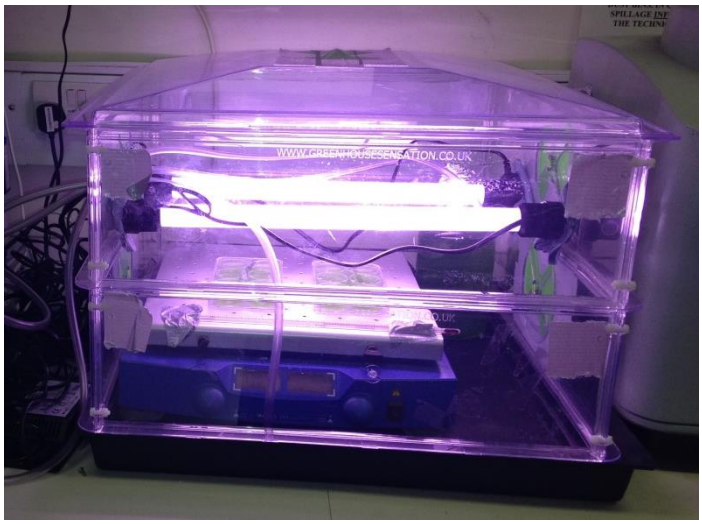

Figure V.2. Greenhouse box.

Calibration curves of the spectrophotometers for *Chlorella sorokiniana* cultures

The measurements of the biomass ODs, and their corresponding dry weight and concentrations are shown in Table V.2. Some optical densities were by mistake measured when the cuvette was oriented vertically to the orientation suggested in the specifications (light passing through the non-arrow side), thus these data were also converted to dry biomass using the same procedure. Calibration curves are shown in Figure V.3. The equation used to convert the optical density measurements from the Camspec spectrophotometer (using the arrow side of the cuvettes) is the following.

The difference of Lizzul's method is that the samples to be measured were diluted in order to always maintain an optical density below 0.8, due to the spectrophotometer's precision requirements. This dilution was not realised during the experiments and calibration measurements, hence, the calibration Eq.91 was used. The implication of following this method is mainly the accuracy of the optical density measurementswhich at high biomass concentration could be responsible for an incorrect exponential calibration curve's shape, instead of the linear suggested by Lambert-Beer law (Myers et al., 2013). It gave a difference of up to 70 % from a linear curve produced by fellow doctoral student Alessandro Marco Lizzul, although having an RMSE greater than 0.99. On top of that, the Thermo Electron UV/Vis

Spectrophotometer was last calibrated in 2002, which might have caused significant errors to the optical densities of Series 1 Try 2, Series 4 and the last day of Series 3.

$$C_b = 0.0492e^{1.7944 \cdot OD} \quad (91)$$

During the period February 2nd to 13th when the spectrophotometer was being serviced, a Thermo Electron UV/Vis Spectrometer was used for Series 1 Try 2, Series 4 and the last day of Series 3, with conversion of optical density based on a separate calibration curve. The calibration curves for conversion of optical density to biomass concentration for the two spectrophotometers are all shown in Table V.2, Table V.3, Table V.4, Figure V.3 and Figure V.4.

Table V.2. *Chlorella* biomass dry weight and optical density (OD) measurements with Campspec for the calibration curve.

OD arrow side	**OD non-arrow side**	**Volume Filtered (ml)**	**Dry Biomass (g)**	**Biomass Concentration (g/L)**
0.2881	0.1415	200	0.0162	0.081
0.6195	0.3747	100	0.0162	0.162
1.2390	0.7493	98.5	0.0381	0.387
1.5600		100	0.0897	0.897
1.9730		100	0.1693	1.693

Table V.3. Camspec spectrophotometer calibration curve data (optical density, OD) measured by Alessandro Marco Lizzul.

OD	**Biomass Concentration (g/L)**
0.134	0.004
0.778	0.100
2.496	0.520
4.124	0.840
4.64	0.928
9.164	2.246

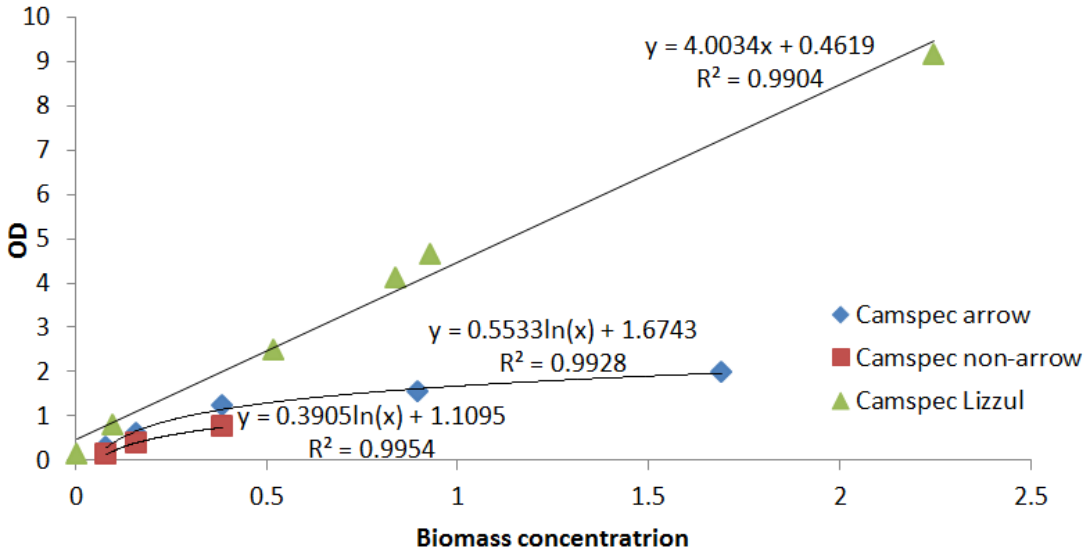

Figure V.3. *Chlorella* biomass measurement calibration curve.

Table V.4. Conversion between the optical densities (OD) of the two spectrophotometers used.

Thermo Electron UV/Vis Spectrometer OD readings	Camspec M550 Double Beam UV/V Spectrophotometer OD
0.665	0.4826
0.701	0.5072
0.623	0.4946
0.36	0.459
0.746	0.54
0.556	0.4035
1.904	1.4396

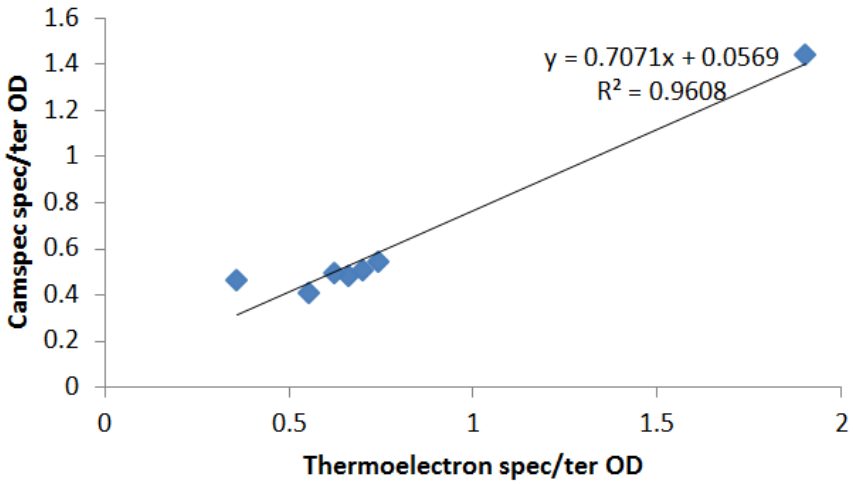

Figure V.4. Optical density values measured with the two spectrophotometers and the conversion equation.

Pictures of the set-up (continued)

Figure V.5. Sealable vessel for the measurement of the highest CO_2 concentration used in the preliminary experiments.

gPROMS script for the full kinetic model form

```
VARIABLE
maint    AS Maintenance_Algal
m_N      AS Maintenance_Consumpt
m_P      AS Maintenance_Consumpt
K_N      AS Half_Saturation_Con_Substrate
K_P      AS Half_Saturation_Con_Substrate
Y_bN     AS Yield_Substrate
Y_bP     AS Yield_Substrate
m_max    AS Growth_Rate
K_I      AS Light_Utilisation_Effic
K_CO2    AS Half_Saturation_Con_CO2
K_i_CO2  AS Inhibition_Con_CO2
C_CO2    AS Concentration_CO2
I_0      AS Illumination_Average
K_a      AS Light_Absorption_Coeff
L_to_m3  AS L_to_m3
R        AS Gas_constant
T        AS Temperature
T_opt    AS Temperature
E_a      AS Activation_Energy
Dil      AS Dilution_rate
C_N0     AS Concentration_Substrate
C_P0     AS Concentration_Substrate
d        AS Radial_Distance
C_B    AS Concentration_Biomass
```

```
m     AS Growth_Rate
C_N   AS Concentration_Substrate
C_P   AS Concentration_Substrate
f_N   AS Efficiency_Factor
f_P   AS Efficiency_Factor
f_I     AS Efficiency_Factor
I_av    AS Illumination_Average
C_CO2_D AS Concentration_CO2_Dissolved
k_H     AS Henry_Constant_CO2
f_T     AS Efficiency_Factor
f_CO2   AS Efficiency_Factor


EQUATION
# Efficiency factors
f_N=C_N/(K_N+C_N);
f_P=C_P/(K_P+C_P);
I_av=I_0*((1-exp(-K_a*L_to_m3*C_B*d))/(K_a*L_to_m3*C_B*d));
f_I=I_av/(K_I+I_av);
f_T=(2*exp((E_a*(T-T_opt))/(R*T*T_opt)))/(1+((exp((E_a*(T-
T_opt))/(R*T*T_opt)))^2));
k_H=exp(-8.1403+(842.9/(T+151.5)));
C_CO2_D=k_H*C_CO2;
f_CO2=C_CO2_D/(K_CO2+C_CO2_D+(C_CO2_D^2/K_i_CO2));

# Substrate&CO2&light growth rate
m=m_max*f_N*f_P*f_I*f_T*f_CO2;

# Cell Concentration
$C_B=C_B*(m-maint-Dil);

# Substrate concentration
-$C_N=((1/Y_bN)*(C_B*m))+(m_N*C_B)-((1/Y_bN)*Dil*(C_N0-C_N));
-$C_P=((1/Y_bP)*(C_B*m))+(m_P*C_B)-((1/Y_bP)*Dil*(C_P0-C_P));
```

gPROMS script for the simple kinetic model form

```
VARIABLE
maint     AS Maintenance_Algal
m_S       AS Maintenance_Consumpt
K_S       AS Half_Saturation_Con_Substrate
Y_bS      AS Yield_Substrate
K_I       AS Light_Utilisation_Effic
I_0_1       AS Illumination_Average
I_0_2       AS Illumination_Average
I_0_3       AS Illumination_Average
I_0_4       AS Illumination_Average
K_a       AS Light_Absorption_Coeff
L_to_m3   AS L_to_m3
R         AS Gas_constant
T_1         AS Temperature
T_2         AS Temperature
T_3         AS Temperature
T_4         AS Temperature
E_a       AS Activation_Energy
k_0       AS Preexponential_Factor
Dil       AS Dilution_rate
C_S0_05    AS Concentration_Substrate
C_S0_10   AS Concentration_Substrate
C_S0_20   AS Concentration_Substrate
d         AS Radial_Distance
```

```
f_S_1_05_S   AS Efficiency_Factor
f_S_1_05_R   AS Efficiency_Factor
f_S_1_10_S  AS Efficiency_Factor
f_S_1_10_R  AS Efficiency_Factor
f_S_1_20_S  AS Efficiency_Factor
f_S_1_20_R  AS Efficiency_Factor
I_av_1_05_S  AS Illumination_Average
I_av_1_05_R  AS Illumination_Average
I_av_1_10_S AS Illumination_Average
I_av_1_10_R AS Illumination_Average
I_av_1_20_S AS Illumination_Average
I_av_1_20_R AS Illumination_Average
f_I_1_05_S   AS Efficiency_Factor
f_I_1_05_R   AS Efficiency_Factor
f_I_1_10_S  AS Efficiency_Factor
f_I_1_10_R  AS Efficiency_Factor
f_I_1_20_S  AS Efficiency_Factor
f_I_1_20_R  AS Efficiency_Factor
f_T_1       AS Efficiency_Factor
m_1_05_S     AS Growth_Rate
m_1_05_R     AS Growth_Rate
m_1_10_S    AS Growth_Rate
m_1_10_R    AS Growth_Rate
m_1_20_S    AS Growth_Rate
m_1_20_R    AS Growth_Rate
C_B_1_05_S   AS Concentration_Biomass
C_B_1_05_R   AS Concentration_Biomass
C_B_1_10_S  AS Concentration_Biomass
C_B_1_10_R  AS Concentration_Biomass
C_B_1_20_S  AS Concentration_Biomass
C_B_1_20_R  AS Concentration_Biomass
C_S_1_05_S   AS Concentration_Substrate
C_S_1_05_R   AS Concentration_Substrate
C_S_1_10_S  AS Concentration_Substrate
C_S_1_10_R  AS Concentration_Substrate
C_S_1_20_S  AS Concentration_Substrate
C_S_1_20_R  AS Concentration_Substrate

f_S_2_05_S   AS Efficiency_Factor
f_S_2_05_R   AS Efficiency_Factor
f_S_2_10_S  AS Efficiency_Factor
f_S_2_10_R  AS Efficiency_Factor
f_S_2_20_S  AS Efficiency_Factor
f_S_2_20_R  AS Efficiency_Factor
I_av_2_05_S  AS Illumination_Average
I_av_2_05_R  AS Illumination_Average
I_av_2_10_S AS Illumination_Average
I_av_2_10_R AS Illumination_Average
I_av_2_20_S AS Illumination_Average
I_av_2_20_R AS Illumination_Average
f_I_2_05_S   AS Efficiency_Factor
f_I_2_05_R   AS Efficiency_Factor
f_I_2_10_S  AS Efficiency_Factor
f_I_2_10_R  AS Efficiency_Factor
f_I_2_20_S  AS Efficiency_Factor
f_I_2_20_R  AS Efficiency_Factor
f_T_2       AS Efficiency_Factor
m_2_05_S     AS Growth_Rate
m_2_05_R     AS Growth_Rate
m_2_10_S    AS Growth_Rate
m_2_10_R    AS Growth_Rate
m_2_20_S    AS Growth_Rate
m_2_20_R    AS Growth_Rate
C_B_2_05_S   AS Concentration_Biomass
C_B_2_05_R   AS Concentration_Biomass
C_B_2_10_S  AS Concentration_Biomass
C_B_2_10_R  AS Concentration_Biomass
```

```
C_B_2_20_S  AS Concentration_Biomass
C_B_2_20_R  AS Concentration_Biomass
C_S_2_05_S   AS Concentration_Substrate
C_S_2_05_R   AS Concentration_Substrate
C_S_2_10_S  AS Concentration_Substrate
C_S_2_10_R  AS Concentration_Substrate
C_S_2_20_S  AS Concentration_Substrate
C_S_2_20_R  AS Concentration_Substrate

f_S_3_05_S   AS Efficiency_Factor
#f_S_3_05_R   AS Efficiency_Factor
f_S_3_10_S  AS Efficiency_Factor
#f_S_3_10_R  AS Efficiency_Factor
f_S_3_20_S  AS Efficiency_Factor
#f_S_3_20_R  AS Efficiency_Factor
I_av_3_05_S  AS Illumination_Average
#I_av_3_05_R  AS Illumination_Average
I_av_3_10_S AS Illumination_Average
#I_av_3_10_R AS Illumination_Average
I_av_3_20_S AS Illumination_Average
#I_av_3_20_R AS Illumination_Average
f_I_3_05_S   AS Efficiency_Factor
#f_I_3_05_R   AS Efficiency_Factor
f_I_3_10_S  AS Efficiency_Factor
#f_I_3_10_R  AS Efficiency_Factor
f_I_3_20_S  AS Efficiency_Factor
#f_I_3_20_R  AS Efficiency_Factor
f_T_3       AS Efficiency_Factor
m_3_05_S     AS Growth_Rate
#m_3_05_R     AS Growth_Rate
m_3_10_S    AS Growth_Rate
#m_3_10_R    AS Growth_Rate
m_3_20_S    AS Growth_Rate
#m_3_20_R    AS Growth_Rate
C_B_3_05_S   AS Concentration_Biomass
#C_B_3_05_R   AS Concentration_Biomass
C_B_3_10_S  AS Concentration_Biomass
#C_B_3_10_R  AS Concentration_Biomass
C_B_3_20_S  AS Concentration_Biomass
#C_B_3_20_R  AS Concentration_Biomass
C_S_3_05_S   AS Concentration_Substrate
#C_S_3_05_R   AS Concentration_Substrate
C_S_3_10_S  AS Concentration_Substrate
#C_S_3_10_R  AS Concentration_Substrate
C_S_3_20_S  AS Concentration_Substrate
#C_S_3_20_R  AS Concentration_Substrate

f_S_4_05_S   AS Efficiency_Factor
f_S_4_05_R   AS Efficiency_Factor
f_S_4_10_S  AS Efficiency_Factor
f_S_4_10_R  AS Efficiency_Factor
f_S_4_20_S  AS Efficiency_Factor
f_S_4_20_R  AS Efficiency_Factor
I_av_4_05_S  AS Illumination_Average
I_av_4_05_R  AS Illumination_Average
I_av_4_10_S AS Illumination_Average
I_av_4_10_R AS Illumination_Average
I_av_4_20_S AS Illumination_Average
I_av_4_20_R AS Illumination_Average
f_I_4_05_S   AS Efficiency_Factor
f_I_4_05_R   AS Efficiency_Factor
f_I_4_10_S  AS Efficiency_Factor
f_I_4_10_R  AS Efficiency_Factor
f_I_4_20_S  AS Efficiency_Factor
f_I_4_20_R  AS Efficiency_Factor
f_T_4       AS Efficiency_Factor
m_4_05_S     AS Growth_Rate
```

```
m_4_05_R     AS Growth_Rate
m_4_10_S    AS Growth_Rate
m_4_10_R    AS Growth_Rate
m_4_20_S    AS Growth_Rate
m_4_20_R    AS Growth_Rate
C_B_4_05_S   AS Concentration_Biomass
C_B_4_05_R   AS Concentration_Biomass
C_B_4_10_S  AS Concentration_Biomass
C_B_4_10_R  AS Concentration_Biomass
C_B_4_20_S  AS Concentration_Biomass
C_B_4_20_R  AS Concentration_Biomass
C_S_4_05_S   AS Concentration_Substrate
C_S_4_05_R   AS Concentration_Substrate
C_S_4_10_S  AS Concentration_Substrate
C_S_4_10_R  AS Concentration_Substrate
C_S_4_20_S  AS Concentration_Substrate
C_S_4_20_R  AS Concentration_Substrate
mytime    AS timeline

EQUATION
# Efficiency factors
f_S_1_05_S=C_S_1_05_S/(K_S+C_S_1_05_S);
f_S_1_05_R=C_S_1_05_R/(K_S+C_S_1_05_R);
f_S_1_10_S=C_S_1_10_S/(K_S+C_S_1_10_S);
f_S_1_10_R=C_S_1_10_R/(K_S+C_S_1_10_R);
f_S_1_20_S=C_S_1_20_S/(K_S+C_S_1_20_S);
f_S_1_20_R=C_S_1_20_R/(K_S+C_S_1_20_R);
I_av_1_05_S=I_0_1*((1-exp(-
K_a*L_to_m3*C_B_1_05_S*d))/(K_a*L_to_m3*C_B_1_05_S*d));
I_av_1_05_R=I_0_1*((1-exp(-
K_a*L_to_m3*C_B_1_05_R*d))/(K_a*L_to_m3*C_B_1_05_R*d));
I_av_1_10_S=I_0_1*((1-exp(-
K_a*L_to_m3*C_B_1_10_S*d))/(K_a*L_to_m3*C_B_1_10_S*d));
I_av_1_10_R=I_0_1*((1-exp(-
K_a*L_to_m3*C_B_1_10_R*d))/(K_a*L_to_m3*C_B_1_10_R*d));
I_av_1_20_S=I_0_1*((1-exp(-
K_a*L_to_m3*C_B_1_20_S*d))/(K_a*L_to_m3*C_B_1_20_S*d));
I_av_1_20_R=I_0_1*((1-exp(-
K_a*L_to_m3*C_B_1_20_R*d))/(K_a*L_to_m3*C_B_1_20_R*d));
f_I_1_05_S=I_av_1_05_S/(K_I+I_av_1_05_S);
f_I_1_05_R=I_av_1_05_R/(K_I+I_av_1_05_R);
f_I_1_10_S=I_av_1_10_S/(K_I+I_av_1_10_S);
f_I_1_10_R=I_av_1_10_R/(K_I+I_av_1_10_R);
f_I_1_20_S=I_av_1_20_S/(K_I+I_av_1_20_S);
f_I_1_20_R=I_av_1_20_R/(K_I+I_av_1_20_R);
f_T_1=k_0*exp(-E_a/R/T_1);

# Substrate&CO2&light growth rate
m_1_05_S=f_S_1_05_S*f_I_1_05_S*f_T_1;
m_1_05_R=f_S_1_05_R*f_I_1_05_R*f_T_1;
m_1_10_S=f_S_1_10_S*f_I_1_10_S*f_T_1;
m_1_10_R=f_S_1_10_R*f_I_1_10_R*f_T_1;
m_1_20_S=f_S_1_20_S*f_I_1_20_S*f_T_1;
m_1_20_R=f_S_1_20_R*f_I_1_20_R*f_T_1;

# Cell Concentration
$C_B_1_05_S=C_B_1_05_S*(m_1_05_S-maint-Dil);
$C_B_1_05_R=C_B_1_05_R*(m_1_05_R-maint-Dil);
$C_B_1_10_S=C_B_1_10_S*(m_1_10_S-maint-Dil);
$C_B_1_10_R=C_B_1_10_R*(m_1_10_R-maint-Dil);
$C_B_1_20_S=C_B_1_20_S*(m_1_20_S-maint-Dil);
$C_B_1_20_R=C_B_1_20_R*(m_1_20_R-maint-Dil);

# Substrate concentration
-$C_S_1_05_S=((1/Y_bS)*(C_B_1_05_S*m_1_05_S))+(m_S*C_B_1_05_S)-
((1/Y_bS)*Dil*(C_S0_05-C_S_1_05_S));
```

```
-$C_S_1_05_R=((1/Y_bS)*(C_B_1_05_R*m_1_05_R))+(m_S*C_B_1_05_R)-
((1/Y_bS)*Dil*(C_S0_05-C_S_1_05_R));
-$C_S_1_10_S=((1/Y_bS)*(C_B_1_10_S*m_1_10_S))+(m_S*C_B_1_10_S)-
((1/Y_bS)*Dil*(C_S0_10-C_S_1_10_S));
-$C_S_1_10_R=((1/Y_bS)*(C_B_1_10_R*m_1_10_R))+(m_S*C_B_1_10_R)-
((1/Y_bS)*Dil*(C_S0_10-C_S_1_10_R));
-$C_S_1_20_S=((1/Y_bS)*(C_B_1_20_S*m_1_20_S))+(m_S*C_B_1_20_S)-
((1/Y_bS)*Dil*(C_S0_20-C_S_1_20_S));
-$C_S_1_20_R=((1/Y_bS)*(C_B_1_20_R*m_1_20_R))+(m_S*C_B_1_20_R)-
((1/Y_bS)*Dil*(C_S0_20-C_S_1_20_R));


#Experiment 2
# Efficiency factors
f_S_2_05_S=C_S_2_05_S/(K_S+C_S_2_05_S);
f_S_2_05_R=C_S_2_05_R/(K_S+C_S_2_05_R);
f_S_2_10_S=C_S_2_10_S/(K_S+C_S_2_10_S);
f_S_2_10_R=C_S_2_10_R/(K_S+C_S_2_10_R);
f_S_2_20_S=C_S_2_20_S/(K_S+C_S_2_20_S);
f_S_2_20_R=C_S_2_20_R/(K_S+C_S_2_20_R);
I_av_2_05_S=I_0_2*((1-exp(-
K_a*L_to_m3*C_B_2_05_S*d))/(K_a*L_to_m3*C_B_2_05_S*d));
I_av_2_05_R=I_0_2*((1-exp(-
K_a*L_to_m3*C_B_2_05_R*d))/(K_a*L_to_m3*C_B_2_05_R*d));
I_av_2_10_S=I_0_2*((1-exp(-
K_a*L_to_m3*C_B_2_10_S*d))/(K_a*L_to_m3*C_B_2_10_S*d));
I_av_2_10_R=I_0_2*((1-exp(-
K_a*L_to_m3*C_B_2_10_R*d))/(K_a*L_to_m3*C_B_2_10_R*d));
I_av_2_20_S=I_0_2*((1-exp(-
K_a*L_to_m3*C_B_2_20_S*d))/(K_a*L_to_m3*C_B_2_20_S*d));
I_av_2_20_R=I_0_2*((1-exp(-
K_a*L_to_m3*C_B_2_20_R*d))/(K_a*L_to_m3*C_B_2_20_R*d));
f_I_2_05_S=I_av_2_05_S/(K_I+I_av_2_05_S);
f_I_2_05_R=I_av_2_05_R/(K_I+I_av_2_05_R);
f_I_2_10_S=I_av_2_10_S/(K_I+I_av_2_10_S);
f_I_2_10_R=I_av_2_10_R/(K_I+I_av_2_10_R);
f_I_2_20_S=I_av_2_20_S/(K_I+I_av_2_20_S);
f_I_2_20_R=I_av_2_20_R/(K_I+I_av_2_20_R);
f_T_2=k_0*exp(-E_a/R/T_2);

# Substrate&CO2&light growth rate
m_2_05_S=f_S_2_05_S*f_I_2_05_S*f_T_2;
m_2_05_R=f_S_2_05_R*f_I_2_05_R*f_T_2;
m_2_10_S=f_S_2_10_S*f_I_2_10_S*f_T_2;
m_2_10_R=f_S_2_10_R*f_I_2_10_R*f_T_2;
m_2_20_S=f_S_2_20_S*f_I_2_20_S*f_T_2;
m_2_20_R=f_S_2_20_R*f_I_2_20_R*f_T_2;

# Cell Concentration
$C_B_2_05_S=C_B_2_05_S*(m_2_05_S-maint-Dil);
$C_B_2_05_R=C_B_2_05_R*(m_2_05_R-maint-Dil);
$C_B_2_10_S=C_B_2_10_S*(m_2_10_S-maint-Dil);
$C_B_2_10_R=C_B_2_10_R*(m_2_10_R-maint-Dil);
$C_B_2_20_S=C_B_2_20_S*(m_2_20_S-maint-Dil);
$C_B_2_20_R=C_B_2_20_R*(m_2_20_R-maint-Dil);

# Substrate concentration
-$C_S_2_05_S=((1/Y_bS)*(C_B_2_05_S*m_2_05_S))+(m_S*C_B_2_05_S)-
((1/Y_bS)*Dil*(C_S0_05-C_S_2_05_S));
-$C_S_2_05_R=((1/Y_bS)*(C_B_2_05_R*m_2_05_R))+(m_S*C_B_2_05_R)-
((1/Y_bS)*Dil*(C_S0_05-C_S_2_05_R));
-$C_S_2_10_S=((1/Y_bS)*(C_B_2_10_S*m_2_10_S))+(m_S*C_B_2_10_S)-
((1/Y_bS)*Dil*(C_S0_10-C_S_2_10_S));
-$C_S_2_10_R=((1/Y_bS)*(C_B_2_10_R*m_2_10_R))+(m_S*C_B_2_10_R)-
((1/Y_bS)*Dil*(C_S0_10-C_S_2_10_R));
-$C_S_2_20_S=((1/Y_bS)*(C_B_2_20_S*m_2_20_S))+(m_S*C_B_2_20_S)-
((1/Y_bS)*Dil*(C_S0_20-C_S_2_20_S));
```

```
-$C_S_2_20_R=((1/Y_bS)*(C_B_2_20_R*m_2_20_R))+(m_S*C_B_2_20_R)-
((1/Y_bS)*Dil*(C_S0_20-C_S_2_20_R));

#Experiment 3
# Efficiency factors
f_S_3_05_S=C_S_3_05_S/(K_S+C_S_3_05_S);
#f_S_3_05_R=C_S_3_c05_R/(K_S+C_S_3_c05_R);
f_S_3_10_S=C_S_3_10_S/(K_S+C_S_3_10_S);
#f_S_3_10_R=C_S_3_c10_R/(K_S+C_S_3_c10_R);
f_S_3_20_S=C_S_3_20_S/(K_S+C_S_3_20_S);
#f_S_3_20_R=C_S_3_c20_R/(K_S+C_S_3_c20_R);
I_av_3_05_S=I_0_3*((1-exp(-
K_a*L_to_m3*C_B_3_05_S*d))/(K_a*L_to_m3*C_B_3_05_S*d));
#I_av_3_05_R=I_0_3*((1-exp(-
K_a*L_to_m3*C_B_3_05_R*d))/(K_a*L_to_m3*C_B_3_05_R*d));
I_av_3_10_S=I_0_3*((1-exp(-
K_a*L_to_m3*C_B_3_10_S*d))/(K_a*L_to_m3*C_B_3_10_S*d));
#I_av_3_10_R=I_0_3*((1-exp(-
K_a*L_to_m3*C_B_3_10_R*d))/(K_a*L_to_m3*C_B_3_10_R*d));
I_av_3_20_S=I_0_3*((1-exp(-
K_a*L_to_m3*C_B_3_20_S*d))/(K_a*L_to_m3*C_B_3_20_S*d));
#I_av_3_20_R=I_0_3*((1-exp(-
K_a*L_to_m3*C_B_3_20_R*d))/(K_a*L_to_m3*C_B_3_20_R*d));
f_I_3_05_S=I_av_3_05_S/(K_I+I_av_3_05_S);
#f_I_3_05_R=I_av_3_05_R/(K_I+I_av_3_05_R);
f_I_3_10_S=I_av_3_10_S/(K_I+I_av_3_10_S);
#f_I_3_10_R=I_av_3_10_R/(K_I+I_av_3_10_R);
f_I_3_20_S=I_av_3_20_S/(K_I+I_av_3_20_S);
#f_I_3_20_R=I_av_3_20_R/(K_I+I_av_3_20_R);
f_T_3=k_0*exp(-E_a/R/T_3);

# Substrate&CO2&light growth rate
m_3_05_S=f_S_3_05_S*f_I_3_05_S*f_T_3;
#m_3_05_R=f_S_3_05_R*f_I_3_05_R*f_T_3;
m_3_10_S=f_S_3_10_S*f_I_3_10_S*f_T_3;
#m_3_10_R=f_S_3_10_R*f_I_3_10_R*f_T_3;
m_3_20_S=f_S_3_20_S*f_I_3_20_S*f_T_3;
#m_3_20_R=f_S_3_20_R*f_I_3_20_R*f_T_3;

# Cell Concentration
$C_B_3_05_S=C_B_3_05_S*(m_3_05_S-maint-Dil);
#$C_B_3_05_R=C_B_3_05_R*(m_3_05_R-maint-Dil);
$C_B_3_10_S=C_B_3_10_S*(m_3_10_S-maint-Dil);
#$C_B_3_10_R=C_B_3_10_R*(m_3_10_R-maint-Dil);
$C_B_3_20_S=C_B_3_20_S*(m_3_20_S-maint-Dil);
#$C_B_3_20_R=C_B_3_20_R*(m_3_20_R-maint-Dil);

# Substrate concentration
-$C_S_3_05_S=((1/Y_bS)*(C_B_3_05_S*m_3_05_S))+(m_S*C_B_3_05_S)-
((1/Y_bS)*Dil*(C_S0_05-C_S_3_05_S));
#-$C_S_3_05_R=((1/Y_bS)*(C_B_3_c05_R*m_3_c05_R))+(m_S*C_B_3_c05_R)-
((1/Y_bS)*Dil*(C_S0_05-C_S_3_05_R));
-$C_S_3_10_S=((1/Y_bS)*(C_B_3_10_S*m_3_10_S))+(m_S*C_B_3_10_S)-
((1/Y_bS)*Dil*(C_S0_10-C_S_3_10_S));
#-$C_S_3_10_R=((1/Y_bS)*(C_B_3_c10_R*m_3_c10_R))+(m_S*C_B_3_c10_R)-
((1/Y_bS)*Dil*(C_S0_10-C_S_3_10_R));
-$C_S_3_20_S=((1/Y_bS)*(C_B_3_20_S*m_3_20_S))+(m_S*C_B_3_20_S)-
((1/Y_bS)*Dil*(C_S0_20-C_S_3_20_S));
#-$C_S_3_20_R=((1/Y_bS)*(C_B_3_c20_R*m_3_c20_R))+(m_S*C_B_3_c20_R)-
((1/Y_bS)*Dil*(C_S0_20-C_S_3_20_R));

#Experiment 4
# Efficiency factors
f_S_4_05_S=C_S_4_05_S/(K_S+C_S_4_05_S);
f_S_4_05_R=C_S_4_05_R/(K_S+C_S_4_05_R);
f_S_4_10_S=C_S_4_10_S/(K_S+C_S_4_10_S);
f_S_4_10_R=C_S_4_10_R/(K_S+C_S_4_10_R);
```

```
f_S_4_20_S=C_S_4_20_S/(K_S+C_S_4_20_S);
f_S_4_20_R=C_S_4_20_R/(K_S+C_S_4_20_R);
I_av_4_05_S=I_0_4*((1-exp(-
K_a*L_to_m3*C_B_4_05_S*d))/(K_a*L_to_m3*C_B_4_05_S*d));
I_av_4_05_R=I_0_4*((1-exp(-
K_a*L_to_m3*C_B_4_05_R*d))/(K_a*L_to_m3*C_B_4_05_R*d));
I_av_4_10_S=I_0_4*((1-exp(-
K_a*L_to_m3*C_B_4_10_S*d))/(K_a*L_to_m3*C_B_4_10_S*d));
I_av_4_10_R=I_0_4*((1-exp(-
K_a*L_to_m3*C_B_4_10_R*d))/(K_a*L_to_m3*C_B_4_10_R*d));
I_av_4_20_S=I_0_4*((1-exp(-
K_a*L_to_m3*C_B_4_20_S*d))/(K_a*L_to_m3*C_B_4_20_S*d));
I_av_4_20_R=I_0_4*((1-exp(-
K_a*L_to_m3*C_B_4_20_R*d))/(K_a*L_to_m3*C_B_4_20_R*d));
f_I_4_05_S=I_av_4_05_S/(K_I+I_av_4_05_S);
f_I_4_05_R=I_av_4_05_R/(K_I+I_av_4_05_R);
f_I_4_10_S=I_av_4_10_S/(K_I+I_av_4_10_S);
f_I_4_10_R=I_av_4_10_R/(K_I+I_av_4_10_R);
f_I_4_20_S=I_av_4_20_S/(K_I+I_av_4_20_S);
f_I_4_20_R=I_av_4_20_R/(K_I+I_av_4_20_R);
f_T_4=k_0*exp(-E_a/R/T_4);

# Substrate&CO2&light growth rate
m_4_05_S=f_S_4_05_S*f_I_4_05_S*f_T_4;
m_4_05_R=f_S_4_05_R*f_I_4_05_R*f_T_4;
m_4_10_S=f_S_4_10_S*f_I_4_10_S*f_T_4;
m_4_10_R=f_S_4_10_R*f_I_4_10_R*f_T_4;
m_4_20_S=f_S_4_20_S*f_I_4_20_S*f_T_4;
m_4_20_R=f_S_4_20_R*f_I_4_20_R*f_T_4;

# Cell Concentration
$C_B_4_05_S=C_B_4_05_S*(m_4_05_S-maint-Dil);
$C_B_4_05_R=C_B_4_05_R*(m_4_05_R-maint-Dil);
$C_B_4_10_S=C_B_4_10_S*(m_4_10_S-maint-Dil);
$C_B_4_10_R=C_B_4_10_R*(m_4_10_R-maint-Dil);
$C_B_4_20_S=C_B_4_20_S*(m_4_20_S-maint-Dil);
$C_B_4_20_R=C_B_4_20_R*(m_4_20_R-maint-Dil);

# Substrate concentration
-$C_S_4_05_S=((1/Y_bS)*(C_B_4_05_S*m_4_05_S))+(m_S*C_B_4_05_S)-
((1/Y_bS)*Dil*(C_S0_05-C_S_4_05_S));
-$C_S_4_05_R=((1/Y_bS)*(C_B_4_05_R*m_4_05_R))+(m_S*C_B_4_05_R)-
((1/Y_bS)*Dil*(C_S0_05-C_S_4_05_R));
-$C_S_4_10_S=((1/Y_bS)*(C_B_4_10_S*m_4_10_S))+(m_S*C_B_4_10_S)-
((1/Y_bS)*Dil*(C_S0_10-C_S_4_10_S));
-$C_S_4_10_R=((1/Y_bS)*(C_B_4_10_R*m_4_10_R))+(m_S*C_B_4_10_R)-
((1/Y_bS)*Dil*(C_S0_10-C_S_4_10_R));
-$C_S_4_20_S=((1/Y_bS)*(C_B_4_20_S*m_4_20_S))+(m_S*C_B_4_20_S)-
((1/Y_bS)*Dil*(C_S0_20-C_S_4_20_S));
-$C_S_4_20_R=((1/Y_bS)*(C_B_4_20_R*m_4_20_R))+(m_S*C_B_4_20_R)-
((1/Y_bS)*Dil*(C_S0_20-C_S_4_20_R));

$mytime=1;
```

Table V.5. Parameter values used in the literature and used as initial bounds for the parameter estimation.

Parameter	Value	Reference
μ_{max} [1/h]	0.8 d^{-1}	(Arrigo & Sullivan, 1994)
	0.7-1.3 d^{-1}	(Bernard & Rémond, 2010)
	0.046 h-1	(Molina Grima et al., 1994),
	0.025 h-1	(Quinn et al., 2011)
K_N [mol/m^3]	0.3 – 2.3 µM	(Arrigo & Sullivan, 1994)
	12.1 mg/L	(Xin et al., 2010)
	0.005 g/L	(Quinn et al., 2011)
K_P [mol/m^3]	0.3 & 2.3 µM	(Arrigo & Sullivan, 1994)
	0.27 mg/L	(Xin et al., 2010)
K_{CO2} [mol/m^3]	0.0003 mol/m3	(He et al., 2012)
	(=7.3 x 10^-6 L/L)	
K_I [µE/m^2/sec]	18 µE/m^2/s	(Arrigo & Sullivan, 1994)
	14 µmol/m^2/s	(He et al., 2012)
	94.3 µE/m^2/s	(Molina Grima et al., 1999)
K_a [m^2/g]	0.2	(Huesemann et al., 2013)
	0.127-0.233	(Vejrazka et al., 2011)
	0.0752	(Quinn et al., 2011)
E_a [J/mol]	75 – 85 kJ/mol	(Ribeiro et al., 2008)
	65 kJ/mol (grass)	(Koutsoumanis et al., 2000)
	85 – 222 kJ/mol (bacteria)	(Alexandrov & Yamagata, 2007)
	63 kJ/mol (microalgae)	(Giannuzzi et al., 1998)
	36 kJ/mol (microalgae)	(Quinn et al., 2011)
	36.72 kJ/mol	(Ashokkumar et al., 2014)
	75 – 85 kJ/mol	(Koutsoumanis et al., 2000)
T_{opt} [K]	298 K	(Alexandrov & Yamagata, 2007)
	300 K	(Zheng-Rong et al., 2010)
m_a [1/h]	0.005 h-1	(Cabello et al., 2014)
	0.000432 h-1	(Quinn et al., 2011)
	0.01800.03 h-1	(Ruiz et al., 2011)
	0.00385 h-1	(Molina Grima et al., 1994)
$m_{s/N}$[gsubstrate/g cells/h]	<2x10^{-4}	(Ruiz et al., 2011)
$Y_{b/N}$ [g/g]	0.65 g_b/g_{O2}	(Molina Grima et al., 1994)
	130	(Concas et al., 2012)
	11.51-49 gcells/gN	(Ruiz et al., 2011)
$m_{s/P}$[gsubstrate/g cells/h]	<2x10^{-4}	(Ruiz et al., 2011)
$Y_{b/P}$ [g/g]	0.2 g_b/g_{O2}	(Molina Grima et al., 1994)
	10.4	(Concas et al., 2012)
	0.046-470 gcells/gPO4	(Ruiz et al., 2011)
k_0 [1/h]	148-1.3E42 days-1 (bacteria)	(Giannuzzi et al., 1998)
	0.16-0.28 h-1	(Ribeiro et al., 2008)
	31/sec	(Ashokkumar et al., 2014)
K_S [mol/m^3]	0.27 mg/L	(Xin et al., 2010)
	0.3 – 2.3 µM	(Arrigo & Sullivan, 1994)
$Y_{b/S}$ [g/g]	0.0199 m2/g	(Molina Grima et al., 1994)
	0.6 g/g	(van Bodegom, 2007)
	470 gcells/gPO4	(Ruiz et al., 2011)
$m_{s/S}$[gsubstrate/g cells/h]	<2x10^{-4}	(Ruiz et al., 2011)

Table V.6. Average bounds used for the final stage parameter estimation for all the experiments.

	Lower bound	**Upper bound**
E_a	609	917500
K_A	0.00001	58.5833
K_{CO2}	2.51E-10	47.5833
K_I	1.71E-05	117.25
K_N	9.43E-09	0.01258
K_P	5.00E-07	0.05633
μ_{max}	0.020	0.16
m_N	8.53E-08	0.00025
m_P	0.000001	0.00092
m_a	0.00011	0.05426
T_{opt}	295	303
$Y_{b/N}$	0.93	12
$Y_{b/P}$	8.92	60

Experimental measurements

Table V.7. Sacrificial (S) and resampling (R) measurements of the different substances (in g/L) for the CO_2 experiments.

CO_2 experiment	Substance measured	Time (h)	Nutrient dilution 1:200		1:100		1:50	
			S	R	S	R	S	R
700 mg/L	Biomass	0	0.0710		0.0683		0.0805	
		23	0.1011	0.0978	0.0898	0.0896	0.0792	0.0747
		95	0.2341	0.2518	0.1702	0.2151	0.0914	0.1287
		167	0.2527	0.2542	0.3475	0.6316	0.5853	1.3624
	Nitrates	0	0.0705		0.0068		1.7295	
		23	0.0395	0.0401	0.1180	0.1341	0.3598	0.3550
		95	0.0019	0.0043	0.0032	0.0021	0.0360	0.0159
		167	0.0001	0.0029	0.0011	0.0050	0.0049	0.0057
	Phosphates	0	0.0502		0.0050		1.1708	
		23	0.0540	0.0621	0.1168	0.1344	0.2704	0.2425
		95	0.0482	0.0560	0.0998	0.1048	0.2049	0.2005
		167	0.0021	0.0684	0.0184	0.1621	0.2781	0.2765
4,300 mg/L	Biomass	0	0.1069		0.1083		0.1077	
		45	0.7286	0.6979	0.7800	0.8640	0.9761	0.9451
		94	0.4838	0.5323	0.7975	0.9319	1.1229	1.2569
	Nitrates	0	0.0599		0.6128		0.1648	
		45	0.0012	0.0101	0.0011	0.0033	0.0033	0.0047
		94	0.0012	0.0318	0.0005	0.0034	0.0007	0.0020
	Phosphates	0	0.0438		0.4294		0.1193	
		45	0.0105	0.0086	0.0162	0.0640	0.1332	0.1380
		94	0.0350	0.0549	0.0696	0.0710	0.1271	0.1049
50,000 mg/L	Biomass	0	0.1027		0.1016		0.1016	
		43	0.4963	0.5124	0.6306	0.6274	0.6306	0.6274
		89.5	0.3484	0.3668	0.5150	0.5423	0.5150	0.5423
		167	0.2354	0.1458	0.1804	0.4482	0.5069	0.5909
	Nitrates	0	0.1247		0.0379		0.0111	
		43	0	0.0010	0.0089	0.0094	0.0026	0.0162
		89.5	0.0019	0.0058	0.0020	0.0041	0.0091	0.0004
		167	0.0007	0.0007	0.0038	0.0095	0.0129	0.0138
	Phosphates	0	0.0848		0.0270		0.0320	
		43	0.0015	0.1451	0.1142	0.0607	0.0078	0.1142
		89.5	0.0113	0.1210	0.0200	0.2894	0.0549	0.0050
		167	0.0368	0.0037	0.1834	0.0539	0.0983	0.1024

Table V.8. Sacrificial (S) and resampling (R) measurements of the different substances (in g/L) for the factorial experiments.

Experiment substance measure		Time (h)	Nutrient dilution								
			5			10			20		
			S (A)	S (B)	R	S (A)	S (B)	R	S (A)	S (B)	R
Series 1, Try 1	Biomass	0.0	0.0946			0.1054			0.1011		
		41.5	0.4940		0.5284	0.5350		0.6728	0.7218		0.4619
		93.0	0.2635		0.1638	0.2196		0.1479	0.7212		0.6824
	Nitrates	0.0	0.0423			0.0693			0.1926		
		41.5	0.0097		0.0016	0.0144		0.0010	0.0037		0.0030
		93.0	0.0006		0.0000	0.0046		0.0262	0.0031		0.0053
	Phosphates	0.0	0.0136			0.0216			0.0619		
		41.5	0.0122		0.0153	0.0249		0.0159	0.0419		0.0797
		93.0	0.0084		0.0085	0.0331		0.0689	0.0345		0.0612
Series 1, Try 2	Biomass	0.0	0.0906		0.0920	0.0907		0.0925	0.0886		0.0928
		23.3	0.3211		0.3340	0.3768		0.3687	0.2912		0.2935
		47.0	0.4015		0.3711	0.5006		0.4371	0.5800		0.6071
		94.9	0.2890		0.1948	0.3577		0.1904	0.6087		0.4962
	Nitrates	0.0	0.0497	0.0443	0.0273	0.0856	0.0883	0.0690	0.1738	0.1951	0.1468
		23.3	0.0019	0.0000	0.0000	0.0589	0.0013	0.0015	0.0845	0.0562	0.0516
		47.0	0.0000	0.0135	0.0018	0.0000	0.0010	0.0030	0.0000	0.0000	0.0012
		94.9	0.0000	0.0015	0.0012	0.0000	0.0012	0.0000	0.0000	0.0000	0.0009
	Phosphates	0.0	0.0306	0.0388	0.0225	0.0586	0.0624	0.0488	0.1158	0.1346	0.0978
		23.3	0.0318	0.0302	0.0168	0.0956	0.0483	0.0486	0.1260	0.1006	0.1004
		47.0	0.0206	0.0258	0.0441	0.0391	0.0399	0.0369	0.0991	0.1061	0.0747
		94.9	0.0268	0.0239	0.0193	0.0371	0.0381	0.0302	0.0923	0.1010	0.0580
Series 2, Try 1	Biomass	0.0	0.0848		0.0830	0.0946		0.0898	0.0905		0.0800
		24.5	0.2802		0.3988	0.3210		0.3671	0.2969		0.3850
		46.0	0.5581		0.6784	0.6458		0.7794	0.7683		0.9724
	Nitrates	0.0	0.0502		0.0684	0.0850		0.0843	0.1701		0.1754
		24.5	0.0000		0.0101	0.0040		0.0000	0.0105		0.0994
		46.0	0.0000		0.0103	0.0044		0.0117	0.0043		0.0000
	Phosphates	0.0	0.0336		0.0444	0.0569		0.0506	0.1161		0.1116
		24.5	0.0306		0.0471	0.0492		0.0583	0.0062		0.1308
		46.0	0.0021		0.0368	0.0410		0.0467	0.0946		0.1051
Series 2, Try 2	Biomass	0.0	0.1170		0.1222	0.1195		0.1121	0.1297		0.1015
		20.9	0.3586		0.5162	0.3955		0.3485	0.3376		0.2110
		46.9	0.6758		0.6595	0.8131		0.8404	0.8968		0.6665
		117.3	0.5278		0.5699	0.7161		0.7390	1.4886		1.2145
	Nitrates	0.0	0.0715	0.0446	0.0424	0.1069	0.0930	0.0819	0.1555	0.1737	0.1762
		20.9	0.0005	0.0000	0.0000	0.0067	0.0054	0.0009	0.0893	0.0982	0.0643
		46.9	0.0000	0.0006	0.0000	0.0000	0.0014	0.0000	0.0000	0.0000	0.0000
		117.3	0.0011	0.0000	0.0051	0.0121	0.0000	0.0007	0.0012	0.0010	0.0013
	Phosphates	0.0	0.0565	0.0338	0.0366	0.0728	0.0705	0.0680	0.1081	0.1172	0.1089
		20.9	0.0367	0.0289	0.0285	0.0651	0.0640	0.0451	0.1124	0.1228	0.0901
		46.9	0.0249	0.0315	0.0212	0.0641	0.0650	0.0442	0.0951	0.0928	0.0833
		117.3	0.0195	0.0288	0.0134	0.0349	0.0424	0.0286	0.0719	0.0811	0.0778
Series 3	Biomass	0.0	0.0958		0.0964	0.1061		0.1064	0.0940		0.0948
		22.0	0.3172		0.3035	0.3437		0.2978	0.2475		0.2457
		41.8	0.6008		0.6976	0.8010		0.8147	0.7658		0.8177

		164.3	0.6884			0.7288			0.8222		
	Nitrates	0.0	0.0770	0.0726	0.0761	0.1156	0.1189	0.1115	0.2555	0.2397	0.1961
		22.0	0.0053	0.0056	0.0035	0.0059	0.0048	0.0132	0.1194	0.1191	0.1473
		41.8	0.0031	0.0029	0.0020	0.0026	0.0000	0.0000	0.0022	0.0029	0.0014
		164.3	0.0026	0.0020		0.0010	0.0021		0.0010	0.0015	
	Phosphates	0.0	0.0513	0.0495	0.0530	0.0768	0.0797	0.0747	0.1663	0.1548	0.1280
		22.0	0.0461	0.0607	0.0539	0.0805	0.0830	0.0769	0.1305	0.1392	0.1597
		41.8	0.0318	0.0277	0.0288	0.0347	0.0453	0.0435	0.0933	0.1069	0.0685
		164.3	0.0367	0.0362		0.0554	0.0592		0.0913	0.1001	
Series 4	Biomass	0.0	0.0984		0.0962	0.0897		0.0946	0.0984		0.0943
		22.4	0.3179		0.2782	0.2938		0.2872	0.2148		0.2283
		45.9	0.4155		0.3924	0.5142		0.5382	0.5423		0.5972
		93.6	0.3107		0.2097	0.5221		0.5749	0.7590		0.7875
	Nitrates	0.0	0.0800	0.0602	0.0508	0.0856	0.0697	0.0856	0.1801	0.1858	0.1257
		22.4	0.0052	0.0058	0.0294	0.0193	0.0000	0.0084	0.1023	0.0717	0.0565
		45.9	0.0032	0.0037	0.0471	0.0029	0.0019	0.0076	0.0136	0.0061	0.0027
		93.6	0.0000	0.0136	0.0027	0.0000	0.0085	0.0000	0.0000	0.0000	0.0039
	Phosphates	0.0	0.0449	0.0406	0.0437	0.0611	0.0520	0.0541	0.1265	0.1258	0.0883
		22.4	0.0406	0.0458	0.0517	0.0400	0.0491	0.0444	0.1226	0.1061	0.0743
		45.9	0.0261	0.0329	0.0514	0.0385	0.0405	0.0319	0.1277	0.0988	0.0790
		93.6	0.0000	0.0231	0.0110	0.0410	0.0502	0.0432	0.0818	0.0917	0.0555

Parameter Estimation of the full model

Figure V.8 to Figure V.11 plot the biomass and substrate dynamic behaviour according to each model that uses the parameters estimated with either correct or wrong bounds used in the estimation procedure. A significantly better fit to the biomass data is shown when relaxed bounds are used and some parameters take extreme values which might not be physically correct, so those values need to be checked with the literature if they are rational. Table V.9 Table V.14 show the parameters estimated from each case.

Table V.9. Parameters estimated from stage 1 for all the factorial (main) experiments.

	1:200 T20 I100	**1:200 T20 I150**	**1:200 T30 I100**	**1:200 T30 I150**	**1:100 T20 I100**	**1:100 T20 I150**	**1:100 T30 I100**	**1:100 T30 I150**	**1:50 T20 I100**	**1:50 T20 I150**	**1:50 T30 I100**	**1:50 T30 I150**
$(^{x10^{-6}})K_N$	21.377	5.903	4.971	58.014	6908.886	2855.088	0.252	10.000	74.921	99.893	9995.038	107.617
$(^{x10^{-3}})K_P$	0.0089	2.00	0.0217	25.989	83.660	0.00164	0.00174	0.00112	0.01485	0.01698	18.663	50.6335
μ_{max}	0.064	0.075	0.063	0.123	0.160	0.076	0.050	0.071	0.053	0.051	0.052	0.083
$(^{x10^{-10}})$ m_N	1.00	10000.0	10000.0	145.37	12.40	0.10	10.00	90.09	12207.80	999.04	0	3201.76
$(^{x10^{-7}})$ m_P	1.00	2000.00	2000.00	518.73	0	2000.00	0.00099	25.72	11.09	23.01	7953.24	7289.01
$(^{x10^{-3}})$ m_a	0.005	0.203	1.744	3.901	0.050	0.203	0.203	7.610	0.200	0.204	0.200	0.203
$Y_{b/N}$	4.20	7.00	4.47	7.12	2.82	4.41	3.55	5.14	2.62	3.65	3.07	2.61
$Y_{b/P}$	19.13	28.17	12.11	52.22	12.31	18.30	18.82	24.85	9.90	21.77	90.00	50.31

Table V.10. Parameters estimated from stage 2 for all the factorial (main) experiments.

	1:200 T20 I100	1:200 T20 I150	1:200 T30 I100	1:200 T30 I150	1:100 T20 I100	1:100 T20 I150	1:100 T30 I100	1:100 T30 I150	1:50 T20 I100	1:50 T20 I150	1:50 T30 I100	1:50 T30 I150
$(\times 10^{-2})K_a$	13.38	9.44	11.84	0.007	56.21	19.56	4.68	0.02	0.01	0.01	1.21E-7	5.00
K_I	2.85	1.0E-5	0.17	1.40	7.2E-12	1.0E-10	9.64	1.58E-4	1.21E-04	1.00	5.95E-03	4.02E-03
$(\times 10^{-6})K_N$	27.73	2.52	8.58	71.70	5993.58	521.68	0.82	10.33	82.97	99.89	90.01	115.75
$(\times 10^{-3})K_P$	8.898	1.666	3.584	33.90	0.001	26.461	1.0E-6	1.0E-9	0.015	0.017	3.0E-4	0.064
μ_{max}	0.079	0.056	0.076	0.140	0.164	0.100	0.068	0.071	0.051	0.040	0.041	0.056
$(\times 10^{-10})m_N$	1.00	2.0E6	0.60	100.00	0.66	0.10	10.00	100.00	18646.80	999.04	479.90	327.61
$(\times 10^{-7})m_P$	1.000	0.010	0.137	707.26	0.100	2000.00	0.001	0.002	11.21	23.01	7104.59	7253.33
$(\times 10^{-3})m_a$	0.100	2.030	2.181	3.737	0.050	0.103	0.203	7.610	0.199	0.204	0.200	0.200
$Y_{b/N}$	4.24	9.00	4.45	7.00	2.75	4.32	3.90	5.15	2.77	8.00	3.18	2.64
$Y_{b/P}$	18.98	30.00	6.89	53.15	12.19	18.17	19.97	25.16	10.33	38.00	67.33	55.20

Table V.11. Parameters estimated from stage 3 for all the CO_2 experiments (T30, I150).

	C700 1:50	C4,300 1:200	C4,300 1:100	C4,300 1:50	C50,000 1:200	C50,000 1:100
E_a	13442.00	1000.00	1000.00	1000.00	1.0E-11	2.16
$(\times 10^{-2})K_a$	4.28	1.00	0.63	6.96	1.0E-8	1.98E-3
$(\times 10^{-7})K_{CO2}$	100.00	5.17	1000.00	40.88	8.5E-16	3.5E-14
K_I	3.6E-03	1.000	1.0E-05	1.000	1.0E-05	1.0E-05
$(\times 10^{-7})K_N$	2.922	0.414	261.674	3.849	5.000	5.000
$(\times 10^{-7})K_P$	0.010	5.807	0.000001	0.000001	10.000	10.000
μ_{max}	0.120	0.120	0.121	0.150	0.208	0.208
$(\times 10^{-6})m_N$	2000.00	0.494	0.100	20.000	0.080	5.0E-5
$(\times 10^{-6})m_P$	2.00	2.00	1.36	1.36	70.00	10.0
$(\times 10^{-3})m_a$	0.0002	7.221	0.229	0.229	0.203	6.030
T_{opt}	302.4	297.7	297.0	297.0	305.0	299.0
$Y_{b/N}$	0.90	11.00	2.00	5.00	0.65	1.18
$Y_{b/P}$	2.59	21.00	7.00	80.00	80.00	200.00

Table V.12. Parameters estimated from stage 4 for all the factorial (main) experiments.

	1:200 T20 I100	**1:200 T20 I150**	**1:200 T30 I100**	**1:200 T30 I150**	**1:100 T20 I100**	**1:100 T20 I150**	**1:100 T30 I100**	**1:100 T30 I150**	**1:50 T20 I100**	**1:50 T20 I150**	**1:50 T30 I100**	**1:50 T30 I150**
E_a	2.0	421.7	22459.1	1000.0	59354.9	1000.0	1000.0	1000.0	1200.0	900.0	2.0	9995.8
($\times 10^{-2}$) K_a	13.53	100.76	4.69	0.007	0.006	19.56	4.68	0.019	0.010	0.010	1.2E-7	5.00
($\times 10^{-7}$) K_{CO2}	0.010	0.043	1.0E-5	1.0E-5	1.0E-4	1.0E-5	0.339	0.010	0.010	0.010	0.010	1.0E-5
K_I	2.857	1.0E-05	0.094	1.400	1.400	1.0E-10	1.0E-05	1.6E-04	1.2E-04	1.000	5.9E-03	4.0E-03
($\times 10^{-6}$) K_N	27.73	4.58	0.50	7.17	0.60	521.68	0.22	10.33	83.25	99.89	90.00	114.77
($\times 10^{-3}$) K_P	8.898	1.666	2.012	33.898	0.100	26.395	0.0015	1.0E-9	0.015	0.017	0.0003	0.064
μ_{max}	0.0794	0.056	0.062	0.140	0.154	0.100	0.071	0.071	0.051	0.040	0.041	0.056
($\times 10^{-10}$) m_N	1.00	10000000	0.60	100.00	661.63	0.10	10.0	100.00	18646.840	8999.04	479.90	327.61
($\times 10^{-7}$) m_P	1.0	2000.0	0.14	707.26	0.10	2000.0	0.001	0.002	11.2	23.0	7103.8	7253.3
$\times 10^{-3}$) m_a	0.100	2.030	0.207	3.737	3.000	0.103	0.203	7.610	0.199	0.204	0.200	0.201
T_{opt}	295.0	297.4	302.2	295.0	295.0	300.3	302.8	299.0	303.0	303.0	303.0	302.8
$Y_{b/N}$	4.23	9.00	3.67	7.00	6.00	4.32	2.77	5.15	2.77	8.00	3.18	2.63
$Y_{b/P}$	19.16	30.00	5.68	53.15	41.00	17.77	39.87	25.16	10.28	38.00	67.33	55.20

Table V.13. Parameters estimated from stage 5 for all the factorial (main) experiments.

	1:200 T20 I100	1:200 T20 I150	1:200 T30 I100	1:200 T30 I150	1:100 T20 I100	1:100 T20 I150	1:100 T30 I100	1:100 T30 I150	1:50 T20 I100	1:50 T20 I150	1:50 T30 I100	1:50 T30 I150
($\times 10^{-2}$) E_a	1000.0	1000.0	222.7	1000.0	531.6	10.0	10.1	10.0	12.0	9.0	25.9	7.0
($\times 10^{-2}$) K_a	3.526	5.000	4.694	0.007	0.006	19.6	4.681	0.017	0.016	17.128	50.00	1.272
($\times 10^{-7}$) K_{Cl}	0.3448	0.00001	0.00001	0.05857	15.900	0.00001	12.2713	0.0100	0.01384	0.0100	10.2947	22.7613
K_I	3.704E-05	1.954E-06	0.0939	1.40	1.40	1.000E-10	1.262E-05	1.418E-04	3.587E-05	1.0E-09	0.24849	1.013E-04
($\times 10^{-6}$) K_N	6.758	1.717	5.002	71.702	0.599	0.172	1.562	9.297	21.973	99.893	8.092	30.929
($\times 10^{-3}$) K_P	20.00	0.11	2.01	0.798	0.143	0.001	0.0015	1.00E-9	0.0148	0.001	0.0003	0.0179
μ_m	0.169	0.140	0.087	0.150	0.154	0.10	0.13	0.07	0.05	0.05	0.07	0.15
($\times 10^{-10}$) m_N	1.00	1000.00	0.60	100.00	661.63	0.10	10.00	100.00	18646.8	999.04	479.90	10.00
($\times 10^{-7}$) m_P	1.00	2.00	0.137	0.00007	168.5	2000.0	2.62	2000.0	11.21	23.01	710.38	5109.55
($\times 10^{-3}$) m_a	1.000	2.030	0.2072	3.193	0.050	0.0103	0.586	7.560	0.199	0.204	0.04400	0.1515
T_{op}	299.83	300.22	299.96	295.02	302.69	300.33	302.45	299.40	303.00	299.43	303.00	302.74
$Y_{b/}$	6.00	10.00	3.94	6.80	2.62	5.00	3.54	5.15	2.77	3.63	3.18	2.62
$Y_{b/}$	23.00	30.00	8.68	41.26	12.03	10.03	17.86	34.75	10.30	21.69	19.01	26.52

Table V.14. Parameters estimated from stage 6 for the 1:100 T20 I100 factorial (main) experiment tested.

Parameter	Estimated value
E_a	5.236E+04
K_a	1.00E-05
K_{CO2}	2.23E-06
K_I	0.100
K_P	0.0256
μ_{max}	0.1600
m_P	3.33E-04
m_a	5.00E-05
T_{opt}	302.47
$Y_{b/P}$	19.383

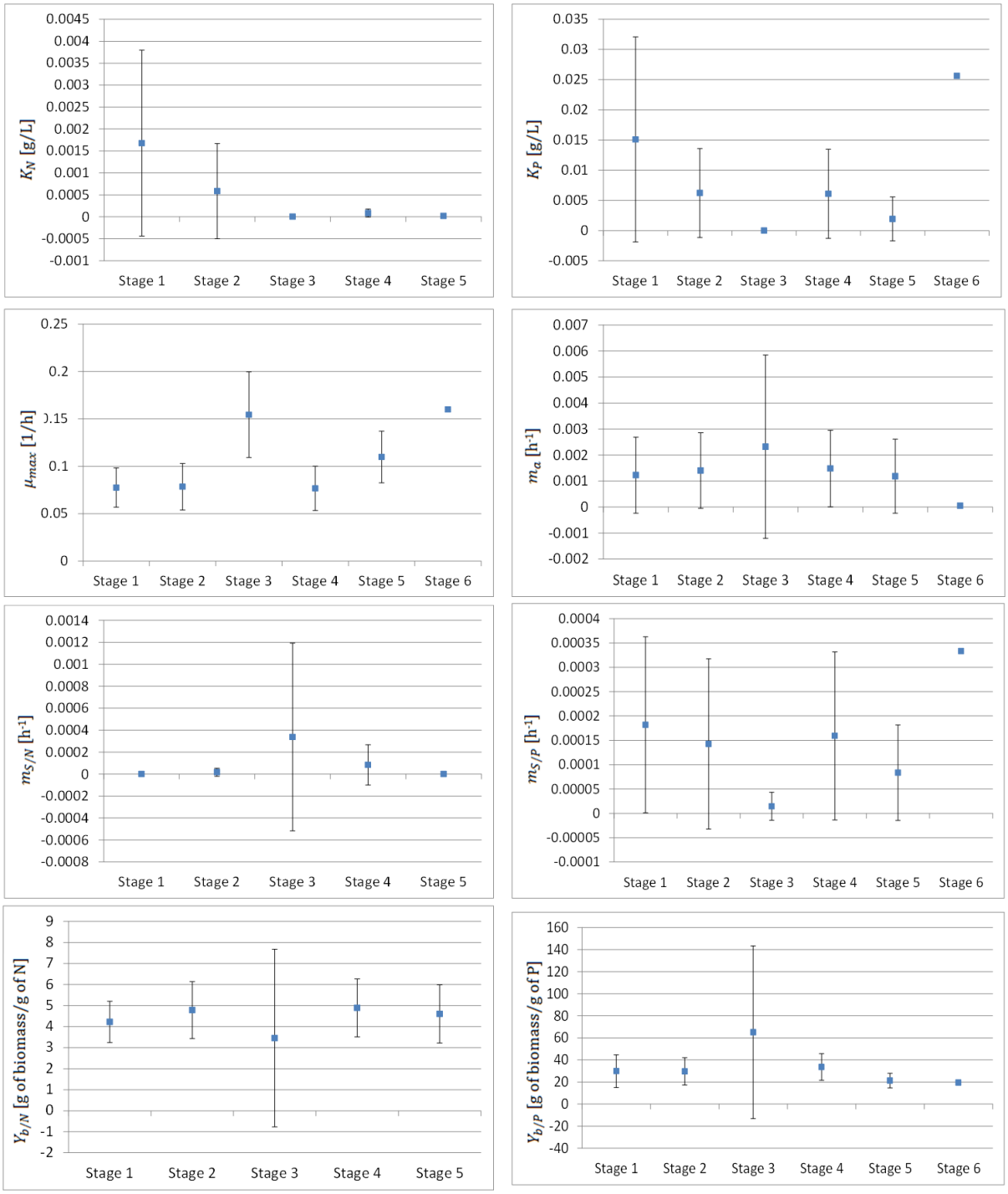

Figure V.6. Average values of the estimated parameters half saturation constant for nitrates and phosphates, K_N, K_P, maximum growth rate, μ_{max}, specific maintenance rate, m_a, maintenance supply rate of minimum nitrates and phosphates consumption $m_{S/N}$, $m_{S/P}$, yield over nitrates and phosphates, $Y_{b/N}$, $Y_{b/P}$ from the full model calibration with their 95% confidence levels.

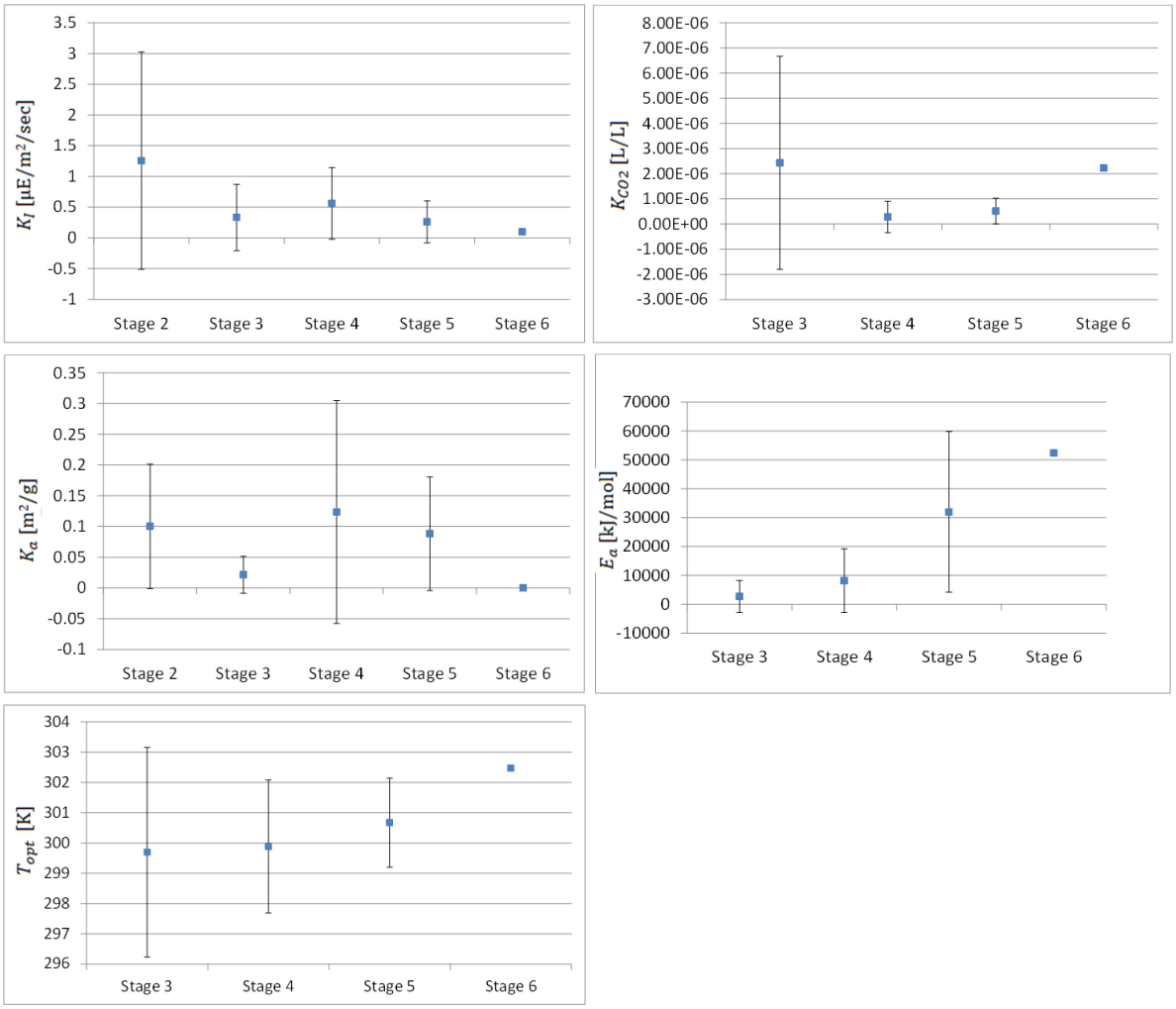

Figure V.7. Average values of the estimated parameters bioenergetics efficiency of light utilisation, K_I, half saturation constant for CO_2, K_{CO2}, biomass light absorption coefficient, K_a, activation energy, E_a, and optimal temperature T_{opt}, from the full model calibration with their 95% confidence levels.

The values of the parameters shown in the tables above were used in the simulation process for all conditions, and plots are shown below to show the fit of each experiment to the model that it contributed to calibrate. Below, the plots of each experiment, plots with its percentage deviations of the measured with the predicted values are shown.

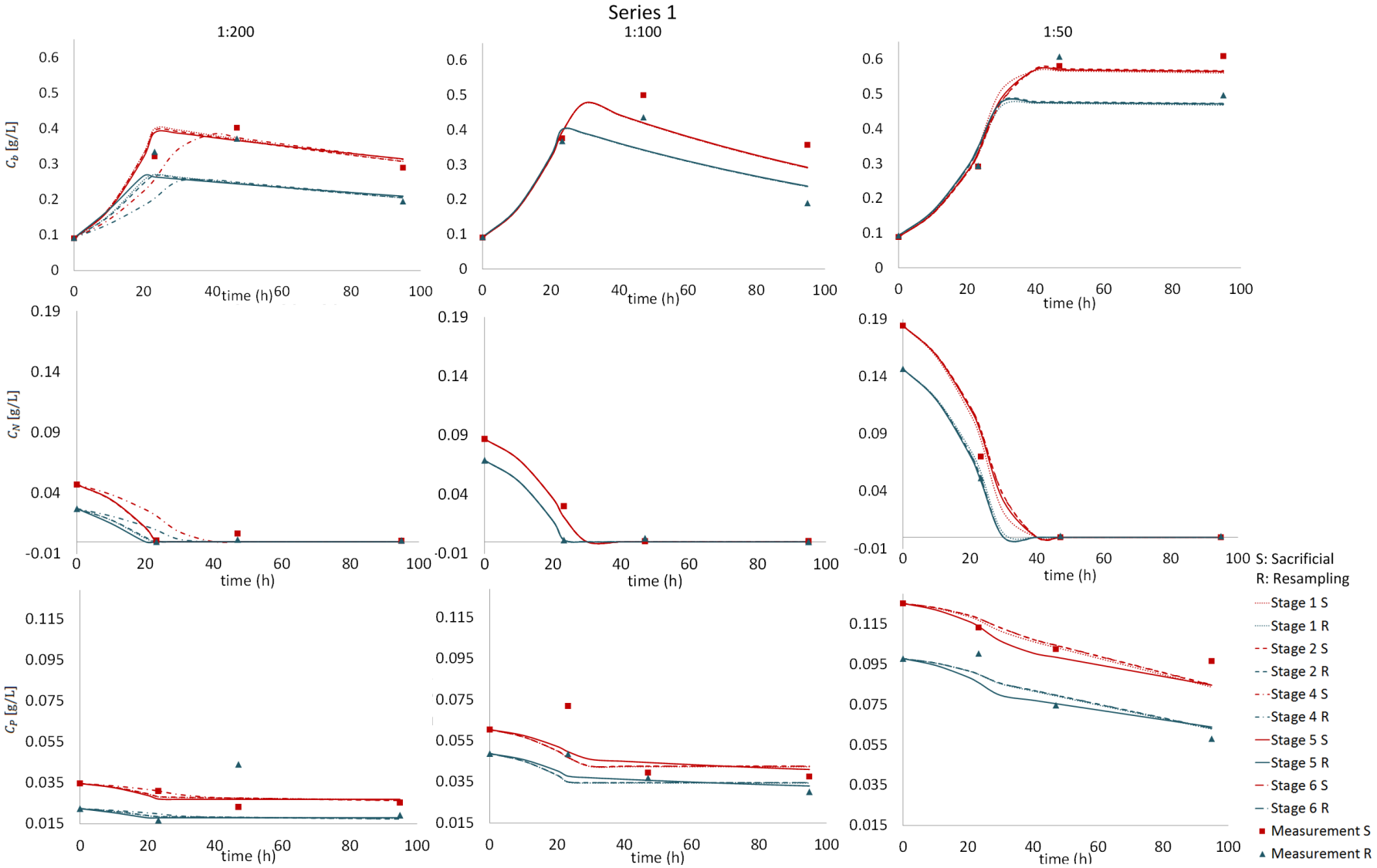

Figure V.8. Factorial experimental measurements of Series 1 and model predictions for the sacrifical (S) resampling (R) wells measurements during the 6 stages of the calibration.

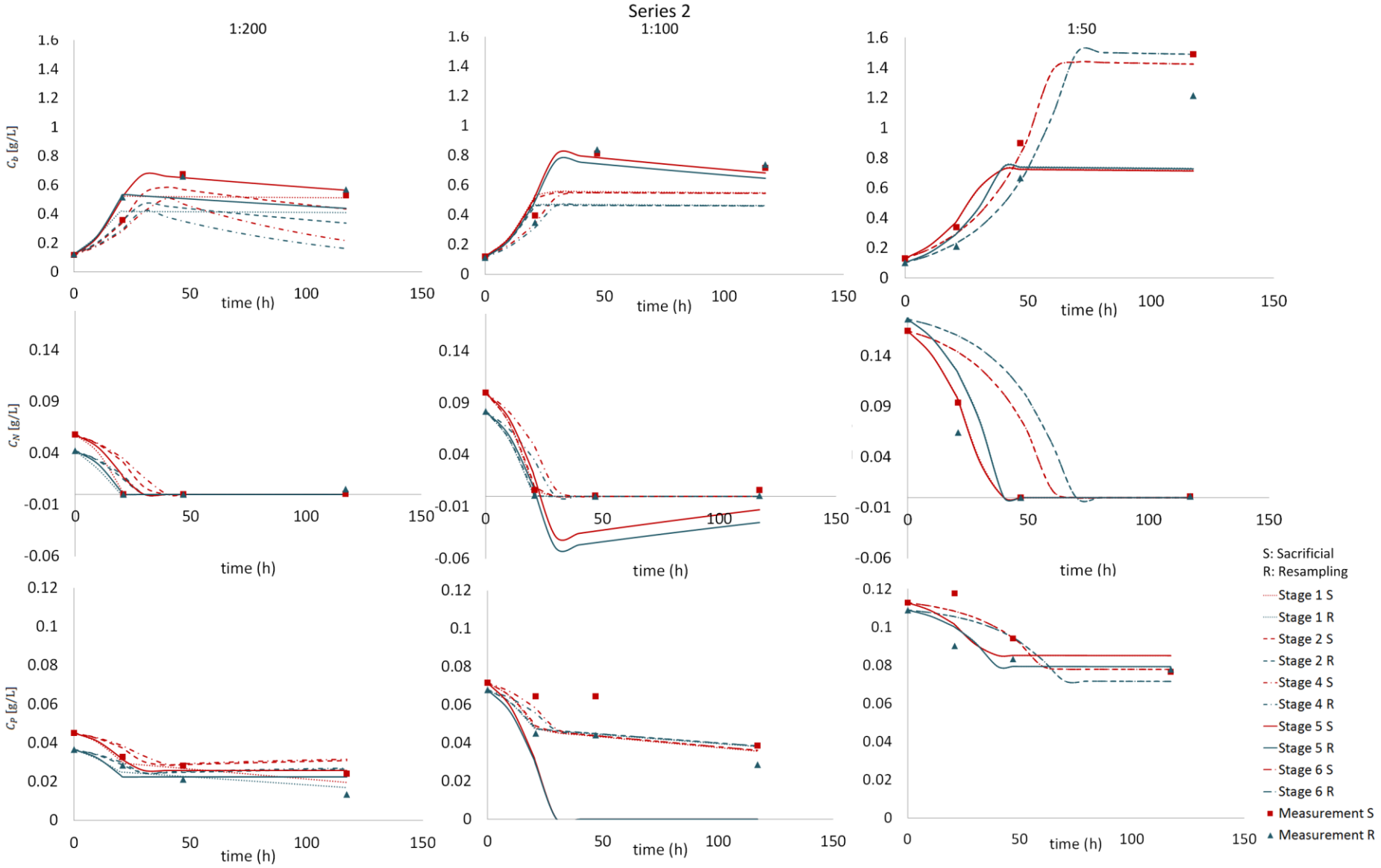

Figure V.9. Factorial experimental measurements of Series 2 and model predictions for the sacrifical (S) resampling (R) wells measurements during the 6 stages of the calibration.

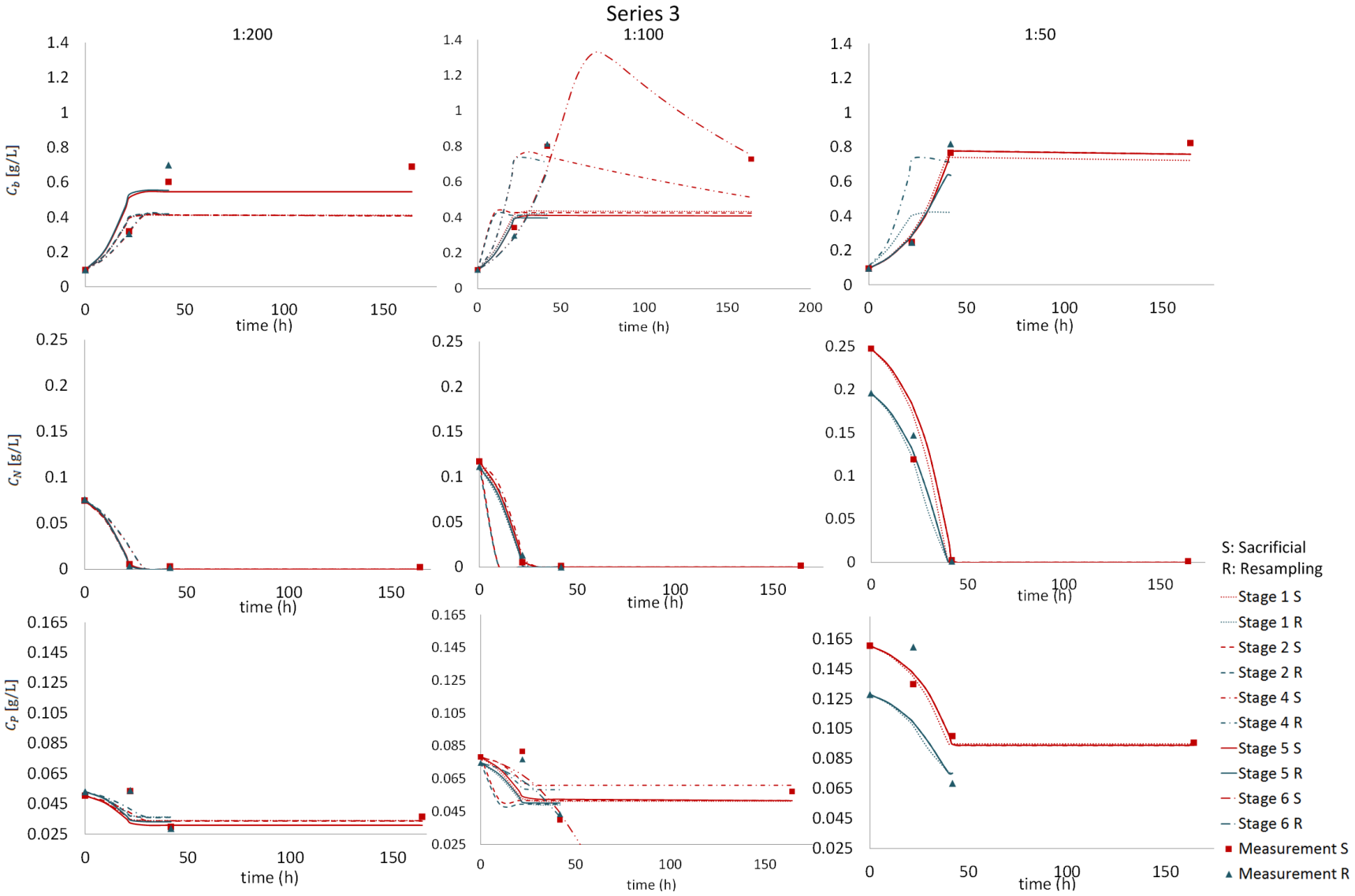

Figure V.10. Factorial experimental measurements of Series 3 and model predictions for the sacrifical (S) resampling (R) wells measurements during the 6 stages of the calibration.

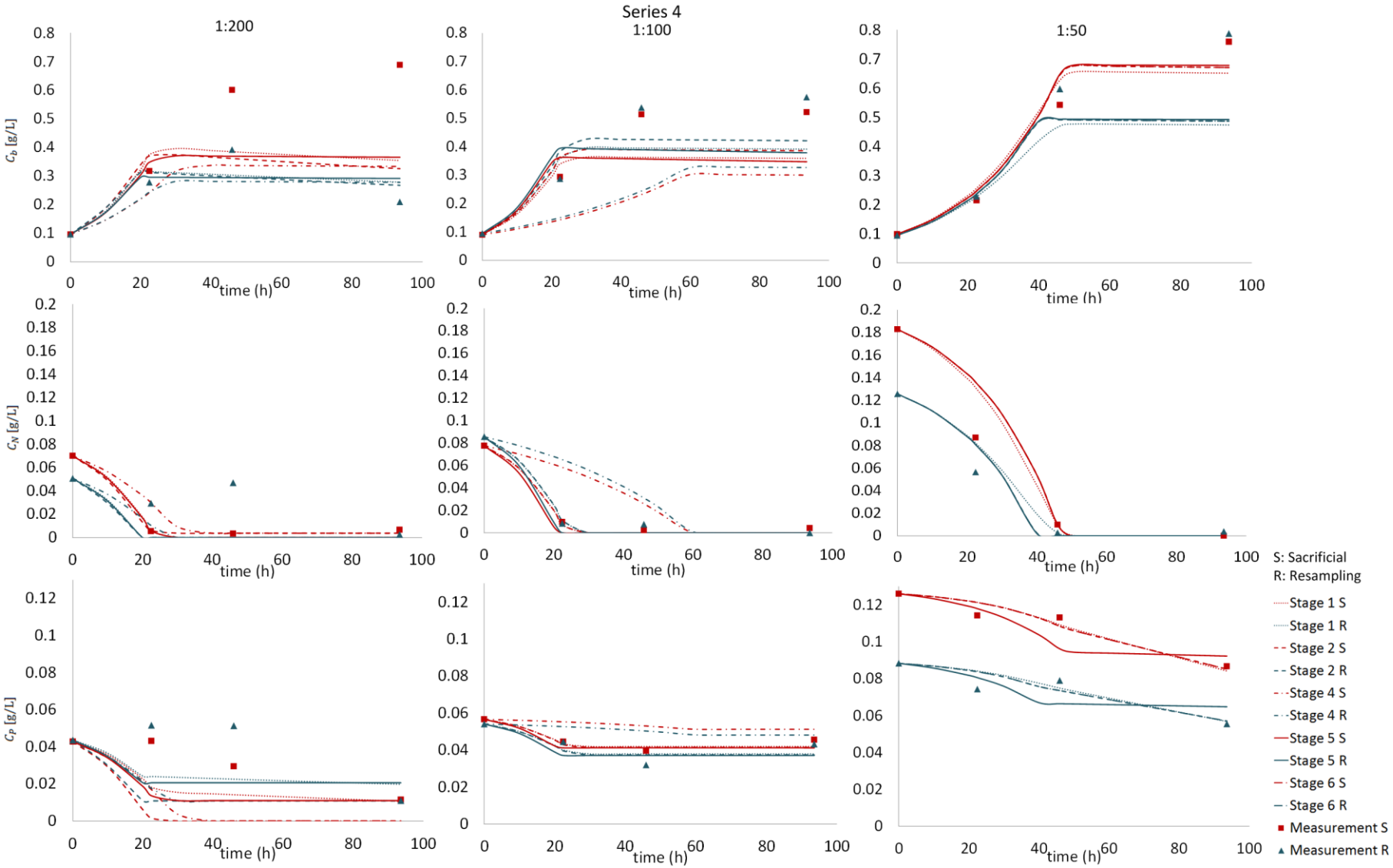

Figure V.11. Factorial experimental measurements of Series 4 and model predictions for the sacrifical (S) resampling (R) wells measurements during the 6 stages of the calibration.

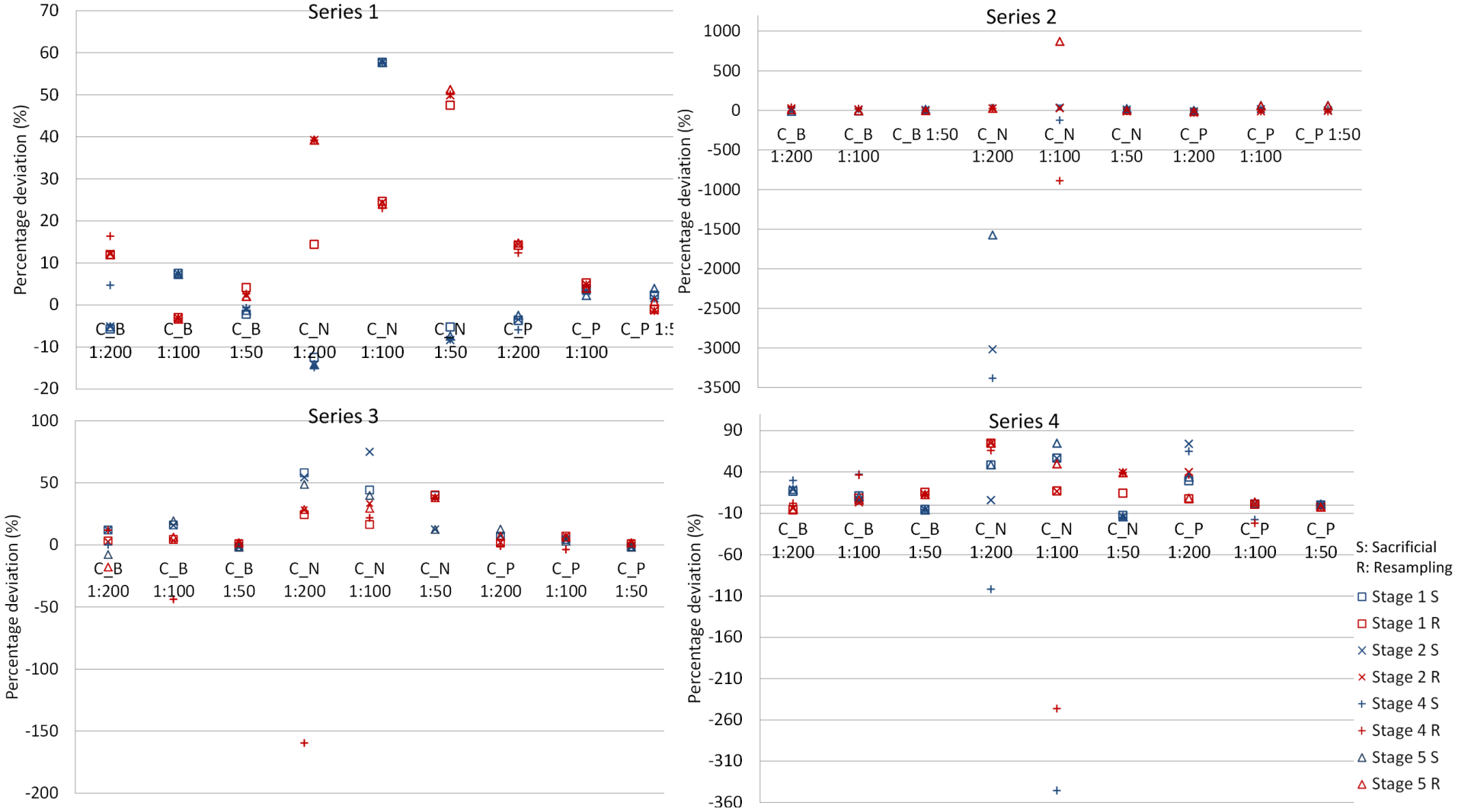

Figure V.12. Percentage deviation of the predicted values of the different measured variables among the 6 stages of the calibration and the 4 factorial experiments series.

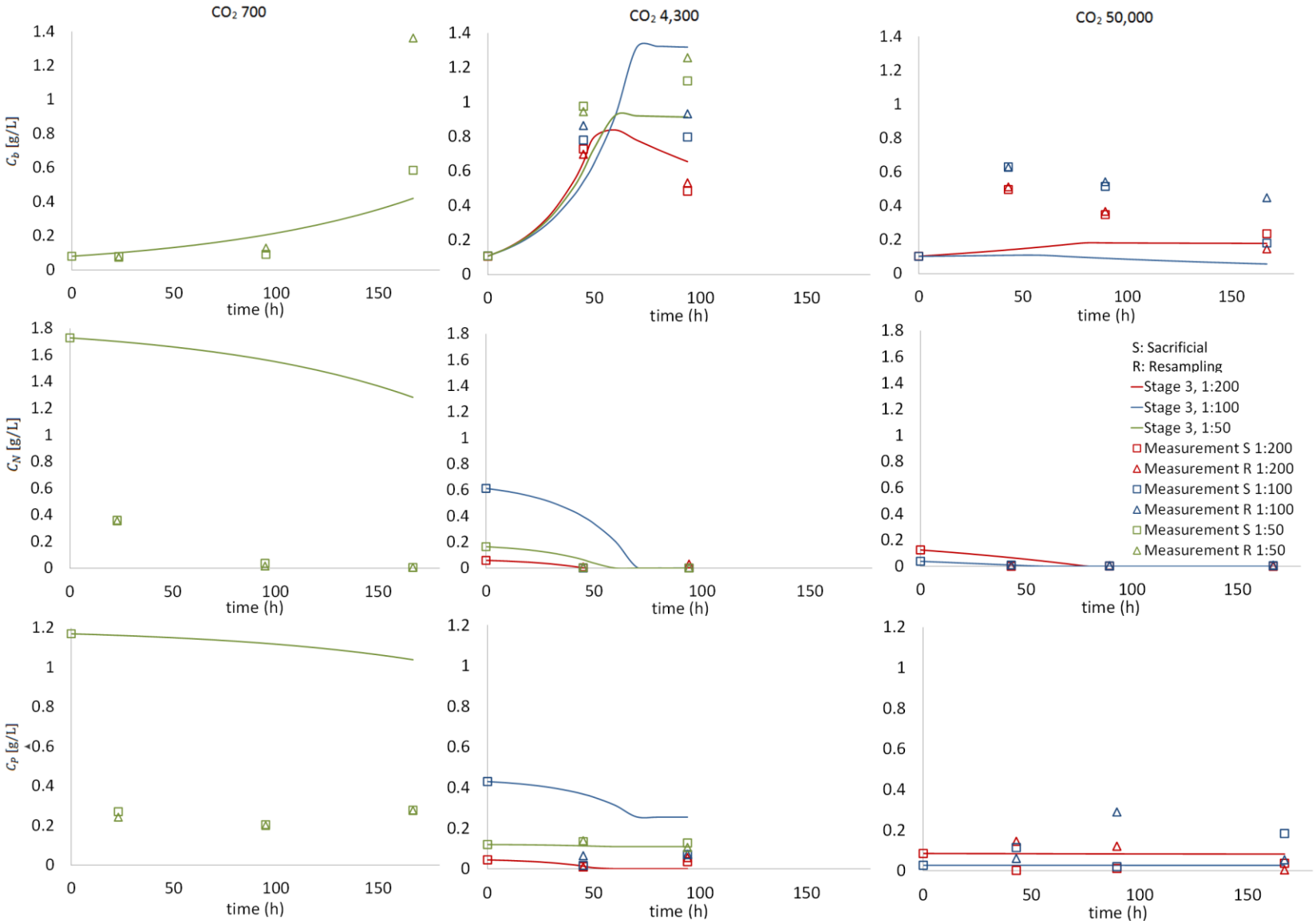

Figure V.13. Model predictions of the variables in the CO_2 experiments during Stage 3 of the calibration.

Table V.15. Average values of the parameters estimated from Stage 5 of the calibration and used for the process simulation.

Parameter	Average estimation
E_a	31986.53
K_a	0.08826
K_{CO2}	5.13E-07
K_I	0.261896
K_N	0.00002
K_P	0.00193
μ_{max}	0.1099
m_N	1.83E-07
m_P	8.36E-05
m_a	0.00119
T_{opt}	300.67
$Y_{b/N}$	4.6033
$Y_{b/P}$	21.2610

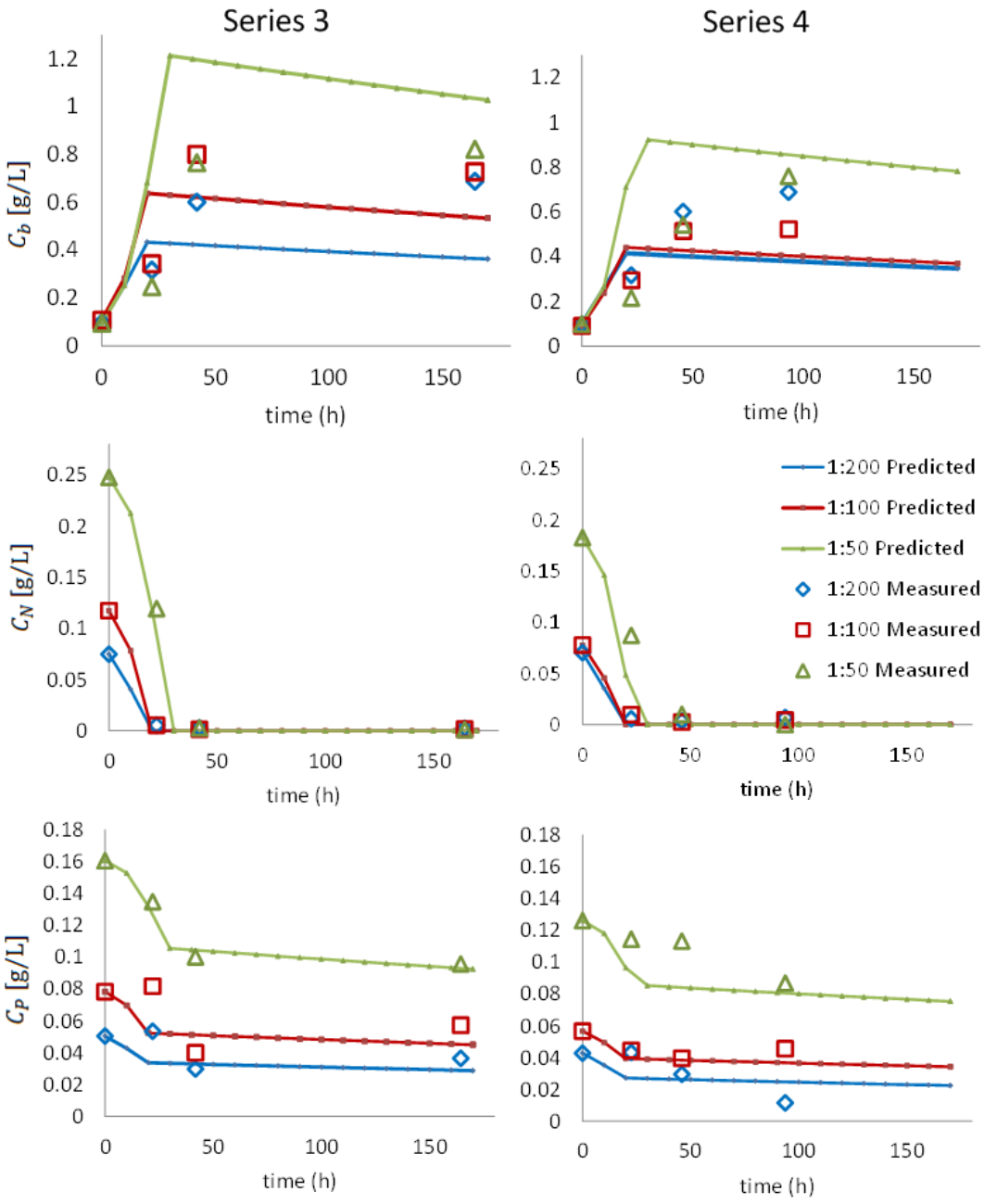

Figure V.14. Model predictions of the processes corresponding to the experimental Series 3 and 4, using the average values of the parameters estimated during Stage 5 of the calibration (shown in Table V.15).

Table V.16. Parameter values used for to adjust the full model to the typical growth stages shown in Figure 2.12.

Parameters	Value
d [m]	0.12
I_0 [µE/m^2/sec]	90
T [K]	298
R [J/mol/K]	8.314
D [1/h]	0
$C_{b,0}$ [g/L]	0.03
$C_{N,0}$ [g/L]	2.99
$C_{P,0}$ [g/L]	2.92
C_{CO2} [L/L]	0.01
μ_{max}[1/h]	0.2
m_a [1/h]	0.060
$m_{s/N}$[gnitrates/g cells/h]	0.060
$m_{s/P}$[gphosphates/g cells/h]	0.060
K_I [µE/m^2/sec]	10
K_a [m^2/g]	0.8
K_N [mol/m^3]	0.03
K_P [mol/m^3]	0.027
K_{CO2} [m^3/m^3]	0.0000073
$Y_{b/N}$ [-]	46
$Y_{b/P}$ [-]	45
E_a [J/mol]	100,000
T_{opt} [K]	303

Appendix VI. Photobioreactor heating and waste heat recovery

Method of the flowsheet development in gPROMS Model Builder

The hot water is stored in the storage tank (Tank 001 of Figure VI.1) which has two level controllers (PID_controller002 and 003) to prevent overflow and cavitation. Since the default variable specification of the tank component model is not dependent on the temperature, an extra heat input controller is added which stops the heat loss from the tank when its temperature reaches the ambient temperature. Two radiators (Heater001 and 001) are simulated after the storage tank, which are represented by coolers of defined heat input rate. At the end of the flow a HE (Heater003) simulates the HE design suggested for the PBR. It needs to be simulated by a shell and tube exchanger than has only one tube, but for the moment it is represented as a third cooler. The model was run as dynamic for a period of 24 hours assuming 8 hours of flue gas provision and 24 hours of heating requirements.

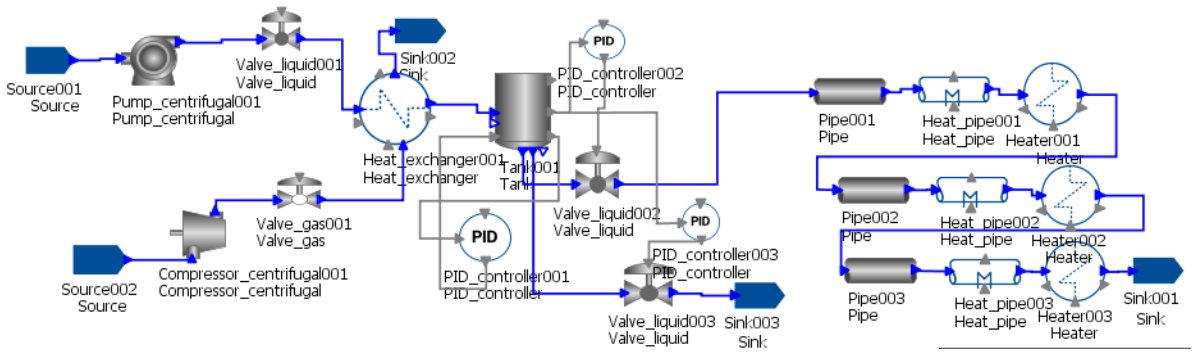

Figure VI.1. Actual flowsheet run on gPROMS for the 5 cases examined.

The parameters of the component models have default values able to be modified and their variables are set. The different component models are connected with streams through their ports. In order to run the simulation, a Process has to be created that makes a call to the flowsheet model where the timing schedule of the simulation is defined. The description of each component model used is presented below and Table VI.1 lists the model parameters, variables, initial conditions and outputs. Some variables specifications have the option of advanced setting which can be used to define more variables, depending on the requirements of the problem and the degrees of freedom.

Source: The source models are used to define the materials entry into the streams. One source model for the flue gas inlet from the engine exhaust and one for the water inlet from the river are used.

Tank: This model is used to simulate the storage tank of the ships. It has multiple inlet and outlet ports. It has includes control ports for the measurement and control of the pressure, liquid level and the temperature. Tank outlet is driven by the hydrostatic pressure.

Sink: The sink model is the exit of a material stream out of the flowsheet process. One sink model is used to represent the cooled flue gas emitted to the environment and two sink models for the dump of the heated water streams back to the river are used. It describes an infinite volume sink.

Compressor centrifugal: The compression is modelled as polytropic. Fan laws are used. The model relates the gas flow rate to the pressure head, the compressor speed and the characteristic performance curves of the compressor which are provided by the foreign object LookupTableFO. A compressor is used to transfer the flue gas from the engine exhaust to the ambient through the HE and the PBR.

Pump centrifugal: The pump model is simulated to transport the river water to the tank through the HE. Isenthalpic flow is assumed and the model is based on the quadratic relationship between the head and flow.

Gas and liquid valves: The models are used to control the flow rate of the material streams. Isenthalpic, isothermal flow is assumed.

Pipe*:* The pipe models are used to simulate the head loss at the piping connecting the tank with the radiators and the PBR HE. Adiabatic flow is assumed.

Heat exchanger: This model is used to simulate the HE – or series of HEs – that cool down the flue gas form the engine and heat up the water pumped from the river. It calculates the heat exchanged by lumping two models of the heater pipe model. The mean temperature difference is selected to be calculated using the log-mean method. Counter-current type of flow is selected and the heat transfer coefficient is selected as constant.

Heat exchanger tubular: The tubular HE represents a tube and shell type exchanger and is used to simulate the PBR double pipe HE (assuming one tube in the model). Counter current operation mode is selected. Heat transfer coefficient can be selected as either constant or related to the flow rates

Heater: This model can be used as either a heater or a cooler and in the existing problem it represents radiators of the ships, hence, it works as a cooler for the heating water stream. This component model uses a lumped heater pipe model as a sub-model.

Heat pipe: It calculates the change in temperature of a flowing fluid when subjected to an external heat input term. This model is not designed to be used separately and it is used as a sub-model in the HEs. However, the heat pipes models are used in the existing flowsheet to simulate the same piping simulated by the pipes models, but this time the heat loss from them is computed.

PID controller: The controllers used are for the heat input and level control of the storage tank. Two level controllers are introduced. One for the low level, to stop the flow in order to avoid cavitation when tank empties, and one high level controller to prevent overflow, by dumping extra water back to the river. The heat input controller, measures the temperature and stops the heat loss when the tank temperature reaches the ambient temperature. This component model describes a PID controller and any of the classes combinations of proportional, integral and derivative action can be selected (P, PI, PID, D, PD and I). The controller action in calculating the error term can also be selected between direct and reverse mode. Reverse approach has been selected for all of them.

Table VI.1. Parameters and variables that need to be specified, initial conditions selected for the dynamic models and outputs of each model.

	Parameters specifications	Variables specifications	Initial conditions	Output
Source	Physical properties foreign object, Components	Pressure, Temperature, Phase, Mass fractions, Advanced: Flow rate	-	Normalised mass fraction Mass specific enthalpy
Tank	-	Height, Diameter, Pressure, Heat input	Selection among different. In this study: Temperature, Mass hold up	Mass fraction Enthalpy Flow rate Holdup, Liquid volume, Liquid level, Pressure
Sink	-	Mass fraction, Temperature, Pressure, (only used in case of backflow)	-	Flow rate
Compressor centrifugal	Head flow equation Flow efficiency equation	Design speed, Load speed	-	Power consumed, Load torque, Discharge, Temperature

	(stored in foreign object).			
Pump centrifugal	-	Head at zero flow, Flow at zero head, Design speed, Advanced: Flow rate, Efficiency, Operating fraction	-	Flow rate, Load power, Load torque
Gas and liquid valves	-	Flow coefficient, Recovery factor, Stem position setting, Gas valve also: Leakage fraction, Time constant	Dynamic mode: Actual valve stem position	Flow rate
Pipe	-	Length, Diameter, Wall roughness, Fittings head loss coefficients, Inlet and outlet elevations	-	Pressure difference
Heat exchanger	-	Heat transfer area, Multipass correction factor, Fouling resistance, Flow coefficients, Design heat transfer coefficient, Design mass flow rates, Advanced:, Outlet temperatures, Mean differential temperature	-	Both pipes: Outlet temperatures, Flow rates
Heat exchanger tubular	Number of tubes and grids	For tubes: Length, Diameter, Metal density, Specific heat capacity, For tubes and shell: Flow coefficients, Flow exponents, Design mass flow rates, Heat transfer coefficients	Dynamic option: initial tube metal, tube fluid and shell fluid temperatures	Flow rates, Change in fluids temperatures
Heater	-	Heat transfer coefficient, Heat transfer area, Energy input rate, Flow coefficient	-	Fluid flow rate, Change in temperature
Heat pipe	-	Heat input rate, Pipe flow coefficient	-	Exit temperature
PID controller	Percentage factor of output	Min measured variable, Max measured variable, min controller output, max controller output, P class: bias, gain, set point	(-) for the proportional class controller	Heat input controller: heat input value, Level controllers: stem position setting

The constant values of the parameters and variables are shown in Table VI.2. The variables that changed are presented with their values at the different scenarios in Table VI.3. Some assumptions used for the flowsheet model are that:

1. No pump is used after the storage tank, due to cavitation problems appearing in the flowsheet. Flow is driven with hydrostatic pressure. The height-to-diameter ratio used for the storage tank examined was 0.55.
2. The pump could not be completely terminated in the simulation after the 8 hours of operation, due to a non-typical error appearing in the model.

3. The PBR HE is simulated as a simple heater and not a double pipe HE as suggested in 7.4, due to complexities with the pressure drop in the model and the addition of a pump downstream.
4. The radiators needs are also simulated for 24 hours, although in most cases, only the PBR will require heat for the whole day. In order to resolve this, the hot water stream needs to be split before the radiators series and create a by-pass straight to the PBR.
5. The heat loss from the tank is 200,000 W and an IF loop sets it to zero when temperature is equal or below the ambient temperature.

Table VI.2. Parameter and variables values given for the model simulation during the five cases examined.

Component model	Representation	Variables	Values	Units
Source 1	River water	Phase	Liquid	-
		Components	Water	-
		Pressure	1.013×10^5	Pa
		Temperature	280.15	K
		Mass fraction	1	-
Pump centrifugal 1	Centrifugal pump	Design head at 0 flow	3×10^5	Pa
		Design speed	276.45	rps
		Operating speed fraction	1	-
		Efficiency	60%	-
		Mass flow rate	Varied	kg/s
Valve liquid 1	Liquid valve 1	Stem position specification	Manual	
		Leakage fraction	1×10^{-2}	-
		Time constant	0.5	s
		Flow coefficient	20	$gpm/psi^{0.5}$
		Stem position setting	1	-
		Initial actual stem position	1	-
Source 2	Engine flue gas	Phase	Gas	-
		Components	N_2, O_2, CO_2	-
		Pressure	1.6×10^5	Pa
		Temperature	653.15	K
		Mass fraction	0.79, 0.16, 0.05	-
Compressor centrifugal 1	Centrifugal compressor	Design speed	50.45	rps
		Load speed	10.45	rps
Valve gas 1	Gas valve 1	Stem position specification	Dynamic	
		Flow coefficient	1×10^4	scf/h/psia
		Recovery factor	60	-
		Stem position setting	1	-
		Initial actual stem position	1	-
Heat exchanger 1	Heat exchanger	Heat transfer area	3	m^2
		Multipass correction factor	1	-
		Fouling resistance	0	m^2K/W
		Water pipe flow coefficient	1E-2	kg/sPa
		Water pipe design heat transfer coefficient	1000	W/ m^2K
		Water pipe design mass flow rate	1	kg/s
		Water pipe flow coefficient	1E-2	kg/sPa
		Water pipe design heat transfer coefficient	1000	W/ m^2K
		Water pipe design mass flow rate	0.5	kg/s

Sink 2	Flue gas to scrubbers	Phase	Gas	-
		Components	N_2, O_2, CO_2	-
		Pressure	1.5×10^5	Pa
		Temperature	373.15	K
		Mass fraction	0.79, 0.16, 0.05	-
Tank 1	Storage tank	Heat input	Controlled	
		Liquid protection	True	
		Liquid initial flow protection	Normal	
		Height	2.5	m
		Diameter	4.5	m
		Pressure	3E5	Pa
		Initial conditions temperature	280	K
		Initial conditions mass holdup	1	kg
PID controller 1	Heat input controller	Class	P	-
		Mode	Automatic	-
		Action	Direct	-
		Min input	278	K
		Max input	900	K
		Min output	0	W
		Max output	-900000	W
		Bias	0	-
		Gain	1	-
		Set point	600	-
PID controller 3	High level controller	Class	P	-
		Mode	Automatic	-
		Action	Reverse	-
		Min input	0	m
		Max input	2.2	m
		Min output	0	-
		Max output	1	-
		Bias	0	-
		Gain	1	-
		Set point	1	-
PID controller 2	Low level controller	Class	P	-
		Mode	Automatic	-
		Action	Reverse	-
		Min input	0.1	m
		Max input	3	m
		Min output	0.1	-
		Max output	Varied	-
		Bias	0	-
		Gain	1	-
		Set point	1	-
Valve liquid 3	Liquid valve 3	Stem position specification	Controlled	
		Leakage fraction	1×10^{-3}	-
		Time constant	0.5	s
		Flow coefficient	10	$gpm/psi^{0.5}$
Sink 3	Overflow water to river	Phase	Liquid	-
		Components	Water	-
		Pressure	0.9×10^5	Pa
		Temperature	280	K
		Mass fraction	1	Kg/kg
Valve liquid 2	Liquid valve 2	Stem position specification	Controlled	
		Leakage fraction	Varied	-
		Time constant	1	s
		Flow coefficient	Varied	$gpm/psi^{0.5}$
Pipe 1	Piping 1 flow calculations	Turbulent friction factor correlation	Constant	-
		Length	10	m
		Internal diameter	0.1	m
		Inlet elevation	0.5	m
		Outlet elevation	3	m
		Fittings heat loss coefficient	1	-
		Wall roughness	5E-6	m

Heat pipe 1	Piping 1 heat loss calculations	Flow coefficient Heat input rate	1E-3 -400	kg/sPa J/s
Heater 1	Radiator 1	phase Heat transfer coefficient Heat transfer area Rate of energy input Flow coefficient	Liquid 100 2 -2000 1E-3	- W/ m^2K m^2 J/s kg/sPa
Pipe 2	Piping 2 flow calculations	Turbulent friction factor correlation Length Internal diameter Inlet elevation Outlet elevation Fittings heat loss coefficient Wall roughness	Constant 10 0.1 3 3 1 5E-6	- m m m m - m
Heat pipe 2	Piping 2 heat loss calculations	Flow coefficient Heat input rate	1E-3 -400	kg/sPa J/s
Heater 2	Radiator 2	phase Heat transfer coefficient Heat transfer area Rate of energy input Flow coefficient	Liquid 100 2 -2000 1E-3	- W/ m^2K m^2 J/s kg/sPa
Pipe 3	Pipeline 3 flow calculations	Turbulent friction factor correlation Length Internal diameter Inlet elevation Outlet elevation Fittings heat loss coefficient Wall roughness	Constant 5 0.1 3 3 1 5E-6	- m m m m - m
Heat pipe 3	Pipeline 3 heat loss calculations	Flow coefficient Heat input rate	1E-3 -400	kg/sPa J/s
Heater 3	PBR double pipe HE	phase Heat transfer coefficient Heat transfer area Rate of energy input Flow coefficient	Liquid 100 0.5 -800 1E-3	- W/ m^2K m^2 J/s kg/sPa
Sink 3	Overflow water to river	Phase Components Pressure Temperature Mass fraction	Liquid Water $1*10^5$ 280 1	- - Pa K Kg/kg

Table VI.3. Values of the control variables for the cases examined (for a given storage capacity, given number of radiators and heat transfer areas of the heat exchangers and given flow rate and temperature of the flue gas).

	Case 1	Case2	Case 3	Case4	Case 5
Centrifugal pump flow rate [kg/s]	1.3	2.8	2.8	0.85	0.85
Valve liquid 2 leakage fraction [-]	0.1	0.01	0.01	0.01	0.01
Valve liquid 2 flow coefficient [gpm/$psi^{0.5}$]	8	20.5	30.5	20	10
PID controller 2 max output [-]	0.2	0.9	0.9	0.9	0.9

The following figures show the response of the tank level and temperatures of the two fluids in the various streams according to the water flow rates output, corresponding to the settings of the five cases in Table VI.3. Pumping requirements

during the engine working hours are shown in Table VI.4. The reason why the water flow rate after the first 8 hours (time 28,800 seconds) is not zero is because the pump could not be switched off. The compressor had the same issue and the gas flow rate after the first 8 hours was set to 0.015 kg/s. Case 4 in Figure VI.2 has a continuous step change after the time that the tank empties, because of the low level controller and the minor inlet flow rate. The same happens with the water temperature of this case in Figure VI.3.

Table VI.4. Pumping requirements for the 5 cases examined.

	Centrifugal compressor (J/s)	Centrifugal pump (J/s)
Case 1	10,122	449
Case 2	10,122	1,096
Case 3	10,122	1,096
Case 4	10,122	288
Case 5	10,122	288

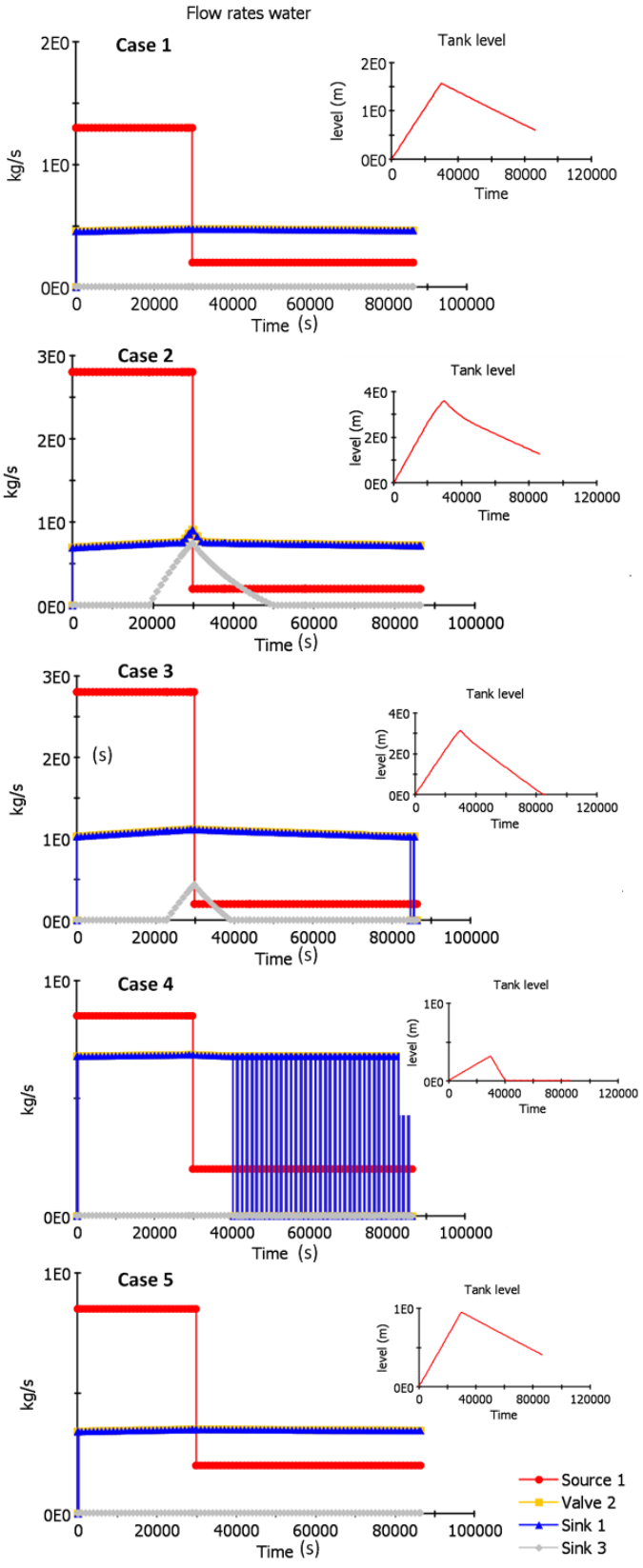

Figure VI.2.Water flow rates along with the corresponding transient level of the storage tank response for the five cases examined.

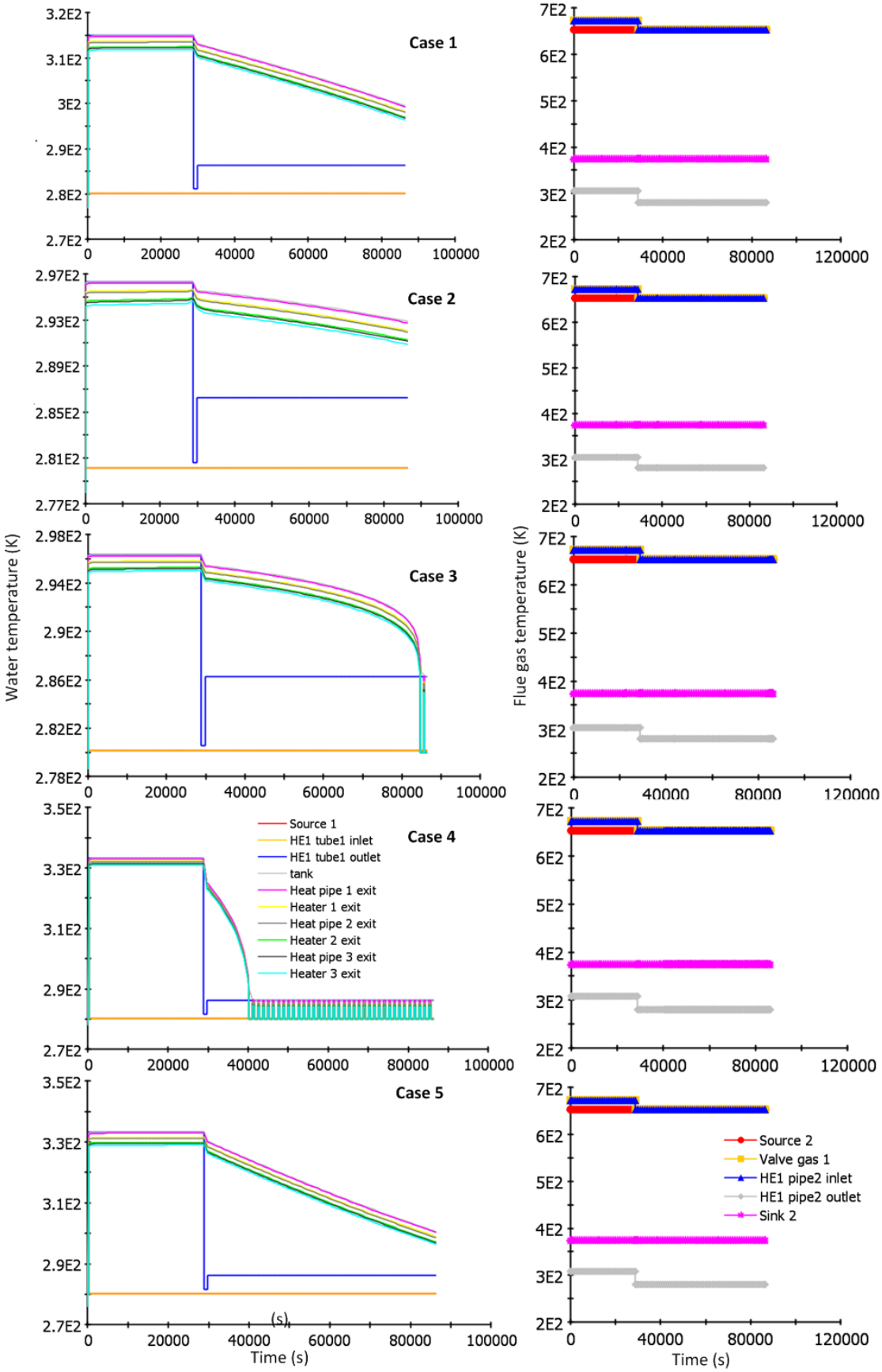

Figure VI.3. Temperature response of the water and gas streams for the five cases examined.

Method and script for the temperature control methods suggested

Prandtl (Pr) number can be found from Eq.92 by using the properties of the mixture for simplification, although it is related to the properties of the continuous phase in a more complex way (Brennen, 2005). Graetz (Gz) number from Eq.93 and Nusselt ($\overline{Nu_d}$) number is found from Eq.94 to Eq.96, for the laminar flow ($Re < 2100$), the transition Reynolds numbers ($2100 < Re < 4000$), and the turbulent pipe flow ($Re > 4000$), respectivly. Finally, $\overline{h_m}$ is computed from Eq.1 and can be replaced in Eq.82 (Lienhard Iv & Lienhard, 2008 (chapters 7.2-7.4); Perry et al., 1999).

$$Pr = \frac{\mu_m c_{p_m}}{k_m} \tag{92}$$

$$Gz = \frac{Re_l Prd_r}{l} \tag{93}$$

$$\overline{Nu_{d_{laminar}}} = 3.657 + \frac{0.0668 Gz^{1/3}}{0.04 + Gz^{-2/3}} \tag{94}$$

$$Nu_{d_{transition}} = \frac{\left(\frac{f}{8}\right)(Re - 1000)Pr}{1 + 12.7\sqrt{\frac{f}{8}}(Pr^{2/3} - 1)} \tag{95}$$

$$Nu_{d_{turbulent}} = \frac{\left(\frac{f}{8}\right)RePr}{1.07 + 12.7\sqrt{\frac{f}{8}}(Pr^{2/3} - 1)} \tag{96}$$

$$\overline{h_m} = \frac{\overline{Nu_d} k_m}{d_r} \tag{97}$$

Code for Figure 7.12, Figure 7.14 and Figure 7.13:

```
clear all; close all; clc;

clear all; close all; clc;

% The following code estimates the temperature needed for the flue gas to
% enter the reactor in order to maintain the temperature until the end of
% the tube above the lower limit that does not harm algae, by using the
% heat transfer model produced in the report.

%PARAMETERS
d_r=0.06; %[m]
d_b=0.005; %[m]
l_d=1.5; %[m]
q_g=0.00004; %[m3/s]
```

```
v_l=0.000000801; %[m2/s]
K_avg=(1.5+1.5+1.3+0.75)/4;
e_yo=0.0000025;
l_r=6;
l=l_r+l_d;
m_l=0.000798; %[kg/m/s]
m_g=0.00001983; %[kg/m/s]
p_l=1000; %[kg/m3]
p_g=1.225; %[kg/m3]
cp_l=4181.3; %[JK-1kg-1]
cp_g=1012; %[JK-1kg-1]
pi=3.142; %[dimensionless]
g=9.81; %[m/s2]
c_s=0; %[dimensionless parameter of solids]
k_t=0.195; %[Wm-1K-1]
k_l=0.55; %[Wm-1K-1]
k_g=0.027; %[Wm-1K-1]
r_i=d_r/2; %[m]
s=0.002; %[m]
r_e=r_i+s; %[m]
d_o=d_r+(2*s); %[m] outer diameter
h_e=12; %[Wm-2K-1]
T_m_out=296; %[K]
T_e=283; %[K]
T_max= 345;
n=1000000; %linspace for T_m_in
x=1000; %linspace for u_b
z=100; %linspace for q_g_row

%ESTIMATION OF u_b
u_b_t=linspace(0.0005,2,x); %[m/s]
u_b_e_numerator=4*g*d_b.*(p_l-p_g);
u_b_e_denom_0 = 3*p_l;
u_b_e_denom_1 = 24*((u_b_t.*d_b./v_l).^(-1));
u_b_e_denom_2 = 2.6*u_b_t.*d_b.*((5*v_l)^(-1)).*((1+((u_b_t.*d_b.*((v_l*5)^(-
1))).^1.52)).^(-1));
u_b_e_denom_3 = 0.411*((u_b_t.*d_b./(263000*v_l)).^(-
7.94))./(1+((u_b_t.*d_b.*((v_l*263000))^(-1)).^(-8)));
u_b_e_denom_4 = ((u_b_t.*d_b./v_l).^0.8)./461000;
u_b_e =
(u_b_e_numerator*((u_b_e_denom_0*(u_b_e_denom_1+u_b_e_denom_2+u_b_e_denom_3+u_
b_e_denom_4)).^(-1))).^0.5; %[m/s]
u_b_error = abs(u_b_e-u_b_t);
[inVal, position] =min(u_b_error);
u_b = u_b_e(position);

d_r_chan=0.04:0.02:0.1;
d_r_col=reshape(d_r_chan,size(d_r_chan,2),1);
q_g_row=linspace(0.000001,0.0001,z);
d_r_mat=repmat(d_r_col,1,z);
d_o_mat=repmat(d_r_col+(2*s),1,z);
q_g_mat=repmat(q_g_row,size(d_r_col,1),1);


%ESTIMATION OF u_l
% Approach Force Bualance

u_l=zeros(size(d_r_chan,2),z);
% q_g_row=linspace(0.000001,0.0001,x);
% q_g_col=reshape(q_g_row,x,1);

for m=1:size(d_r_chan,2);
    for k=1:z;
        u_l_t=linspace(0.0005,2,n);
        u_l_e_1=(u_l_t.^3).*(u_l_t+u_b*ones(1,n));
        u_l_e_num1=8*g*(p_l-p_g)*u_b.*l_r.*q_g_mat(m,k);
        u_l_e_den1=pi*p_l*d_r_mat(m,k);
```

```
        u_l_e_den2=4*K_avg*d_r_mat(m,k)*ones(1,n);
        u_l_e_den3=l;
        u_l_e_den4=-
4*log((0.27*e_yo./d_r_mat(m,k)).*ones(1,n)+((7*v_l./(u_l_t.*d_r_mat(m,k))).^0.
9));

u_l_e_2=u_l_e_num1./(u_l_e_den1.*(u_l_e_den2+u_l_e_den3.*(u_l_e_den4.^(-2))));
        u_l_e_error = abs(u_l_e_1-u_l_e_2);
        [inVal, position] =min(u_l_e_error);
        u_l(m,k)=u_l_t(position);
    end
end




% Re
Re=u_l.*d_r_mat./v_l ;

% e_r
e_r=(4*q_g_mat)./(pi*(d_r_mat.^2).*(u_b.*ones(size(q_g_mat,1),size(q_g_mat,2))
+u_l));

% cp_m, k_m, m_m, p_m, q_m, m, n,
q_m=2*q_g_mat;
k_m= (k_g.*e_r) + (k_l.*(ones(size(q_g_mat,1),size(q_g_mat,2))-e_r));
m_m=(m_g.*e_r) + (m_l.*(ones(size(q_g_mat,1),size(q_g_mat,2))-e_r));
cp_m=(cp_g.*e_r) + (cp_l.*(ones(size(q_g_mat,1),size(q_g_mat,2))-e_r));
p_m=(p_g.*e_r) + (p_l.*(ones(size(q_g_mat,1),size(q_g_mat,2))-e_r));
m= p_m.*u_l.*pi.*(d_r_mat.^2)./4;

% Pr
Pr=m_m.*cp_m./k_m;

clr=jet(size(d_r_col,1));
Nu_d_mat=zeros(size(q_g_mat,1),size(q_g_mat,2));
for i=1:size(d_r_col,1);
    for e=1:size(q_g_row,2);
        % Nu_d
        if Re(i,e)<=2100;
            Gz=Re(i,e)*Pr(i,e)*d_r_mat(i)./l;
            Nu_d= 3.657+ (0.0668*(Gz.^(1/3))./(0.04+(Gz.^(-2/3)))) ;
        else
                if Re(i,e)<=4000;
                    f=(-4*log((0.27*e_yo/d_r_mat(i))+((7/Re(i,e))^0.9)))^(-2);
                    Nu_d= ((f./8)*(Re(i,e)-
1000).*Pr(i,e))/(1+12.7*((f./8)^0.5)*((Pr(i,e)^(2/3))-1));
                else
                        % Re(i,e)>4000;
                        f=(-
4*log((0.27*e_yo/d_r_mat(i))+((7/Re(i,e))^0.9)))^(-2);
                        Nu_d=
((f./8).*Re(i,e).*Pr(i,e))./(1.07+12.7*((f./8)^0.5).*((Pr(i,e)^(2/3))-1));
                end
        end
        Nu_d_mat(i,e)=Nu_d;
    end


    figure(1)
    hold on
    plot(q_g_row,Nu_d_mat(i,:),'Color', clr(i,:));

end
hold off
xlabel('q_g (m^3/s)');
```

```
ylabel('Nu_d');
zlabel('d_r(m)');
str=cellstr(num2str(d_r_col));
legend(str);
v=get(legend(str),'title');
set(v,'string','d_r (m)');

% h_m
h_m= Nu_d_mat.*k_m./d_r_mat;

figure(5)
plot(q_g_row,h_m(4,:),'g');  % test for d_r= d_r(4)
xlabel('q_g (m^3/s)');
ylabel('h_m');

figure (6)
plot(q_g_row,Re(4,:),'g'); % test for d_r= d_r(4)
xlabel('q_g (m^3/s)');
ylabel('Re');

% Thermal resistances
R_t_m=1./(h_m.*pi.*d_r_mat.*l);
R_t_t=(log(d_o_mat./d_r_mat))./(2*k_t.*pi.*l);
R_t_e=1./(h_e.*pi.*d_o_mat.*l);


% T_1


T_m_in=zeros(size(d_r_col,1),size(q_g_row,2));
q=zeros(size(d_r_col,1),size(q_g_row,2));
T_g_in=zeros(size(d_r_col,1),size(q_g_row,2));

clr=cool(size(d_r_col,1));
% clr=colormap(winter);
for i=1:size(d_r_col,1);
    for e=1:size(q_g_row,2);

        T_m_in(i,e)=((T_m_out-T_e)/(exp(-
4*((p_m(i,e)*u_l(i,e)*pi*(d_r_mat(i,e)^2)*cp_m(i,e)*(R_t_m(i,e)+R_t_t(i,e)+R_t
_e(i,e))).^(-1))))+T_e;
        q(i,e)=m(i,e)*cp_m(i,e)*(T_m_in(i,e)-T_m_out);

        T_g_in(i,e)=T_m_in(i,e)+((cp_l*p_l*u_l(i,e)*(1-
e_r(i,e))*pi*((d_r_mat(i,e).^2)/4))/(cp_g*p_g*q_g_mat(i,e)))*(T_m_in(i,e)-
T_m_out);
    end

    figure(2)
    hold on
    clr_inv=gray(size(d_r_col,1)+1);
    clr_inv(size(clr_inv,1),:)=[];
    clr=flipud(clr_inv);
    plot(q_g_row,T_m_in(i,:),'Color', clr(i,:),'Linewidth',1.2);
    axis ([0.000001 0.0001 296 296.14]);
    title('Temperature of the mixture required at the entrance of the
reactor');
    xlabel('Gas flow rate (m^3/s)');
    ylabel('Temperature in the mixture (K)');
    zlabel('d_r(m)');
    str=cellstr(num2str(d_r_col));
    legend(str);
    v=get(legend(str),'title');
    set(v,'string','d_r (m)');

    figure(4)
    hold on
```

```
    plot(q_g_row,T_g_in(i,:),'Color', clr(i,:),'Linewidth',1.2);
    axis ([0.000001 0.0001 0 250000]);
    title('Temperature of the gas required at the entrance of the reactor');
    xlabel('Gas flow rate (m^3/s)');
    ylabel('Temperature of the gas required (K)');
    zlabel('d_r(m)');
    str=cellstr(num2str(d_r_col));
    legend(str);
    v=get(legend(str),'title');
    set(v,'string','d_r (m)');

    figure(3)
    hold on
    plot (q_g_row,q(i,:),'Color', clr(i,:),'Linewidth',1.2);
    axis ([0.000001 0.0001 110 330]);
    title('Heat loss through the walls along the reactor');
xlabel('Gas flow rate (m^3/s)');
ylabel('Heat transferred (W)');
zlabel('d_r(m)');
str=cellstr(num2str(d_r_col));
legend(str);
v=get(legend(str),'title');
set(v,'string','d_r (m)');
end

hold off;
```

Code for Figure 7.15 :

```
clear all; close all; clc;

% The following code estimates the temperature needed for the flue gas to
% enter the reactor in order to maintain the temperature until the end of
% the tube above the lower limit that does not harm algae, by using the
% heat transfer model produced in the report.

%PARAMETERS
d_r=0.06; %[m]
d_b=0.005; %[m]
l_d=1.5; %[m]
q_g=0.00004; %[m3/s]
v_l=0.000000801; %[m2/s]
K_avg=(1.5+1.5+1.3+0.75)/4;
e_yo=0.0000025;
l_r=6;
l=l_r+l_d;
m_l=0.000798; %[kg/m/s]
m_g=0.00001983; %[kg/m/s]
p_l=1000; %[kg/m3]
p_g=1.225; %[kg/m3]
cp_l=4181.3; %[JK-1kg-1]
cp_g=1012; %[JK-1kg-1]
pi=3.142; %[dimensionless]
g=9.81; %[m/s2]
c_s=0; %[dimensionless parameter of solids]
k_t=0.195; %[Wm-1K-1]
k_l=0.55; %[Wm-1K-1]
k_g=0.027; %[Wm-1K-1]
r_i=d_r/2; %[m]
s=0.002; %[m]
r_e=r_i+s; %[m]
```

```
d_o=d_r+(2*s); %[m] outer diameter
h_e=12; %[Wm-2K-1]
T_m_out=296; %[K]
T_e=283; %[K]
T_max= 400;
n=100000; %linspace for T_m_in
x=1000; %linspace for u_b
z=100; %linspace for q_g_row

%ESTIMATION OF u_b
u_b_t=linspace(0.0005,2,x); %[m/s]
u_b_e_numerator=4*g*d_b.*(p_l-p_g);
u_b_e_denom_0 = 3*p_l;
u_b_e_denom_1 = 24*((u_b_t.*d_b./v_l).^(-1));
u_b_e_denom_2 = 2.6*u_b_t.*d_b.*((5*v_l)^(-1)).*((1+((u_b_t.*d_b.*((v_l*5)^(-
1))).^1.52)).^(-1));
u_b_e_denom_3 = 0.411*((u_b_t.*d_b./(263000*v_l)).^(-
7.94))./(1+((u_b_t.*d_b.*((v_l*263000))^(-1)).^(-8)));
u_b_e_denom_4 = ((u_b_t.*d_b./v_l).^0.8)./461000;
u_b_e =
(u_b_e_numerator*((u_b_e_denom_0*(u_b_e_denom_1+u_b_e_denom_2+u_b_e_denom_3+u_
b_e_denom_4)).^(-1))).^0.5; %[m/s]
u_b_error = abs(u_b_e-u_b_t);
[inVal, position] =min(u_b_error);
u_b = u_b_e(position);

s_chan=0.002:0.002:0.008;
s_col=reshape(s_chan,size(s_chan,2),1);
q_g_row=linspace(0.000001,0.0001,z);
s_mat=repmat(s_col,1,z);
q_g_mat=repmat(q_g_row,size(s_col,1),1);
d_o=d_r*ones(size(s_col,1),size(q_g_row,2))+(2*s_mat);

%ESTIMATION OF u_l
% Approach Force Balance

u_l=zeros(size(s_chan,2),z);

for m=1:size(s_chan,2);
    for k=1:z;
        u_l_t=linspace(0.0005,2,n);
        u_l_e_1=(u_l_t.^3).*(u_l_t+u_b*ones(1,n));
        u_l_e_num1=8*g*(p_l-p_g)*u_b.*l_r.*q_g_mat(m,k);
        u_l_e_den1=pi*p_l*d_r;
        u_l_e_den2=4*K_avg*d_r*ones(1,n);
        u_l_e_den3=1;
        u_l_e_den4=-
4*log((0.27*e_yo./d_r).*ones(1,n)+((7*v_l./(u_l_t.*d_r)).^0.9));

u_l_e_2=u_l_e_num1./(u_l_e_den1.*(u_l_e_den2+u_l_e_den3.*(u_l_e_den4.^(-2))));
        u_l_e_error = abs(u_l_e_1-u_l_e_2);
        [inVal, position] =min(u_l_e_error);
        u_l(m,k)=u_l_t(position);
    end
end


% Re
Re=u_l.*d_r./v_l ;

% e_r
e_r=(4*q_g_mat)./(pi*(d_r.^2).*(u_b.*ones(size(q_g_mat,1),size(q_g_mat,2))+u_l
));

% cp_m, k_m, m_m, p_m, q_m, m, n,
q_m=2*q_g_mat;
k_m= (k_g.*e_r) + (k_l.*(ones(size(q_g_mat,1),size(q_g_mat,2))-e_r));
```

```
m_m=(m_g.*e_r) + (m_l.*(ones(size(q_g_mat,1),size(q_g_mat,2))-e_r));
cp_m=(cp_g.*e_r) + (cp_l.*(ones(size(q_g_mat,1),size(q_g_mat,2))-e_r));
p_m=(p_g.*e_r) + (p_l.*(ones(size(q_g_mat,1),size(q_g_mat,2))-e_r));
m= p_m.*u_l.*pi.*(d_r.^2)./4;

% Pr
Pr=m_m.*cp_m./k_m;

clr=cool(size(s_col,1));
Nu_d_mat=zeros(size(q_g_mat,1),size(q_g_mat,2));
for i=1:size(s_col,1);
    for e=1:size(q_g_row,2);
        % Nu_d
        if Re(i,e)<=2100;
            Gz=Re(i,e)*Pr(i,e)*d_r./l(i,e);
            Nu_d= 3.657+ (0.0668*(Gz.^(1/3))./(0.04+(Gz.^(-2/3)))) ;
        else
                if Re(i,e)<=4000;
                    f=(-4*log((0.27*e_yo/d_r_mat(i))+((7/Re(i,e))^0.9)))^(-2);
                    Nu_d= ((f./8)*(Re(i,e)-
1000).*Pr(i,e))/(1+12.7*((f./8)^0.5)*((Pr(i,e)^(2/3))-1));
                else
                        % Re(i,e)>4000;
                        f=(-4*log((0.27*e_yo/d_r)+((7/Re(i,e))^0.9)))^(-2);
                        Nu_d=
((f./8).*Re(i,e).*Pr(i,e))./(1.07+12.7*((f./8)^0.5).*((Pr(i,e)^(2/3))-1));
                end
        end
        Nu_d_mat(i,e)=Nu_d;
    end


    figure(1)
    hold on
    plot(q_g_row,Nu_d_mat(i,:),'Color', clr(i,:));

end
hold off
xlabel('q_g (m^3/s)');
ylabel('Nu_d');
zlabel('s(m)');
str=cellstr(num2str(s_col));
legend(str);
v=get(legend(str),'title');
set(v,'string','s (m)');

% h_m
h_m= Nu_d_mat.*k_m./d_r;

figure(5)
plot(q_g_row,h_m(4,:),'g');  % test for d_r= d_r(4)
xlabel('q_g (m^3/min)');
ylabel('h_m');

figure (6)
plot(q_g_row,Re(4,:),'g'); % test for d_r= d_r(4)
xlabel('q_g (m^3/min)');
ylabel('Re');

% Thermal resistances
R_t_m=1./(h_m.*pi.*d_r*l);
R_t_t=(log(d_o./d_r.*ones(size(s_col,1),size(q_g_row,2)))./(2*k_t.*pi.*l);
R_t_e=1./(h_e.*pi.*d_o.*l);

% T_1

T_m_in=zeros(size(s_col,1),size(q_g_row,2));
```

```
q=zeros(size(s_col,1),size(q_g_row,2));
T_g_in=zeros(size(s_col,1),size(q_g_row,2));

for i=1:size(s_col,1);
    for e=1:size(q_g_row,2);
        T_m_in(i,e)=((T_m_out-T_e)/(exp(-
4*((p_m(i,e)*u_l(i,e)*pi*(d_r^2)*cp_m(i,e)*(R_t_m(i,e)+R_t_t(i,e)+R_t_e(i,e)))
.^(-1)))))+T_e;
        q(i,e)=m(i,e)*cp_m(i,e)*(T_m_in(i,e)-T_m_out);
        T_g_in(i,e)=T_m_in(i,e)+((cp_l*p_l*u_l(i,e)*(1-
e_r(i,e))*pi*((d_r.^2)/4))/(cp_g*p_g*q_g_mat(i,e)))*(T_m_in(i,e)-T_m_out);
    end

    figure(2)
    hold on
    clr_inv=gray(size(s_col,1)+1);
    clr_inv(size(clr_inv,1),:)=[];
    clr=flipud(clr_inv);
    plot(q_g_row,T_m_in(i,:),'Color', clr(i,:),'Linewidth',1.2);
    axis ([0.000001 0.0001 296.02 296.1]);
    title('Temperature of the mixture required at the entrance of the
reactor');
    xlabel('Gas flow rate (m^3/s)');
    ylabel('Temperature in the mixture (K)');
    zlabel('s(m)');
    str=cellstr(num2str(s_col));
    legend(str);
    v=get(legend(str),'title');
    set(v,'string','s (m)');

    figure(4)
    hold on
    plot(q_g_row,T_g_in(i,:),'Color', clr(i,:),'Linewidth',1.2);
    axis ([0.000001 0.0001 0 150000]);
    title('Temperature of the gas required at the entrance of the reactor');
    xlabel('Gas flow rate (m^3/s)');
    ylabel('Temperature of the gas required (K)');
    zlabel('s(m)');
    str=cellstr(num2str(s_col));
    legend(str);
    v=get(legend(str),'title');
    set(v,'string','s (m)');

    figure(3)
    hold on
    plot (q_g_row,q(i,:),'Color', clr(i,:),'Linewidth',1.2);
    title('Heat loss through the walls along the reactor');
    axis ([0.000001 0.0001 160 200]);
xlabel('Gas flow rate (m^3/s)');
ylabel('Heat transferred (W)');
zlabel('s(m)');
str=cellstr(num2str(s_col));
legend(str);
v=get(legend(str),'title');
set(v,'string','s (m)');

end

hold off;
```

Code for Figure 7.16:

```
clear all; close all; clc;

% The following code estimates the temperature needed for the flue gas to
% enter the reactor in order to maintain the temperature until the end of
% the tube above the lower limit that does not harm algae, by using the
% heat transfer model produced in the report.

%PARAMETERS
d_r=0.06; %[m]
d_b=0.005; %[m]
l_d=1.5; %[m]
q_g=0.00004; %[m3/s]
v_l=0.000000801; %[m2/s]
K_avg=(1.5+1.5+1.3+0.75)/4;
e_yo=0.0000025;
l_r=6;
l=l_r+l_d;
m_l=0.000798; %[kg/m/s]
m_g=0.00001983; %[kg/m/s]
p_l=1000; %[kg/m3]
p_g=1.225; %[kg/m3]
cp_l=4181.3; %[JK-1kg-1]
cp_g=1012; %[JK-1kg-1]
pi=3.142; %[dimensionless]
g=9.81; %[m/s2]
c_s=0; %[dimensionless parameter of solids]
k_t=0.195; %[Wm-1K-1]
k_l=0.55; %[Wm-1K-1]
k_g=0.027; %[Wm-1K-1]
r_i=d_r/2; %[m]
s=0.002; %[m]
r_e=r_i+s; %[m]
d_o=d_r+(2*s); %[m] outer diameter
h_e=12; %[Wm-2K-1]
T_m_out=296; %[K]
T_e=283; %[K]
T_max= 400;
n=100000; %linspace for T_m_in
x=1000; %linspace for u_b
z=100; %linspace for q_g_row

%ESTIMATION OF u_b
u_b_t=linspace(0.0005,2,x); %[m/s]
u_b_e_numerator=4*g*d_b.*(p_l-p_g);
u_b_e_denom_0 = 3*p_l;
u_b_e_denom_1 = 24*((u_b_t.*d_b./v_l).^(-1));
u_b_e_denom_2 = 2.6*u_b_t.*d_b.*((5*v_l)^(-1)).*((1+((u_b_t.*d_b.*((v_l*5)^(-
1))).^1.52)).^(-1));
u_b_e_denom_3 = 0.411*((u_b_t.*d_b./(263000*v_l)).^(-
7.94))./(1+((u_b_t.*d_b.*((v_l*263000))^(-1)).^(-8)));
u_b_e_denom_4 = ((u_b_t.*d_b./v_l).^0.8)./461000;
u_b_e =
(u_b_e_numerator*((u_b_e_denom_0*(u_b_e_denom_1+u_b_e_denom_2+u_b_e_denom_3+u_
b_e_denom_4)).^(-1))).^0.5; %[m/s]
u_b_error = abs(u_b_e-u_b_t);
[inVal, position] =min(u_b_error);
u_b = u_b_e(position);

k_t_chan=0.2:0.4:1;
k_t_col=reshape(k_t_chan,size(k_t_chan,2),1);
q_g_row=linspace(0.000001,0.0001,z);
k_t_mat=repmat(k_t_col,1,z);
q_g_mat=repmat(q_g_row,size(k_t_col,1),1);
```

```
%ESTIMATION OF u_l
% Approach Force Balance

u_l=zeros(size(k_t_chan,2),z);

for m=1:size(k_t_chan,2);
    for k=1:z;
        u_l_t=linspace(0.0005,2,n);
        u_l_e_1=(u_l_t.^3).*(u_l_t+u_b*ones(1,n));
        u_l_e_num1=8*g*(p_l-p_g)*u_b.*l_r.*q_g_mat(m,k);
        u_l_e_den1=pi*p_l*d_r;
        u_l_e_den2=4*K_avg*d_r*ones(1,n);
        u_l_e_den3=1;
        u_l_e_den4=-
4*log((0.27*e_yo./d_r).*ones(1,n)+((7*v_l./(u_l_t.*d_r)).^0.9));

u_l_e_2=u_l_e_num1./(u_l_e_den1.*(u_l_e_den2+u_l_e_den3.*(u_l_e_den4.^(-2))));
        u_l_e_error = abs(u_l_e_1-u_l_e_2);
        [inVal, position] =min(u_l_e_error);
        u_l(m,k)=u_l_t(position);
    end
end


% Re
Re=u_l.*d_r./v_l ;

% e_r
e_r=(4*q_g_mat)./(pi*(d_r.^2).*(u_b.*ones(size(q_g_mat,1),size(q_g_mat,2))+u_l
));

% cp_m, k_m, m_m, p_m, q_m, m, n,
q_m=2*q_g_mat;
k_m= (k_g.*e_r) + (k_l.*(ones(size(q_g_mat,1),size(q_g_mat,2))-e_r));
m_m=(m_g.*e_r) + (m_l.*(ones(size(q_g_mat,1),size(q_g_mat,2))-e_r));
cp_m=(cp_g.*e_r) + (cp_l.*(ones(size(q_g_mat,1),size(q_g_mat,2))-e_r));
p_m=(p_g.*e_r) + (p_l.*(ones(size(q_g_mat,1),size(q_g_mat,2))-e_r));
m= p_m.*u_l.*pi.*(d_r.^2)./4;

% Pr
Pr=m_m.*cp_m./k_m;

clr=cool(size(k_t_col,1));
Nu_d_mat=zeros(size(q_g_mat,1),size(q_g_mat,2));
for i=1:size(k_t_col,1);
    for e=1:size(q_g_row,2);
        % Nu_d
        if Re(i,e)<=2100;
            Gz=Re(i,e)*Pr(i,e)*d_r./l;
            Nu_d= 3.657+ (0.0668*(Gz.^(1/3))./(0.04+(Gz.^(-2/3)))) ;
        else
                if Re(i,e)<=4000;
                    f=(-4*log((0.27*e_yo/d_r)+((7/Re(i,e))^0.9)))^(-2);
                    Nu_d= ((f./8)*(Re(i,e)-
1000).*Pr(i,e))/(1+12.7*((f./8)^0.5)*((Pr(i,e)^(2/3))-1));
                else
                        % Re(i,e)>4000;
                    f=(-4*log((0.27*e_yo/d_r)+((7/Re(i,e))^0.9)))^(-2);
                        Nu_d=
((f./8).*Re(i,e).*Pr(i,e))./(1.07+12.7*((f./8)^0.5).*((Pr(i,e)^(2/3))-1));
                end
        end
        Nu_d_mat(i,e)=Nu_d;
    end


    figure(1)
```

```
    hold on
    plot(q_g_row,Nu_d_mat(i,:),'Color', clr(i,:));

end
hold off
xlabel('q_g (m^3/s)');
ylabel('Nu_d');
zlabel('k_t(W/m/K)');
str=cellstr(num2str(k_t_col));
legend(str);
v=get(legend(str),'title');
set(v,'string','k_t (W/m/K)');

% h_m
h_m= Nu_d_mat.*k_m./d_r;

figure(5)
plot(q_g_row,h_m(3,:),'g');  % test for d_r= d_r(4)
xlabel('q_g (m^3/min)');
ylabel('h_m');

figure (6)
plot(q_g_row,Re(3,:),'g'); % test for d_r= d_r(4)
xlabel('q_g (m^3/min)');
ylabel('Re');

% Thermal resistances
R_t_m=1./(h_m.*pi.*d_r*l);
R_t_t=(log(d_o./d_r))./(2.*k_t_mat.*pi.*l);
R_t_e=1./(h_e.*pi.*d_o*l);

% T_1

T_m_in=zeros(size(k_t_col,1),size(q_g_row,2));
q=zeros(size(k_t_col,1),size(q_g_row,2));
T_g_in=zeros(size(k_t_col,1),size(q_g_row,2));


for i=1:size(k_t_col,1);
    for e=1:size(q_g_row,2);
        T_m_in(i,e)=((T_m_out-T_e)/(exp(-
4*((p_m(i,e)*u_l(i,e)*pi*(d_r.^2)*cp_m(i,e)*(R_t_m(i,e)+R_t_t(i,e)+R_t_e)).^(-
1)))))+T_e;
        q(i,e)=m(i,e)*cp_m(i,e)*(T_m_in(i,e)-T_m_out);
        T_g_in(i,e)=T_m_in(i,e)+((cp_l*p_l*u_l(i,e)*(1-
e_r(i,e))*pi*((d_r.^2)/4))/(cp_g*p_g*q_g_mat(i,e)))*(T_m_in(i,e)-T_m_out);
    end

    figure(2)
    hold on
    clr_inv=gray(size(k_t_col,1)+1);
    clr_inv(size(clr_inv,1),:)=[];
    clr=flipud(clr_inv);
    plot(q_g_row,T_m_in(i,:),'Color', clr(i,:),'Linewidth',1.2);
    axis ([0 0.0001 296.02 296.1]);
    title('Temperature of the mixture required at the entrance of the
reactor');
    xlabel('Gas flow rate (m^3/s)');
    ylabel('Temperature in the mixture (K)');
    zlabel('k_t(W/m/K)');
    str=cellstr(num2str(k_t_col));
    legend(str);
    v=get(legend(str),'title');
    set(v,'string','k_t (W/m/K)');

    figure(4)
    colormap cool;
```

```
    hold on
    plot(q_g_row,T_g_in(i,:),'Color', clr(i,:),'Linewidth',1.2);
    axis ([0 0.0001 0 160000]);
    title('Temperature of the gas required at the entrance of the reactor');
    xlabel('Gas flow rate (m^3/s)');
    ylabel('Temperature of the gas required (K)');
    zlabel('k_t(W/m/K)');
    str=cellstr(num2str(k_t_col));
    legend(str);
    v=get(legend(str),'title');
    set(v,'string','k_t (W/m/K)');

    figure(3)
    hold on
    plot (q_g_row,q(i,:),'Color', clr(i,:),'Linewidth',1.2);
    axis ([0 0.0001 185 220]);
end

hold off;

title('Heat loss through the walls along the reactor');
xlabel('Gas flow rate (m^3/s)');
ylabel('Heat transferred (W)');
zlabel('k_t(W/m/K)');
str=cellstr(num2str(k_t_col));
legend(str);
v=get(legend(str),'title');
set(v,'string','k_t (W/m/K)');
```

Code for Figure 7.17:

```
clear all; close all; clc;

% The following code estimates the temperature needed for the flue gas to
% enter the reactor in order to maintain the temperature until the end of
% the tube above the lower limit that does not harm algae, by using the
% heat transfer model produced in the report.

%PARAMETERS
d_r=0.06; %[m]
d_b=0.005; %[m]
l_d=1.5; %[m]
q_g=0.0003; %[m3/s]
v_l=0.000000801; %[m2/s]
K_avg=(1.5+1.5+1.3+0.75)/4;
e_yo=0.0000025;
l_r=6;
l=l_r+l_d;
m_l=0.000798; %[kg/m/s]
m_g=0.00001983; %[kg/m/s]
p_l=1000; %[kg/m3]
p_g=1.225; %[kg/m3]
cp_l=4181.3; %[JK-1kg-1]
cp_g=1012; %[JK-1kg-1]
pi=3.142; %[dimensionless]
g=9.81; %[m/s2]
c_s=0; %[dimensionless parameter of solids]
k_t=0.195; %[Wm-1K-1]
k_l=0.55; %[Wm-1K-1]
k_g=0.027; %[Wm-1K-1]
r_i=d_r/2; %[m]
s=0.002; %[m]
```

```
r_e=r_i+s; %[m]
d_o=d_r+(2*s); %[m] outer diameter
h_e=12; %[Wm-2K-1]
T_m_out=296; %[K]
T_e=283; %[K]
T_max= 400;
n=100000; %linspace for T_m_in
x=1000; %linspace for u_b
z=100; %linspace for q_g_row

%ESTIMATION OF u_b
u_b_t=linspace(0.0005,2,x); %[m/s]
u_b_e_numerator=4*g*d_b.*(p_l-p_g);
u_b_e_denom_0 = 3*p_l;
u_b_e_denom_1 = 24*((u_b_t.*d_b./v_l).^(-1));
u_b_e_denom_2 = 2.6*u_b_t.*d_b.*((5*v_l)^(-1)).*((1+((u_b_t.*d_b.*((v_l*5)^(-
1))).^1.52)).^(-1));
u_b_e_denom_3 = 0.411*((u_b_t.*d_b./(263000*v_l)).^(-
7.94))./(1+((u_b_t.*d_b.*((v_l*263000))^(-1)).^(-8)));
u_b_e_denom_4 = ((u_b_t.*d_b./v_l).^0.8)./461000;
u_b_e =
(u_b_e_numerator*((u_b_e_denom_0*(u_b_e_denom_1+u_b_e_denom_2+u_b_e_denom_3+u_
b_e_denom_4)).^(-1))).^0.5; %[m/s]
u_b_error = abs(u_b_e-u_b_t);
[inVal, position] =min(u_b_error);
u_b = u_b_e(position);

h_e_chan=5:70:215;
h_e_col=reshape(h_e_chan,size(h_e_chan,2),1);
q_g_row=linspace(0.000001,0.00012,z);
h_e_mat=repmat(h_e_col,1,z);
q_g_mat=repmat(q_g_row,size(h_e_col,1),1);


%ESTIMATION OF u_l
% Approach Force Balance

u_l=zeros(size(h_e_chan,2),z);

for m=1:size(h_e_chan,2);
    for k=1:z;
        u_l_t=linspace(0.0005,2,n);
        u_l_e_1=(u_l_t.^3).*(u_l_t+u_b*ones(1,n));
        u_l_e_num1=8*g*(p_l-p_g)*u_b.*l_r.*q_g_mat(m,k);
        u_l_e_den1=pi*p_l*d_r;
        u_l_e_den2=4*K_avg*d_r*ones(1,n);
        u_l_e_den3=1;
        u_l_e_den4=-
4*log((0.27*e_yo./d_r).*ones(1,n)+((7*v_l./(u_l_t.*d_r)).^0.9));

u_l_e_2=u_l_e_num1./(u_l_e_den1.*(u_l_e_den2+u_l_e_den3.*(u_l_e_den4.^(-2))));
        u_l_e_error = abs(u_l_e_1-u_l_e_2);
        [inVal, position] =min(u_l_e_error);
        u_l(m,k)=u_l_t(position);
    end
end



% Re
Re=u_l.*d_r./v_l ;

% e_r
e_r=(4*q_g_mat)./(pi*(d_r.^2).*(u_b.*ones(size(q_g_mat,1),size(q_g_mat,2))+u_l
));

% cp_m, k_m, m_m, p_m, q_m, m, n,
```

```
q_m=2*q_g_mat;
k_m= (k_g.*e_r) + (k_l.*(ones(size(q_g_mat,1),size(q_g_mat,2))-e_r));
m_m=(m_g.*e_r) + (m_l.*(ones(size(q_g_mat,1),size(q_g_mat,2))-e_r));
cp_m=(cp_g.*e_r) + (cp_l.*(ones(size(q_g_mat,1),size(q_g_mat,2))-e_r));
p_m=(p_g.*e_r) + (p_l.*(ones(size(q_g_mat,1),size(q_g_mat,2))-e_r));
m= p_m.*u_l.*pi.*(d_r.^2)./4;

% Pr
Pr=m_m.*cp_m./k_m;

clr=cool(size(h_e_col,1));
Nu_d_mat=zeros(size(q_g_mat,1),size(q_g_mat,2));
for i=1:size(h_e_col,1);
    for e=1:size(q_g_row,2);
        % Nu_d
        if Re(i,e)<=2100;
            Gz=Re(i,e)*Pr(i,e)*d_r./l;
            Nu_d= 3.657+ (0.0668*(Gz.^(1/3))./(0.04+(Gz.^(-2/3)))) ;
        else
                if Re(i,e)<=4000;
                    f=(-4*log((0.27*e_yo/d_r)+((7/Re(i,e))^0.9)))^(-2);
                    Nu_d= ((f./8)*(Re(i,e)-
1000).*Pr(i,e))/(1+12.7*((f./8)^0.5)*((Pr(i,e)^(2/3))-1));
                else
                        % Re(i,e)>4000;
                        f=(-4*log((0.27*e_yo/d_r)+((7/Re(i,e))^0.9)))^(-2);
                        Nu_d=
((f./8).*Re(i,e).*Pr(i,e))./(1.07+12.7*((f./8)^0.5).*((Pr(i,e)^(2/3))-1));
                end
        end
        Nu_d_mat(i,e)=Nu_d;
    end


    figure(1)
    hold on
    plot(q_g_row,Nu_d_mat(i,:),'Color', clr(i,:));

end
hold off
xlabel('q_g (m^3/s)');
ylabel('Nu_d');
zlabel('h_e(W/m^2/K)');
str=cellstr(num2str(h_e_col));
legend(str);
v=get(legend(str),'title');
set(v,'string','h_e (W/m^2/K)');

% h_m
h_m= Nu_d_mat.*k_m./d_r;

figure(5)
plot(q_g_row,h_m(4,:),'g');  % test for d_r= d_r(4)
xlabel('q_g (m^3/min)');
ylabel('h_m');

figure (6)
plot(q_g_row,Re(4,:),'g'); % test for d_r= d_r(4)
xlabel('q_g (m^3/min)');
ylabel('Re');

% Thermal resistances
R_t_m=1./(h_m.*pi.*d_r*l);
R_t_t=(log(d_o./d_r))./(2.*k_t.*pi.*l);
R_t_e=1./(h_e_mat.*pi.*d_o*l);

% T_1
```

```
T_m_in=zeros(size(h_e_col,1),size(q_g_row,2));
q=zeros(size(h_e_col,1),size(q_g_row,2));
T_g_in=zeros(size(h_e_col,1),size(q_g_row,2));


for i=1:size(h_e_col,1);
    for e=1:size(q_g_row,2);
        T_m_in(i,e)=((T_m_out-T_e)/(exp(-
4*((p_m(i,e)*u_l(i,e)*pi*(d_r.^2)*cp_m(i,e)*(R_t_m(i,e)+R_t_t+R_t_e(i,e))).^(-
1)))))+T_e;
        q(i,e)=m(i,e)*cp_m(i,e)*(T_m_in(i,e)-T_m_out);
        T_g_in(i,e)=T_m_in(i,e)+((cp_l*p_l*u_l(i,e)*(1-
e_r(i,e))*pi*((d_r.^2)/4))/(cp_g*p_g*q_g_mat(i,e)))*(T_m_in(i,e)-T_m_out);
    end

    figure(2)
    hold on
    clr_inv=gray(size(h_e_col,1)+1);
    clr_inv(size(clr_inv,1),:)=[];
    clr=flipud(clr_inv);
    plot(q_g_row,T_m_in(i,:),'Color', clr(i,:),'Linewidth',1.2);
    axis ([0 0.0001 296 296.35]);
    title('Temperature of the mixture required at the entrance of the
reactor');
    xlabel('Gas flow rate (m^3/s)');
    ylabel('Temperature in the mixture (K)');
    zlabel('h_e(W/m^2/K)');
    str=cellstr(num2str(h_e_col));
    legend(str);
    v=get(legend(str),'title');
    set(v,'string','h_e (W/m^2/K)');

    figure(4)
    colormap cool;
    hold on
    plot(q_g_row,T_g_in(i,:),'Color', clr(i,:),'Linewidth',1.2);
    axis ([0 0.0001 0 500000]);
    title('Temperature of the gas required at the entrance of the reactor');
    xlabel('Gas flow rate (m^3/s)');
    ylabel('Temperature of the gas required (K)');
    zlabel('h_e(W/m^2/K)');
    str=cellstr(num2str(h_e_col));
    legend(str);
    v=get(legend(str),'title');
    set(v,'string','h_e (W/m^2/K)');

    figure(3)
    hold on
    plot (q_g_row,q(i,:),'Color', clr(i,:),'Linewidth',1.2);
    axis ([0 0.0001 0 1000]);
end

hold off;

title('Heat loss through the walls along the reactor');
xlabel('Gas flow rate (m^3/s)');
ylabel('Heat transferred (W)');
zlabel('h_e(W/m^2/K)');
str=cellstr(num2str(h_e_col));
legend(str);
v=get(legend(str),'title');
set(v,'string','h_e (W/m^2/K)');
```

Code for Figure 7.18:

```
clear all; close all; clc;

% The following code estimates the temperature needed for the flue gas to
% enter the reactor in order to maintain the temperature until the end of
% the tube above the lower limit that does not harm algae, by using the
% heat transfer model produced in the report.

%PARAMETERS
d_r=0.06; %[m]
d_b=0.005; %[m]
l_d=1.5; %[m]
q_g=0.0003; %[m3/s]
v_l=0.000000801; %[m2/s]
K_avg=(1.5+1.5+1.3+0.75)/4;
e_yo=0.0000025;
l_r=6;
l=l_r+l_d;
m_l=0.000798; %[kg/m/s]
m_g=0.00001983; %[kg/m/s]
p_l=1000; %[kg/m3]
p_g=1.225; %[kg/m3]
cp_l=4181.3; %[JK-1kg-1]
cp_g=1012; %[JK-1kg-1]
pi=3.142; %[dimensionless]
g=9.81; %[m/s2]
c_s=0; %[dimensionless parameter of solids]
k_t=0.195; %[Wm-1K-1]
k_l=0.55; %[Wm-1K-1]
k_g=0.027; %[Wm-1K-1]
r_i=d_r/2; %[m]
s=0.002; %[m]
r_e=r_i+s; %[m]
d_o=d_r+(2*s); %[m] outer diameter
h_e=12; %[Wm-2K-1]
T_m_out=296; %[K]
T_e=283; %[K]
T_max= 400;
n=100000; %linspace for T_m_in
x=1000; %linspace for u_b
z=100; %linspace for q_g_row

%ESTIMATION OF u_b
u_b_t=linspace(0.0005,2,x); %[m/s]
u_b_e_numerator=4*g*d_b.*(p_l-p_g);
u_b_e_denom_0 = 3*p_l;
u_b_e_denom_1 = 24*((u_b_t.*d_b./v_l).^(-1));
u_b_e_denom_2 = 2.6*u_b_t.*d_b.*((5*v_l)^(-1)).*((1+((u_b_t.*d_b.*((v_l*5)^(-
1))).^1.52)).^(-1));
u_b_e_denom_3 = 0.411*((u_b_t.*d_b./(263000*v_l)).^(-
7.94))./(1+((u_b_t.*d_b.*((v_l*263000))^(-1)).^(-8)));
u_b_e_denom_4 = ((u_b_t.*d_b./v_l).^0.8)./461000;
u_b_e =
(u_b_e_numerator*((u_b_e_denom_0*(u_b_e_denom_1+u_b_e_denom_2+u_b_e_denom_3+u_
b_e_denom_4)).^(-1))).^0.5; %[m/s]
u_b_error = abs(u_b_e-u_b_t);
[inVal, position] =min(u_b_error);
u_b = u_b_e(position);

T_e_chan=268:8:292;
T_e_col=reshape(T_e_chan,size(T_e_chan,2),1);
q_g_row=linspace(0.000001,0.00012,z);
T_e_mat=repmat(T_e_col,1,z);
q_g_mat=repmat(q_g_row,size(T_e_col,1),1);
```

```
%ESTIMATION OF u_l
% Approach Force Balance
u_l=zeros(size(T_e_chan,2),z);

for m=1:size(T_e_chan,2);
    for k=1:z;
        u_l_t=linspace(0.0005,2,n);
        u_l_e_1=(u_l_t.^3).*(u_l_t+u_b*ones(1,n));
        u_l_e_num1=8*g*(p_l-p_g)*u_b.*l_r.*q_g_mat(m,k);
        u_l_e_den1=pi*p_l*d_r;
        u_l_e_den2=4*K_avg*d_r*ones(1,n);
        u_l_e_den3=l;
        u_l_e_den4=-
4*log((0.27*e_yo./d_r).*ones(1,n)+((7*v_l./(u_l_t.*d_r)).^0.9));

u_l_e_2=u_l_e_num1./(u_l_e_den1.*(u_l_e_den2+u_l_e_den3.*(u_l_e_den4.^(-2))));
        u_l_e_error = abs(u_l_e_1-u_l_e_2);
        [inVal, position] =min(u_l_e_error);
        u_l(m,k)=u_l_t(position);
    end
end

% Re
Re=u_l.*d_r./v_l ;

% e_r
e_r=(4*q_g_mat)./(pi*(d_r.^2).*(u_b.*ones(size(q_g_mat,1),size(q_g_mat,2))+u_l
));

% cp_m, k_m, m_m, p_m, q_m, m, n,
q_m=2*q_g_mat;
k_m= (k_g.*e_r) + (k_l.*(ones(size(q_g_mat,1),size(q_g_mat,2))-e_r));
m_m=(m_g.*e_r) + (m_l.*(ones(size(q_g_mat,1),size(q_g_mat,2))-e_r));
cp_m=(cp_g.*e_r) + (cp_l.*(ones(size(q_g_mat,1),size(q_g_mat,2))-e_r));
p_m=(p_g.*e_r) + (p_l.*(ones(size(q_g_mat,1),size(q_g_mat,2))-e_r));
m= p_m.*u_l.*pi.*(d_r.^2)./4;

% Pr
Pr=m_m.*cp_m./k_m;

clr=cool(size(T_e_col,1));
Nu_d_mat=zeros(size(q_g_mat,1),size(q_g_mat,2));
for i=1:size(T_e_col,1);
    for e=1:size(q_g_row,2);
        % Nu_d
        if Re(i,e)<=2100;
            Gz=Re(i,e)*Pr(i,e)*d_r./l;
            Nu_d= 3.657+ (0.0668*(Gz.^(1/3))./(0.04+(Gz.^(-2/3)))) ;
        else
                if Re(i,e)<=4000;
                    f=(-4*log((0.27*e_yo/d_r)+((7/Re(i,e))^0.9)))^(-2);
                    Nu_d= ((f./8)*(Re(i,e)-
1000).*Pr(i,e))/(1+12.7*((f./8)^0.5)*((Pr(i,e)^(2/3))-1));
                else
                        % Re(i,e)>4000;
                    f=(-4*log((0.27*e_yo/d_r)+((7/Re(i,e))^0.9)))^(-2);
                        Nu_d=
((f./8).*Re(i,e).*Pr(i,e))./(1.07+12.7*((f./8)^0.5).*((Pr(i,e)^(2/3))-1));
                end
        end
        Nu_d_mat(i,e)=Nu_d;
    end


    figure(1)
    hold on
    plot(q_g_row,Nu_d_mat(i,:),'Color', clr(i,:));
```

```
end
hold off
xlabel('q_g (m^3/s)');
ylabel('Nu_d');
zlabel('T_e(K)');
str=cellstr(num2str(T_e_col));
legend(str);
v=get(legend(str),'title');
set(v,'string','T_e (K)');

% h_m
h_m= Nu_d_mat.*k_m./d_r;

figure(5)
plot(q_g_row,h_m(4,:),'g');  % test for d_r= d_r(4)
xlabel('q_g (m^3/min)');
ylabel('h_m');

figure (6)
plot(q_g_row,Re(4,:),'g'); % test for d_r= d_r(4)
xlabel('q_g (m^3/min)');
ylabel('Re');

% Thermal resistances
R_t_m=1./(h_m.*pi.*d_r*l);
R_t_t=(log(d_o./d_r))./(2.*k_t.*pi.*l);
R_t_e=1./(h_e.*pi.*d_o*l);


% T_1

T_m_in=zeros(size(T_e_col,1),size(q_g_row,2));
q=zeros(size(T_e_col,1),size(q_g_row,2));
T_g_in=zeros(size(T_e_col,1),size(q_g_row,2));

for i=1:size(T_e_col,1);
    for e=1:size(q_g_row,2);
        T_m_in(i,e)=((T_m_out-T_e_mat(i,e))/(exp(-
4*((p_m(i,e)*u_l(i,e)*pi*(d_r.^2)*cp_m(i,e)*(R_t_m(i,e)+R_t_t+R_t_e)).^(-
1)))))+T_e_mat(i,e);
        q(i,e)=m(i,e)*cp_m(i,e)*(T_m_in(i,e)-T_m_out);
        T_g_in(i,e)=T_m_in(i,e)+((cp_l*p_l*u_l(i,e)*(1-
e_r(i,e))*pi*((d_r.^2)/4))/(cp_g*p_g*q_g_mat(i,e)))*(T_m_in(i,e)-T_m_out);

    end

    figure(2)
    hold on
    clr_inv=gray(size(T_e_col,1)+1);
    clr_inv(size(clr_inv,1),:)=[];
    clr=flipud(clr_inv);
    plot(q_g_row,T_m_in(i,:),'Color', clr(i,:),'Linewidth',1.2);
    axis ([0 0.0001 296 296.2]);
    title('Temperature of the mixture required at the entrance of the
reactor');
    xlabel('Gas flow rate (m^3/s)');
    ylabel('Temperature in the mixture (K)');
    zlabel('T_e(K)');
    str=cellstr(num2str(T_e_col));
    legend(str);
    v=get(legend(str),'title');
    set(v,'string','T_e (K)');

    figure(4)
    colormap cool;
    hold on
```

```
    plot(q_g_row,T_g_in(i,:),'Color', clr(i,:),'Linewidth',1.2);
   axis ([0 0.0001 0 300000]);
    title('Temperature of the gas required at the entrance of the reactor');
    xlabel('Gas flow rate (m^3/s)');
    ylabel('Temperature of the gas required (K)');
    zlabel('T_e(K)');
    str=cellstr(num2str(T_e_col));
    legend(str);
    v=get(legend(str),'title');
    set(v,'string','T_e (K)');

    figure(3)
    hold on
    plot (q_g_row,q(i,:),'Color', clr(i,:),'Linewidth',1.2);
    axis ([0 0.0001 50 450]);
end

hold off;

title('Heat loss through the walls along the reactor');
xlabel('Gas flow rate (m^3/s)');
ylabel('Heat transferred (W)');
zlabel('T_e(K)');
str=cellstr(num2str(T_e_col));
legend(str);
v=get(legend(str),'title');
set(v,'string','T_e (K)');
```

Table VI.5. Parameters used for the production of Figure 7.19 and variables computed.

Parameters	Values	Variables	Values estimated
d_r	0.060	u_b	0.392
d_b	0.005	$\bar{u}_l$	0.133
l_d	1.50	Re_l	9959
q_g	0.00015	ε_r	0.2
l_r	7.98	l	9.00
ν_l	0.801 x 10^{-6}	c_{p_m}	3,541
μ_l	0.798 x 10^{-3}	r_e	0.032
μ_g	1.983 x 10^{-5}	f	0.0317
ρ_l	1000	Nu_d	28.5
ρ_g	1.225	Pr	5.85
c_{p_l}	4,181.3	h_m	249.7
c_{p_g}	1,012	k_m	0.527
π	3.142	μ_m	7.6 x10^{-4}
g	9.810	q_m	0.0003
k_t	0.195	q_{loss}	199.8
k_l	0.55	$T_{m_{in}}$	296.02
k_{HE}	16	$T_{hf_{out}}$	306
k_g	0.027		
s	0.002		
$h_{e,l}$	300		
$h_{e,g}$	200		
$T_{m_{out}}$	296 (23° C)		
T_e	283 (10° C)		

Code for Figure 7.19**:**

```
clear all; close all; clc;

% The following code estimates the temperature needed for the flue gas to
% enter the reactor in order to maintain the temperature until the end of
% the tube above the lower limit that does not harm algae, by using the
% heat transfer model produced in the report.

%PARAMETERS
d_r=0.06; %[m]
d_b=0.005; %[m]
q_g=0.00015; %[m3/s]
```

```
l_d=1.5;
v_l=0.000000801; %[m2/s]
K_avg=(1.5+1.5+1.3+0.75)/4;
e_yo=0.0000025;
l_r=6;
l=l_r+l_d;
m_l=0.000798; %[kg/m/s]
m_g=0.00001983; %[kg/m/s]
p_l=1000; %[kg/m3]
p_g=1.225; %[kg/m3]
p_hf_l=p_l; %for the heating fluid if water
p_hf_g=p_g; %for the heating fluid if gas
cp_l=4181.3; %[JK-1kg-1]
cp_g=1012; %[JK-1kg-1]
cp_hf_l=cp_l; %for the heating fluid if liquid
cp_hf_g=cp_g; % for the heating fluid if gas
h_e=12;
h_e_he_l=300; % for the heating fluid if liquid
h_e_he_g=200; %for the heating fluid if gas
pi=3.142; %[dimensionless]
g=9.81; %[m/s2]
k_t=0.195; %[Wm-1K-1] for the plastic
k_t_he=16; %for stailess steel
k_l=0.55; %[Wm-1K-1]
k_g=0.027; %[Wm-1K-1]
r_i=d_r/2; %[m]
s=0.002; %[m]
s_he=s; %width of metal part
r_e=r_i+s; %[m]
d_o=d_r+(2*s); %[m] outer diameter
T_dif=10; % temperature difference between the heatinf fluid
T_e=283; % ambient temperature
T_m_out=296; %[K]
T_hf_out=T_m_out+T_dif; %[K]
T_max= 345;
n=1000; %linspace for T_m_in
x=1000; %linspace for u_b
z=100; %linspace for q_g_row

%ESTIMATION OF u_b
u_b_t=linspace(0.0005,2,x); %[m/s]
u_b_e_numerator=4*g*d_b.*(p_l-p_g);
u_b_e_denom_0 = 3*p_l;
u_b_e_denom_1 = 24*((u_b_t.*d_b./v_l).^(-1));
u_b_e_denom_2 = 2.6*u_b_t.*d_b.*((5*v_l)^(-1)).*((1+((u_b_t.*d_b.*((v_l*5)^(-
1))).^1.52)).^(-1));
u_b_e_denom_3 = 0.411*((u_b_t.*d_b./(263000*v_l)).^(-
7.94))./(1+((u_b_t.*d_b.*((v_l*263000))^(-1)).^(-8)));
u_b_e_denom_4 = ((u_b_t.*d_b./v_l).^0.8)./461000;
u_b_e =
(u_b_e_numerator*((u_b_e_denom_0*(u_b_e_denom_1+u_b_e_denom_2+u_b_e_denom_3+u_
b_e_denom_4)).^(-1))).^0.5; %[m/s]
u_b_error = abs(u_b_e-u_b_t);
[inVal, position] =min(u_b_error);
u_b = u_b_e(position);


%ESTIMATION OF u_l
% Approach Force Balance

u_l_t=linspace(0.0005,2,n);
u_l_e_1=(u_l_t.^3).*(u_l_t+u_b*ones(1,n));
u_l_e_num1=8*g*(p_l-p_g)*u_b.*l_r.*q_g;
u_l_e_den1=pi*p_l*d_r;
u_l_e_den2=4*K_avg*d_r*ones(1,n);
u_l_e_den3=l;
u_l_e_den4=-4*log((0.27*e_yo./d_r).*ones(1,n)+((7*v_l./(u_l_t.*d_r)).^0.9));
```

```
u_l_e_2=u_l_e_num1./(u_l_e_den1.*(u_l_e_den2+u_l_e_den3.*(u_l_e_den4.^(-2))));
u_l_e_error = abs(u_l_e_1-u_l_e_2);
[inVal, position] =min(u_l_e_error);
u_l=u_l_t(position);


% Re
Re=u_l.*d_r./v_l ;

% e_r
e_r=(4*q_g)./(pi*(d_r.^2).*(u_b.*ones(size(q_g,1),size(q_g,2))+u_l));


% cp_m, k_m, m_m, p_m, q_m, m, n,
q_m=2*q_g;
k_m= (k_g.*e_r) + (k_l.*(1-e_r));
m_m=(m_g.*e_r) + (m_l.*(1-e_r));
cp_m=(cp_g.*e_r) + (cp_l.*(1-e_r));
p_m=(p_g.*e_r) + (p_l.*(1-e_r));
m= p_m.*u_l.*pi.*(d_r.^2)./4;

% Pr
Pr=m_m.*cp_m./k_m;

% clr=jet(size(d_r,1));
Nu_d_mat=zeros(size(q_g,1),size(q_g,2));
for i=1:size(d_r,1);
    for e=1:size(q_g,2);
        % Nu_d
        if Re(i,e)<=2100;
            Gz=Re(i,e)*Pr(i,e)*d_r./l_r;
            Nu_d= 3.657+ (0.0668*(Gz.^(1/3))./(0.04+(Gz.^(-2/3)))) ;
        else
                if Re(i,e)<=4000;
                    f=(-4*log((0.27*e_yo/d_r)+((7/Re(i,e))^0.9)))^(-2);
                    Nu_d= ((f./8)*(Re(i,e)-
1000).*Pr(i,e))/(1+12.7*((f./8)^0.5)*((Pr(i,e)^(2/3))-1));
                else
                        % Re(i,e)>4000;
                    f=(-4*log((0.27*e_yo/d_r)+((7/Re(i,e))^0.9)))^(-2);
                        Nu_d=
((f./8).*Re(i,e).*Pr(i,e))./(1.07+12.7*((f./8)^0.5).*((Pr(i,e)^(2/3))-1));
                end
        end
        Nu_d_mat(i,e)=Nu_d;
    end


%     figure(1)
%     hold on
%     plot(q_g,Nu_d_mat(i,:),'Color', clr(i,:));

end
% hold off
% xlabel('q_g (m^3/s)');
% ylabel('Nu_d');
% zlabel('d_r(m)');
% str=cellstr(num2str(d_r));
% legend(str);
% v=get(legend(str),'title');
% set(v,'string','d_r (m)');
%
% h_m
h_m= Nu_d_mat.*k_m./d_r;

% Thermal resistances
R_t_m=1./(h_m.*pi.*d_r*l);
```

```
R_t_t=(log(d_o./d_r))./(2.*k_t.*pi.*l);
R_t_e=1./(h_e.*pi.*d_o*l);


% T_m_in
T_m_in=((T_m_out-T_e)/(exp(-
4*((p_m*u_l*pi*(d_r.^2)*cp_m*(R_t_m+R_t_t+R_t_e)).^(-1))))+T_e;
q=m*cp_m*(T_m_in-T_m_out);

% l_he

T_hf_in=linspace(T_m_in+11,T_m_out+62, n);

%lmtd according to counter flow het exchanger. be carefull T in and Tout
%are confusing because for the mixture Tin is in for the riser but out of
%the HE

lmtd_he=((T_hf_in-T_m_in*ones(1,n))-(T_hf_out-
T_m_out)*ones(1,n))./(log((T_hf_in-T_m_in.*ones(1,n))./(T_hf_out-
T_m_out).*ones(1,n)));
R_t_m_he=1./(h_m.*pi.*d_r);
R_t_t_he=(log(d_o./d_r))./(2.*k_t.*pi);
R_t_e_he_l=1./(h_e_he_l.*pi.*d_o);
R_t_e_he_g=1./(h_e_he_g.*pi.*d_o);
UA_he_l= (1/(R_t_m_he+R_t_t_he+R_t_e_he_l));
UA_he_g= (1/(R_t_m_he+R_t_t_he+R_t_e_he_g));

m_hf_l=q./(cp_hf_l*(T_hf_in-T_hf_out));

l_he_l=q./UA_he_l./lmtd_he;

m_hf_g=q./(cp_hf_g*(T_hf_in-T_hf_out));

l_he_g=q./UA_he_g./lmtd_he;


figure(2)
hold on
[AX,h1,h2]=plotyy(T_hf_in,m_hf_g,T_hf_in, l_he_g,'plot');

axes(AX(1));
lh=line(T_hf_in,m_hf_l,'Linewidth',3);
set(get(AX(1),'Ylabel'),'String','Mass flow rate of the heating fluid (kg/s)')
axis([307 358 0 0.2]);

axes(AX(2));
lh=line(T_hf_in,l_he_l,'Linewidth',3);
set(get(AX(2),'Ylabel'),'String','Length of the metal part (m)')
axis ([307 358 0 2]);
xlabel('Temperature of the entering heating fluid (K)')
%title('Mass flow rate and length required for the heat exchanger')

figure(3)
plot (T_hf_in,l_he_l);
```